

1. Report No. NASA CR-134587		2. Government Accession No.		3. Recipient's Catalog No.	
4. Title and Subtitle FRACTURE CHARACTERISTICS OF STRUCTURAL AEROSPACE ALLOYS CONTAINING DEEP SURFACE FLAWS				5. Report Date DECEMBER 1973	
				6. Performing Organization Code	
7. Author(s) J. N. MASTERS, W. D. BIXLER AND R. W. FINGER				8. Performing Organization Report No. D180-17759-1	
9. Performing Organization Name and Address BOEING AEROSPACE COMPANY RESEARCH AND ENGINEERING DIVISION P. O. BOX 3999 SEATTLE, WASHINGTON 98124				10. Work Unit No.	
				11. Contract or Grant No. NAS 3-14341	
12. Sponsoring Agency Name and Address NATIONAL AERONAUTICS AND SPACE ADMINISTRATION LEWIS RESEARCH CENTER 21000 BROOKPARK ROAD CLEVELAND, OHIO 44135				13. Type of Report and Period Covered CONTRACTOR REPORT JUNE 1970 THROUGH MARCH 1972	
				14. Sponsoring Agency Code	
15. Supplementary Notes PROJECT MANAGER, JOHN A. MISENICK MATERIALS AND STRUCTURES DIVISION NASA LEWIS RESEARCH CENTER CLEVELAND, OHIO 44135					
16. Abstract <p>THIS EXPERIMENTAL PROGRAM WAS UNDERTAKEN TO FURTHER INVESTIGATE CONDITIONS CONTROLLING THE GROWTH AND FRACTURE OF DEEP SURFACE FLAWS IN AEROSPACE ALLOYS. THE PROGRAM WAS BASED ON PRIOR WORK PERFORMED UNDER CONTRACT NAS3-10290 "INVESTIGATION OF DEEP FLAWS IN THIN WALLED TANKS". STATIC FRACTURE TESTS WERE PERFORMED ON 7075-T651 AND 2219-T87 ALUMINUM, AND 6Al-4V STA TITANIUM. CYCLIC FLAW GROWTH TESTS WERE PERFORMED ON THE TWO LATTER ALLOYS, AND SUSTAIN LOAD TESTS WERE PERFORMED ON THE TITANIUM ALLOY. BOTH THE CYCLIC AND THE SUSTAIN LOAD TESTS WERE PERFORMED WITH AND WITHOUT A PRIOR PROOF OVERLOAD CYCLE TO INVESTIGATE POSSIBLE GROWTH RETARDATION EFFECTS. VARIABLES INCLUDED IN ALL TEST SERIES WERE THICKNESS, FLAW DEPTH-TO-THICKNESS RATIO, AND FLAW SHAPE. RESULTS WERE ANALYZED AND COMPARED WITH PREVIOUSLY DEVELOPED DATA TO DETERMINE THE LIMITS OF APPLICABILITY OF AVAILABLE MODIFIED LINEAR ELASTIC FRACTURE SOLUTIONS.</p>					
17. Key Words (Suggested by Author(s)) SURFACE FLAW 7075-T651 ALUMINUM 2219-T87 ALUMINUM 6Al-4V STA TITANIUM FRACTURE CONTROL				18. Distribution Statement UNCLASSIFIED, UNLIMITED	
19. Security Classif. (of this report) UNCLASSIFIED		20. Security Classif. (of this page) UNCLASSIFIED		21. No. of Pages 238	22. Price* 3.00

* For sale by the National Technical Information Service, Springfield, Virginia 22151

FOREWORD

This report describes an investigation of flaw growth and fracture characteristics of structural aerospace alloys containing deep surface flaws performed by the Boeing Aerospace Company from June 1970 through March 1972 under Contract NAS3-14341. The work was administered by Mr. John A. Misencik of the NASA Lewis Research Center.

This program was conducted by the Research and Engineering Division of the Boeing Aerospace Company, Seattle, Washington under the supervision of H. W. Klopfenstein, Structures Research and Development Manager. The Program Leader was J. N. Masters, Supervisor, Failure Mechanisms Group. The Technical Leader was R. W. Finger and W. D. Bixler performed the flaw growth analysis. A. A. Ottlyk provided test engineering support, and D. G. Good produced the technical illustrations and art work. This technical report is also released as Boeing Document D180-17759-1.

PRECEDING PAGE BLANK NOT FILMED

PRECEDING PAGE BLANK NOT FILMED

TABLE OF CONTENTS

	<u>Page</u>
1.0 INTRODUCTION	1
2.0 BACKGROUND	3
3.0 MATERIALS AND PROCEDURES	7
3.1 Materials	—
3.2 Specimen Preparation	8
3.3 Experimental Procedures	9
3.3.1 Instrumentation	
3.3.2 Mechanical Property Tests	10
3.3.3 Static Fracture Tests	—
3.3.4 Cyclic Tests	—
3.3.5 Overload Tests	11
4.0 PRESENTATION AND DISCUSSION OF RESULTS	13
4.1 Mechanical Property Tests	—
4.2 Static Fracture Tests	14
4.2.1 Stress-Flaw Depth Relationship	—
4.2.2 Comparison of Magnification Factors	20
4.2.3 Back Surface Dimpling	24
4.2.4 Resistance Curve Considerations	26
4.2.5 Static Test Summary	29
4.3 Cyclic Tests	32
4.3.1 Baseline da/dN Data	—
4.3.2 Proof Overload Effects on Baseline da/dN Data	35
4.3.3 Environmental Effects on Baseline da/dN Data	38
4.3.4 Environment/Proof Overload Effects on da/dN Data	39

TABLE OF CONTENTS (Continued)

	<u>Page</u>
4.3.5 Frequency/Proof Overload Effects on da/dN Data	39
4.3.6 Cyclic Test Summary	40
4.4 Sustained Load Tests	—
5.0 CONCLUSIONS	45
APPENDIX A - STRAIN MEASUREMENTS	47
APPENDIX B - CALCULATION OF CRACK GROWTH RATES FROM SURFACE FLAW OPENING MEASUREMENTS	49
REFERENCES	53

LIST OF FIGURES

Figure No.	Title	Page
Figure 1 -	Shape Parameter Curves for Surface Flaws	55
Figure 2 -	Effect of Flaw Depth on Apparent K Values	56
Figure 3 -	Deep Flaw Magnification Curves (Reference 4)	57
Figure 4 -	Tensile Specimen	58
Figure 5 -	6Al-4V Titanium Surface Flaw Specimen	—
Figure 6 -	6Al-4V Titanium Surface Flaw Specimen	59
Figure 7 -	6Al-4V Titanium Surface Flaw Specimen	—
Figure 8 -	6Al-4V Titanium Surface Flaw Specimen	60
Figure 9 -	Surface Flaw Specimen	61
Figure 10 -	Surface Flaw Specimen	62
Figure 11 -	Surface Flaw Specimen	63
Figure 12 -	Aluminum Surface Flaw Specimen	64
Figure 13 -	Flaw Opening Measurement of Surface Flaw Specimens	65
Figure 14 -	Tensile Properties of 2219-T87 Aluminum Base Metal	66
Figure 15 -	Tensile Properties of 6Al-4V (STA) Titanium Plate	67
Figure 16 -	2219-T87 Aluminum Stress Versus Flaw Size t = 0.38 cm (0.15 Inch)	68
Figure 17 -	2219-T87 Aluminum Stress Versus Flaw Size t = 0.51 cm (0.20 Inch)	69
Figure 18 -	2219-T87 Aluminum Stress Versus Flaw Size t = 1.27 cm (0.50 Inch)	70
Figure 19 -	2219-T87 Aluminum Stress Versus Flaw Size t = 1.90 cm (0.75 Inch)	71
Figure 20 -	7075-T651 Aluminum Stress Versus Flaw Size (Room Temperature, WT)	72

LIST OF FIGURES (Continued)

Figure No.	Page
Figure 21 - 6A1-4V STA Titanium Stress Versus Flaw Size t = 0.15 cm (0.06 Inch)	73
Figure 22 - 6A1-4V STA Titanium Stress Versus Flaw Size t = 0.32 cm (0.125 Inch)	74
Figure 23 - 6A1-4V STA Titanium Stress Versus Flaw Size t = 0.53 cm (0.21 Inch)	75
Figure 24 - 6A1-4V STA Titanium Stress Versus Flaw Size t = 0.76 cm (0.30 Inch)	76
Figure 25 - Comparison of Magnification Terms, 2219-T87 Base Metal at 79°K (-320°F), WT Direction	77
Figure 26 - Comparison of Magnification Terms, 2219-T87 Base Metal at Room Temperature, RT Direction (Data Taken From Ref. (4))	78
Figure 27 - Comparison of Magnification Terms, 2219-T87 Base Metal at 78°K (-320°F), RT Direction (Data Taken From Ref. (4))	79
Figure 28 - Comparison of Magnification Terms, 2219-T87 Base Metal at 20°K (-423°F), RT Direction (Data Taken From Ref. 4)	80
Figure 29 - Comparison of Magnification Terms, 7075-T651 Aluminum at Room Temperature, WT Direction	81
Figure 30 - Comparison of Magnification Terms, 6A1-4V Titanium STA at Room Temperature, RT Direction, a/2c = 0.10	82
Figure 31 - Comparison of Magnification Terms, 6A1-4V Titanium STA at Room Temperature, RT Direction, a/2c = 0.25	83
Figure 32 - Comparison of Magnification Terms, 6A1-4V Titanium STA at Room Temperature, RT Direction, a/2c = 0.40	84
Figure 33 - Variation of Applied and Critical Stress Intensity Around the Periphery of a Surface Flaw 6A1-4V Titanium STA at Room Temperature (RT Direction)	85
Figure 34 - Dimpling Thresholds for 6A1-4V STA Titanium at Room Temperature (RT Direction)	86

LIST OF FIGURES (Continued)

Figure No.	Page
Figure 35 - Comparison of Experimental and Theoretical Dimpling Threshold for 6Al-4V STA Titanium at Room Temperature RT Direction	87
Figure 36 - 2219-T87 Aluminum Dimpling Threshold at 78K(-320F), WT Direction	—
Figure 37 - 6Al-4V STA Titanium Dimple Threshold at Room Temperature (RT Direction)	88
Figure 38 - Crack-Growth-Resistance Curve and Crack Driving Force Curves for Load Controlled Test - Schematic	89
Figure 39 - Stable Growth Measurements for 2219-T87 Base Metal at Room Temperature	90
Figure 40 - Crack Growth-Resistance and -Driving Curves for 2219-T87 Base Metal ($a/2c = 0.40$)	91
Figure 41 - Crack Growth-Resistance and -Driving Curves for 2219-T87 Base Metal ($a/2c = 0.10$)	92
Figure 42 - Generalized Stress Versus Flaw Depth Relationship for Static Fracture	93
Figure 43 - Summary of Static Fracture Test Results	94
Figure 44 - Cyclic Crack Growth for 1.27 cm (0.50 Inch) Thick 2219-T87 Aluminum (WT Direction) at 78°K (-320°F) with $\sigma_o = 0.67 \sigma_{ys}$ and $(a/2c)_i \approx 0.37$	95
Figure 45 - Cyclic Crack Growth Rates for 1.27 cm (0.50 Inch) Thick 2219-T87 Aluminum (WT Direction) at 78°K (-320°F) with $\sigma_o = 0.67 \sigma_{ys}$ and $(a/2c)_i \approx 0.30$	96
Figure 46 - Cyclic Growth Rates for 1.27 cm (0.50 Inch) Thick 2219-T87 Aluminum (WT Direction) at 78°K (-320°F) with $\sigma_o = 0.91 \sigma_{ys}$ and $(a/2c)_i \approx 0.41$	97
Figure 47 - Cyclic Growth Rates for 1.27 cm (0.50 Inch) Thick 2219-T87 Aluminum (WT Direction) at 78°K (-320°F) with $\sigma_o = 0.91 \sigma_{ys}$ and $(a/2c)_i \approx 0.11$	98

LIST OF FIGURES (Continued)

Figure No.	Page
Figure 48 - Cyclic Growth Rates for 0.51 cm (0.20 Inch) Thick 2218-T87 Aluminum (WT Direction) at 78°K (-320°F) with $\sigma_o = 0.91 \sigma_{ys}$ and $(a/2c)_i \approx 0.40$	99
Figure 49 - Cyclic Crack Growth Rates for 0.51 cm (0.20 Inch) Thick 2219-T87 Aluminum (WT Direction) at 78°K (-320°F) with $\sigma_o = 0.91 \sigma_{ys}$ and $(a/2c)_i \approx 0.09$	100
Figure 50 - Cyclic Crack Growth Rates for 0.38 cm (0.15 Inch) Thick 2219-T87 Aluminum (WT Direction) at 78°K (-320°F) with $\sigma_o = 0.67 \sigma_{ys}$ and $(1/2c)_i \approx 0.37$	101
Figure 51 - Cyclic Crack Growth Rates for 0.38 cm (0.15 Inch) Thick 2219-T87 Aluminum (WT Direction) at 78°K (-320°F) with $\sigma_o = 0.67 \sigma_{ys}$ and $(a/2c)_i \approx 0.11$	102
Figure 52 - Cyclic Crack Growth Rates for 0.38 cm (0.15 Inch) Thick 2219-T87 Aluminum (WT Direction) at 78°K (-320°F) with $\sigma_o = 0.91 \sigma_{ys}$ and $(a/2c)_i \approx 0.38$	103
Figure 53 - Cyclic Crack Growth Rates for 0.38 cm (0.15 Inch) Thick 2219-T87 Aluminum (WT Direction) at 78°K (-320°F) with $\sigma_o = 0.91 \sigma_{ys}$ and $(a/2c)_i \approx 0.10$	104
Figure 54 - Summary of Baseline Cyclic Crack Growth Rates for 2219-T87 Aluminum (WT Direction at 78°K (-320°F))	105
Figure 55 - Comparison of 2219-T87 Aluminum (WT Direction) Fatigue Crack Growth Rate Data at 78°K (-320°F)	106
Figure 56 - Cyclic Crack Growth Rates for 0.54 cm (0.21 Inch) Thick 6Al-4V STA Titanium (RT Direction) at 295°K (72°F) in Air with $\sigma_o = 0.77 \sigma_{ys}$ and $(a/2c)_i \approx 0.39$	107
Figure 57 - Cyclic Crack Growth Rates for 0.54 cm (0.21 Inch) Thick 6Al-4V STA Titanium (RT Direction) at 295°K (72°F) in Air with $\sigma_o = 0.77 \sigma_{ys}$ and $(a/2c)_i \approx 0.10$	108
Figure 58 - Cyclic Crack Growth Rates for 0.31 cm (0.12 Inch) Thick 6Al-4V STA Titanium (RT Direction) at 295°K (72°F) in Air with $\sigma_o = 0.77 \sigma_{ys}$ and $(a/2c)_i \approx 0.34$	109

LIST OF FIGURES (Continued)

Figure No.	Page
Figure 59 - Cyclic Crack Growth Rates for 0.31 cm (0.12 Inch) Thick 6Al-4V STA Titanium (RT Direction) at 295°K (72°F) in Air with $\sigma_o = 0.77 \sigma_{ys}$ and $(a/2c)_i = 0.10$	110
Figure 60 - Cyclic Crack Growth Rates for 0.16 cm (0.063 Inch) Thick 6Al-4V STA Titanium (RT Direction) at 295°K (72°F) in Air with $\sigma_o = 0.77 \sigma_{ys}$ and $(a/2c)_i = 0.40$	111
Figure 61 - Cyclic Crack Growth Rates for 0.16 cm (0.063 Inch) Thick 6Al-4V STA Titanium (RT Direction) at 295°K (72°F) in Air with $\sigma_o = 0.77 \sigma_{ys}$ and $(a/2c)_i = 0.10$	112
Figure 62 - Summary of Baseline Cyclic Crack Growth Rates for 6Al-4V STA Titanium (RT Direction) Plate at 295°K (72°F)	113
Figure 63 - Comparison of 6Al-4V STA Titanium (RT Direction) Fatigue Crack Growth Rate Data at 295°K (72°F)	114
Figure 64 - Cyclic Crack Growth Rates for 0.31 cm (0.12 Inch) Thick 6Al-4V STA Titanium (WT Direction) at 295°K in Argon with $\sigma_o = 0.68 \sigma_{ys}$ and $(a/2c)_i = 0.37$	115
Figure 65 - Cyclic Crack Growth Rates for 0.16 cm (0.063 Inch) Thick 6Al-4V STA Titanium (WT Direction) at 295°K (72°F) in Argon with $\sigma_o = 0.68 \sigma_{ys}$ and $(a/2c)_i = 0.10$	116
Figure 66 - Effect of Crack Orientation on Fatigue Crack Growth Rate Data for 6Al-4V STA Titanium at 295°K (72°F)	117
Figure 67 - Cyclic Crack Growth Rates (After a Cryogenic Proof Test) for 1.27 cm (0.50 Inch) Thick 2219-T87 Aluminum (WT Direction) at 78°K (-320°F) with $\sigma_o = 0.67 \sigma_{ys}$ and $(a/2c)_i = 0.39$	118
Figure 68 - Cyclic Crack Growth Rates (After a Cryogenic Proof Test) for 1.27 cm (0.50 Inch) Thick 2219-T87 Aluminum (WT Direction) at 78°K (-302°F) with $\sigma_o = 0.67 \sigma_{ys}$ and $(a/2c)_i = 0.28$	119

LIST OF FIGURES (Continued)

Figure No.	Page
Figure 69 - Cyclic Crack Growth Rates (After a Cryogenic Proof Test) for 1.27 cm (0.50 Inch) Thick 2219-T87 Aluminum (WT Direction) at 78°K (-320°F) with $\sigma_o = 0.91 \sigma_{ys}$ and $(a/2c)_i \approx 0.40$ and 0.10	120
Figure 70 - Cyclic Crack Growth Rates (After a Cryogenic Proof Test) for 0.38 cm (0.15 Inch) Thick 2219-T87 Aluminum (WT Direction) at 78°K (-320°F) with $\sigma_o = 0.67 \sigma_{ys}$ and $(a/2c)_i \approx 0.37$	121
Figure 71 - Cyclic Crack Growth Rates (After a Cryogenic Proof Test) for 0.38 cm (0.15 Inch) Thick 2219-T87 Aluminum (WT Direction) at 78°K (-320°F) with $\sigma_o = 0.67 \sigma_{ys}$ and $(a/2c)_i \approx 0.11$	122
Figure 72 - Cyclic Crack Growth Rates (After a Cryogenic Proof Test) for 0.38 cm (0.15 Inch) Thick 2219-T87 Aluminum (WT Direction) at 78°K (-320°F) with $\sigma_o = 0.76 \sigma_{ys} \rightarrow 0.91 \sigma_{ys}$ and $(a/2c)_i \approx 0.11$ and 0.36	123
Figure 73 - Cyclic Crack Growth Rates (After a Proof Test) For 0.54 cm (0.21 Inch) Thick 6Al-4V STA Titanium (RT Direction) at 295°K (72°F) in Air with $\sigma_o = 0.77 \sigma_{ys}$ and $(a/2c)_i \approx 0.37$	124
Figure 74 - Cyclic Crack Growth Rates (After a Proof Test) For 0.54 cm (0.21 Inch) Thick 6Al-4V STA Titanium (RT Direction) at 295°K (72°F) in Air with $\sigma_o = 0.77 \sigma_{ys}$ and $(a/2c)_i \approx 0.10$	125
Figure 75 - Cyclic Crack Growth Rates (After a Proof Test) For 0.16 cm (0.063 Inch) Thick 6Al-4V STA Titanium (RT Direction) at 295°K (72°F) in Air with $\sigma_o = 0.77 \sigma_{ys}$ and $(a/2c)_i \approx 0.33$	126
Figure 76 - Cyclic Crack Growth Rates (After a Proof Test) For 0.16 cm (0.063 Inch) Thick 6Al-4V STA Titanium (RT Direction) at 295°K (72°F) in Air with $\sigma_o = 0.77 \sigma_{ys}$ and $(a/2c)_i \approx 0.09$	127
Figure 77 - Cyclic Crack Growth Rates (After a Proof Test) For 0.31 cm (0.12 Inch) Thick 6Al-4V STA Titanium (WT Direction) at 295°K (72°F) in Argon with $\sigma_o = 0.68 \sigma_{ys}$ and $(a/2c)_i \approx 0.38$	128

LIST OF FIGURES (Continued)

Figure No.	Page
Figure 78 - Cyclic Crack Growth Rates (After a Proof Test) For 0.16 cm (0.063 Inch) Thick 6Al-4V STA Titanium (WT Direction) at 295°K (72°F) in Argon with $\sigma_o = 0.68 \sigma_{ys}$ and $(a/2c)_i \approx 0.10$	129
Figure 79 - Cyclic Crack Growth Rates for 0.31 cm (0.12 Inch) Thick 6Al-4V STA Titanium (WT Direction) at 295°K (72°F) Salt Water with $\sigma_o = 0.68 \sigma_{ys}$ and $(a/2c)_i \approx 0.37$	130
Figure 80 - Cyclic Crack Growth Rates for 0.16 cm (0.063 Inch) Thick 6Al-4V STA Titanium (WT Direction) at 295°K (72°F) Salt Water with $\sigma_o = 0.68 \sigma_{ys}$ and $(a/2c)_i \approx 0.10$	131
Figure 81 - Cyclic Crack Growth Rates (After a Proof Test) For 0.31 cm (0.12 Inch) Thick 6Al-4V STA Titanium (WT Direction) at 295°K (72°F) in Salt Water with $\sigma_o = 0.68 \sigma_{ys}$ and $(a/2c)_i \approx 0.38$	132
Figure 82 - Cyclic Crack Growth Rates (After a Proof Test) For 0.16 cm (0.063 Inch) Thick 6Al-4V STA Titanium (WT Direction) at 295°K (72°F) in Salt Water with $\sigma_o = 0.68 \sigma_{ys}$ and $(a/2c)_i \approx 0.10$	133
Figure 83 - Cyclic Crack Growth Rates (After a Proof Test) for 0.31 cm (0.12 Inch) Thick 6Al-4V STA Titanium (WT Direction) at 295°K (72°F) in Salt Water with $\sigma_o = 0.68 \sigma_{ys}$ and $(a/2c)_i \approx 0.38$	134
Figure 84 - Cyclic Crack Growth Rates (After a Proof Test) for 0.16 cm (0.063 Inch) Thick 6Al-4V STA Titanium (WT Direction) at 295°K (72°F) in Salt Water with $\sigma_o = 0.68 \sigma_{ys}$ and $(a/2c)_i \approx 0.10$	135
Figure 85 - Summary of Baseline da/dN Developed for 2219-T87 Aluminum and 6Al-4V STA Titanium in Inert Environments	136
Figure 86 - Summary of 6Al-4V STA Titanium (WT Direction) Sustained Loaded Data* in Salt Water at 295°K (72°F)	137
Figure A-1 - Rear Surface Strain Gage Data for 0.381 cm (0.150 Inch) and 0.508 cm (0.200 Inch) Thick 7075-T651 Aluminum at Room Temperature	139

LIST OF FIGURES (Continued)

Figure No.	Page
Figure A-2 - Rear Surface Strain Gage Data for 1.27 cm (0.500 Inch) Thick 7075-T651 Aluminum at Room Temperature	140
Figure A-3 - Rear Surface Strain Gage for 1.905 cm (0.750 Inch) Thick 7075-T651 Aluminum at Room Temperature	141
Figure A-4 - Rear Surface Strain Gage for 0.508 cm (0.200 Inch) Thick 2219-T87 Aluminum at 78°K (-320°F)	142
Figure A-5 - Rear Surface Strain Measurements as a Function of Flaw Depth for 7075-T651 Aluminum at Room Temperature	143
Figure A-6 - Rear Surface Strain Measurement as a Function of Flaw Depth for 2219-T87 Aluminum at 78°K (-320°F)	144
Figure A-7 - Rear Surface Strain Gage for 1.27 cm (0.500 Inch) Thick 2219-T87 Aluminum at -320°F	145
Figure B-1 - EDI Clip Gage Installation	147
Figure B-2 - Variation of C with Flaw Depth for 2219-T87 Aluminum at 78°K (-320°F) and an $(a/2c)_i \approx 0.40$	148
Figure B-3 - Variation of C with Flaw Depth for 2219-T87 Aluminum at 78°K (-320°F) and an $(a/2c)_i \approx 0.25$	149
Figure B-4 - Variation of C with Flaw Depth for 2219-T87 Aluminum at 78°K (-320°F) and an $(a/2c)_i \approx 0.10$	150
Figure B-5 - Variation of C with Flaw Depth for 7075-T651 Aluminum at Room Temperature and an $(a/2c)_i \approx 0.25$	151

LIST OF TABLES

Table No.	Title	Page
1	Summary: NAS3-10290 Investigation of Deep Flaws in Thin Walled Tanks	153
2	Test Summary	154
3	Chemical Compositions of Materials	155
4	Tensile Properties 2219-T87 Aluminum Parent Metal	156
5	Tensile Properties 7075-T6 Aluminum Parent Metal	157
6	Tensile Properties 6Al-4V STA Titanium Parent Metal	158
7	Static Fracture Data for 0.38 cm (0.15 Inch) 2219-T87 Aluminum Parent Metal (WT Direction)	159
8	Static Fracture Data for 0.51 cm (0.20 Inch) 2219-T87 Aluminum Parent Metal (WT Direction)	160
9	Static Fracture Data for 1.27 cm (0.50 Inch) 2219-T87 Aluminum Parent Metal (WT Direction)	161
10	Static Fracture Data for 1.91 cm (0.75 Inch) 2219-T87 Aluminum Parent Metal (WT Direction)	163
11	Static Fracture Data for 7075-T651 Aluminum Parent Metal (WT Direction)	164
12	Static Fracture Data for 0.08 cm (0.03 Inch) and 0.15 cm (0.06 Inch) 6Al-4V STA Titanium Parent Metal (RT Direction)	166
13	Static Fracture Data for 0.31 cm (0.12 Inch) 6Al-4V STA Titanium Parent Metal (RT Direction)	167
14	Static Fracture Data for 0.53 cm (0.21 Inch) 6Al-4V STA Titanium Parent Metal (RT Direction)	168
15	Static Fracture Data for 0.76 cm (0.30 Inch) 6Al-4V STA Titanium Parent Metal (RT Direction)	170
16	2219-T87 Aluminum Cyclic Flaw Growth Data at 78°K (-320°F); t = 1.27 cm (0.50 Inch), $\sigma_o = 0.67 \sigma_{ys}$ and $(a/2c)_i \approx 0.37$	171

LIST OF TABLES (Continued)

Table No.	Title	Page
17	2219-T87 Aluminum Cyclic Flaw Growth Data at 78°K (-320°F); $t = 1.27$ cm (0.50 Inch), $\sigma_o = 0.67 \sigma_{ys}$ and $(a/2c)_i \approx 0.30$	172
18	2219-T87 Aluminum Cyclic Flaw Growth Data at 78°K (-320°F); $t = 1.27$ cm (0.50 Inch), $\sigma_o = 0.91 \sigma_{ys}$ and $(a/2c)_i \approx 0.41$	173
19	2219-T87 Aluminum Cyclic Flaw Growth Data at 78°K (-320°F); $t = 1.27$ cm (0.50 Inch), $\sigma_o = 0.91 \sigma_{ys}$ and $(a/2c)_i \approx 0.11$	174
20	2219-T87 Aluminum Cyclic Flaw Growth Data at 78°K (-320°F); $t = 0.51$ cm (0.20 Inch), $\sigma_o = 0.91 \sigma_{ys}$ and $(a/2c)_i \approx 0.40$	175
21	2219-T87 Aluminum Cyclic Flaw Growth Data at 78°K (-320°F); $t = 0.51$ cm (0.20 Inch), $\sigma_o = 0.91 \sigma_{ys}$ and $(a/2c)_i \approx 0.09$	176
22	2219-T87 Aluminum Cyclic Flaw Growth Data at 78°K (-320°F); $t = 0.38$ cm (0.20 Inch), $\sigma_o = 0.67 \sigma_{ys}$ and $(a/2c)_i \approx 0.37$	177
23	2219-T87 Aluminum Cyclic Flaw Growth Data at 78°K (-320°F); $t = 0.38$ cm (0.15 Inch), $\sigma_o = 0.67 \sigma_{ys}$ and $(a/2c)_i \approx 0.11$	178
24	2219-T87 Aluminum Cyclic Flaw Growth Data at 78°K (-320°F); $t = 0.38$ cm (0.15 Inch), $\sigma_o = 0.91 \sigma_{ys}$ and $(a/2c)_i \approx 0.38$	179
25	2219-T87 Aluminum Cyclic Flaw Growth Data at 78°K (-320°F); $t = 0.38$ cm (0.15 Inch), $\sigma_o = 0.91 \sigma_{ys}$ and $(a/2c)_i \approx 0.09$	180
26	6AL-4V STA Titanium (RT Direction) Cyclic Flaw Growth Data at 295°K (72°F); $t = 0.51$ cm (0.21 Inch), $\sigma_o = 0.77 \sigma_{ys}$ and $(a/2c)_i \approx 0.39$	181
27	6AL-4V STA Titanium (RT Direction) Cyclic Flaw Growth Data at 295°K (72°F); $t = 0.51$ cm (0.21 Inch), $\sigma_o = 0.77 \sigma_{ys}$ and $(a/2c)_i \approx 0.10$	182
28	6AL-4V STA Titanium (RT Direction) Cyclic Flaw Growth Data at 295°K (72°F); $t = 0.31$ cm (0.12 Inch), $\sigma_o = 0.77 \sigma_{ys}$ and $(a/2c)_i \approx 0.34$	183

LIST OF TABLES (Continued)

Table No.	Title	Page
29	6AL-4V STA Titanium (RT Direction) Cyclic Flaw Growth Data at 295°K (72°F); $t = 0.31$ cm (0.12 Inch), $\sigma_o = 0.77 \sigma_{ys}$ and $(a/2c)_i \approx 0.10$	184
30	6AL-4V STA Titanium (RT Direction) Cyclic Flaw Growth Data at 295°K (72°F); $t = 0.16$ cm (0.063 Inch), $\sigma_o = 0.77 \sigma_{ys}$ and $(a/2c)_i \approx 0.40$	185
31	6AL-4V STA Titanium (RT Direction) Cyclic Flaw Growth Data at 295°K (72°F); $t = 0.16$ cm (0.063 Inch), $\sigma_o = 0.77 \sigma_{ys}$ and $(a/2c)_i \approx 0.10$	186
32	6AL-4V STA Titanium (WT Direction) Cyclic Flow Growth Data at 295°K (72°F) in Argon and Salt Water at 10 cpm; $t = 0.31$ cm (0.12 Inch), $\sigma_o = 0.68 \sigma_{ys}$ and $(a/2c)_i \approx 0.37$	187
33	6AL-4V STA Titanium (WT Direction) Cyclic Flow Growth Data at 295°K (72°F) in Argon and Salt Water at 10 cpm; $t = 0.16$ cm (0.063 Inch), $\sigma_o = 0.68 \sigma_{ys}$ and $(a/2c)_i \approx 0.10$	188
34	2219-T87 Aluminum Cyclic Flow Growth Data at 78°K (-320°F) After Cryogenic Proof Test; $t = 1.27$ cm (0.50 Inch), $\sigma_o = 0.67 \sigma_{ys}$ and $(a/2c)_i \approx 0.39$	189
35	2219-T87 Aluminum Cyclic Flow Growth Data at 78°K (-320°F) After Cryogenic Proof Test; $t = 1.27$ cm (0.50 Inch), $\sigma_o = 0.67 \sigma_{ys}$ and $(a/2c)_i \approx 0.28$	190
36	2219-T87 Aluminum Cyclic Flow Growth Data at 78°K (-320°F) After Cryogenic Proof Test; $t = 1.27$ cm (0.50 Inch), $\sigma_o = 0.91 \sigma_{ys}$ and $(a/2c)_i \approx 0.40$ and 0.18	191
37	2219-T87 Aluminum Cyclic Flow Growth Data at 78°K (-320°F) After Cryogenic Proof Test; $t = 0.38$ cm (0.15 Inch), $\sigma_o = 0.67 \sigma_{ys}$ and $(a/2c)_i \approx 0.37$	192
38	2219-T87 Aluminum Cyclic Flow Growth Data at 78°K (-320°F) After Cryogenic Proof Test; $t = 0.38$ cm (0.15 Inch), $\sigma_o = 0.67 \sigma_{ys}$ and $(a/2c)_i \approx 0.11$	193

LIST OF TABLES (Continued)

Table No.	Title	Page
39	2219-T87 Aluminum Cyclic Flaw Growth Data at 78°K (-320°F) After Cryogenic Proof test; $t = 0.38$ cm (0.15 Inch), $\sigma_o = 0.76 \sigma_{ys}$ and $(a/2c)_i \approx 0.37$	194
40	2219-T87 Aluminum Cyclic Flaw Growth Data at 78°K (-320°F) After Cryogenic Proof Test; $t = 0.38$ cm (0.15 Inch), $\sigma_o = 0.91 \sigma_{ys}$ and $(a/2c)_i \approx 0.11$	195
41	6AL-4V STA Titanium (RT Direction) Cyclic Flaw Growth Data at 295°K (72°F) After An Ambient Proof Test; $t = 0.54$ cm (0.21 Inch), $\sigma_o = 0.77 \sigma_{ys}$ and $(a/2c)_i \approx 0.37$	196
42	6AL-4V STA Titanium (RT Direction) Cyclic Flaw Growth Data at 295°K (72°F) After An Ambient Proof Test; $t = 0.54$ cm (0.21 Inch), $\sigma_o = 0.77 \sigma_{ys}$ and $(a/2c)_i = 0.10$	197
43	6A1-4V STA Titanium (RT Direction) Cyclic Flaw Growth Data at 295°K (72°F) After an Ambient Proof Test; $t = 0.16$ cm (0.063 inch), $\sigma_o = 0.77 \sigma_{vs}$ and $(a/2c)_i \approx 0.33$	199
44	6A1-4V STA Titanium (RT Direction) Cyclic Flaw Growth Data at 295°K (72°F) After an Ambient Proof Test; $t = 0.16$ cm (0.063 inch), $\sigma_o = 0.77 \sigma_{vs}$ and $(a/2c)_i \approx 0.09$	200
45	6A1-4V STA Titanium (WT Direction) Cyclic Flaw Growth Data at 295°K (72°F) in Argon at 10 cpm After an Ambient Proof Test; $t = 0.31$ cm (0.12 inch); $\sigma_o = 0.68 \sigma_{ys}$ and $(a/2c)_i \approx 0.38$	201
46	6A1-4V STA Titanium (WT Direction) Cyclic Flaw Growth Data at 295°K (72°F) in Argon at 10 cpm After an Ambient Proof Test; $t = 0.16$ cm (0.063 inch), $\sigma_o = 0.68 \sigma_{ys}$ and $(a/2c)_i = 0.10$	202
47	6A1-4V STA Titanium (WT Direction) Cyclic Flaw Growth Data at 295°K (72°F) in Salt Water at 10 cpm After an Ambient Proof Test; $t = 0.31$ cm (0.12 inch), $\sigma_o = 0.68 \sigma_{ys}$ and $(a/2c)_i \approx 0.38$	203

LIST OF TABLES (Continued)

Table No.	Title	Page
48	6A1-4V STA Titanium (WT Direction) Cyclic Flow Growth Data at 295°K (72°F) in Salt Water at 10 cpm After an Ambient Proof Test; $t = 0.16$ cm (0.063 inch), $\sigma_o = 0.68 \sigma_{ys}$ and $(a/2c)_i \approx 0.10$	204
49	6A1-4V STA Titanium (WT Direction) Cyclic Flow Growth Data at 295°K (72°F) in Salt Water at 0.2 cpm After an Ambient Proof Test; $t = 0.31$ (0.12 inch), $\sigma_o = 0.68 \sigma_{ys}$ and $(a/2c)_i \approx 0.38$	205
50	6A1-4V STA Titanium (WT Direction) Cyclic Flow Growth Data at 295°K (72°F) in Salt Water at 0.2 cpm After an Ambient Proof Test, $t = 0.16$ cm (0.063 inch), $\sigma_o \approx 0.68 \sigma_{ys}$ and $(a/2c)_i \approx 0.10$	206
51	Proof Overload Effects on da/dN for 2219-T87 Aluminum at 78°K (-320°F) (WT Direction)	207
52	Proof Overload Effects on da/dN in Inert Environment for 6A1-4V STA Titanium at 295°K (72°F)	208
53	6A1-4V STA Titanium (WT Direction) Sustained Load Flow Growth Data at 295°K (72°F) in Salt Water, $t = 0.54$ cm (0.21 inch), $\sigma_o = 0.68 \sigma_{ys}$ and $(a/2c)_i \approx 0.37$	209
54	6A1-4V STA Titanium (WT Direction) Sustained Load Flow Growth Data at 295°K (72°F) in Salt Water, $t = 0.31$ cm (0.12 inch), $\sigma_o = 0.68 \sigma_{ys}$ and $(a/2c)_i \approx 0.37$	210
55	6A1-4V STA Titanium (WT Direction) Sustained Load Flow Growth Data at 295°K (72°F) in Salt Water; $t = 0.16$ cm (0.063 inch), $\sigma_o = 0.62 \rightarrow 0.76 \sigma_{ys}$ and $(a/2c)_i \approx 0.09$	211

1.0 INTRODUCTION

The semi-elliptical surface flaw is an excellent model of common failure origins in aerospace structure and so has been the object of considerable study. This type of defect is especially prevalent in failure analysis reports of welded aerospace pressure vessels and to a lesser degree, percentage wise, in aircraft primary structures.

Pressure vessel design methods have been developed (1)* for assuring that crack-like defects will not grow sufficiently to initiate failure during the required operational life. Similar efforts are now underway to develop more effective guidelines for assuring structural integrity of military aircraft⁽²⁾. A large part of the data used in the formulation of the philosophies of the reference 1 monograph resulted from testing and analysis of surface flaws in relatively brittle materials. Flaw and plastic zone sizes usually were relatively small with respect to other specimen or structure dimensions. The most significant structural failures of high performance aircraft, those prompting accelerated Air Force research efforts, also involved surface defects in high strength (brittle) materials.

With the above situations the defect becomes critical before it can grow through the thickness and become detectable. Catastrophic failure can and has occurred. Exact stress intensity solutions for these conditions are not available, however, the solution due to Irwin⁽³⁾ for shallow surface flaws and combined with Kobayashi's original deep flaw magnification values has proven to be quite useful in solving practical engineering problems.

Recognition of the factors causing these past failure problems has resulted in gradual but marked changes in new designs and structures. Improved materials and material processing, and reduced strength and stress levels have combined to result in conditions in which critical flaw sizes approach or exceed the wall thickness of the structure. While this improves structural safety and durability, it complicates the failure mode and life prediction efforts. The previously developed analytical procedures based upon modified

* numbers in parenthesis refer to references at end of report

linear elastic fracture theory become increasingly ineffective as flaw and plastic zone size become large with respect to other dimensions, and one must rely heavily on experimental results.

Initial experimental work devoted strictly to the deep flaw problem was initiated in 1967 and is published in Reference 4. This work involved static and cyclic testing of 2219-T87 aluminum and 5Al-2.5Sn titanium base metal and weldments. Very thick and very thin gages of material were tested to bracket the problem. a/t and $a/2c$ values were systematically varied to cover a complete range of flaw sizes and shapes. The resulting data were analyzed to determine deep flaw magnification factors, M_K , which could be applied to the Irwin stress intensity solution. It was concluded that these values of M_K applied for net failure stresses up to $0.90\sigma_y$ and ligament thicknesses ($t_n = t - a$) greater than $0.20 (K_{IE}/\sigma_y)^2$. Instrumentation was not available during the reference 4 program to detect stable flaw growth preceding fracture, however, it was suspected that such behavior did affect both static and cyclic behavior.

This experimental program had two major objectives. The first objective was to further explore the static and cyclic behavior of combinations of flaw depths, flaw shapes, and thicknesses thru that range where failure mode changed from "catastrophic failure" to "leak-before-failure". Titanium 6Al-4V and aluminum 7075-T651 were added to the 2219, and several intermediate thicknesses were added in order to expand applicability of the results.

The second objective was to evaluate the effects of a prior proof overload cycle on subsequent cyclic or sustained load behavior. 6Al-4V titanium specimens were either sustain loaded or cycled in air or in a 3½% salt solution at room temperature after receiving a simulated proof overload cycle. 2219-T87 specimens were cycled at 78° (-320°F) after receiving a proof cycle.

The following sections of this report describe related background data, materials and experimental approach, and presentation and discussion of results. Applicable data from reference 4 are combined with results of this program in the discussion section.

2.0 BACKGROUND

Relationships between stress intensity, flaw size, and nominal stress field have been derived for a number of crack geometries and loading conditions. Solutions for the semi-elliptical surface flaws have proved to be the most useful in the prediction of pressure vessel performance. To date several approximate solutions are available.

Irwin⁽³⁾ first obtained a solution for a semi-elliptical surface flaw in a plate and estimated that the solution may be valid for flaws with depth to about one-half the material thickness. This derivation was based on Green and Sneddon's solution⁽⁵⁾ of an elliptical crack in an infinite solid and Wigglesworth's solution⁽⁶⁾ of an edgecracked semi-infinite solid. The stress intensity factor at the deepest penetration of a semi-elliptical flaw was then given by:

$$K_{IE} = 1.1\sigma \sqrt{\frac{\pi a}{Q}} \quad (1)$$

where σ is the applied gross stress
 Q is as shown in Figure 1

Equation (1) has proven to be quite useful in practical applications for relatively shallow flaws and at stress levels below the material yield strength. There are no acceptable theoretical solutions for surface flaws fracturing in the presence of largescale yielding. Several theoretical solutions are now available for estimating the magnification factors for deep surface flaws.⁽⁷⁾ The work of Smith, and of Shah and Kobayashi reported in reference (7) are believed to be particularly important contributions to the increased understanding of the problem. Due to the extensive coverage of the surface flaw problem reported in reference (7) a detailed description is not attempted here. It is important to note that these recent solutions generally take the form of equation (1), but modify it to better account for front surface effects, and to account for back surface effects. For example, the 1.1 factor estimated by Irwin to account for the front surface effects is replaced by a variable which ranges from a value of about 1.03 to 1.12, and is a function of flaw shape. Additionally, back surface effects are accounted for by multiplying

equation (1) by a correction factor (M_K or M_2) which varies primarily with flaw shape and flaw depth-to-thickness ratio.

The first systematic experimental study of deep surface flaws⁽⁴⁾ was undertaken in 1967. This work involved static and cyclic testing of aluminum 2219-T87 and titanium 5A1-2.5Sn base metal and weldment. Each material was tested in very thick and in very thin gages in an attempt to bracket the problem; a/t and $a/2c$ values were systematically varied to cover a complete range of flaw sizes and shapes for each of the materials. A summary of testing parameters included in the reference (4) work is shown in Table 1.

The approach used to calculate magnification factors consisted of, first, plotting all data in terms of apparent toughness (K_{IE} per equation 1) versus depth-to-thickness ratio, a/t for each of the thicknesses, test temperatures, and flaw shapes. Earlier data (e.g., reference 8) had shown that at net section stresses above about 90% of yield strength, K_{IE} values are suppressed, and thus data in this range was not included. A baseline toughness was then selected as the apparent K_{IE} as a/t approached 0. The M_K value then was set equal to the baseline toughness divided by the calculated apparent toughness for the particular value of depth and shape tested. Figure 2 shows typical data for 2219-T87 aluminum base metal at a test temperature of 20°K (-423°F). Note that net section stress for all points is less than 90% of yield strength except as noted, and that the curve of apparent toughness is faired above the high stress points.

Resultant M_K curves for 2219-T87 base metal for varying a/t and $a/2c$ values are shown in Figure 3. As a result of the analysis of this data, it was concluded that these curves apply for failure stresses up to $0.90\sigma_{ys}$ and ligament thicknesses ($t_n = t - a$) greater than $0.20 (K_{IE}/\sigma_{ys})^2$. Similar curves for the 5A1-2-1/2Sn material exhibited slightly higher M_K values. With only a few exceptions, the actual data fell within a ± 10 percent scatter band around the curves shown, with the titanium data showing a tendency for greater scatter than that of the aluminum.

The ligament restriction noted above was an estimate, although very few data points were obtained in this area. It was hypothesized that at this point, excessive flaw growth preceded failure. In the extreme case, growth through-the-thickness could occur prior to fracture. Obviously, a surface flaw "model" would not be expected to describe the failure process in this case--the specimen actually contains a through-crack at failure. As a result of analysis of the cyclic test data, it was also concluded that cyclic flaw growth rates increased markedly when the above noted ligament restrictions were exceeded.

NAS 3-10290 provided considerable data which verified a significant increase in flaw tip stress intensity for deep flaws, and identified a range of flaw depth-to-thickness ratios where important deviations from theoretical predictions occur. This range of depths roughly corresponded with the departure from "catastrophic failure" versus "leak before failure" condition. Thus, additional data in this range were considered vital for accurate prediction of failure mode of pressure vessels. The program reported herein was initiated to further explore this area. 6Al-4V-Ti and 7075-T651 were added to the 2219, and several intermediate thicknesses were added in order to expand applicability of the results.

PRECEDING PAGE BLANK NOT FILMED

3.0 MATERIALS AND PROCEDURES

Table 2 shows an overall summary of tests performed. As can be seen, mechanical property and static fracture tests were performed on 7075-T651 aluminum, 6Al-4V STA titanium, and 2219-T87 aluminum. Additionally, simulated proof tests, cyclic flaw growth tests, and cyclic and sustain load tests following a simulated proof overload cycle were performed on the latter two alloys. Other test variables included specimen thickness, flaw shape, and flaw depth-to-thickness ratio. Specimens of all thicknesses were machined from a common gage for each alloy with the specimen neutral axis coincident with the plate neutral axis. The following paragraphs give specific details on test materials and procedures.

3.1 Materials

The 2219 aluminum plate material, 25.4 by 914 by 2134mm (1.0 by 36.0 x 84.0 inches) was purchased in the T87 condition per Boeing BMS 7-105C (equivalent to MIL-A-8920-ASG). The 7075 aluminum plate material, 25.4 by 914 by 2134mm (1.0 by 36.0 by 84.0 inches) was purchased in the T651 condition per QQ-A-250/12D. The 6Al-4V titanium plate material, 9.5 by 609 by 1829mm (0.375 by 24.0 by 72.0 inches) was purchased in the annealed condition per MIL-T-9046F, Type II, Composition C.

Both aluminum alloys were tested in the as received condition without subsequent thermal treatment. The titanium plates were subjected to the following treatment:

- a) solution treat at 1227K (1750F) for 30 minutes
- b) water quench with 6 second maximum delay
- c) age at 769K (925F) for 8 hours.

Chemical composition of the titanium alloy and the specification limits for the aluminum alloys are listed in Table 3. All plates of each alloy were obtained from a common heat.

3.2 Specimen Preparation

Mechanical properties were obtained by testing specimens of the configuration shown in Figure 4. Tests were performed with the specimen axis oriented both parallel and perpendicular to the major plate rolling direction.

All fracture and flaw growth tests were performed using uniaxially loaded surface flaw specimens. The many thickness, flaw depth, and flaw shape variables investigated resulted in requirements for the many different specimen configurations as shown in Figures 5 through 12. To prevent configuration variables from affecting test results dimensions were generally controlled to the following:

specimen length \geq 3 times width
specimen width \geq 5 times flaw length.

These constraints were practical for all but a few of the thickest specimens with the longest flaws. However, as shown in Appendix A, strain gage data indicate that specimen dimensions were adequate even on those excepted cases. The objective of this program was to investigate flaw growth characteristics only up to the point at which the flaw penetrated the thickness (i.e., leakage). Of course, for studies involving growth after this point, greater widths would be required.

All aluminum surface flaws were oriented with the flaw plane parallel to the major plate rolling direction (referred to as WT orientation/propagation direction). All titanium surface flaws to be tested in air were oriented with the flaw plane perpendicular to the major plate rolling direction (RT). The titanium specimens tested in argon and salt water (Reference Section 4.0) were oriented in the WT direction.

All of the test specimens were drilled using drill jigs in which the holes had been located to within a tolerance of $\pm 0.025\text{mm}$ (± 0.001 inch). The specimen grips were also drilled using the same drill jigs to ensure an accurate fit between specimen and loading grip.

All surface flaws were prepared by initially introducing a starter notch by means of an Electric Discharge Machine (EDM) and then extending the starter notch by means of low stress cyclic fatigue. Since the stress level used to initially fatigue the crack specimen is dependent upon the material and size of the EDM starter slot, and a wide variety of flaw sizes were tested, many different stress levels were used during the initial fatigue cracking. All of the aluminum specimens, both 2219-T87 and 7075-T651 alloys, were precracked using a maximum fatigue stress level between 41 and 110 MN/m² (6 and 16 ksi). All of the 6Al-4V STA titanium specimens were precracked using a stress level between 103 and 310 MN/m² (15 and 45 ksi). Care was taken in all cases to ensure that the precracking stress level was small compared to the anticipated test stress level. The low stress fatigue cracking was continued on all specimens until a fatigue crack existed over the entire periphery of the EDM starter slot. A microscope was used to monitor the size of the fatigue crack during the precracking operation.

3.3 Experimental Procedures

The following sections describe the instrumentation and experimental procedures used to accomplish all of the mechanical property, static fracture, cyclic, overload and load-unload testing performed during the subject program.

3.3.1 Instrumentation

All mechanical property tests were conducted using both extensometer and strain gages for determination of yield strength, modulus of elasticity and Poisson's ratio. All of the surfaced flaw specimens were instrumented with an electrical displacement indicator (EDI) clip gage for determination of crack opening displacement (COD). The EDI clip gage was attached to the flaw either by means of tabs micro-spot welded to the specimen or by integrally machined knife edges. Figure 13 illustrates the two different means of attaching the EDI gage. In addition to the EDI clip gage, the majority of the surface flawed specimens were also instrumented with strain gages attached on the rear surface, in order to monitor the strain field behind the flaw. A discussion of the placement of the strain gages and the results obtained is given in Appendix A. Initially, pressure cups were used on selected specimens for determination of flaw break-through. This system consists of placing a pressure cup either directly over

the flaw or directly behind the flaw and then filling one cup with pressurized gas. The pressure in the cup is then monitored throughout the test; a decrease in pressure in one cup is accompanied by an increase in pressure in the other, indicating flaw breakthrough.

3.3.2 Mechanical Property Tests

Mechanical property tests were conducted at RT, 78K (-320F), and 20K (-423F) in air, LN₂ and LH₂, respectively. A strain rate of 0.005 mm/mm/minute was used on all specimens until the material yield stress was obtained. A strain rate of 0.02 mm/mm/minute was then used for the remaining portion of the loading until failure.

3.3.3 Static Fracture Tests

Static fracture tests were conducted using surface flawed specimens, in air at room temperature and in liquid nitrogen (LN₂) at 78K (-320F). All specimens tested at 78K (-320F) were submerged in LN₂ by means of an open top cryostat. The liquid level within the cryostat was visually monitored to ensure that the test section of the specimen had been completely submerged for a minimum of 15 minutes prior to the application of any test load. All specimens were loaded at a rate such that failure would occur between 1 and 3 minutes after the initiation of loading.

All specimens were equipped with an EDI clip gage to monitor crack opening displacement and strain gages to monitor the rear surface strain.

3.3.4 Cyclic Tests

Cyclic tests were conducted, using surface flawed specimens, at both room temperature and 78K (-320F). All of the 6Al-4V STA titanium specimens were tested at room temperature and all of the 2219-T87 aluminum specimens were tested at 78K (-320F). The technique used to ensure thermal stability for the LN₂ tests was identical to that used for the static fracture tests. A cyclic speed of 0.33Hz (20 CPM) was used for all of the testing. In order to define the flaw size at the time back surface dimpling occurred, the cyclic tests were interrupted and low stress fatigue cycles were applied to mark the flaw

periphery. (Refer to Section 4.0 for a discussion of back surface dimpling.) The tests were then continued and finally terminated either at flaw breakthrough or immediately prior to failure. Flaw breakthrough was detected by means of pressure cups using the method described in Section 2.3.1. Continual monitoring of the EDI output allowed the test machine operator to estimate the remaining cycles to failure. When failure appeared to be imminent, the operator stopped the cyclic test and then loaded the specimen to failure. Employment of this method, rather than cycling all the way to failure, results in a more easily distinguishable final flaw size. Since the failure stress of all the tests terminated in this manner were near the prior cyclic stress, it can be concluded that these tests were stopped within a very few cycles of failure.

3.3.5 Overload Tests

Overload tests were conducted at 78°K (-320°F) using 2219-T87 aluminum specimens and at room temperature using 6Al-4V STA titanium specimens. The tests consisted of a proof overload applied at a rate such that maximum load would be obtained in one minute, followed by either sustained loading or cyclic loading.

For the aluminum specimens tested in LN₂, the cyclic loading consisted of a 0.33Hz (20 CPM) sinusoidal profile. Three different cyclic profiles were used for the titanium specimens. The three cyclic profiles used were 0.33Hz (20 CPM) sinusoidal, 0.17Hz (10 CPM) triangular, 0.003Hz (0.2 CPM) trapezoidal. The 0.003 Hz (0.2 CPM) trapezoidal loading profile consisted of a 3 second linear loading, followed by a 294 second hold, and a 3 second linear unloading. By using the trapezoidal loading just described, it was possible to have identical loading and unloading profiles between this and the 0.17hz (10 CPM) triangular profiles.

All of the aluminum overload cyclic specimens were either cycled until the flaw broke through the rear surface or until failure was imminent. The imminence of failure was detected by means of an EDI gage as described in the previous section. Flaw breakthrough was determined by means of a strain gage mounted on the rear surface slightly above the plane of the flaw. The titanium specimens cycled in salt water using the trapezoidal loading profile were cycled to

failure. For all other cyclic tests the tests were terminated either when the flaw broke through the rear surface or failure was imminent. The same techniques as previously described were employed for determination of these two cases. The sustained load tests which were conducted after overload were held at load for approximately 7.0 hours and then marked and failed at room temperature.

4.0 PRESENTATION AND DISCUSSION OF RESULTS

4.1 Mechanical Property Tests

Results of the mechanical properties tests of the alloys are shown in Tables 4 thru 6. Tests on the 2219 aluminum and the 6Al-4V titanium alloys were performed at room temperature in air, 78⁰K (-320⁰F) in liquid nitrogen, and 20⁰K (-423⁰F) in liquid hydrogen. The 7075 aluminum alloy was tested only at room temperature. Ultimate strength, yield strength, elongation, and Poisson's ratio were determined.

Uniaxial yield strengths were calculated using loads corresponding to a 0.2 percent offset on load-strain curves. Longitudinal strains were measured using 50.8mm (2.0 inch) gage length extensometers.

Poisson's ratio measurements were made from continuous strain gage recordings of load (P) versus longitudinal strain (E_L) and transverse strain (E_T). The elastic Poisson's ratio was then computed from the formula

$$\mu = \frac{d_{E_T}}{dP} \div \frac{d_{E_L}}{dP}$$

where μ is the elastic Poisson's ratio;
and

$\frac{d_{E_T}}{dP}$ and $\frac{d_{E_L}}{dP}$ are the average slopes of the elastic portions of the load-versus-transverse-strain and load-versus-longitudinal-strain recordings, respectively.

Measured properties are plotted as a function of test temperature in Figure 14 for the 2219 alloy, and in Figure 15 for the titanium alloy. All properties of the 2219 alloy are quite similar to those of the 2219 alloy tested in the Reference 4 program.

The elongation and Poisson's ratio measurements for the 6Al-4V titanium are significantly lower than that of the titanium tested in Reference 4 (5Al-2.5Sn), and the strength of course, is substantially higher. Average room temperature properties of the 7075 aluminum alloy are as shown below.

GRAIN DIRECTION	ULTIMATE STRENGTH	YIELD STRENGTH	%ELONG	POISSON'S
	MN/m ² (KSI)	MN/m ² (KSI)	IN 50.8mm (2.0 INCH)	RATIO
Longitudinal	609 (88.4)	551 (79.9)	11.1	0.318
Transverse	607 (88.1)	536 (77.8)	11.1	0.332

4.2 Static Fracture Tests

Results of the static fracture tests of surface flaw specimens are shown in:

Tables 7 thru 10	- 2219-T87 Aluminum
Table 11	- 7075-T651 Aluminum
Tables 12 thru 15	- 6Al-4V Titanium

In each of the above noted tables, specimen dimensions, test conditions, and gross section stresses at maximum load are shown in the first several lefthand columns. The next columns, where applicable, note the gross section stress at which back surface dimpling was detected and the point at which the flaw broke thru the back surface. Subsequent columns show initial flaw dimensions as measured after fracture. For reference purposes, the apparent K_{IE} is shown as calculated from Equation (1), using initial flaw sizes and gross stress at maximum load. In subsequent paragraphs, the data of Tables 7 thru 15 are presented and discussed from several viewpoints in an attempt to describe those conditions controlling fracture instability of specimens containing deep surface flaws. The discussion is covered under the headings of (1) Stress-Flaw Depth Relationship, (2) M_K Comparisons, (3) Backside Dimpling, (4) Resistance Curve Considerations, and (5) Static Fracture Summary.

4.2.1 Stress-Flaw Depth Relationship

The raw data of Tables 7 thru 15 are plotted in terms of stress versus flaw depth in Figures 16 thru 19 (2219 aluminum), Figure 20 (7075 aluminum), and

Figures 21 thru 24 (6A1-4V titanium). The data are grouped by nominal flaw shape, with all test points for a given thickness and alloy plotted on a single page. For example, the 2219-T87 aluminum data for 0.38 cm (0.15 in.) thick specimens are shown in Figure 16(a) for a/2c of 0.40; in Figure 16(b) for a/2c of 0.25 and in Figure 16(c) for a/2c of 0.10. Each illustration shows up to three data points for each specimen; the open triangles indicate stress levels at which back surface dimpling was detected* the solid circles indicate stress levels at which the flaws grew through the thickness, and the open circles indicate stress levels at which the specimens fractured. The first step in analysis of this data was to determine effective toughness values which best described the observed failure locii for the various materials, thicknesses, and flaw geometries. Using the solution and magnification curves of Figure 3, K_{IE} values were calculated for each alloy which matched the majority of the data. The resultant nominal values were

<u>ALLOY</u>	<u>MN/m^{3/2}</u>	<u>K_{IE} (KSI√in)</u>
2219-T87 Aluminum	55.0	(50.0)
7075-T651 Aluminum	39.6	(36.0)
6A1-4V STA Titanium	80.2	(73.0)

Plots of these values with a scatter band of $\pm 10\%$ were then superimposed on the raw data plots of Figures 16 thru 24. Test results can now be compared with those predicted using the Figure 3 solution by observation of each of the above noted figures.

2219 T87 Aluminum

It is seen in Figures 16 through 19 that all of the 2219-T87 aluminum specimens which failed before break-thru at section stresses less than ninety percent of the yield strength (19 data points) fall within the predicted toughness band. Above ninety percent of yield strength, the data points fall below the constant K band. It would appear that a straight line band drawn between this point and the point of zero flaw size and ultimate strength would adequately describe the failure locus through this range.

* See Section 4.2.3 for a discussion of back surface dimpling.

Study of the effects of thickness and flaw shape shows that elastic failure can be expected for all shapes tested ($a/2c$ of 0.10, 0.25 and 0.40) in thicknesses of 1.25 cm (0.50 inches) and above. For 0.51 cm (0.20 inch) material elastic failure can occur only in the two longer flaw shapes, and in the thinnest material tested, 0.38 cm (0.15 inch), only the longest flaw shape can cause elastic failure.

Observation of all of the 2219 T87 specimens which "leaked" before failing reveals that such behavior can be expected if the initial ligament is less than about 0.15 cm (0.060 inch). Three of the eleven specimens involved, as seen in Figure 18(c), had initial ligaments more than 0.15 cm (0.060 inch). It is seen that leakage and complete failure in these three specimens occurred almost simultaneously. In a pressure vessel it is doubtful that leakage would have been detected prior to complete rupture.

The specimens tested in Reference 4 were not instrumented to detect flaw breakthrough, however, it was speculated that break through probably did occur in several of the thinner specimens and tougher materials. If this did occur the failures could best be described by consideration of the original surface flaw length ($2c$) and the plane stress toughness. A comparison of this type was shown in Figure 71 of Reference 4 for thin titanium surface flaw specimens. A plot of failure stress versus initial surface length compared quite well with that obtained from through-cracked specimens over a wide range of crack lengths. A similar comparison can be made from the data developed in this program. For example, Figure 18(c) contains the three data points from surface flaws with $a/2c$ values of 0.10 in 1.27 cm (0.50 inch) plate which broke through before failing. K_{CN} values were calculated using initial flaw lengths and failure stresses. The average value was $63.3 \text{ MN/m}^{3/2}$ ($57.6 \text{ ksi}\sqrt{\text{in}}$), which agrees well with the value of $60.6 \text{ MN/m}^{3/2}$ ($55.1 \text{ ksi}\sqrt{\text{in}}$) which was obtained for 1.58 cm (0.625 inch) 2219-T87 plate at 78°K (-320°F) in Reference 4. The single similar data point on Figure 18(b) for $a/2c$ values of 0.25 in the same thickness represents a K_{CN} value of $68.7 \text{ MN/m}^{3/2}$ ($62.5 \text{ ksi}\sqrt{\text{in}}$). From the above, it is concluded that fracture of surface flaw specimens which leak before failing can

be adequately predicted by considering initial surface flaw length and plane stress (or transitional stress) toughness for the thickness in question. Furthermore, the failure stress may be either higher or lower than that which would be predicted using surface flaw solutions, depending on flaw shape and the ratio of K_{IE} and K_{CN} for the thickness under consideration.

7075-T651 Aluminum

Results of the 7075-T651 aluminum are shown in Figures 20(a) thru 20(d) for the four thicknesses tested, all with $a/2c$ values of 0.25.

As can be seen, failures occurred predominantly in the elastic range for all thicknesses tested. Most of the specimens tested in this series displayed a distinct pop-in before failure. This was detected both on the COD traces and the rear surface strain gages as well as by an audible "click". Pop-in occurred usually at a load of approximately 85 to 90 percent of the subsequent failure load. Observation of the fracture faces of these specimens failed to reveal any signs of growth which may have occurred during the pop-in. Therefore, two specimens of the series (A5-2 and A5-4 of Table 11) were unloaded immediately after the discontinuity, and then were fatigue marked and failed. Both fracture faces revealed growth of about 0.50 cm (0.20 inch) predominately at an angle of about 65 to 75° from the depth direction (i.e., propagation closer to the WR direction). Little or no growth took place at 0 or 90° from the depth direction. Overall average calculated K_I of the specimens was about 35 $\text{MN/m}^{3/2}$ (32 $\text{ksi}\sqrt{\text{in}}$) at the pop-in load as calculated at the bottom of the flaw. The stress intensity at an angle of 70° from the bottom should be about 28.6 $\text{MN/m}^{3/2}$ (26.1 $\text{ksi}\sqrt{\text{in}}$). This value compares favorably with a toughness, K_{IC} , of 28.5-30.6 $\text{MN/m}^{3/2}$ (26.0-28.0 $\text{ksi}\sqrt{\text{in}}$) obtained from bend specimens in 7075-T6 plate tested in the WR direction (Ref. 9). The abrupt extension of the cracks at pop-in was evidently arrested by the pinning action at the surface and the higher toughness in the depth direction. After pop-in the COD trace was relatively straight up to the failure load.

Since flaw sizes after the pop-ins were not discernible on the other specimens, the data in Figure 20 and subsequent K calculations are based on initial flaw dimensions and stress at failure.

As noted earlier, a K_{IE} value of $39.6 \text{ MN/m}^{3/2}$ ($36.0 \text{ ksi}\sqrt{\text{in}}$) with a scatter of ten percent was found to best fit the data. By comparing the data of Figures 20(a) thru (d) it is seen that the failure points in the two thinner gages fall somewhat higher than the overall average toughness band and the points for the two thickest gages generally appear to fall in the lower part of the toughness band. (Recall that all specimens were machined from the same thickness). Such a thickness dependency was not noted in the 2219-T87 data. It may be significant that dimpling was not observed in any specimens of the two thicker gages in the 7075 alloy whereas dimpling was observed in varying degree in all thicknesses in the 2219 tests. It is possible that relief of deformation constraint associated with dimpling would result in increased fracture strength of the thinner specimens.

One specimen from each of the two thinnest gages experienced break through prior to failure. In both cases the initial ligament was less than 0.63 cm (0.025 inch). Leakage did not occur in the two thickest gages, however ligament dimensions were larger than 0.63 cm (0.025 inch) in all of these latter tests. For the two specimens that did leak (Ref. Figures 20(a) and 20(b)) K_{CN} values are calculated to be $49.2 \text{ MN/m}^{3/2}$ ($44.8 \text{ ksi}\sqrt{\text{in}}$) and $51.6 \text{ MN/m}^{3/2}$ ($47.0 \text{ ksi}\sqrt{\text{in}}$), respectively. No published K_{CN} data from center cracked specimens of these thicknesses or test directions could be found, however the values noted appear to be somewhat low. The edgewise tunneling known to occur during a pop-in would result in calculated K_{CN} values on the low side.

6Al-4V STA Titanium

Stress-flaw size relationships for the titanium static fracture tests are shown in Figures 21 thru 24. As noted earlier, a K_{IE} value of $80.2 \text{ MN/m}^{3/2}$ ($73.0 \text{ ksi}\sqrt{\text{in}}$) was initially selected which appeared to fit the overall data best. This nominal value with a plus or minus 10 percent band is shown in the figures for comparison with the raw data.

As with the 2219 fracture results, elastic failure before leakage was not observed in the shorter flaws/thinner gage combinations. Elastic failure was observed in all shapes tested ($a/2c$ of 0.10, 0.25 and 0.40) in thicknesses of 0.318 cm (0.125 inch) and greater. In the thinnest gage of 0.15 cm (0.060 inch) elastic failure was produced only with the longest flaw ($a/2c = 0.10$).

There are no systematic variations in failure behavior as affected by varying thickness. Additionally, dimpling was observed in all thicknesses tested. In this respect the titanium behavior is similar to that of the 2219 data.

There does appear to be a distinct effect attributable to flaw shape; specimens with flaw aspect ratio of 0.40 fall below the nominal K_{IE} band; specimens with shape of 0.25 fall near or slightly below nominal; and the longest flaws fall at or slightly above. This is best illustrated by comparison of the 0.53 cm (0.21 inch) data of Figure 23. This is believed to be caused by unusual directionality of fracture resistance of the plates tested and is discussed in more detail in Section 4.2.2.

Study of the titanium specimens which leaked before breaking indicates that if the initial ligament dimension is less than about 0.051 cm (0.020 inch) then such behavior is highly probable. A few specimens with ligaments of up to 0.102 cm (0.040 inch) also leaked before failing. There were a total of nine specimens which leaked and then failed at less than 90 percent of yield strength, and they represented all flaw shapes tested and all but the thickest of the gages tested. As with the aluminum tests, K_{CN} values were calculated for these nine specimens using initial flaw length ($2c$) and failure stress. The average of the calculated K_{CN} values was $101.2 \text{ MN/m}^{3/2}$ ($92.1 \text{ ksi}\sqrt{\text{in}}$) with a standard deviation of $8.1 \text{ MN/m}^{3/2}$ ($7.4 \text{ ksi}\sqrt{\text{in}}$). These values are well within the range of toughness values developed for similarly processed material tested in SST research⁽¹⁰⁾.

4.2.2 Comparison of Magnification Factors

In the preceding discussion, the surface flaw failure loci of specimens of various alloys, thicknesses, flaw shapes and flaw depth-to-thickness ratios were compared with the experimentally determined back surface magnification factor of Reference 4. Since the development of the Reference 4 data, considerable effort has been directed toward the derivation of analytical solutions for the deep surface flaw.⁽¹¹⁻¹⁴⁾ Two of these solutions, that of Shah and Kobayashi⁽¹²⁾ and that of Smith⁽¹¹⁾, are compared with available experimental data in the following paragraphs.

2219-T87 Aluminum

A comparison of the 2219-T87 Aluminum experimental data obtained in this program with available solutions is shown in Figure 25. The data points included in Figure 25 consist only of those specimens which failed prior to leakage at net section stress levels less than 90 percent of yield strength. The curves are plotted in terms of calculated K_{IE} versus flaw depth-to-thickness ratio (a/t).

Figure 25(a) is a plot of data calculated by equation 1 (Reference 3) and is included to graphically display the magnitude of the back surface effect. The family of curves included represent predicted trends of the Figure 3 solution (i.e., the expected reduction in apparent toughness with increasing a/t if magnification is ignored).

Figures 25 (b), (c) and (d) show results using magnification terms of Masters⁽⁴⁾, Shah and Kobayashi⁽¹²⁾, and Smith⁽¹¹⁾. The solutions for the latter two curves are valid for a Poisson's ratio of 0.30. The Smith data points are calculated for matching flaw depth and length for an equivalent ellipse (Smith's solution is based on a part circular crack). Additionally, Smith's analysis is limited to moderate to high aspect ratios, so data is included only for a/2c ratios of 0.25 and 0.40.

Results of these analyses are shown in terms of the average calculated K_{IE} value and the standard deviation (S.D.) for the set of data. For example, the experimentally defined solution from Reference (4) results in an average K_{IE}

of $57.2 \text{ MN/m}^{3/2}$ ($52.1 \text{ ksi}\sqrt{\text{in}}$) with a S.D. of $3.9 \text{ MN/m}^{3/2}$ ($3.6 \text{ ksi}\sqrt{\text{in}}$). (Note that this average value is slightly higher than that which was visually established in the previous section.) Shah's analysis yields an average K_{IE} of $50.8 \text{ MN/m}^{3/2}$ ($46.3 \text{ ksi}\sqrt{\text{in}}$) and a S.D. of $4.0 \text{ MN/m}^{3/2}$ ($3.7 \text{ ksi}\sqrt{\text{in}}$) while Smith's average for the fewer data points is $59.6 \text{ MN/m}^{3/2}$ ($54.2 \text{ ksi}\sqrt{\text{in}}$) with a S.D. of $4.4 \text{ MN/m}^{3/2}$ ($4.0 \text{ ksi}\sqrt{\text{in}}$).

Data from Reference 4 is illustrated in Figures 26, 27 and 28. This data is for 1.58 cm (0.625 inch) 2219-T87 aluminum tested in the RT direction at room temperature 78°K (-320°F) and 20°K (-423°F). Trends of this data are similar to that of Figure 25. That is the average K_{IE} value calculated from Reference 4 is consistently higher than from the Reference 12 solution, and is either comparable or slightly lower than that calculated from the Reference 11 solution. Calculated S.D.'s are comparable except that those from Reference 11 probably would have been higher had the same number of data points been assessed. Again, observation of all data of Figures 25 thru 28 does not reveal any consistent trends of errors in the handling of the various thickness and flaw shape variables tested.

7075-T651 Aluminum

Data for the 7075-T651 aluminum were analyzed in a similar manner and are shown in Figure 29. A comparison of the three deep flaw solutions again shows the K_{IE} average from Reference 4 higher than that of Reference 12 and close to that of Reference 11. Scatter in the latter values is the highest with a trend of over correcting the deeper flaws in evidence.

As noted in Section 4.2.1, there was a discrepancy between the two thinner gage data as compared to that of the two thicker gages. This is also shown in all plots of Figure 29; the four data points for the 0.38 cm (0.15 inch) and the 0.51 cm (0.20 inch) test are consistently and significantly above those of the thicker specimens. As seen in Figure 29(b), the average K_{IE} value for all data is $40.3 \text{ MN/m}^{3/2}$ ($36.7 \text{ ksi}\sqrt{\text{in}}$). The average for the thin specimens is $46.0 \text{ MN/m}^{3/2}$ ($41.9 \text{ ksi}\sqrt{\text{in}}$) and the average for the thick specimens is $38.3 \text{ MN/m}^{3/2}$ ($34.9 \text{ ksi}\sqrt{\text{in}}$).

6Al-4V STA Titanium

It was noted in Section 4.2.1 that there was a significant flaw shape effect apparent in the titanium data. The average K_{IE} value tentatively set at $80.2 \text{ MN/m}^{3/2}$ ($73.0 \text{ ksi}\sqrt{\text{in}}$) was high for the short flaws and somewhat low for the long flaws. A plot of apparent K_{IE} (per Equation (1)) versus a/t was made, but as would be expected, the data were not well ordered. Because of this the data were separated by flaw shape, and plotted individually as in Figures 30, 31 and 32.

Figure 30 shows the specimens of $a/2c = 0.10$ which failed before breaking through at stresses less than 90 percent of yield strength. Figure 30(a) shows an average K_{IE} of $83.5 \text{ MN/m}^{3/2}$ ($76.0 \text{ ksi}\sqrt{\text{in}}$) using the Reference 4 magnification factors. As with the aluminum data the Shah-Kobayashi average K_{IE} is lower. The specimen with the largest a/t lies significantly higher than the average on both plots. The ligament dimension for this specimen was in the region where leakage could be expected, however a recheck of the instrumentation records did not indicate such.

Figure 32 shows the $a/2c = 0.40$ data, and shows a further drop in calculated K_{IE} values.

This behavior of decreasing calculated K_{IE} with increasing $a/2c$ can possibly be explained if the material in question displays significant directionality with respect to crack propagation resistance. If the material is highly directional, it is probable that fracture will initiate at some point on the flaw periphery other than at the bottom. To check this, two single edge notch tension specimens were tested to determine K_{IC} for this material in the RW direction (i.e., 90° from the bottom of the surface flaw tests). The average K_{IC} of these specimens, valid per ASTM requirements, was $48.1 \text{ MN/m}^{3/2}$ ($43.8 \text{ ksi}\sqrt{\text{in}}$), or less than 60 percent of the K_{IE} values calculated for the long surface flaws. It has been observed that crack-line loaded specimens often display lower toughness values than those obtained from surface flaw specimens⁽¹⁵⁾. However, Hall⁽¹⁶⁾ has shown that when the two types of specimens are tested with identical propagation directions, the toughness results

usually compare quite favorably. Hall's conclusions were based on tests of aluminum and titanium at ambient and cryogenic temperatures. Therefore, it is believed that a large part of the difference between the two directions is truly an indication of directionality and not a specimen configuration effect.

To estimate the location on the flaw periphery where fracture initiation is most likely to occur, it is necessary to compare the variation of applied and critical stress intensities around the crack front. This is shown in Figure 33.

Figure 33(a) describes estimated critical and applied stress intensity as a function of location on the front of a flaw of $a/2c = 0.10$. The solid line is an estimate of the critical stress intensity around the flaw front assuming that the critical value varies linearly with α_2 from $K_{IE}(RT)$ at $\alpha_2 = 0$ to $K_{IC}(RW)$ at $\alpha_2 = 90^\circ$. It is recognized that the effective toughness is higher at the surface than shown, however, it will be seen that this is unimportant for the longer flaws. The dashed curve represents Shah's⁽¹²⁾ theoretical variation in applied stress intensity around the flaw. It is further assumed that fracture will initiate in a direction normal to the flaw front, α_1 . The critical curve is set at a K of $72.8 \text{ MN/m}^{3/2}$ ($66.2 \text{ ksi}\sqrt{\text{in}}$) at $\alpha_1 = 0$ (Shah's average value from Figure 30), and $48.1 \text{ MN/m}^{3/2}$ ($43.8 \text{ ksi}\sqrt{\text{in}}$) at $\alpha_2 = 90^\circ$ (from the SENT specimens). It is seen that the critical curve is relatively flat up to α_1 of about 70° . At this point α_2 increases rapidly with an increase in α_1 , and the K critical drops rapidly. The K applied curve, with known variation is then adjusted upward until the two curves meet. This occurs at $\alpha = 0$, and indicates that fracture initiation would occur at the flaw bottom, $\alpha = 0$, and at a stress intensity at this point of $72.8 \text{ MN/m}^{3/2}$ ($66.2 \text{ ksi}\sqrt{\text{in}}$).

Figure 33(b) is constructed in a similar manner for an $a/2c$ of 0.25. Here the curves meet at α_1 of about 30° and at a stress intensity of $68.1 \text{ MN/m}^{3/2}$ ($62 \text{ ksi}\sqrt{\text{in}}$). Extension of the applied curve to $\alpha_1 = 0$ results in a stress

intensity of about $69.2 \text{ MN/m}^{3/2}$ ($63 \text{ ksi}\sqrt{\text{in}}$). This latter value compares well with Shah's average value for this flaw shape in Figure 31.

Figure 33(c) describes conditions for an $a/2c$ of 0.40. The curve ABD represents critical stress intensity without relief of the front face plasticity. It is estimated that this plastic zone depth is approximately 0.13 cm (0.050 inch) using the expression of Rice⁽¹⁷⁾ of $\rho = \frac{1}{\pi} \left(\frac{K}{\sigma_{YS}}\right)^2$, and a nominal K of $66.0 \text{ MN/m}^{3/2}$ ($60 \text{ ksi}\sqrt{\text{in}}$). This zone would extend from α_1 of about 50° to the front surface. Thus the actual fracture resistance would increase through this range. Curve ABC is a rough estimate of the upper limit of K critical. It is now seen that the K applied curve would intersect the K critical curve at point D. Shah's calculated average K_I is $64.8 \text{ MN/m}^{3/2}$ ($59 \text{ ksi}\sqrt{\text{in}}$) in Figure 32. If the applied curve is set at this value at $\alpha_1 = 0$ the curve intersects the resistance curve at point B. Thus, while there are obviously errors in the values of assumed plastic zone size and the actual shape of the resistance curve in this area, it does appear plausible that fracture of short deep flaws would initiate at α_1 between 45 and 55° ($\alpha_2 = 32^\circ$ to 41°). Fracture would initiate at this point at a stress intensity of about $61.5 \text{ MN/m}^{3/2}$ ($56.0 \text{ ksi}\sqrt{\text{in}}$) but the applied stress intensity calculated at the flaw bottom should be as shown in Figure 31(c).

Notwithstanding the above noted flaw shape considerations, the plots of Figures 30 through 32 may be used to compare the various magnification values. As noted, the results are in line with that of the aluminum data. That is, the calculated K_{IE} values from Shah's solution are consistently the lowest, and the other two solutions are comparable. Scatter appears to be similar for all solutions.

4.2.3 Back Surface Dimpling

Recent studies of back surface dimpling have made use of interferometric techniques to study the surface displacements caused by the formation of plastic zones^(18, 19). Such techniques were not feasible on this program because instrumentation used to detect flaw break through made the rear surface inaccessible for direct observation. For this reason, strain gages were affixed to the rear surface to detect plastic zone penetration. Appendix A describes gage locations and includes example data.

For these tests it was assumed that dimpling had occurred when the maximum strain on the back surface was equal to the yield strain of the material defined by the 0.20 percent offset. The gross section stress at which this strain was reached is noted as the dimpling stress for each specimen in Tables 7 thru 15. It is recognized that this definition of dimpling threshold is somewhat arbitrary, however it does represent a procedure which is fairly reproducible in view of the fact that we are considering lateral deformations in the realm of a few hundred microinches.

Figure 34 shows results for the 6Al-4V STA titanium tests. This is a plot of the crack aspect ratio, $a/2c$, versus crack depth ratio, a/t , at the perceived dimple threshold. This plot shows a definite trend for the data to group together for a given applied stress ratio (σ/σ_{ys}) with the perceived dimple threshold for a deeper crack occurring at a lower stress level as expected. The perceived dimple threshold is also relatively insensitive to changes in crack aspect ratio and at an applied stress level of $\sigma/\sigma_{ys} = 0.99$, such effect is virtually nonexistent. Average perceived dimple threshold curves for the five applied stress levels are thus shown in this figure.

Experimentally determined average threshold curves are also compared with threshold curves estimated by the Dugdale model of plastic yielding proposed in Reference 20. Close agreement between the predicted and observed threshold of dimpling is noted in Figure 35 for applied stress level of $\sigma/\sigma_{ys} = 0.79$. Larger differences, as expected, are noted for larger applied stress levels.

Since the Dugdale model used here does not account for strain hardening effects, the predicted threshold of dimpling would tend to occur at shallower cracks for larger applied stresses as shown in Figure 35. Francis et al⁽¹⁹⁾ tested 0.26 cm (0.10 inch) Ti6Al-4V of a lower strength and visually observed dimpling at a stress somewhat lower than predicted by Kobayashi, even at the very low stress levels (e.g., $<0.30 \sigma_{ys}$). This anomaly probably stems from the methods used to measure the dimpling stress.

Figure 36 shows the effect of flaw shape and depth on dimpling stress for the 2219-T87 aluminum data. The trends are similar to that of the titanium. That is, dimpling stress is strongly dependent on a/t , and relatively insensitive to flaw shape. Francis⁽¹⁸⁾ tested 32.0 cm (0.125 inch) 2219-T87 sheet stock and measured dimple depth as a function of $a/2c$, a/t and stress ratio. This allows a rough comparison of data from the two sources. For example, from Figure 36 it can be seen that for flaw shapes of 0.20 and 0.40 dimpling would occur at $\sigma/\sigma_{ys} = 0.70$ for a/t ratios of about 0.70 and 0.80, respectively. From Reference 18, it is estimated that these conditions would result in dimple depths of about 1524 μcm (600 microinches) for both cases, (data obtained from Figure 6 of Reference 18). Reference 18 notes that the dimple depth, when first detected by eye, was typically on the order of 50 μcm (20 microinches). There was no mention of dimple size after unloading.

It has been suggested⁽²¹⁾ that the dimpling behavior of surface flaws potentially forms the basis for surface flaw detection in thin-walled pressure vessels. Certainly considerably more must be known about such behavior to implement such a procedure. However, the following suggests that such a technique may prove to be feasible. Using the curves of Figure 34, K_{IE} is plotted in Figure 37 in a nondimensionalized form against applied stress.

This figure shows that the threshold of perceived dimple can possibly be used to estimate, within an estimated accuracy of 20%, the corresponding "average" stress intensity factor for a given applied stress level and plate thickness. It should be noted that the above estimated accuracy of predicting the average stress intensity factor is speculative at this time. Figure 37, however, does lend some credence to the suggestion that back surface dimpling can be used to estimate the average stress intensity factor of a surface flaw residing on the inside surfaces of thin-walled pressure vessels and which cannot be conveniently observed by direct NDT methods.

4.2.4 Resistance Curve Considerations

In prior paragraphs, it was noted that K_{IE} values were calculated based upon the initial flaw size and the maximum (failure) stress. However, it is

known that some amount of flaw extension precedes instability in most engineering materials. The actual critical stress intensity may differ from that calculated depending upon the amount and nature of the flaw extension occurring during the rising load. Insight into this behavior can be gained by comparing crack extension driving- and resistance-curves. This concept, developed by Irwin, has normally been applied to specimen types other than the surface flaw specimen^(22, 23, 24 and 25).

The resistance, or R curve, is a plot of crack growth resistance K_R as a function of crack extension in the material as the crack is driven under a continuously increasing stress intensity factor, as shown in Figure 38. Thus, R curves characterize the resistance to fracture of (tough) materials during incremental slow crack growth extension. For through cracked specimens R curves are dependent on material thickness and are normally assumed to be independent of specimen initial crack length, a_i , and specimen configuration. R curves can be used to determine the load necessary to cause unstable crack propagation for a specimen containing a given initial crack size, a_i , as shown in Figure 38. A family of crack driving force curves for the specimen are generated for initial crack length, a_i , as shown in the figure and the unique curve which is tangent to the R curve defines the load at which unstable fracture will occur.

This program was not geared to obtain a comprehensive picture of flaw extension characteristics at or near instability, however, some of the findings obtained in overload/cyclic testing may prove useful in describing, at least qualitatively, the instability conditions for a set of 2219-T87 aluminum tests. As discussed later in Section 4.3, overload/cyclic tests were performed to determine the effect of a simulated proof test on subsequent cyclic flaw growth rates. It is important to note here only that the amount of stable growth which occurred on the single overload cycle could be detected on the fracture face of the specimen. The specimens selected are shown in Tables 34 through 36 as called out in Section 4.3. The data are for 1.27 cm (0.50 inch) thick 2217-T87 tested at 78°K (-320°F) and are plotted in Figure 39 in terms of applied stress intensity versus growth increment. The initial flaw shapes are noted by the various symbols, and the initial flaw depth is

noted in parentheses next to the points. While there is considerable scatter in the data, it does appear that the amount of flaw extension can be described by consideration of both the maximum applied stress intensity and the initial flaw size. It is seen that there is a general trend, at a given stress intensity, that the smallest flaws exhibit the greatest extension. This does not appear to be unreasonable when it is recognized that for a fixed stress intensity, the smaller flaws would have to be loaded to a higher stress level.

On the other hand, there is no strong indication of a flaw shape effect. While considerably more data would be required to confidently describe these interactions, the solid curves in Figure 39 were drawn to represent a best estimate of the average subcritical growth behavior.

The above noted curves were then used to construct the crack extension resistance curves shown in Figures 40 and 41. Figure 40 represents specimens with $a/2c$ of 0.40, comparable to those shown earlier in Figure 18a. The two specimens shown represent the shallowest and the deepest flaws of specimens which failed elastically. The two dotted curves represent resistance curves for specimens AS54-4 and -8 which contained initial flaw depths of 0.71 cm (0.28 inch) and 1.09 cm (0.43 inch), respectively. The solid curves represent driving conditions at constant stress. It is seen that the driving and resistance curves become tangent at a stress intensity of 52.7 to 54.9 $\text{MN/m}^{3/2}$ (48 to 50 $\text{ksi}\sqrt{\text{in}}$) after stable flaw extension on the order of about 0.08 cm (0.030 inches).

Figure 41 shows results of similar calculations for 1.27 cm (0.50 inch) thick 2219 specimens containing flaws with $a/2c$ of 0.10. These specimens are representative of those specimens which failed elastically (refer to Figure 18c) and contained initial flaw depths of 0.41 cm (0.16 inch) through 0.84 cm (0.33 inch). Again it is seen that the points of tangency of the driving and resistance curves occur at a relatively constant stress intensity level of about 53.9 $\text{MN/m}^{3/2}$ (49.0 $\text{ksi}\sqrt{\text{in}}$).

The above examples indicate that crack instability may occur at an applied stress level somewhat less than the maximum stress attained during the fracture test, and after some measurable crack extension. However, the K_{IE} value calculated using maximum stress and initial flaw size in the cases studied compares quite well with that obtained by resistance curve considerations. There is not sufficient subcritical crack extension data available to determine over what range of thickness/flaw geometries this correlation would hold.

4.2.5 Static Test Summary

Some of the more important observations from the preceding discussion are summarized in the following paragraphs.

- (1) When plotted on a linear scale in terms of stress versus flaw size, static test results generally fall into one of three different regions as shown in Figure 42. The first region consists of the range of flaw sizes from zero at ultimate strength to a point at which a flaw causes failure at about 90 percent of typical yield strength. Through this range the failure locus roughly follows a straight line. With a further increase in flaw size, the failure locus follows a path which can be described fairly well with the use of back surface magnification factors of References 4, 11 and 12. With a further increase in flaw size, the third region develops in which the flaw grows through the thickness prior to specimen failure. Failure strength in this region can be predicted by consideration of original flaw length and the applicable through-crack toughness of the material, K_{CN} . Departure from region II to region III appears to be a function of the initial ligament dimensions $(t - a_1)$ and relative toughness of the material $\left(\frac{K_{IE}}{\sigma_{ys}}\right)^2$. This is shown in Figure 43 which summarizes behavior of all the static test results. Data is grouped by alloy, flaw shape, and thicknesses tested. The window in each bar defines the point where failure mode changes from "fracture" to "leakage-before-fracture." It appears for each material and flaw shape,

that a ligament of $0.10 (K_{IE}/\sigma_{ys})^2$ falls quite close to the window. Additionally, for a thickness as small as approximately $0.25 (K_{IE}/\sigma_{ys})^2$ failure can result (prior to leakage) at stresses below the yield strength.

- (2) Within these overall general trends several unique characteristics peculiar to each of the alloys tested (or at least peculiar to the relative thickness of the alloys tested) were observed:
 - (a) Back surface dimpling was detected on the majority of the 2219-T87 aluminum specimens which fell into Region II. There were no systematic variations in calculated K_{IE} values as specimen thickness or flaw shape was varied.
 - (b) Back surface dimpling was detected on the majority of the 6Al-4V STA titanium specimens which fell into Region II. There were no systematic variations in calculated K_{IE} values as specimen thickness was varied. Calculated K_{IE} values (i.e., calculated stress intensity at the bottom of the flaw) decreased with increasing $a/2c$ ratios.
 - (c) For the 7075-T651 aluminum tests, back surface dimpling was observed on the two thinner gages, but was not observed on the two thicker gages. Calculated average K_{IE} values for the thinner gages were about 18% higher than those for the thicker gages.

- (3) Based on COD traces and limited evidence from overload/cyclic tests (Reference Section 4.3) it is believed that varying degrees of flaw extension occurred prior to failure of all specimens with the possible exception of some of the thicker 7075 specimens. Based upon a study of crack driving and resistance curves and very limited crack extension data, it appears that the practice of using initial flaw size and maximum stress for K_{IE} calculations may not result in large errors. Certainly additional data are necessary in this area.

From these observations and related data, four major conclusions are offered.

- (1) When the yield zone penetrates the thickness relatively constant K_{IE} values are obtained over a wide range of thicknesses and flaw dimensions. Calculated K_{IE} values for thicker specimens (where the yield zone does not reach the back surface) may be lower than those obtained from the thinner gages. This was observed in the 7075 data. Considerably thicker gages would be required in 2219-T87 aluminum and the 6Al-4V titanium to test this conclusion (i.e., over 5.0 cm (2.0 inch) and 1.2 cm (0.50 inch), respectively).
- (2) For materials which are not highly directional with regard to crack propagation resistance, relatively constant K_{IE} values result over a wide range of flaw shapes. This implies that the surface flaw specimen measures the material toughness in the direction of the flaw minor axis, and that the flaw shape factor, Φ , adequately describes the flaw geometry variable.
- (3) For materials in which the toughness in the edgewise direction (RW) is significantly lower than in the thickness direction (RT) fracture may not initiate in the depth direction for high $a/2c$ geometries. Calculated K_{IE} values, assuming fracture initiates at the bottom of the flaw, would decrease with increasing $a/2c$ ratio. It is estimated that the actual toughness in the RW direction would have to be less than 70 percent of that in the RT direction before this behavior would result.
- (4) As qualified by the above, failure before leakage can be described by available stress intensity solutions for stress levels below about 90 percent of yield up to the point where the initial remaining flaw ligament is less than about $0.10 \left(\frac{K_{IE}}{\sigma_{ys}} \right)^2$. Through this range, use of either of the available magnification

terms (e.g., References 4, 11, 12) would appear to be acceptable as long as consistency is maintained from data generation to application. Beyond this point, leakage prior to fracture will result, and fracture strength is dependent upon crack length and the K_{CN} value of the material and thickness in question.

4.3 Cyclic Tests

The effects of stress level, flaw shape, proof overload cycle, environment and test frequency on the cyclic flaw growth rates of various thicknesses of 2219-T87 aluminum and 6Al-4V STA titanium were investigated and are presented in this section. Stress intensity values were calculated using Equation 1 with a deep flaw magnification factor as defined in Figure 3.

4.3.1 Baseline da/dN Data

Baseline cyclic flaw growth rate data, da/dN, were generated for 2219-T87 aluminum (WT direction) in liquid nitrogen at 78K (-320F), 6Al-4V STA titanium (RT direction) in air at room temperature and 6Al-4V STA titanium (WT direction) in argon at room temperature. These baseline data were developed at a $\sigma_{min}/\sigma_{max}$ (R ratio) of zero.

2219-T87 Aluminum (WT direction)

Three different thicknesses of 2219-T87 aluminum were cyclic tested in liquid nitrogen with a sinusoidal profile at a frequency of 0.33 Hz (20 cpm). The thicknesses involved were 1.27 cm (0.50 inch), 0.51 cm (0.20 inch), and 0.38 cm (0.15 inch). Material thicknesses of 1.27 cm (0.50 inch) and 0.38 cm (0.15 inch) were tested at moderate stress and high stress levels while a material thickness of 0.51 cm (0.20 inch) was tested only at the high stress level. The moderate and high stress levels were set at $0.67 \sigma_{ys}$ and $0.91 \sigma_{ys}$, respectively. The specimen and test details for these tests are presented in Tables 16 through 25.

The baseline da/dN data developed for the 1.27 cm (0.50 inch) thick material are shown in Figures 44 through 47. The crack growth rate data generated at a moderate cyclic stress level for specimens with initial flaw shapes, $(a/2c)_i$, of 0.37 and 0.30, are shown in Figures 44 and 45, respectively while Figures 46 and 47 present the crack growth rate data developed at a high stress level for specimens with initial flaw shapes of 0.41 and 0.11, respectively. The data scatter bands are established on these plots.

It should be pointed out that not all the fatigue crack growth rate data generated at a high cyclic stress level were included in establishing the data scatter bands. The solid symbols presented in Figures 46 and 47 represent growth rates calculated prior to flaw dimpling. At dimpling, the specimen was slightly marked so that the flaw size at that instant was clearly defined. It is believed that a large amount of flaw growth occurred during the first cycle, based on subsequent visual or photographic observation of the specimen fracture face. If growth-on-loading did occur during the first cycle and if this amount of growth was included in the crack growth rate calculations, it would result in faster apparent fatigue crack growth rates than would actually exist. For this reason the solid symbols were not included in defining the data scatter bands.

The baseline da/dN data developed using 0.51 cm (0.20 inch) thick specimens with initial flaw shapes of 0.40 and 0.09 are shown in Figures 48 and 49. These data were generated at a high cyclic stress level ($\sigma_0 = 0.91 \sigma_{ys}$).

The baseline da/dN data developed for the 0.38 cm (0.15 inch) thick materials are shown in Figures 50 through 53. The crack growth rate data generated at a moderate cyclic stress level for specimens with initial flaw shapes of 0.37 and 0.11, are shown in Figures 50 and 51, respectively while Figures 52 and 53 present the cyclic flaw growth rate data developed at a high stress level for specimens with initial flaw shapes of 0.38 and 0.10, respectively.

A summary of all the baseline da/dN data presented in the preceding paragraphs for 2219-T87 aluminum at 78K (-320F) is shown in Figure 54. The majority of data fall within a relatively narrow scatter band considering the range of material thicknesses, stress levels and flaw shapes presented. Only one set of data fell outside the basic scatter band as shown in Figure 54. These data were developed for the thinnest material tested, 0.38 cm (0.15 inch), as well as at the highest stress level and longest initial flaw shape. A previous investigation (Reference 4) demonstrated that thin sections of 2219-T87 aluminum (less than 0.25 cm (0.10 inch) thick) exhibited increasing crack growth rates as the thickness decreased for a constant stress intensity. The increased growth rate observed for the 0.38 cm (0.15 inch) material over the 0.51 cm (0.20 inch) and 1.27 cm (0.50 inch) materials as tested herein could be the start of the increased crack growth rate for thinner materials tested in Reference 4.

A comparison was made between the baseline cyclic crack growth rate data developed in this program for 2219-T87 aluminum and data presented in Reference 25. These data are directly comparable; the tests being conducted at the same temperature, frequency, environment and flaw plane orientation. This comparison is presented in Figure 55 and shows a very good correlation of the two sets of data at both low cyclic stress ($\sigma_o = 0.46 \sigma_{ys}$) and high cyclic stress ($\sigma_o = 0.91 \sigma_{ys}$) levels.

6Al-4V STA Titanium (RT direction)

Three different thicknesses of 6Al-4V STA titanium (RT direction) were cyclic tested in air with a sinusoidal profile at a frequency of 0.33 Hz (20 cpm). Material thicknesses of 0.54 cm (0.21 inch), 0.31 cm (0.12 inch) and 0.16 cm (0.063 inch) were tested at a moderate stress level of $0.77 \sigma_{ys}$. These data were generated for initial flaw shapes of about 0.40 and 0.10. The specimen and test details for these tests are presented in Tables 26 through 31. The baseline da/dN data developed for the three thicknesses of material tested are shown in Figures 56 through 61.

A summary of all the baseline da/dN data developed in this experimental program for 6Al-4V STA titanium (RT direction) at 295K (72F) is included in Figure 62. The data fall within a relatively narrow scatter band considering the range of material thicknesses and flaw shapes tested.

A comparison was made between the baseline cyclic growth rate data developed in this program for 6Al-4V STA titanium (RT direction) and data presented in Reference 25. These data are directly comparable; the tests being conducted at the same temperature, frequency and flaw plane orientation. The environments were different between the two sets of data; being air for the results presented herein and gaseous helium for the Reference 25 data. This difference is not believed to influence the cyclic crack growth rate results. This comparison is presented in Figure 63 and shows a good correlation of the two sets of data.

6Al-4V STA Titanium (WT direction)

Two different thicknesses of 6Al-4V STA titanium (WT direction) were cyclic tested in argon at a frequency of 0.17 Hz (10 cpm). The loading profile for these tests was triangular. Material thicknesses of 0.31 cm (0.12 inch) and 0.16 cm (0.063 inch) were tested at a moderate stress level of $0.68 \sigma_{ys}$. These data were generated for initial flaw shapes of 0.37 and 0.40. The specimen and test details for these tests are presented in Tables 32 and 33. The baseline da/dN data developed are shown in Figures 64 and 65.

A summary of the data developed for the WT direction is shown in Figure 66 and compares the result with the RT direction results. The scatter band for the WT direction result essentially falls within the scatter band for the RT direction.

4.3.2 Proof Overload Effects on Baseline da/dN Data

The effect of a proof overload on the subsequent fatigue crack growth rates was investigated for 2219-T87 aluminum (WT direction) in liquid nitrogen at 78K (-320F), 6Al-4V STA titanium (RT direction) in air at room temperature

and 6Al-4V STA titanium (WT direction) in argon at room temperature. For these tests, the proof overload was conducted in the same environment and at the same temperature as the subsequent cyclic tests.

2219-T87 Aluminum

The effect of a cryogenic proof overload cycle on the fatigue crack growth rates was investigated for 2219-T87 aluminum using material thicknesses of 1.27 cm (0.50 inch) and 0.38 cm (0.15 inch).

The specimens were cryogenically proof stressed from between $0.85 \sigma_{ys}$ to $1.0 \sigma_{ys}$ and then cycled in liquid nitrogen at stress levels used to develop the baseline fatigue crack growth rate data (i.e., $0.67 \sigma_{ys}$ and $0.91 \sigma_{ys}$). These tests were conducted at a frequency of 0.33 Hz (20 cpm).

The specimen and test details for these tests are presented in Table 34 through 40. For comparison purposes, all figures of cyclic flaw growth rate data presented below show the corresponding baseline growth rate data developed at the same cyclic stress level and initial flaw shape.

The da/dN data for 1.27 cm (0.50 inch) thick material tested after receiving a proof overload cycle are shown in Figures 67 through 69. The growth rate data generated at a moderate cyclic stress level ($\sigma_0 = 0.67 \sigma_{ys}$) for specimens with initial flaw shapes of 0.39 and 0.28, are shown in Figures 67 and 68, respectively. These results show that the fatigue crack growth rates are, in general, significantly retarded initially after receiving the proof overload cycle and then tend to converge with the scatter bands of the baseline data as stress intensity increases. Specimens cycled at stress intensity values approaching critical after receiving a proof overload cycle do not show any retardation in crack growth rates. The crack growth rates at low stress intensity values after receiving an overload cycle are, in general, about one-fifth the non-overload rates. Figure 72 presents the crack growth rate data at a high cyclic stress level after receiving a proof overload cycle for specimens with initial flaw shapes of 0.36 and 0.11. For initial flaw shapes of 0.36 there does not appear to be any detectable retardation in the crack growth rates

after receiving the proof overload cycle (based on a single test) whereas a significant retardation in crack growth rate was apparent for the data generated with an initial flaw shape of 0.11.

It was noted in Section 4.3.1 that growth rates for the 0.38 cm (0.15 inch) thick specimens and the lowest flaw shape tended to be higher than those of any of the other thicknesses and shapes tested. As shown in Figure 72, the overload cycle appears to retard growth rates to values within the range of the thicker specimen data. While only limited data were generated in this area, it might be speculated that retardation may be more significant in thinner gages and lower flaw shape ratios.

6Al-4V STA Titanium (RT direction)

The effect of an ambient proof overload cycle on the fatigue crack growth rates was investigated for 6Al-4V STA titanium (RT direction) using material thicknesses of 0.54 cm (0.21 inch) and 0.16 cm (0.063 inch). The specimens were proof stressed to $0.89 \sigma_{ys}$ and then cycled in air at $0.77 \sigma_{ys}$ (the stress level used to develop the baseline fatigue crack growth rate data). These tests were conducted at a frequency of 0.33 Hz (20 cpm). The specimen and test details for these tests are presented in Tables 41 through 44.

The da/dN data for 0.54 cm (0.21 inch) thick material tested after receiving a proof overload cycle are shown in Figures 73 and 74. All figures of crack growth rate data presented show the corresponding baseline growth rate data developed at the same cyclic stress level and initial flaw shape. These data were developed for initial flaw shapes of 0.37 and 0.10. From the data presented in these two figures it appears that the crack growth rates are only very slightly retarded, if at all, after receiving a proof overload cycle. Figures 75 and 76 present the da/dN data for 0.16 cm (0.063 inch) thick specimens with initial flaw shapes of 0.33 and 0.09, respectively. The data shown in Figure 75 (high $a/2c$) demonstrates a significant initial retardation with a slight retardation effect over the remaining stress intensity range tested. The results obtained at the low initial flaw shape (Figure 76) generally falls within the scatter band of the baseline data with a slight retardation initially.

6Al-4V STA Titanium (WT direction)

The effect of an ambient proof overload cycle on the fatigue crack growth rates was investigated for 6Al-4V STA titanium (WT direction) using material thicknesses of 0.31 cm (0.12 inch) and 0.16 cm (0.063 inch). These specimens were proof tested to $0.91 \sigma_{ys}$ and then cycled in argon at $0.68 \sigma_{ys}$ (the stress level used to develop the baseline fatigue crack growth rate data). The tests were conducted at a frequency of 0.17 hz (10 cpm) with a triangular loading profile. The specimen and test details for these tests are presented in Tables 45 and 46.

Figure 77 presents the da/dN data for the 0.31 cm (0.12 inch) thick material tested after receiving a proof overload cycle. All figures of crack growth rate data presented show the corresponding baseline crack growth rate data developed at the same cyclic stress level and initial flaw shape. These data were developed for an initial flaw shape of 0.38. Figure 78 shows the crack growth rate data for the 0.16 cm (0.063 inch) material tested with an initial flaw shape of 0.10. Both figures show a significant retardation of crack growth rate initially and then the rates approach the baseline scatter band values. The thin material results show more retardation than the moderately thick titanium.

4.3.3 Environmental Effects on Baseline da/dN Data

The effect of cyclic testing surface flawed 6Al-4V STA titanium (WT direction) specimens in a solution of 3.5% NaCl was investigated. These tests were conducted at 295K (72F) and at a test frequency of 0.17 Hz (10 cpm). The loading profile for these tests was triangular. Material thicknesses of 0.31 cm (0.12 inch) and 0.16 cm (0.063 inch) were tested at a moderate stress level of $0.68 \sigma_{ys}$. The specimen and test details for these tests are presented in Tables 32 and 33.

Figures 79 and 80 present the da/dN developed for the thicknesses of material tested in environments of argon and salt water and are compared with baseline data of Figures 64 and 65. These data were generated for initial flaw shapes

of 0.37 and 0.10. The data developed in salt-water show almost an order-of-magnitude increase in the crack growth rates at a given stress intensity compared to those developed in argon.

4.3.4 Environmental/Proof Overload Effects on da/dN Data

The effect of a proof overload on the subsequent fatigue crack growth rates was investigated using surface flawed 6Al-4V STA titanium (WT direction) specimens in a 3.5% NaCl solution. These tests were conducted at room temperature at a frequency of 0.17 Hz (10 cpm) with a triangular loading profile. Material thicknesses of 0.31 cm (0.12 inch) and 0.16 cm (0.063 inch) were tested at a moderate stress level of $0.68 \sigma_{ys}$ after receiving an ambient proof test in air. The specimen and test details for these tests are presented in Tables 47 and 48.

Figure 81 presents the da/dN data for the 0.31 cm (0.12 inch) thick material tested after receiving a proof overload cycle. The figures of crack growth rate data presented show the corresponding no-proof growth rate data developed at the same cyclic stress level, initial flaw shape and in the same environment. These data were developed for an initial flaw shape of 0.38. Figure 82 shows the crack growth rate data for the 0.16 cm (0.063 inch) material tested with an initial flaw shape of 0.10. The data shown in Figure 81 show a significant initial retardation for some specimens compared to the no-proof data but then the crack growth rates appear to accelerate (compared to the no-proof data) as the critical stress intensity is approached. In addition, some specimens did not exhibit the initial retardation at all. The data presented in Figure 82 show no retardation. It appears from this data that a proof overload cannot be relied upon as an effective means of reducing subsequent crack growth in an aggressive environment.

4.3.5 Frequency/Proof Overload Effects on da/dN Data

The effect of frequency on proof overloaded fatigue crack growth rates was investigated using surface flawed 6Al-4V STA titanium (WT direction) specimens

tested in a 3.5% NaCl solution. These tests were conducted at room temperature at a frequency of 3.3 mHz (0.2 cpm) with a trapezoidal loading profile. The rise and fall time for this profile was 3 seconds for each. Material thicknesses of 0.31 cm (0.12 inch) and 0.16 cm (0.063 inch) were tested at a moderate stress level of $0.68 \sigma_{ys}$ after receiving an ambient proof test in air at a stress of about $0.91 \sigma_{ys}$. The specimen and test details for these tests are presented in Tables 49 and 50. Figures 83 and 84 present the da/dN data developed for the thicknesses of material tested. The figures of crack growth rate data presented show the corresponding proof overload crack growth rate data developed at a frequency of 0.17 Hz (10 cpm), and at the same stress level, initial flaw shape and environment. These crack growth rate data were generated for initial flaw shapes of 0.38 and 0.10. From these figures there does not appear to be any effect of decreasing the test frequency from 160 mHz (10 cpm) to 3.3 mHz (0.2 cpm).

4.3.6 Cyclic Test Summary

A summary of the cyclic results are presented in this paragraph.

- (1) Baseline surface flaw da/dN data (that developed with no proof overloads in inert environments) for a variety of stress levels, flaw shapes and material thicknesses can be adequately described as a function of stress intensity for the materials tested herein. Such plots are shown in Figure 85 for 2219-T87 aluminum and 6Al-4V STA titanium and the ranges of applicability are described on this figure.
- (2) The effect of a prior proof overload cycle on surface flaw fatigue crack growth rates was investigated for a variety of materials, cyclic stress levels, flaw shapes and material thicknesses. A summary of the retardation effects observed are presented in Tables 51 and 52 for 2219-T87 aluminum and 6Al-4V STA titanium. In general, retardation can be expected initially after a proof test if the cyclic stress is considerably below the proof stress;

say approximately $0.75 \sigma_p$. As the cyclic stress level approaches the proof stress level the retardation becomes negligible. Generally, the thinner the material, the larger the amount of retardation due to a proof overload cycle.

Retardation of subsequent da/dN rates due to a proof overload is a phenomenon that generally occurs but cannot be relied upon in every instance. Some identical test specimens exhibited no apparent retardation while others showed significant retardation.

- (3) The fatigue crack growth rates developed for 6Al-4V STA titanium exposed to a 3.5% NaCl solution were almost an order of magnitude greater than those rates developed in an inert argon environment.
- (4) The fatigue crack growth rates developed for 6Al-4V STA titanium exposed to a 3.5% NaCl solution after being subjected to a proof overload cycle showed retardation effects ranging from significant to nonexistent. In general, this retardation cannot be relied upon to occur.
- (5) The fatigue crack growth rates for 6Al-4V STA titanium exposed to a 3.5% NaCl solution after being subjected to a proof overload cycle were not affected by cyclic frequency between 3.3 mHz (0.2 cpm) to 160 mHz (10 cpm).

4.4 Sustained Load Results

The influence of a proof overload cycle on the subsequent sustained load flaw growth characteristics was investigated using 6Al-4V STA titanium (WT direction) exposed to a 3.5% NaCl solution. Three different thicknesses of material were tested; 0.54 cm (0.21 inch), 0.31 cm (0.12 inch) and 0.16 cm (0.063 inch). The specimens were, in general, sustain loaded at $0.68 \sigma_{ys}$. Those specimens receiving a proof test were proofed to $0.91 \sigma_{ys}$ in air. The specimen and test details for these tests are presented in Tables 53 through 55.

The results for all three thicknesses of material tested are presented in Figure 86. The data developed using the 0.54 cm (0.21 inch) thick material shows that the threshold stress intensity, K_{TH} , is considerably less than $45.5 \text{ MN/m}^{3/2}$ ($41.3 \text{ ksi}\sqrt{\text{in}}$) for specimens that were not proof tested. All tests conducted with this thickness of material used specimens with initial flaw shapes of 0.37. These specimens all failed within one minute after being sustain loaded. Applying a proof test prior to sustain loading specimens resulted in a significant elevation of the threshold; $45.5 \text{ MN/m}^{3/2}$ ($41.3 \text{ ksi}\sqrt{\text{in}}$) $< K_{TH} < 53.0 \text{ MN/m}^{3/2}$ ($48.2 \text{ ksi}\sqrt{\text{in}}$). In addition to the tests discussed above, two specimens were proof tested, then slightly marked (by low cycle fatigue for less than 0.010 cm (0.004 inch) and then sustain loaded. These tests demonstrated that a small amount of flaw growth caused by cyclic operation could negate any beneficial effect a proof test might have.

The data developed for the 0.31 cm (0.12 inch) thick material showed very similar results as those developed for the 0.54 cm (0.21 inch) material. The non-proof tested specimens indicated a threshold less than $39.2 \text{ MN/m}^{3/2}$ ($35.6 \text{ ksi}\sqrt{\text{in}}$) whereas the proof tested specimens did not show any flaw growth at a stress intensity level of $47.2 \text{ MN/m}^{3/2}$ ($42.9 \text{ ksi}\sqrt{\text{in}}$) when loaded for 8 hours.

The results obtained for the 0.16 cm (0.063 inch) material differed greatly from the thicker material results presented previously. Besides the difference in thickness one other difference should be pointed out between the tests, and that is, that the tests conducted with the 0.16 cm (0.063 inch) thick specimens had initial flaw shapes of 0.09 whereas the tests using thicker gages were conducted with specimens having initial flaw shapes of 0.37. As Figure 86 illustrates, the non-proof loaded/threshold is $47.3 \text{ MN/m}^{3/2}$ ($43.0 \text{ ksi}\sqrt{\text{in}}$). A single specimen was proof tested and then sustain loaded. This specimen failed in the same amount of time as the non-proof specimens loaded to the same stress intensity level thereby indicating no beneficial effect of a proof test on K_{TH} . The non-proof loaded/threshold appears higher for these

tests than those conducted for the tests utilizing thicker material. Again, it must be emphasized that flaw shape differences existed as well as material thicknesses and for this reason it cannot be ascertained whether or not a thickness or flaw shape effect was observed.

From the results presented in Paragraph 4.4 it appears that a proof test is beneficial (elevates K_{TH}) for 6Al-4V STA titanium in thicknesses ranging from 0.31 cm (0.12 inch) to 0.54 cm (0.21 inch) containing flaws with shapes of about 0.40 when sustain loaded in a salt-water environment. Such is not the case for a material thickness of 0.16 cm (0.063 inch) with flaw shapes of about 0.10; the threshold remains unchanged. It also appears from the tests conducted that the beneficial effects of proof overload cycle could be negated by a small amount of flaw growth caused by cyclic operation prior to being sustain loaded.

PRECEDING PAGE BLANK NOT FILMED

5.0 CONCLUSIONS

Major observations and conclusions were listed in detail in Sections 4.2.5 (static tests), 4.3.6 (cyclic tests), and 4.4 (sustained load tests) and are summarized below.

Static Fracture Tests

- (1) Any of the three available deep flaw solutions (4,11,12) can be used to describe failing stress flaw size locii for a wide range of thicknesses, flaw shapes and alloys under the following conditions:
- a) for maximum failing stresses of $0.90 \sigma_{ys}$
 - b) for minimum thickness of about $0.25 \left(\frac{K_{IE}}{\sigma_{ys}} \right)^2$.
 - c) for ligament size greater than about $0.10 \left(\frac{K_{IE}}{\sigma_{ys}} \right)^2$.
 - d) for materials in which the fracture resistance in the edgewise (2c) direction is greater than about 70 percent of that in the depth (a) direction.

Under these conditions K_{IE} values will vary, depending upon which of the three solutions are used and thus the solutions should not be mixed in analyzing and applying the fracture data.

- (2) The thickness of the majority of the specimens tested in this program ranged from $0.25 \left(\frac{K_{IE}}{\sigma_{ys}} \right)^2$ to about $1.50 \left(\frac{K_{IE}}{\sigma_{ys}} \right)^2$. The plastic zone penetrated the back surface on most of these specimens. Thru this range, calculated K_{IE} values did not vary with thickness. Two sets of data were obtained on thicknesses of about $2.5 \left(\frac{K_{IE}}{\sigma_{ys}} \right)^2$ and higher. In these cases back surface dimpling was not observed, and calculated K_{IE} values were somewhat lower than for the thinner gages.

Cyclic Tests

- (1) Baseline cyclic deep flaw growth rate data can be adequately described as a function of applied K_{IE} levels (using deep flaw magnification factors) within the same limits set for static testing noted above.
- (2) Growth rates are usually retarded after a proof overload for operating stresses less than about $0.75 \sigma_p$. The degree of retardation generally increases with decreasing thickness, however, the amount varied widely between presumably identical test conditions.

Sustained Load Tests

- (1) A proof overload cycle will elevate the sustained load threshold (K_{TN}) in thick gage 6Al-4V titanium exposed to a salt water environment. However, this beneficial effect can be negated by a small amount of cyclic loading prior to the application of the sustained load.

APPENDIX A - STRAIN MEASUREMENTS

A considerable amount of rear surface strain data was developed during the course of this program and some of this data is presented in this appendix. Figures A-1 through A-4 show how the rear surface strain varies as a function of distance from the flaw plane, stress level and flaw depth for various thicknesses of 7075-T651 and 2219-T87 aluminum. These figures demonstrate that the maximum strain can be expected at about 45° from the plane of the surface flaw. These figures also show that the rear surface directly behind the flaw goes into compression depending upon the applied stress level and flaw depth-to-thickness ratio. Typical strain results for the two materials are shown in Figures A-5 and A-6 as a function of flaw depth-to-thickness ratio for a constant thickness, flaw shape and stress level. These figures illustrate that significant localized bending exists directly behind the flaw and that this phenomena occurs up to the point where the plastic zone engulfs the remaining ligament, at which point the remaining ligament is fully enveloped in a high tension stress field.

The question of adequate specimen width relative to the surface crack length was also addressed during the course of this program. The results of these tests are presented in Figure A-7 for 2219-T87 aluminum. These test results show that the strains on the back surface reach the nominal P/A value at a distance of about 2 - 2.5 times the crack length. The disturbed strain field behind the flaw appears from these tests to be fairly localized in nature and, therefore, specimen width-to-flaw length ratios greater than 5 appear more than adequate.

PRECEDING PAGE BLANK NOT FILMED

APPENDIX B - CALCULATION OF CRACK GROWTH RATES FROM
SURFACE FLAW OPENING MEASUREMENTS

The specimens in this program that were cyclic tested were instrumented with a crack opening displacement (COD) measurement device as shown in Figure B1 so that the crack depth as a function of the applied cycles could be determined and consequently the crack growth rates calculated. The COD at the diametral center of a completely embedded elliptical flaw under normal stress was first related to the flaw size by Green and Sneddon (Reference 5) and is expressed by the equation

$$\text{COD} = \delta = \frac{4(1 - \mu^2)}{E} \frac{\sigma a}{\phi} \quad (\text{B-1})$$

Although a rigorous solution is not available for flaw opening displacements for a semi-elliptical surface flaw, such displacements would also be proportional to σ and a/ϕ for elastic materials. By following Irwin's procedure (Reference 3) to account for the effect of plastic yielding, the flaw opening displacement for a surface flaw can be approximated by

$$\text{COD} = \delta = C \frac{\sigma a}{\sqrt{Q}} \quad (\text{B-2})$$

where C is a constant, dependent upon material properties.

Tests conducted in this program have shown that C tends to increase with increasing crack size, rather than remain constant. Figures B-2 through B-5 show the variation of C with flaw depth-to-thickness ratio for various flaw shapes. These data were generated from static fracture tests of 2219-T87 and 7075-T651 aluminum using the general equation:

$$d\delta = \sigma \left(\frac{a}{\sqrt{Q}} \right) dC + C \sigma d \left(\frac{a}{\sqrt{Q}} \right) + C \left(\frac{a}{\sqrt{Q}} \right) d\sigma \quad (\text{B-3})$$

The data presented in the figures were generated using a COD and corresponding stress level taken from the linear portion of the load/COD curve and the initial

stress level taken from the linear portion of the load/COD curve and the initial flaw dimension. It is assumed that the flaw size and the value of C remains constant during the linear portion of the load/COD curve, in which case equation (B-3) reduces to

$$d\delta = C \left(\frac{a}{\sqrt{Q}} \right) d\sigma \quad (B-4)$$

From the figures, it can be seen that the value of C does not vary for short flaws, $(a/2c) = 0.40$, but varies significantly with a/t for long flaws, $(a/2c) = 0.10$. In general, long flaws grow in depth significantly more than in the length direction during a cyclic test and therefore the flaw shape increases rapidly. Thus, the variation of C during a cyclic test of a specimen containing a long flaw would never be as severe as presented in Figure B-4. For short flaws or tests where the flaw growth is small, using a constant value of C appears acceptable but to adequately define the flaw size as a function of the COD for long flaws requires that the variation of C with flaw depth-to-thickness be accounted for. Analyses were conducted in which the variation in C between the initial and final flaw size values was assumed to be either linear or a fourth order polynomial and these results have shown that computed crack growth rates are very insensitive to the manner in which C varies. Therefore, the crack growth rate calculations in this report were based on an assumed linear variation in C between the known initial and final flaw size values as calculated below:

$$C_i = \frac{\delta_i}{\sigma} \left(\frac{\sqrt{Q}}{a} \right)_i$$

$$C_f = \frac{\delta_f}{\sigma} \left(\frac{\sqrt{Q}}{a} \right)_f \quad (B-5)$$

where the subscripts i and f refer to initial and final conditions, respectively.

In order to relate the flaw parameter (a/\sqrt{b}) to COD for values of (a/\sqrt{b}) between the initial and final values an assumption must be made as to the manner in which the flaw shape changes from test initiation to termination. It was assumed that

$$\frac{a - a_i}{a_f - a_i} = \frac{2c - (2c)_i}{(2c)_f - (2c)_i} \quad (B-6)$$

i.e., both flaw depth and width growth simultaneously reach the same percentage of their respective total growth from initial to final values. The flaw shape parameter (θ) can now be determined as a function of flaw depth and, in turn, can be related to crack depth using Equation (B-2). The number of cycles (N) corresponding to each selected flaw depth value can be determined from the test record and, consequently, the change in N for each increment of flaw depth is known. With knowledge of the flaw size, the stress intensity can be determined for any point during the cyclic test. For specimens that were proof tested prior to being cycled, the growth-on-loading due to the proof test was not included in the calculation of fatigue flaw growth rates. The fracture face of these specimens clearly indicated the amount of growth-on-loading that had taken place during the proof test. For the specimens that were not proof tested, the fatigue crack growth rates were calculated as outlined above based on the initial and final flaw dimensions. For detailed fatigue growth rate calculations using the above procedure refer to Reference 25. All stress intensity calculations incorporate the use of the deep flaw magnification factors from Reference 4.

PRECEDING PAGE BLANK NOT FILMED

REFERENCES

1. C. F. Tiffany, "Fracture Control of Metallic Pressure Vessels", NASA SP 8040, 1970.
2. Current Efforts at Updating MIL-STD-1530 (USAF), Sent. 1972.
3. G. R. Irwin, "Crack Extension Force for a Part-Through Crack in a Plate," Journal of Applied Mechanics, Vol. 29, Trans, ASME, Vol. 84, Series E, December 1962.
4. J. N. Masters, W. P. Haese and R. W. Finger, "Investigation of Deep Flaws in Thin Walled Tanks," NASA CR-72606, December 1969.
5. A. E. Green and I. N. Sneddon, "The Distribution of Stress in the Neighborhood of a Flat Elliptical Crack in an Elastic Solid," Proc. Cambridge Phil. Soc., 46, 1959 (1950).
6. L. A. Wigglesworth, "Stress Distribution in a Notched Plate," Mathematica, Vol. 4, 1947.
7. "The Surface Crack: Physical Problems and Computational Solutions," edited by J. L. Swedlow, ASME, November 1972.
8. A. E. Smith, "Missile Motor Cases," Metals Engineering Quarterly, Vol. 3 No. 4, Nov. 1963.
9. Damage Tolerant Design Handbook, MCIC-HB-01, December 1972.
10. "Commercial Supersonic Transport Program" Phase 11-C Report - Contract FA-SS-77-5, prepared for Federal Aviation Agency, March 1966.
11. F. W. Smith, "Stress Intensity Factors for a Surface Flawed Fracture Specimen," Tech. Report No. 1, NASA Grant NGR-06-007-063, Colorado State University, 1971.
12. R. C. Shah and A. S. Kobayashi, "On the Surface Flaw Problem," The Surface Crack: Physical Problems and Computational Solutions, edited by J. L. Swedlow, ASME, November 1972.
13. J. R. Rice and N. Levy, "The Part-Through Surface Crack in an Elastic Plate," Journal of Applied Mechanics, Vol. 39, Trans. of ASME, Vol. 94, March 1972.
14. H. Miyamoto and T. Miyoski, "Analysis of Stress Intensity Factor for Surface-Flawed Tension Plate," High Speed Computing of Elastic Structure, Proc. of Symposium of UITAM, Univ. de Liege, 1971.
15. J. N. Masters and J. L. White, "Development of Fracture Toughness Properties of D6-AC Steel of F-111 Applications," AFML-TR-70-310, January 1971.

REFERENCES (Cont'd)

16. L. R. Hall and R. W. Finger, "Investigation of Flaw Geometry and Loading Effects on Plane Strain Fractures in Metallic Materials," NASA CR-726959, Dec. 1971.
17. J. R. Pice, "Mechanics of Crack Tip Deformation and Extension by Fatigue," Fatigue Crack Propagation, ASTM STP 415, Am. Soc. Testing Mats., 1967.
18. P. H. Francis and D. L. Davidson, "Experimental Characterization of Yield Induced by Surface Flaws," The Surface Crack: Physical Problems and Computational Solutions, edited by J. L. Swedlow, ASME, November 1972.
19. P. H. Francis, D. L. Davidson and R. G. Forman, "An Experimental Investigation into the Mechanics of Deep Semielliptical Surface Cracks in Mode I Loading," Engineering Fracture Mechanics, (to be published).
20. A. S. Kobayashi and W. L. Moss, "Stress Intensity Magnification Factors to Surface-Flawed Tension Plate and Notched Round Tension Bar," Fracture Proc. 2nd International Conference on Fracture (Brighton), Chapman and Krell, London, 1969.
21. P. H. Francis, "Elasto-Plastic-Analysis of Mode I Edge Crack with Application to a Surface Notch," International Journal of Fracture Mechanics, Vol. 7, No. 4, Dec. 1971.
22. G. R. Irwin, "Fracture Testing of High-Strength Sheet Materials Under Conditions Appropriate for Stress Analysis," Report 5486, U.S. Navy Research Lab., July 27, 1960.
23. J. M. Krafft, A. M. Sullivan, and R. W. Boyle, "Effect of Dimensions on Test Fracture Instability of Matched Sheets," Proc. Crack Propagation Symposium, College of Aeronautics, Cranfield (Englan), Sept. 1961, Vol. I.
24. J. E. Srawley and W. F. Brown, "Fracture Toughness Testing Methods," Fracture Toughness Testing and Its Application, ASTM Special Technical Publication No. 381, April 1965.
25. L. R. Hall and W. D. Bixler, "Subcritical Crack Growth of Selected Aerospace Pressure Vessel Materials," NASA CR-120834, December 1972.

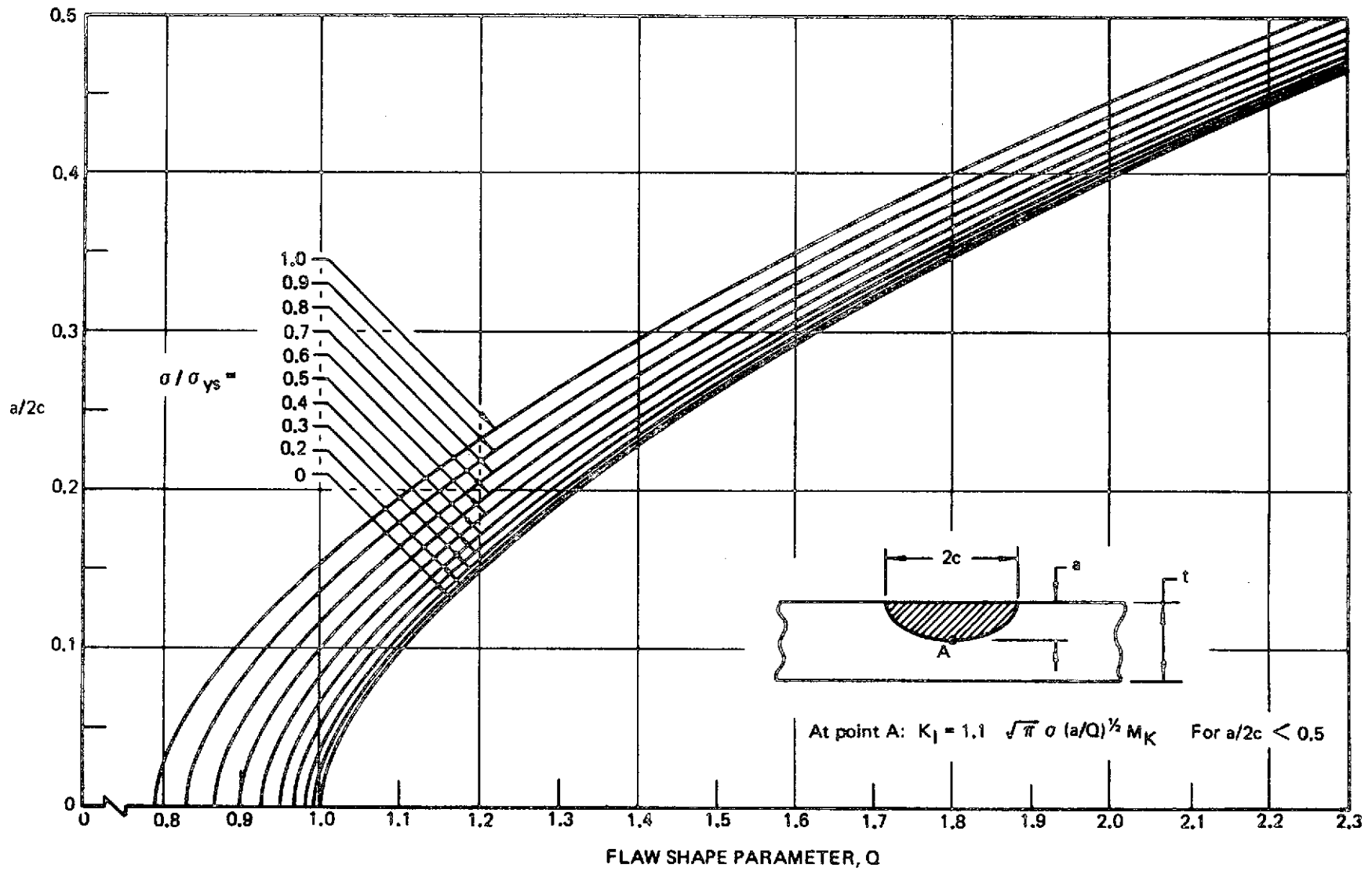


Figure 1: Shape Parameter Curves for Surface Flaws

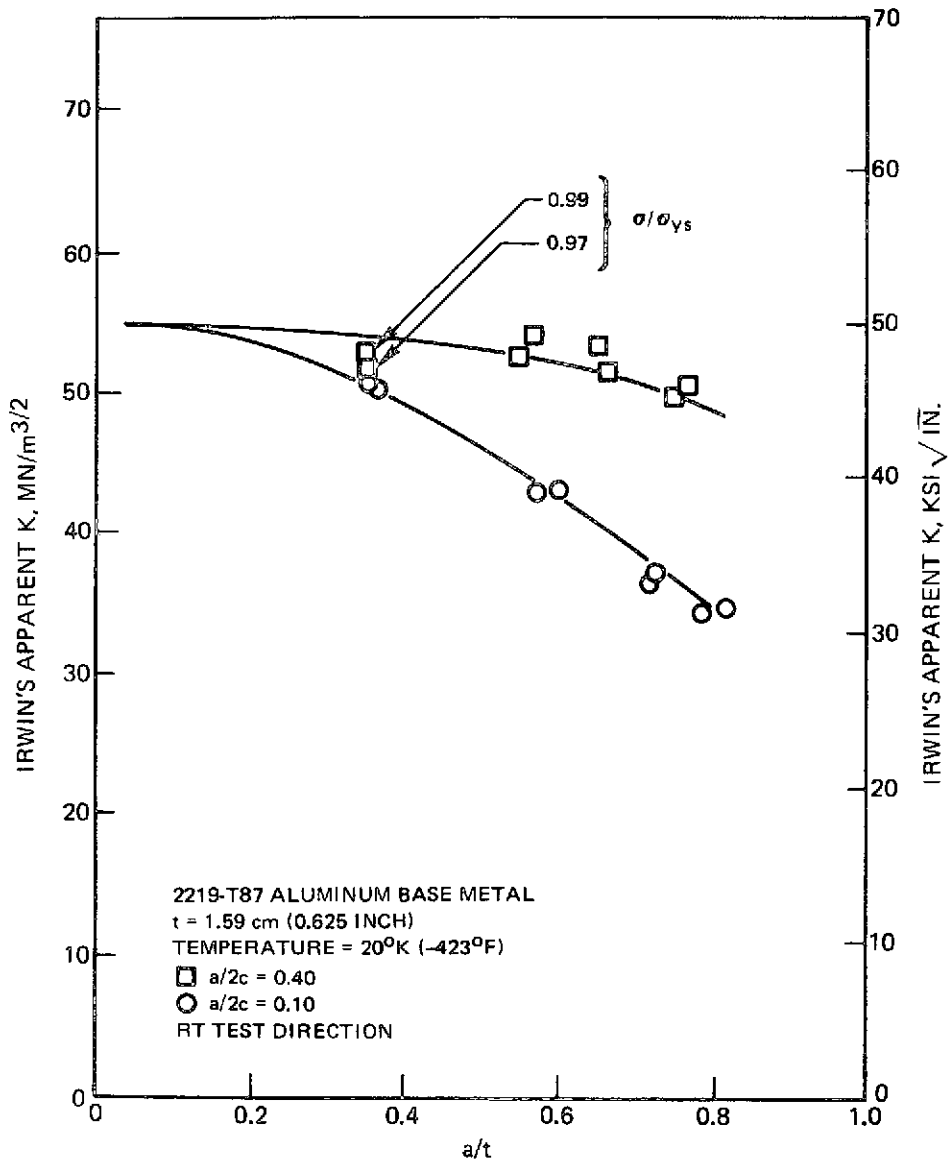


Figure 2: Effect of Flaw Depth on Apparent K Values

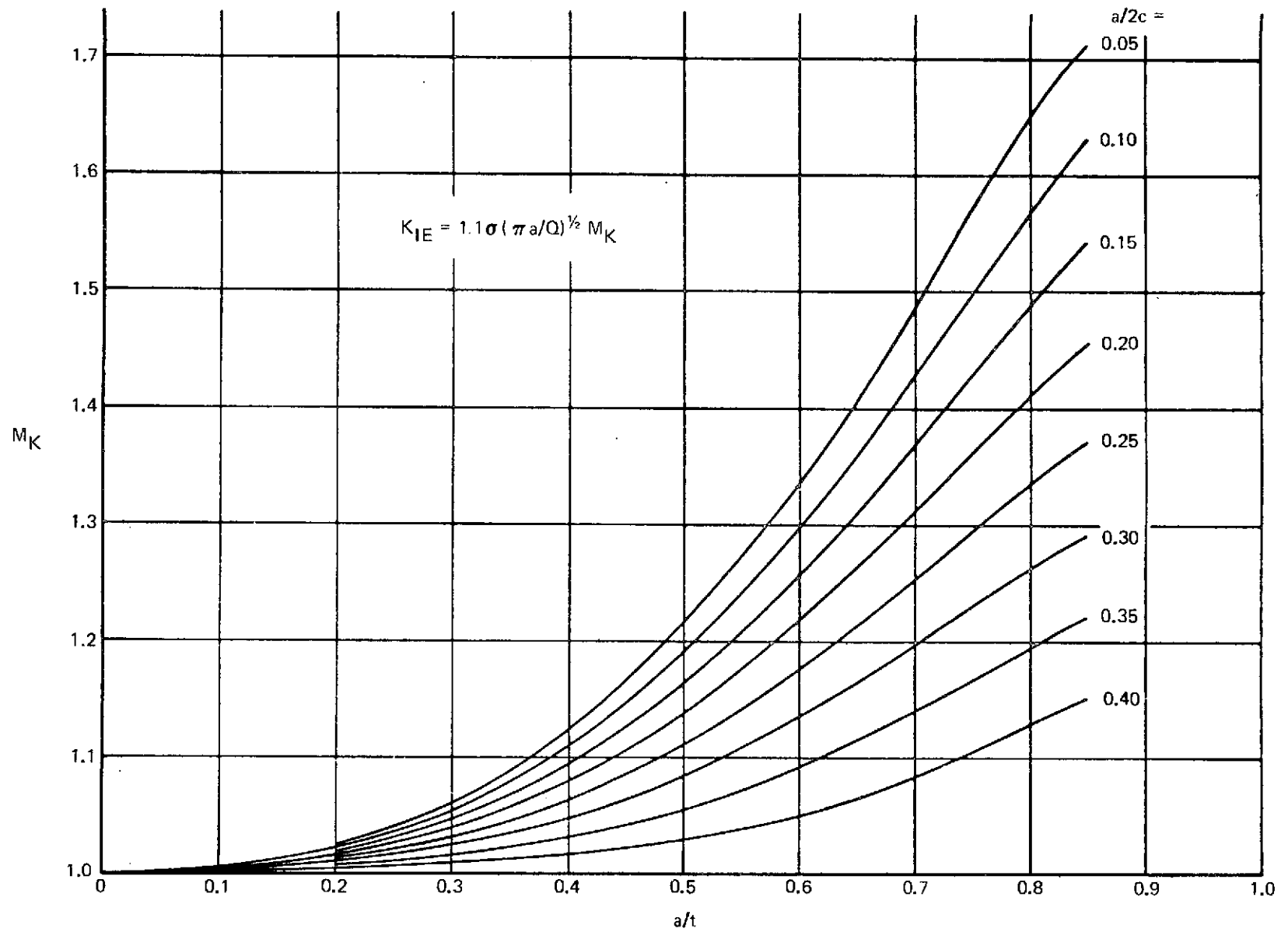
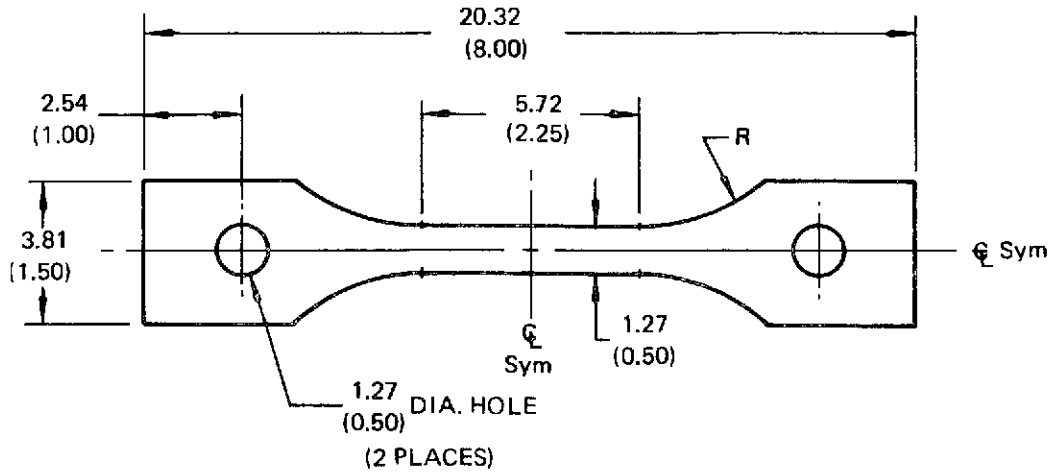
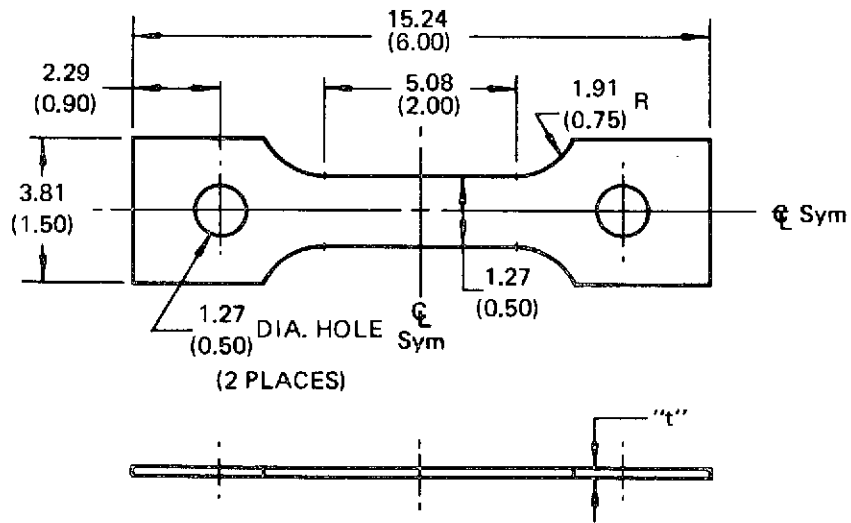


Figure 3: Deep Flaw Magnification Curves (Reference 4)



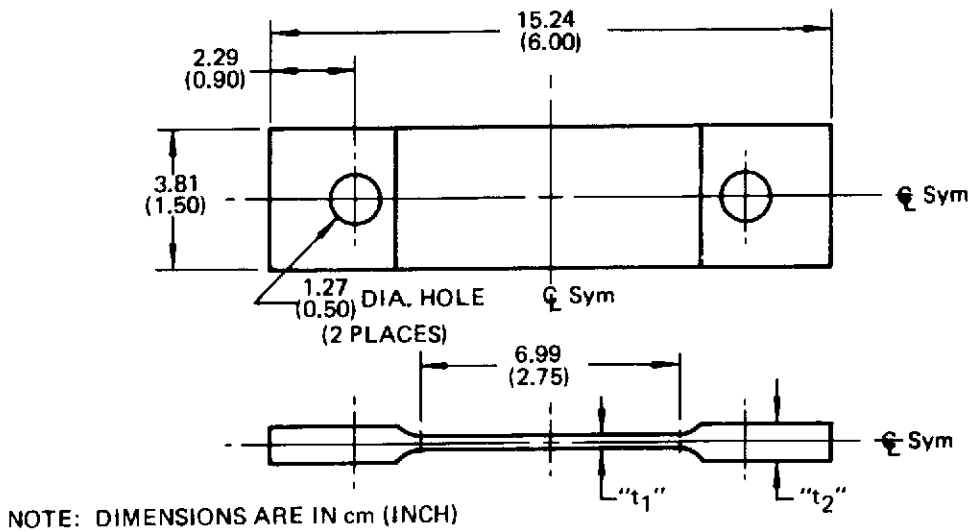
NOTE: DIMENSIONS ARE IN cm (INCH)

Figure 4: Tensile Specimen



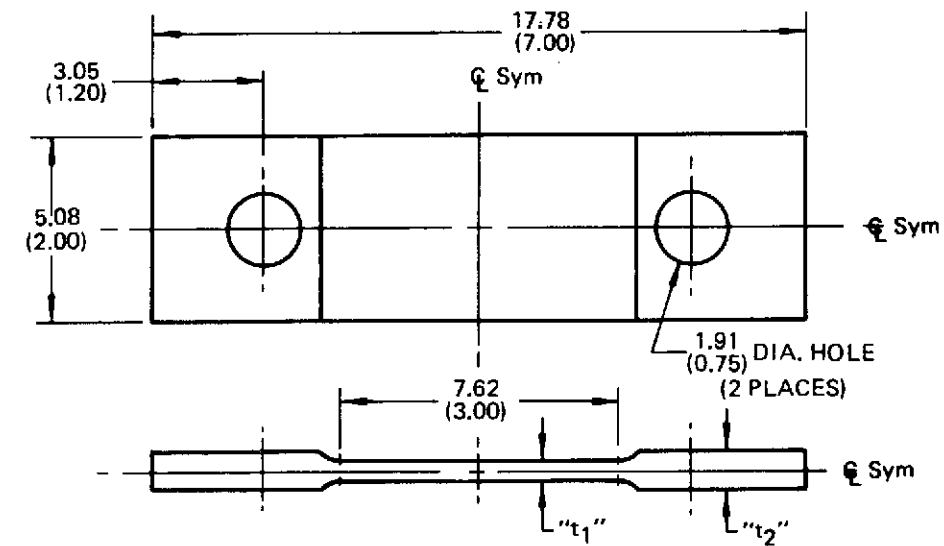
NOTE: DIMENSIONS ARE IN cm (INCH)

Figure 5: 6Al-4V Titanium Surface Flaw Specimen



SPECIMEN CONFIGURATION	"t ₁ "	"t ₂ "
T-4	0.076 (0.030)	0.20 (0.08)
T-5	0.152 (0.060)	0.38 (0.15)
T-6	0.305 (0.120)	0.76 (0.30)

Figure 6: 6Al-4V Titanium Surface Flaw Specimen

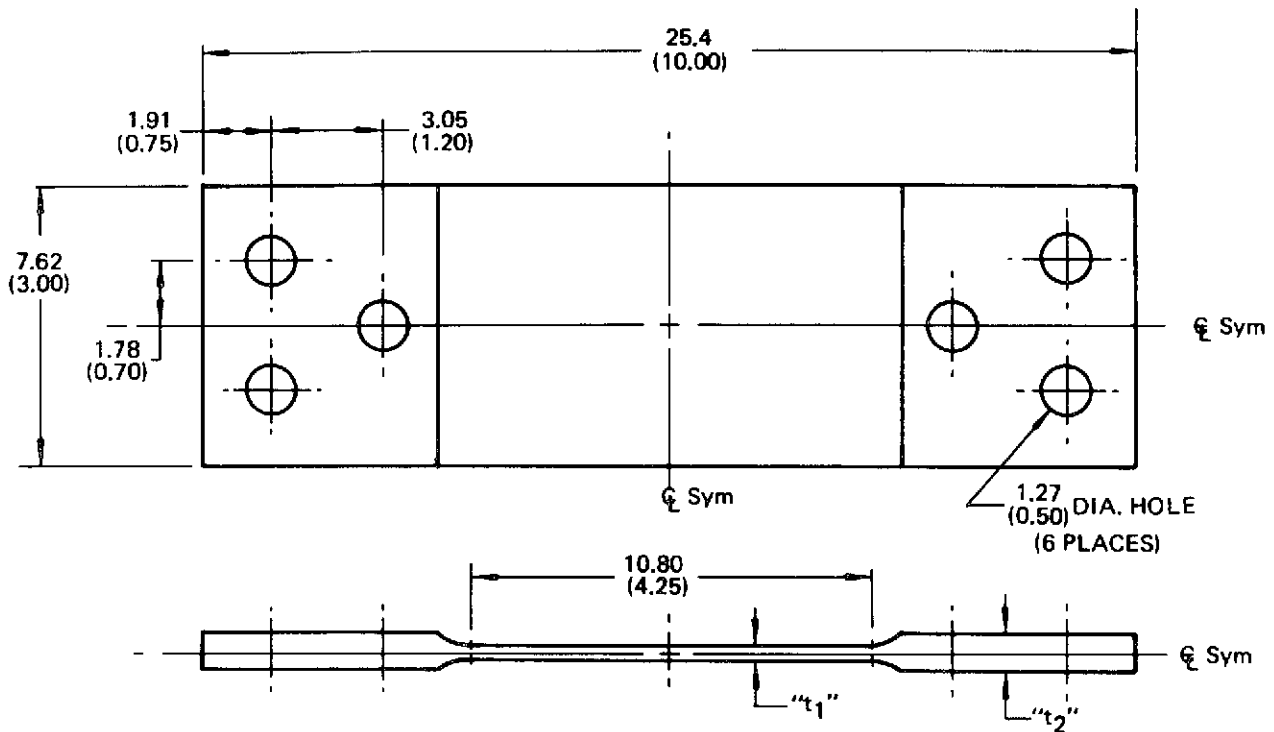


NOTE: DIMENSIONS ARE IN cm (INCH)

SPECIMEN CONFIGURATION	"t ₁ "	"t ₂ "
T-7	0.305 (0.120)	0.762 (0.300)
T-8	0.533 (0.210)	(1)
T-21	0.152 (0.060)	0.381 (0.150)

(1) MAX POSSIBLE AFTER MACHINING CLEANUP

Figure 7: 6Al-4V Titanium Surface Flaw Specimen

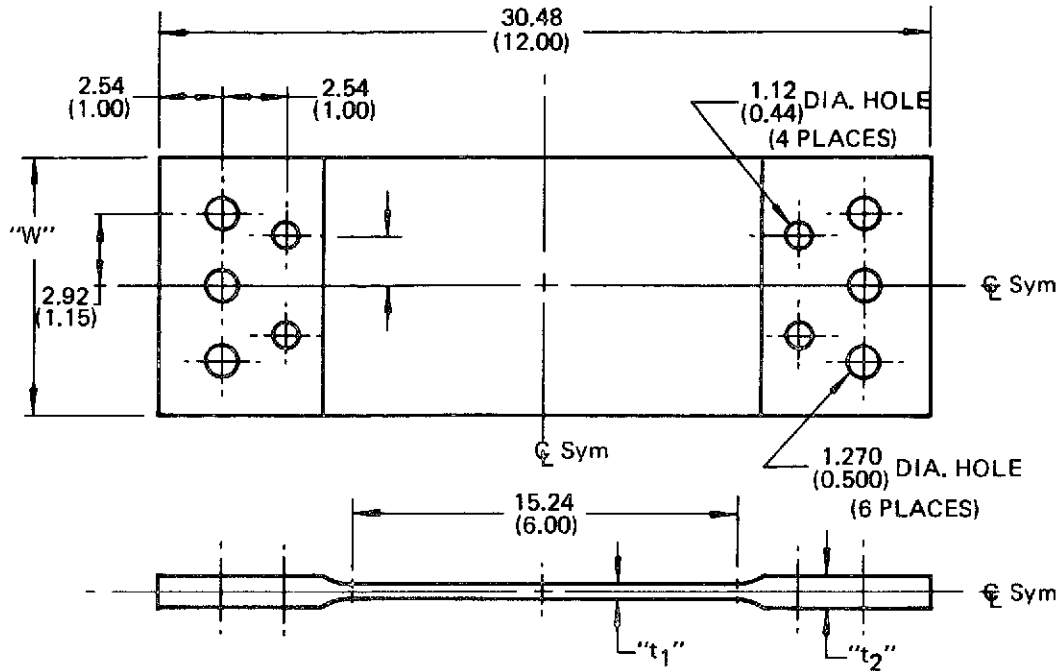


NOTE: DIMENSIONS ARE IN cm (INCH)

SPECIMEN CONFIGURATION	"t ₁ "	"t ₂ "
T-9	0.152 (0.060)	0.305 (0.120)
T-10	0.305 (0.120)	0.635 (0.250)
T-11	0.533 (0.210)	(1)
T-17	0.762 (0.300)	(1)

(1) MAXIMUM POSSIBLE AFTER MACHINING CLEANUP

Figure 8 : 6Al-4V Titanium Surface Flaw Specimen

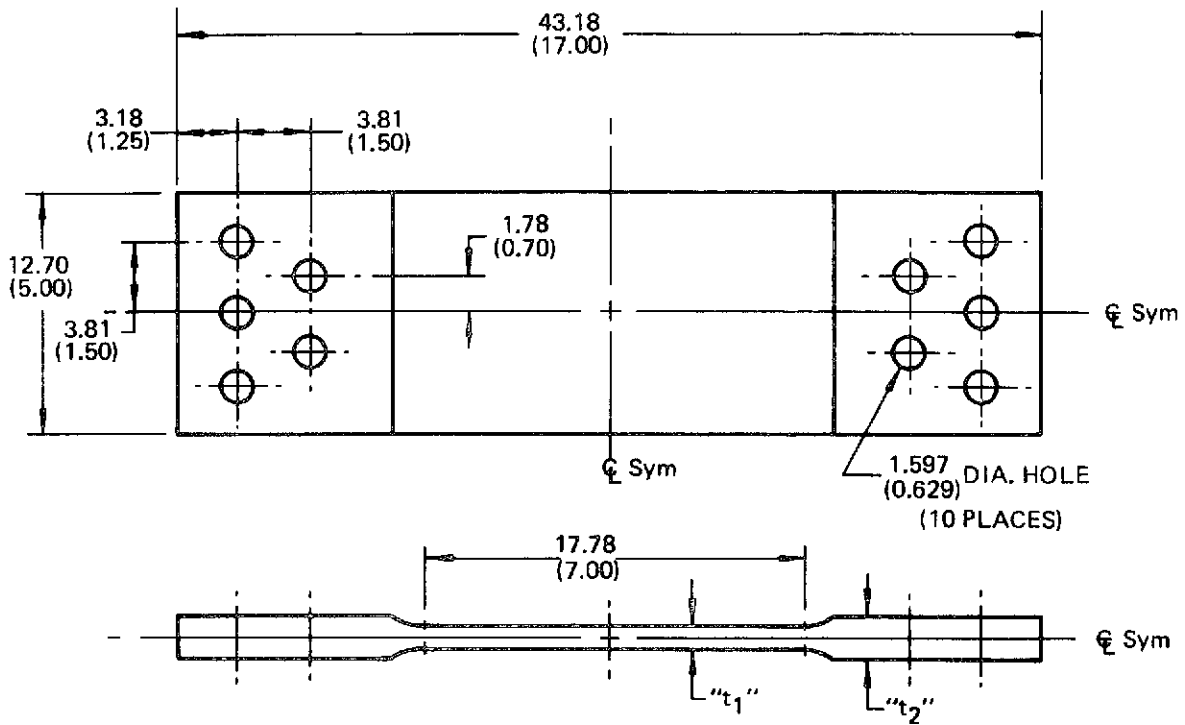


NOTE: DIMENSIONS ARE IN cm (INCH)

MATERIAL	SPECIMEN CONFIGURATION	"t ₁ "	"t ₂ "	"W"
6Al-4V Titanium	T-12	0.305 (0.120)	0.635 (0.250)	10.16 (4.00)
	T-13	0.533 (0.210)	(1)	10.16 (4.00)
	T-18	0.762 (0.300)	(1)	10.16 (4.00)
2219-T87 Aluminum	A8-1	0.508 (0.200)	1.016 (0.400)	10.16 (4.00)
2219-T87 & 7075-T651 Aluminum	A1-1	0.381 (0.150)	1.016 (0.400)	8.89 (3.50)
	A1-2	0.508 (0.200)	1.016 (0.400)	8.89 (3.50)
	A1-3	1.270 (0.500)	2.540 (1.000)	8.89 (3.50)
	A1-4	1.905 (0.750)	2.540 (1.000)	8.89 (3.50)

(1) Maximum Possible After Machining

Figure 9 : Surface Flaw Specimen

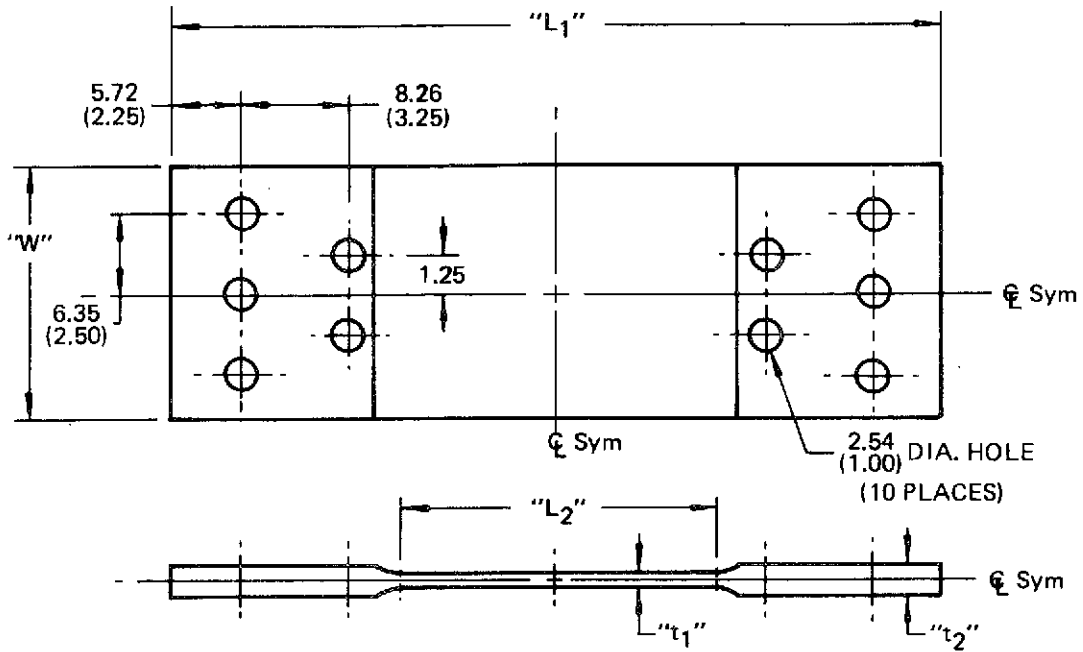


NOTE: DIMENSIONS ARE IN cm (INCH)

MATERIAL	SPECIMEN CONFIGURATION	"t ₁ "	"t ₂ "
2219-T87 & 7075-T651 Aluminum	A2-1	0.381 (0.150)	1.016 (0.400)
	A2-2	0.508 (0.200)	1.016 (0.400)
	A2-3	1.270 (0.500)	2.413 (0.950)
	A2-4	1.905 (0.750)	2.413 (0.950)
6Al-4V Titanium	T-14	0.305 (0.120)	0.635 (0.250)
	T-15	0.533 (0.210)	(1)
	T-16	0.762 (0.300)	(1)

(1) MAXIMUM POSSIBLE AFTER MACHINING CLEANUP

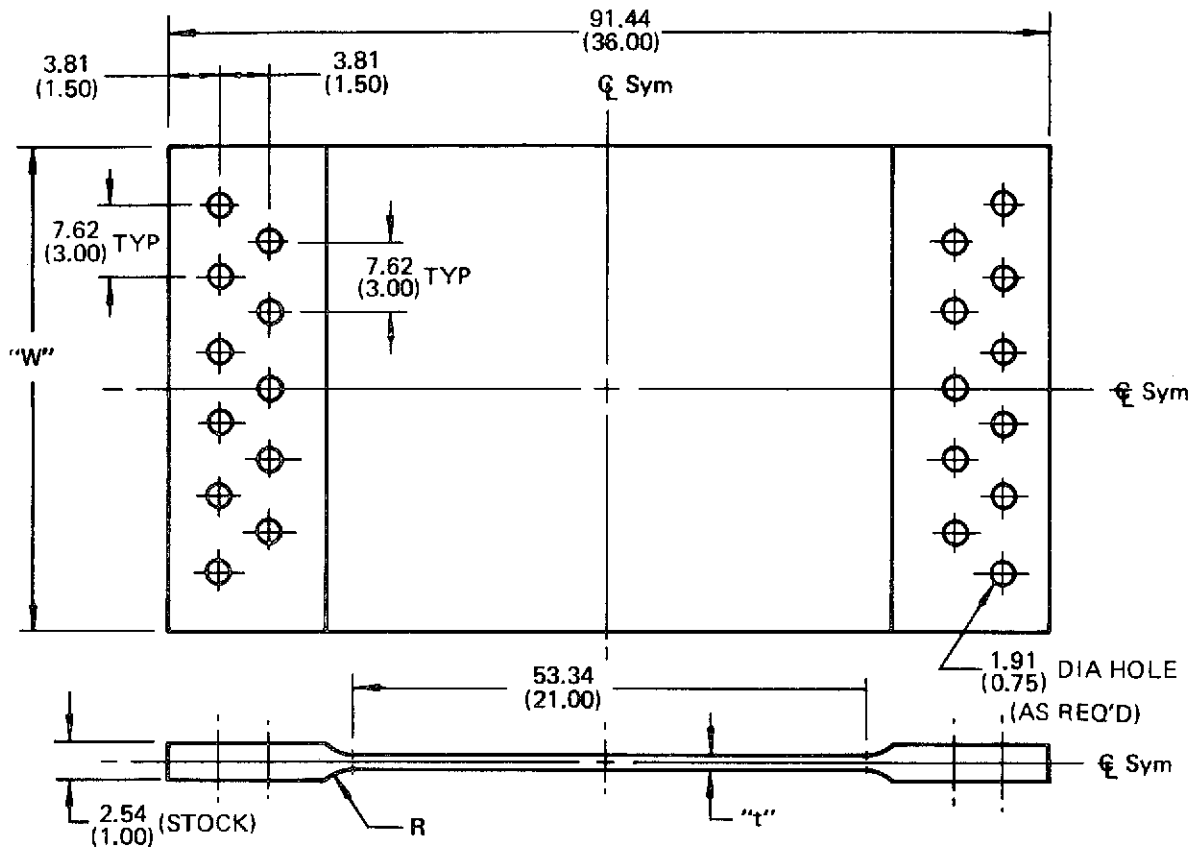
Figure 10: Surface Flaw Specimen



NOTE: DIMENSIONS ARE IN cm (INCH)

MATERIAL	SPECIMEN CONFIGURATION	" t_1 "	" t_2 "	" L_1 "	" L_2 "	" W "
2219-T87 Aluminum	A5-1	1.270 (0.500)	2.540 (1.000)	60.96 (24.00)	25.40 (10.00)	20.32 (8.00)
2219-T87 & 7075-T651 Aluminum	A4-1	0.508 (0.200)	1.016 (0.400)	76.20 (30.00)	35.56 (14.00)	22.86 (9.00)
	A4-2	1.270 (0.500)	2.540 (1.000)	76.20 (30.00)	35.56 (14.00)	22.86 (9.00)
	A4-3	1.905 (0.750)	2.540 (1.000)	76.20 (30.00)	35.56 (14.00)	22.86 (9.00)
6Al-4V Titanium	T-19	0.533 (0.210)	0.533 (0.210)	60.96 (24.00)	25.40 (10.00)	20.32 (8.00)

Figure 11: Surface Flaw Specimen



NOTE: DIMENSIONS ARE IN cm (INCH)

MATERIAL	SPECIMEN CONFIGURATION	"W"	"t"
2219-T87 & 7075-T651 Aluminum	A3-1	30.48 (12.00)	1.270 (0.500)
	A3-2	40.64 (16.00)	1.270 (0.500)
	A3-3	50.80 (20.00)	1.270 (0.500)
	A3-4	30.48 (12.00)	1.905 (0.750)

Figure 12: Aluminum Surface Flaw Specimen

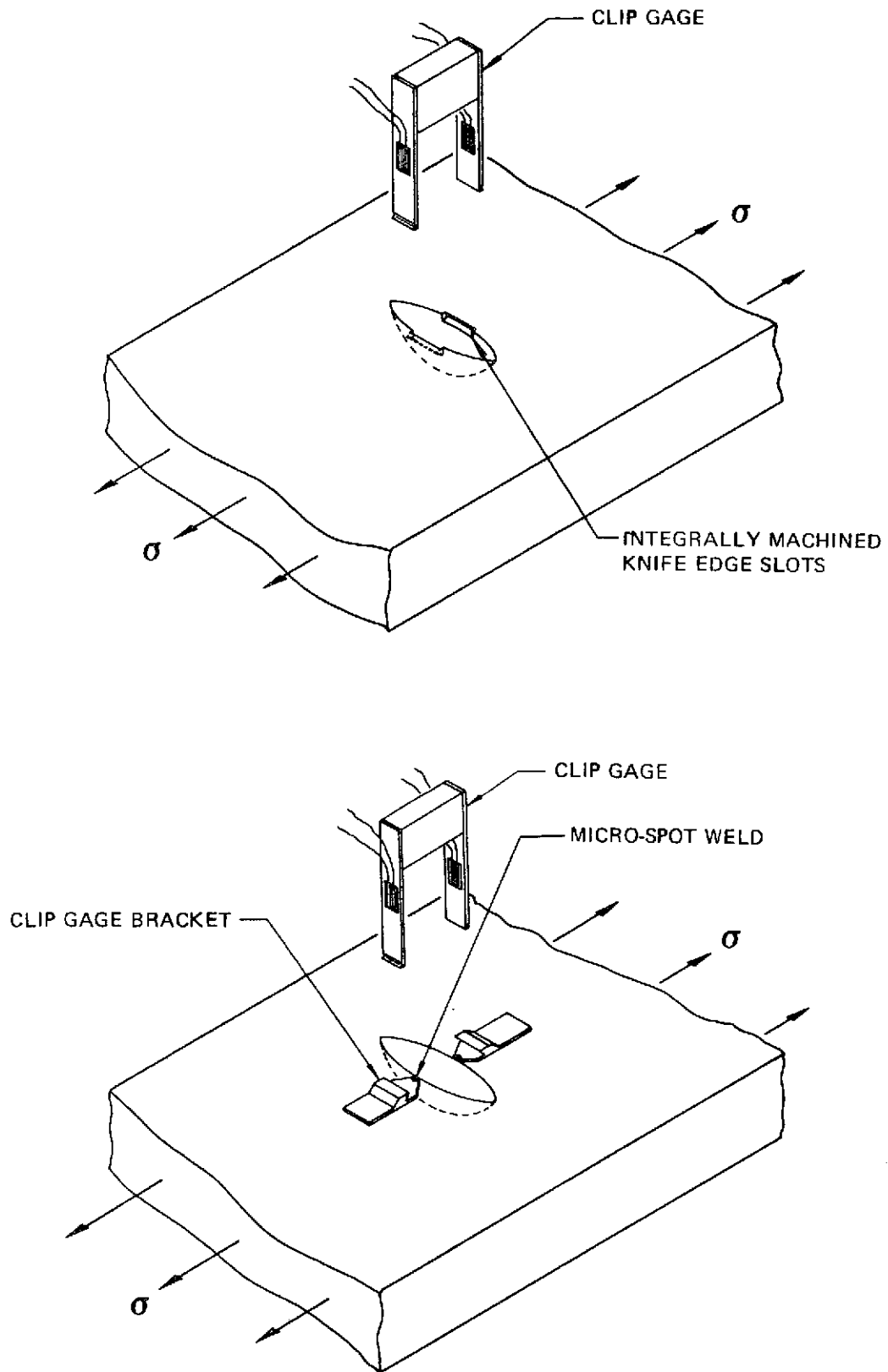


Figure 13: Flaw Opening Measurement of Surface Flaw Specimens

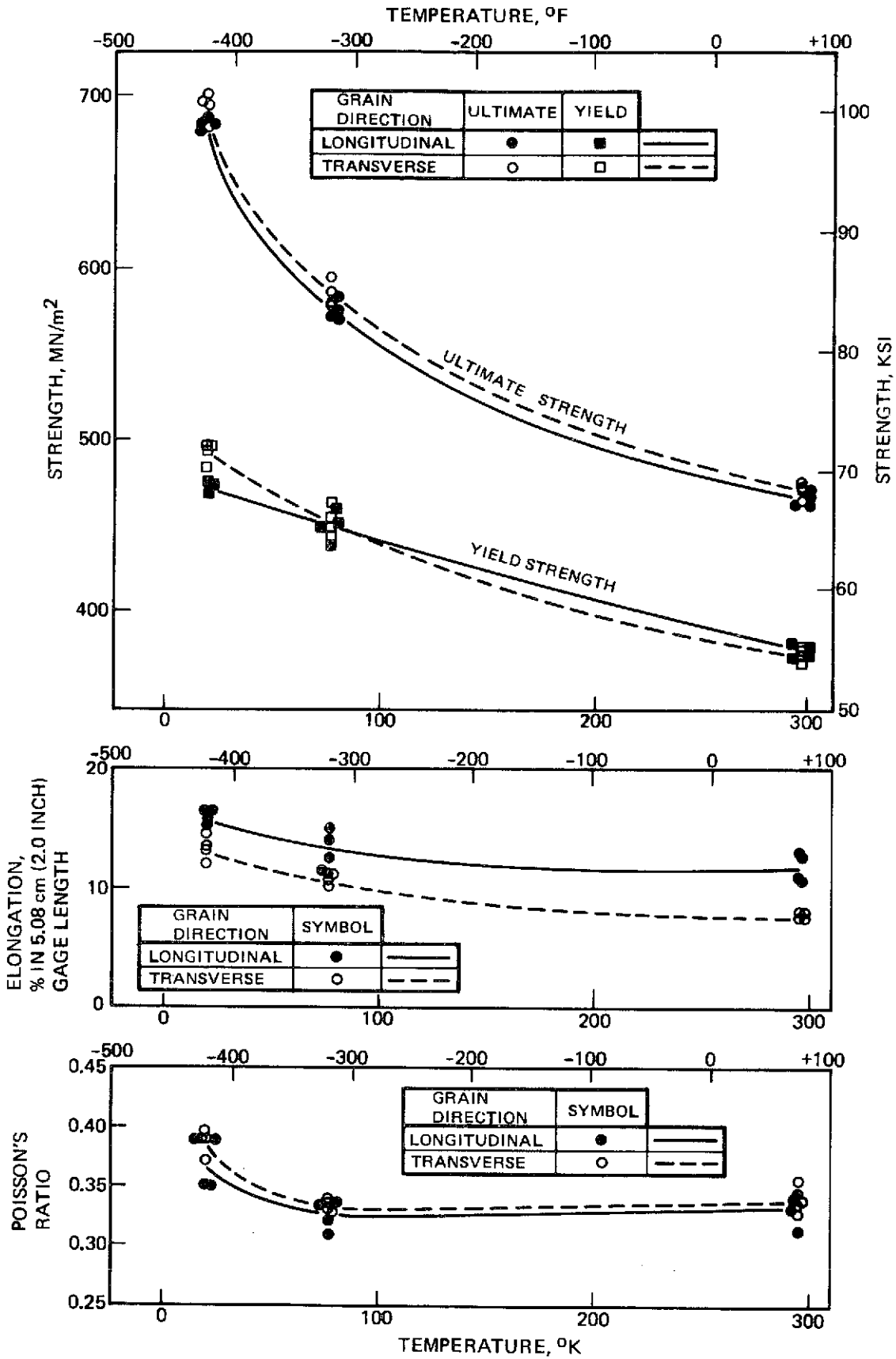


Figure 14: Tensile Properties of 2219-T87 Aluminum Base Metal

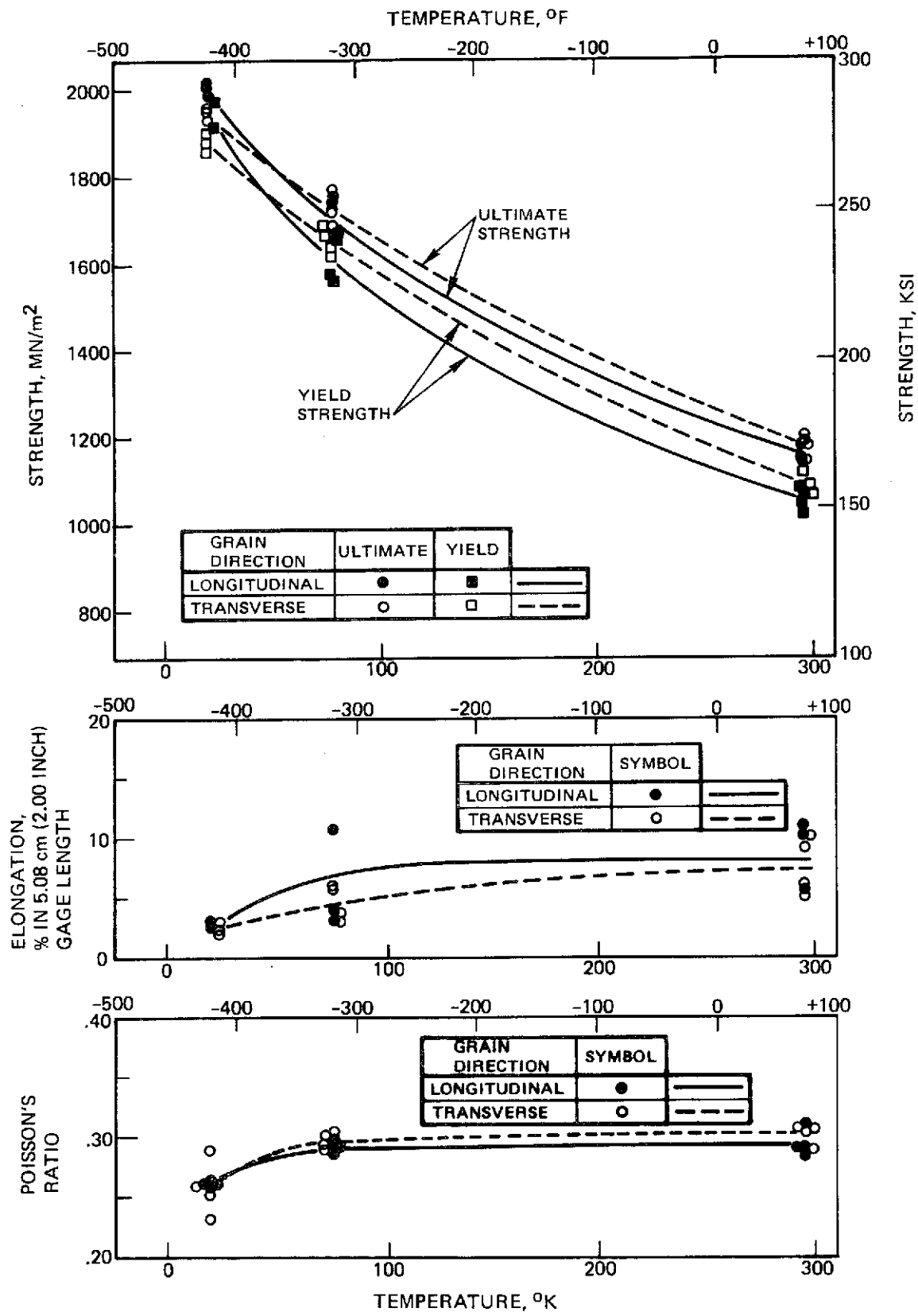
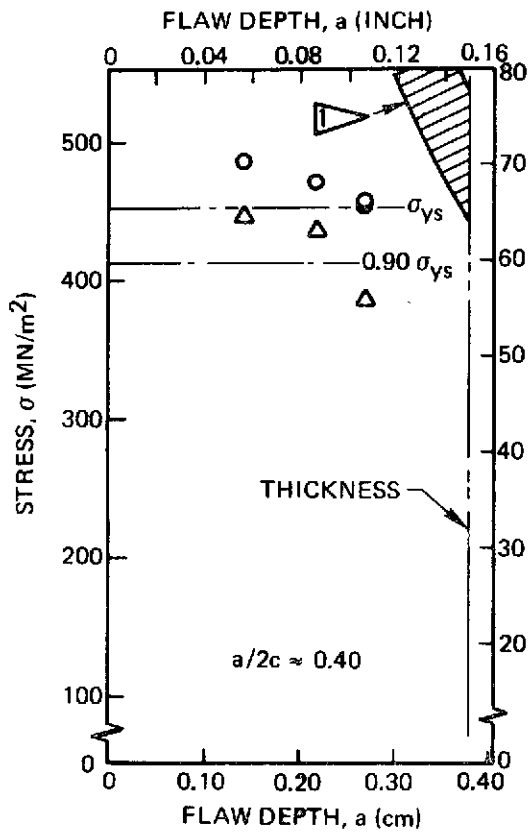
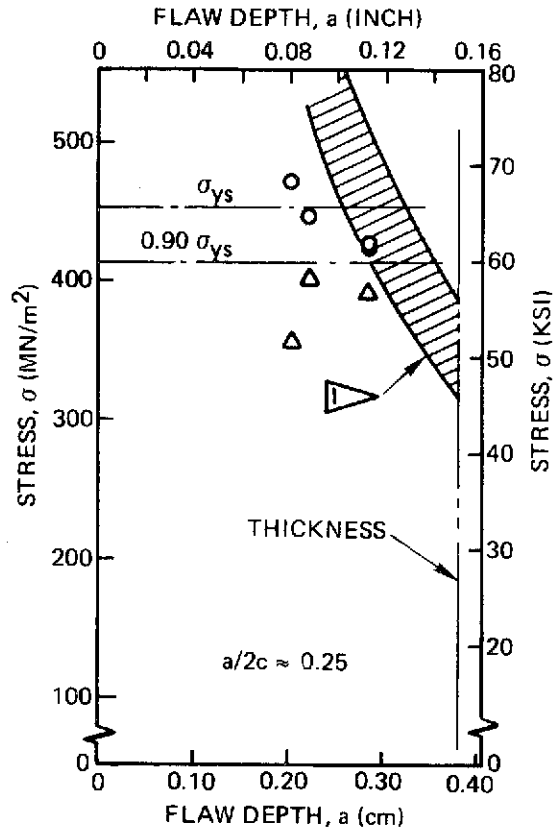


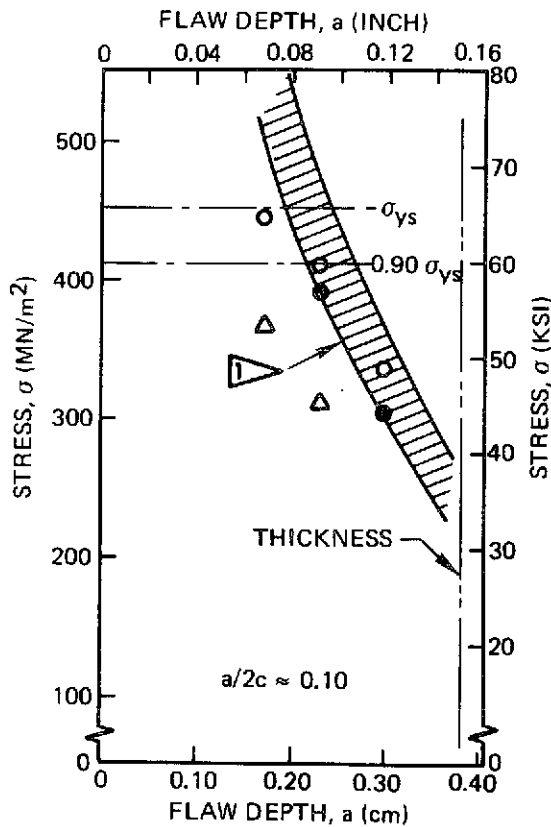
Figure 15: Tensile Properties of 6Al-4V (STA) Titanium Plate



16a:



16b:



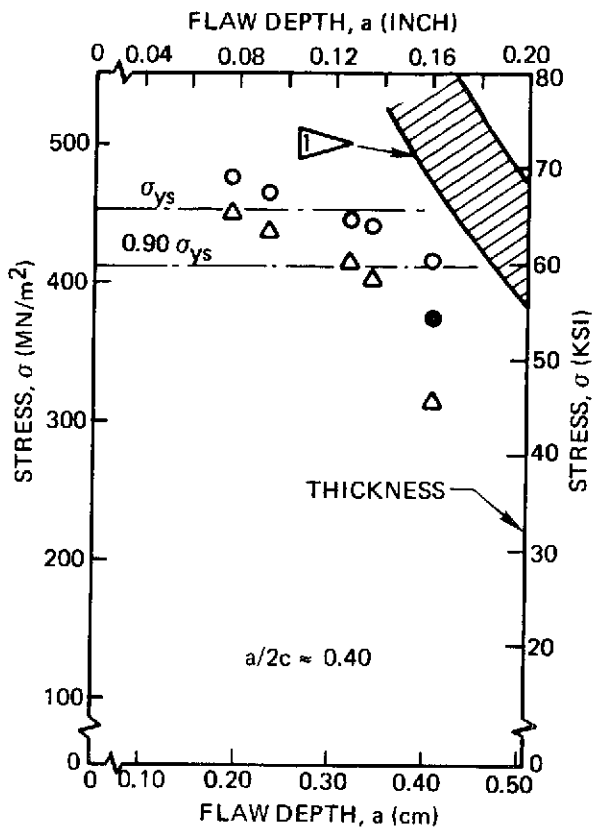
16c:

$\nabla K_{IE} = 55.0 \text{ MN/m}^{3/2} (50.0 \text{ KSI } \sqrt{\text{IN}}.)$
 $\pm 10\% (\text{REF.})$

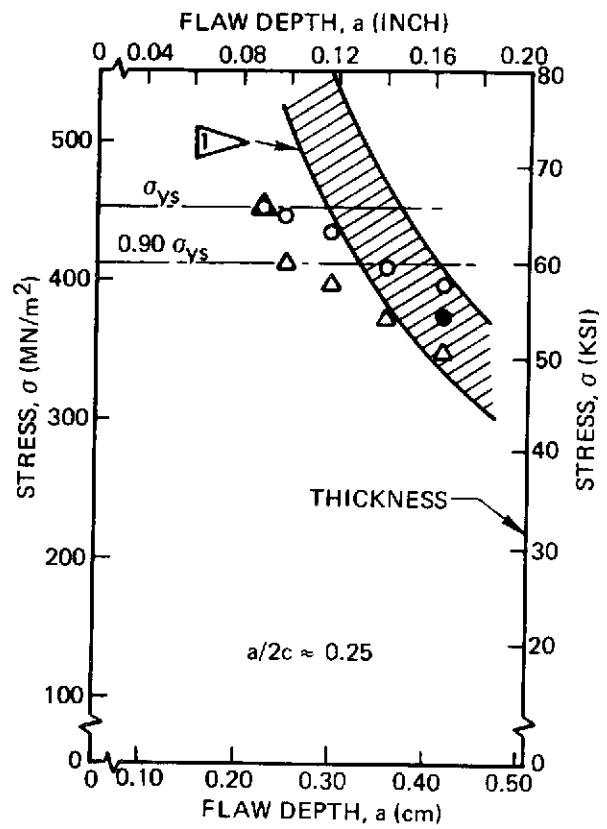
LEGEND:

- FAILURE STRESS
 - BREAKTHROUGH STRESS
 - △ DIMPLING
- TEST TEMPERATURE: 78K (-320F)
 TEST DIRECTION: WT

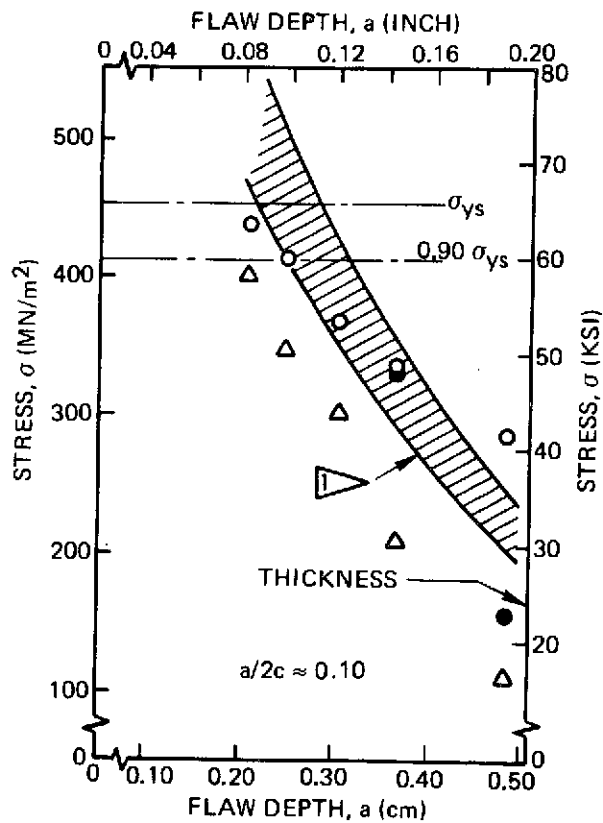
Figure 16: 2219-T87 Aluminum
 Stress Versus Flaw Size
 $t = 0.38 \text{ cm } (0.15 \text{ Inch})$



17a:



17b:



17c:

$\nabla K_{IE} = 55.0 \text{ MN/m}^{3/2} (50.0 \text{ KSI } \sqrt{\text{IN}}.)$
 $\pm 10\% (\text{REF.})$

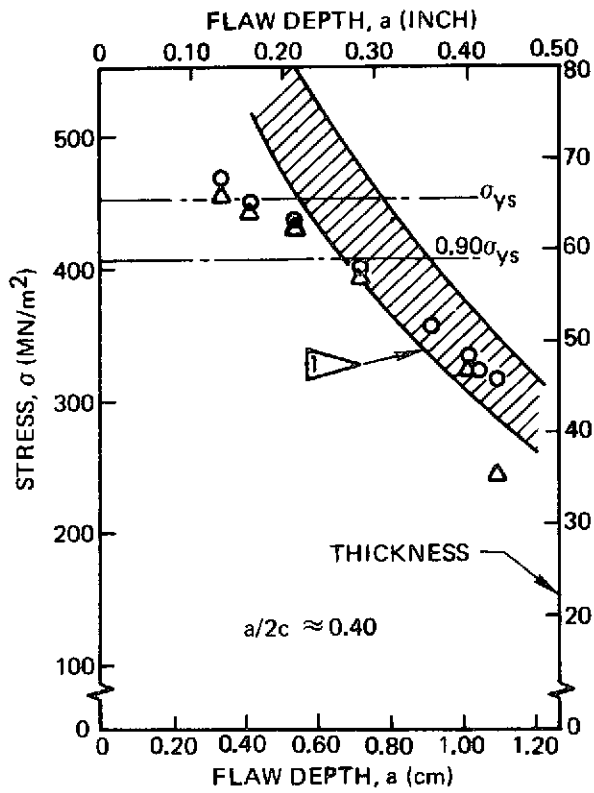
LEGEND:

- FAILURE STRESS
- BREAKTHROUGH STRESS
- △ DIMPLING

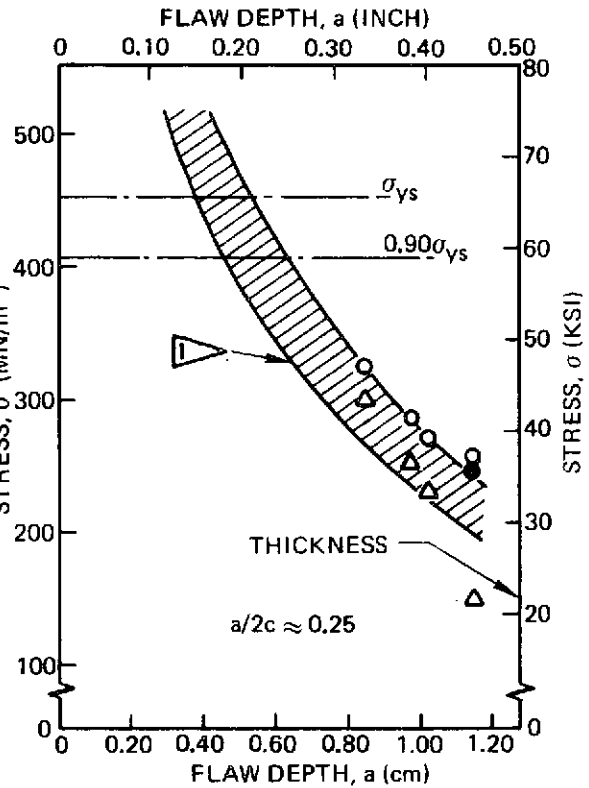
TEST TEMPERATURE: 78 K (-320 F)

TEST DIRECTION: WT

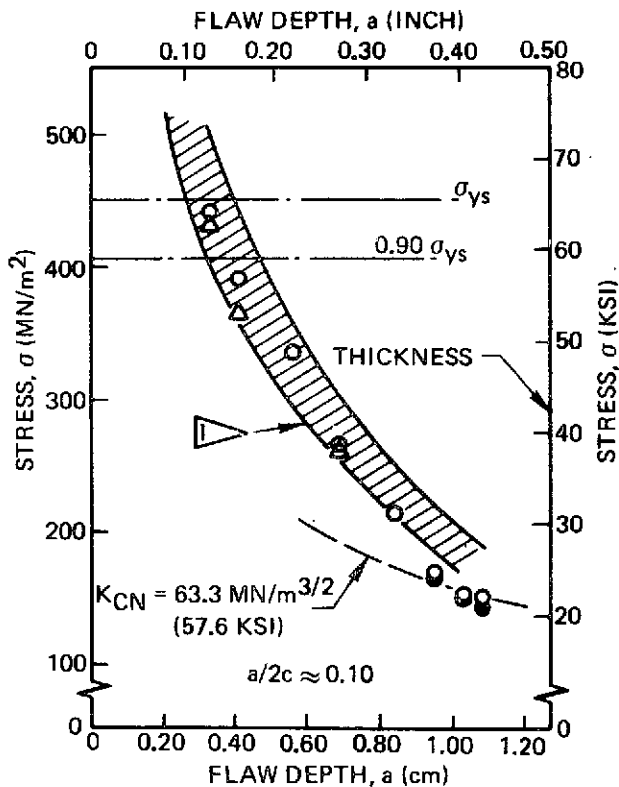
Figure 17: 2219-T87 Aluminum
 Stress Versus Flaw Size
 $t = 0.51 \text{ cm (0.20 Inch)}$



18a:



18b:



18c:

$\triangleleft K_{IE} = 55.0 \text{ MN/m}^{3/2}$ (50.0 KSI $\sqrt{\text{IN.}}$)
± 10% (REF.)

LEGEND:

- FAILURE STRESS
 - BREAKTHROUGH STRESS
 - △ DIMPLING
- TEST TEMPERATURE: 78K (-320F)
TEST DIRECTION: WT

Figure 18: 2219-T87 Aluminum
Stress Versus Flaw Size
 $t = 1.27 \text{ cm}$ (0.50 Inch)

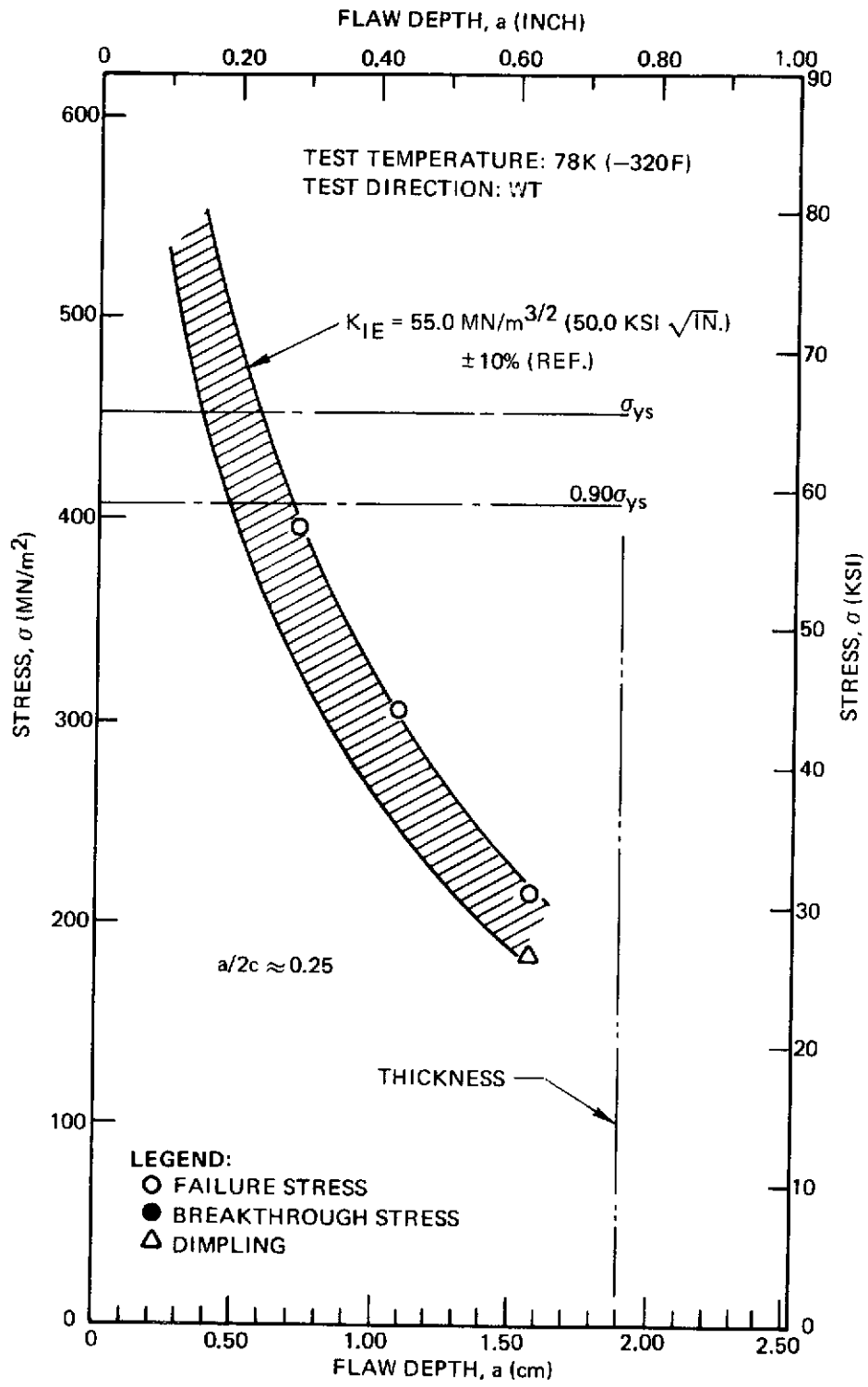


Figure 19: 2219-T87 Aluminum Stress Versus Flaw Size
 $t = 1.90 \text{ cm (0.75 Inch)}$

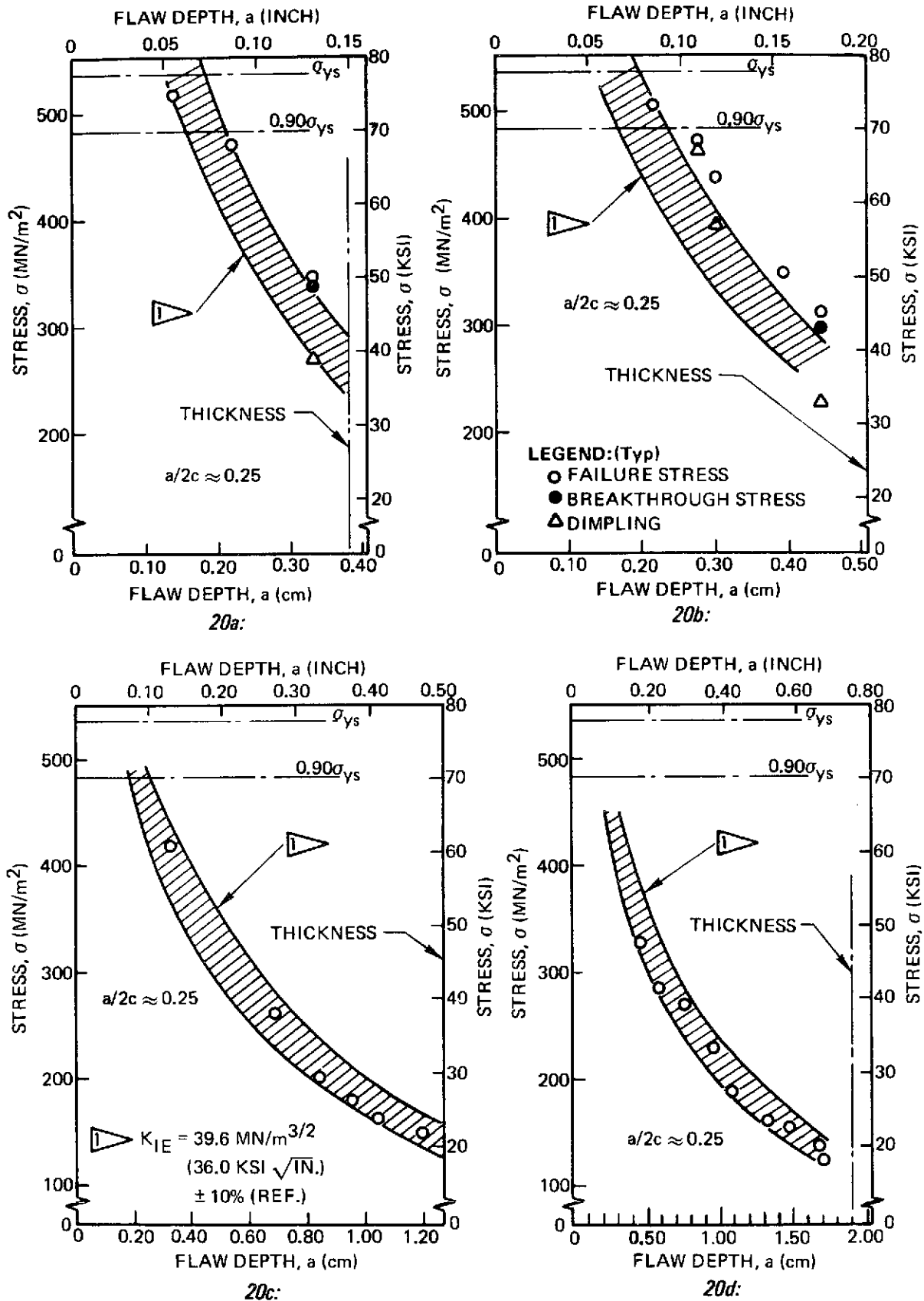
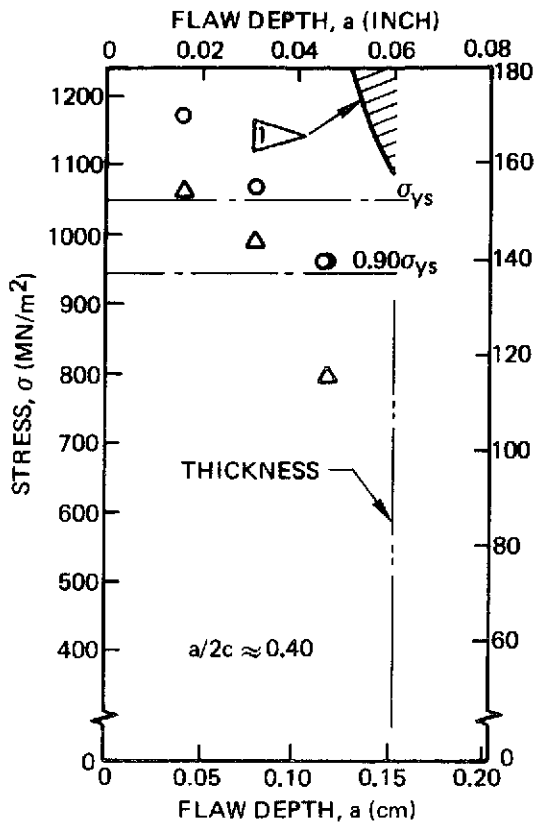
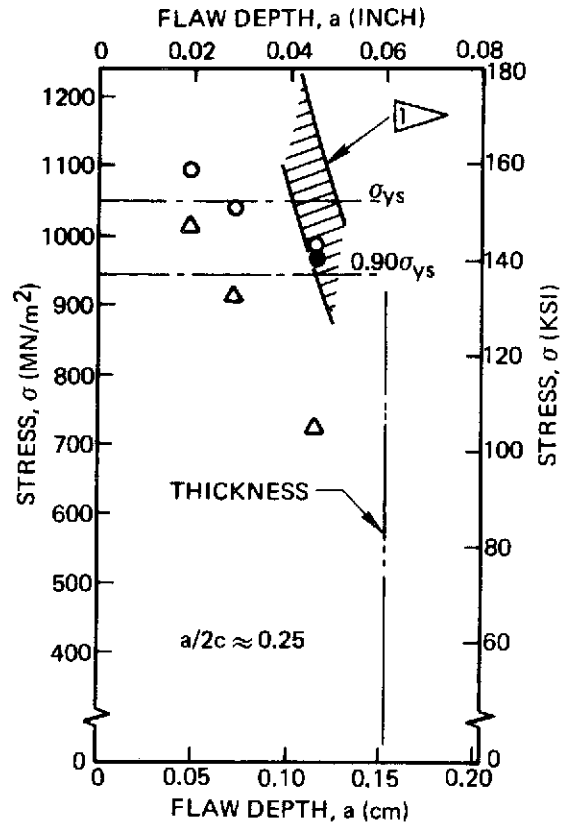


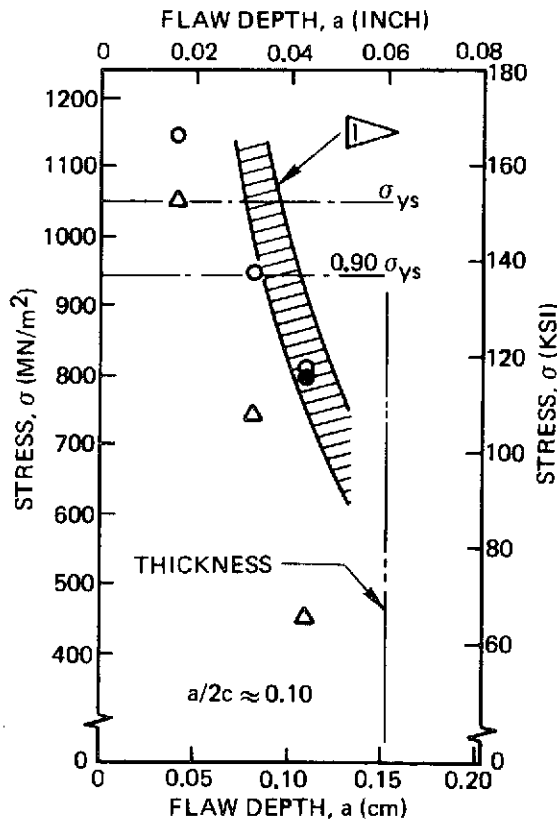
Figure 20: 7075-T651 Aluminum Stress Versus Flaw Size (Room Temperature, WT)



21a:



21b:

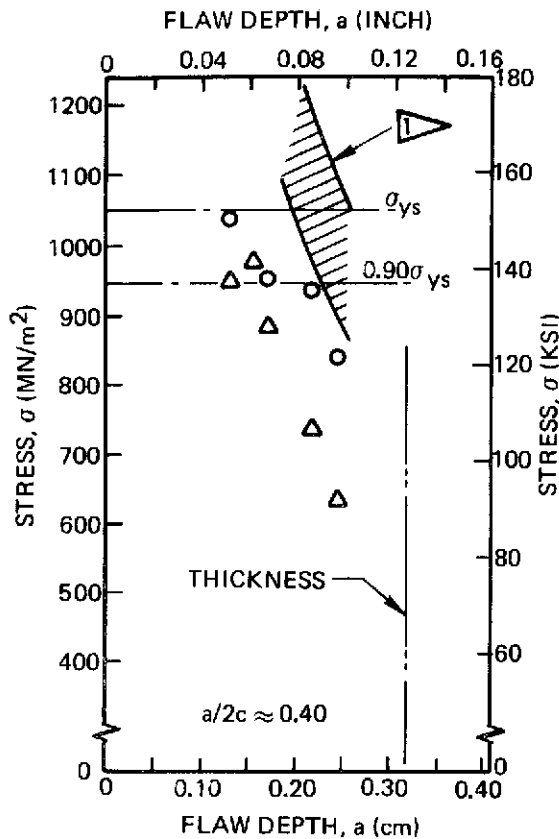


21c:

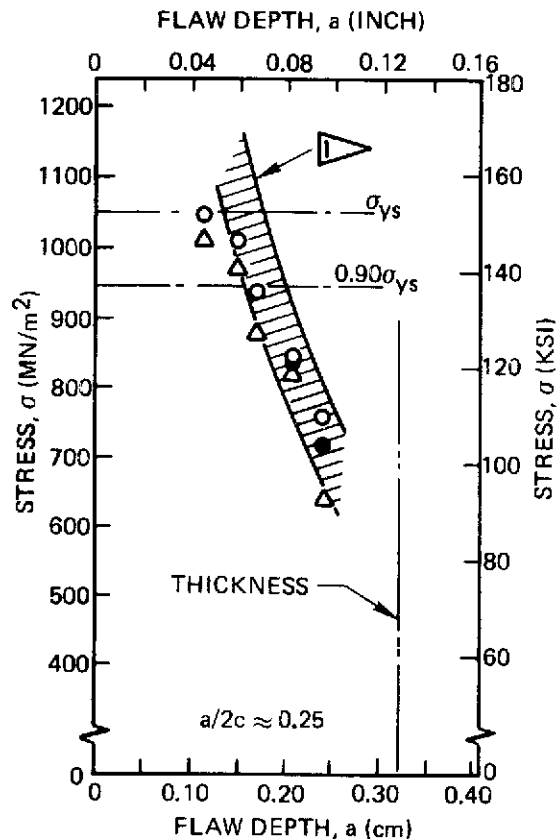
$\nabla K_{IE} = 80.2 \text{ MN/m}^{3/2} (73.0 \text{ KSI } \sqrt{\text{IN}})$
 $\pm 10\% \text{ (REF.)}$

LEGEND:
 ○ FAILURE STRESS
 ● BREAKTHROUGH STRESS
 ▲ DIMPLING
 TEST TEMPERATURE: ROOM
 TEST DIRECTION: RT

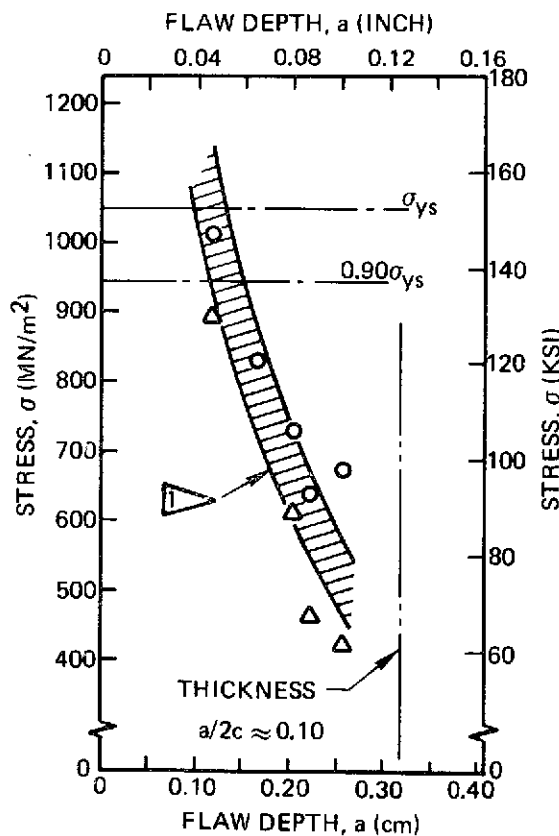
Figure 21: 6Al-4V STA Titanium
 Stress Versus Flaw Size
 t = 0.15 cm (0.06 Inch)



22a:



22b:



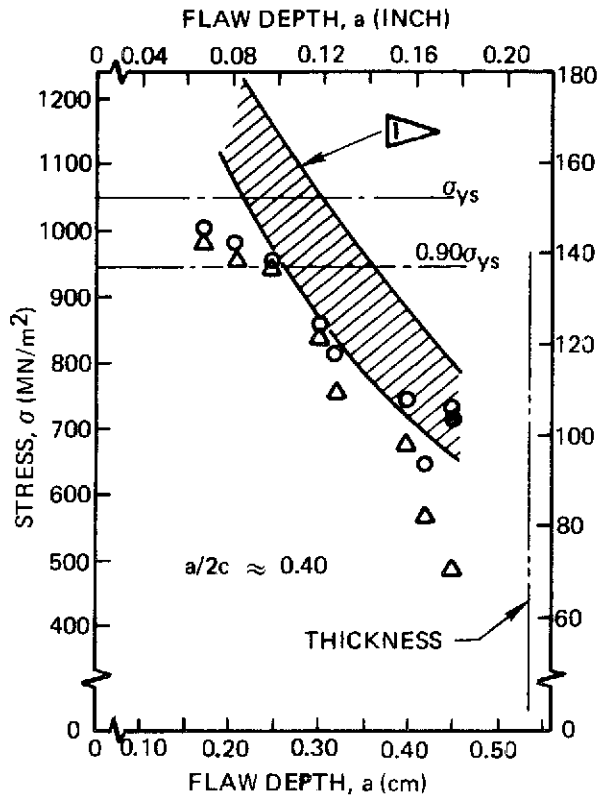
22c:

$\triangle K_{IE} = 80.2 \text{ MN/m}^{3/2} (73.0 \text{ KSI} \sqrt{\text{IN}}.)$
 $\pm 10\% \text{ (REF.)}$

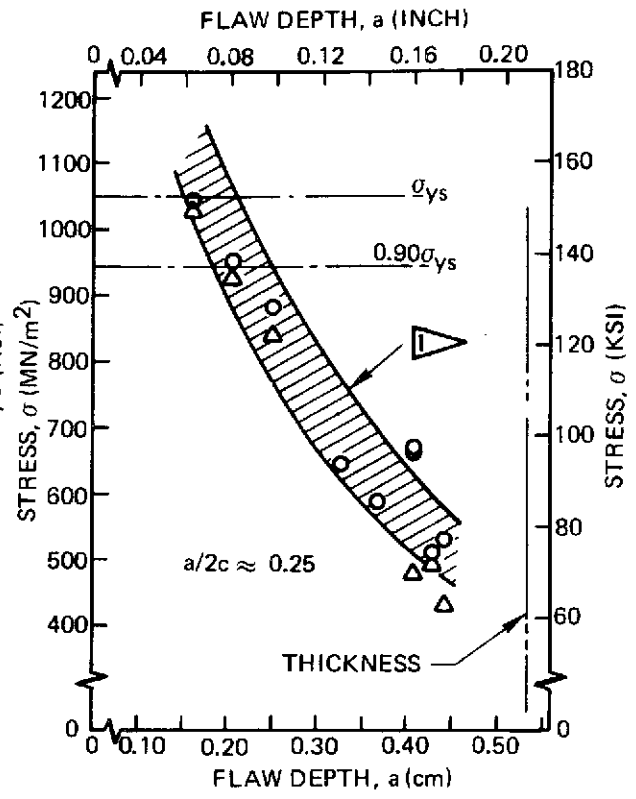
LEGEND:

- FAILURE STRESS
- BREAKTHROUGH STRESS
- △ DIMPLING
- TEST TEMPERATURE: ROOM
- TEST DIRECTION: RT

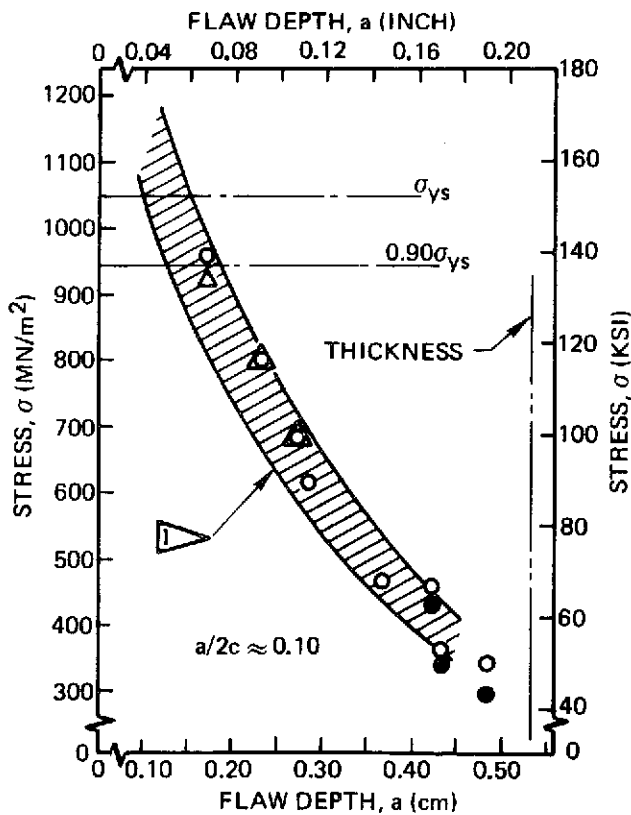
Figure 22: 6Al-4V STA Titanium
 Stress Versus Flaw Size
 $t = 0.32 \text{ cm (0.125 inch)}$



23a:



23b:



23c:

$\triangle K_{IE} = 80.2 \text{ MN/m}^{3/2} (73.0 \text{ KSI } \sqrt{\text{IN}}.)$
 $\pm 10\% (\text{REF.})$

LEGEND:

- FAILURE STRESS
 - BREAKTHROUGH STRESS
 - △ DIMPLING
- TEST TEMPERATURE: ROOM
 TEST DIRECTION: RT

Figure 23: 6Al-4V STA Titanium
 Stress Versus Flaw Size
 $t = 0.53 \text{ cm (0.21 Inch)}$

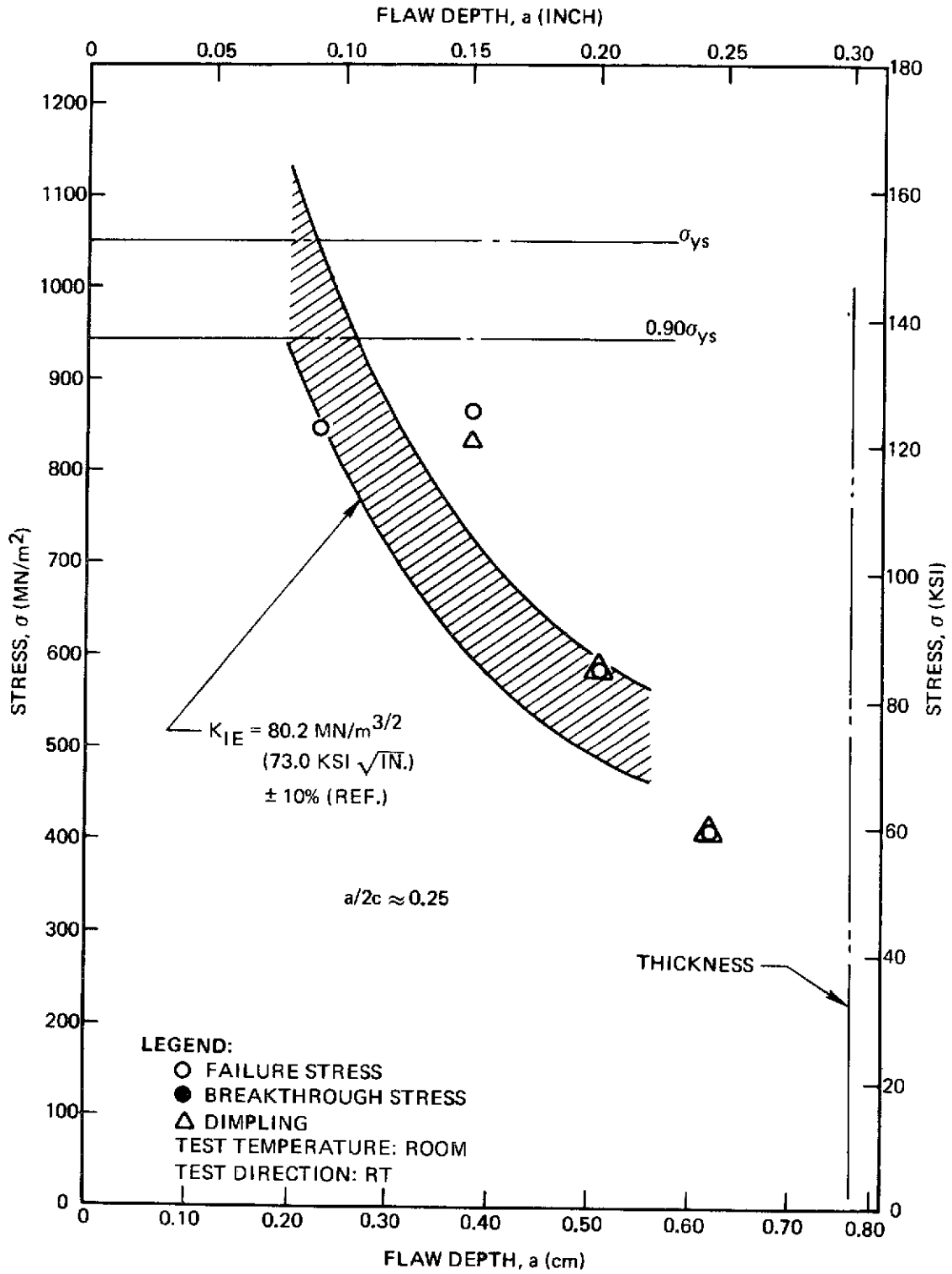


Figure 24: 6Al-4V STA Titanium Stress Versus Flaw Size
 $t = 0.76 \text{ cm (0.30 Inch)}$

THICKNESS cm (INCH)		a/2c		
		0.10	0.25	0.40
0.381	(0.150)	△	□	○
0.508	(0.200)	▲	■	●
1.270	(0.500)	△	□	○
1.906	(0.750)	▲	■	●

2219-T87 ALUMINUM BASE METAL
WT DIRECTION 78°K (-320°F)

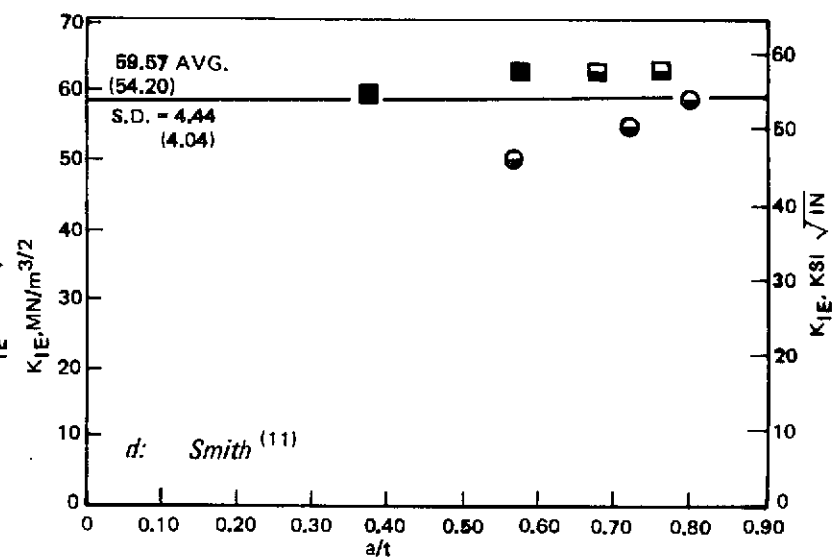
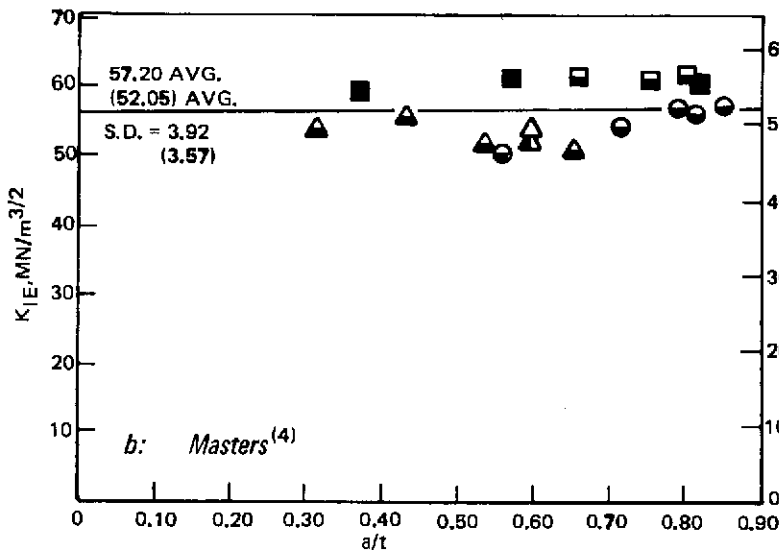
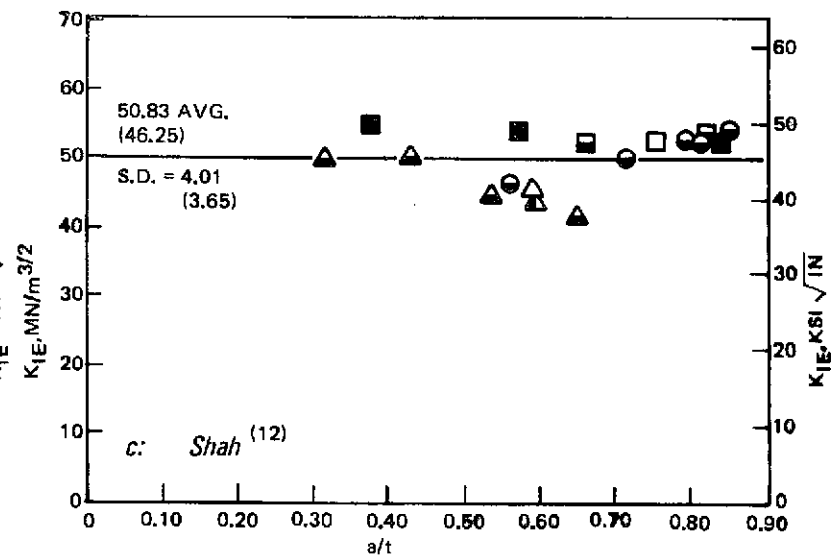
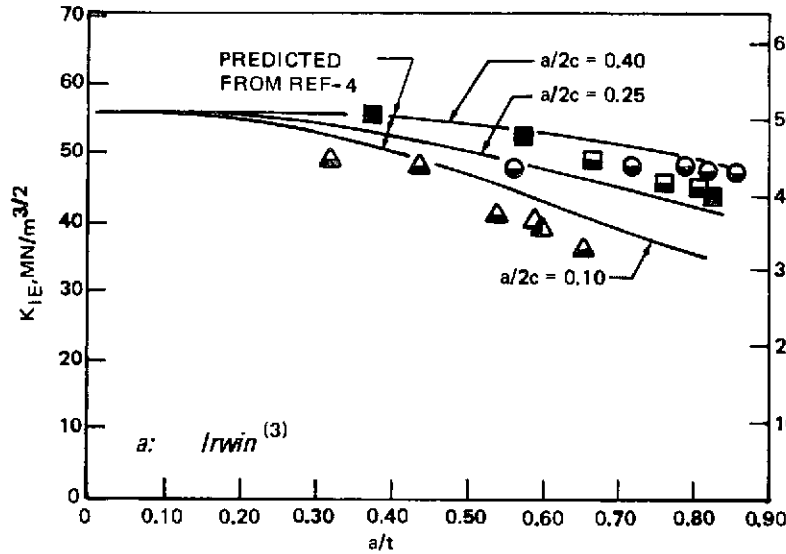


Figure 25: Comparison of Magnification Terms, 2219-T87 Base Metal at 78°K (-320°F), WT Direction

Δ $a/2c \approx 0.10$	2219-T87 ALUMINUM BASE METAL
\circ $a/2c \approx 0.40$	ROOM TEMP, RT DIRECTION $t = 1.588$ cm (0.625 IN.)

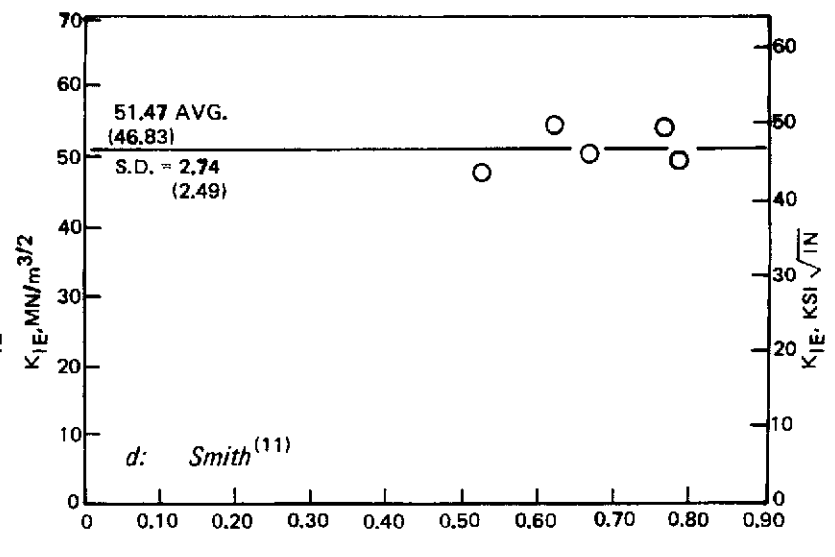
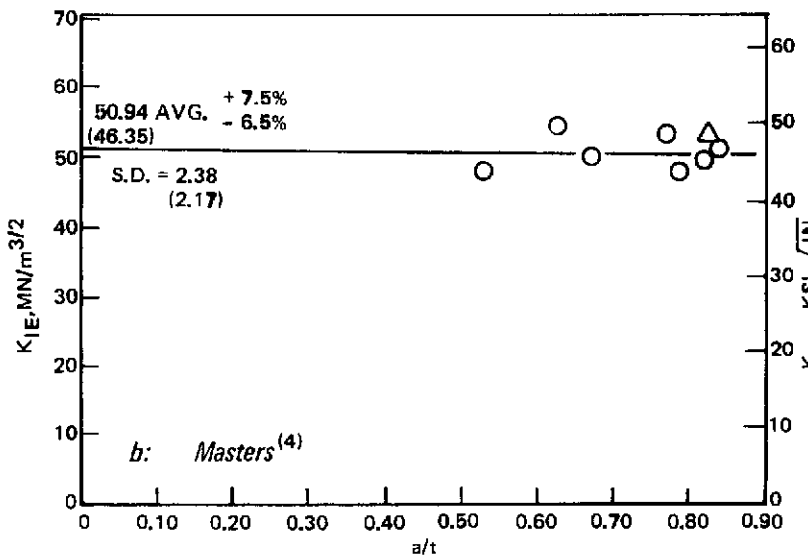
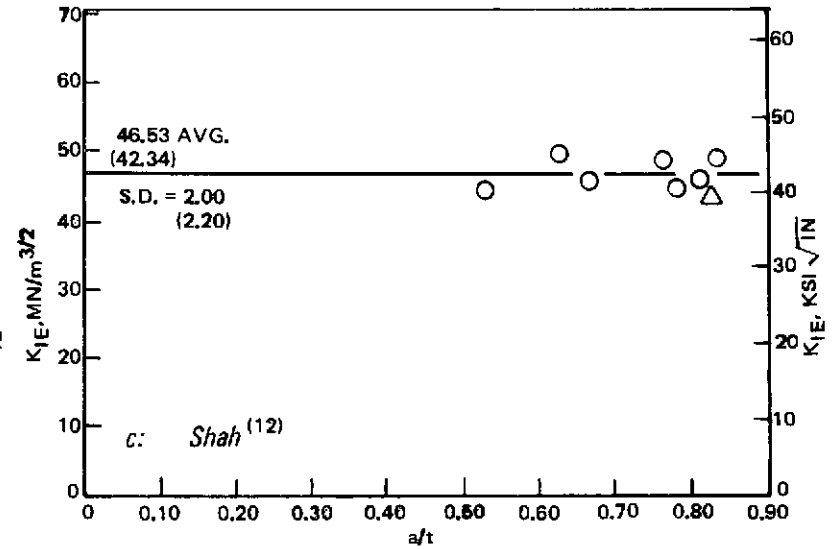
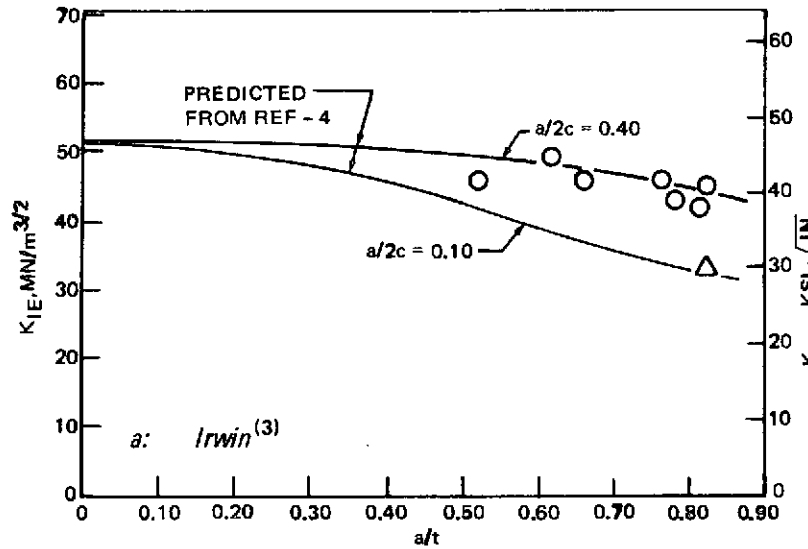


Figure 26: Comparison of Magnification Terms, 2219-T87 Base Metal at Room Temperature, RT Direction (Data Taken From Ref. (4))

△	$a/2c \approx 0.10$	2219-T87 BASE METAL $78^{\circ}\text{K} (-320^{\circ}\text{F})$ RT DIRECTION $t = 1.588 \text{ cm } (0.625 \text{ IN.})$
□	$a/2c \approx 0.25$	
○	$a/2c \approx 0.40$	

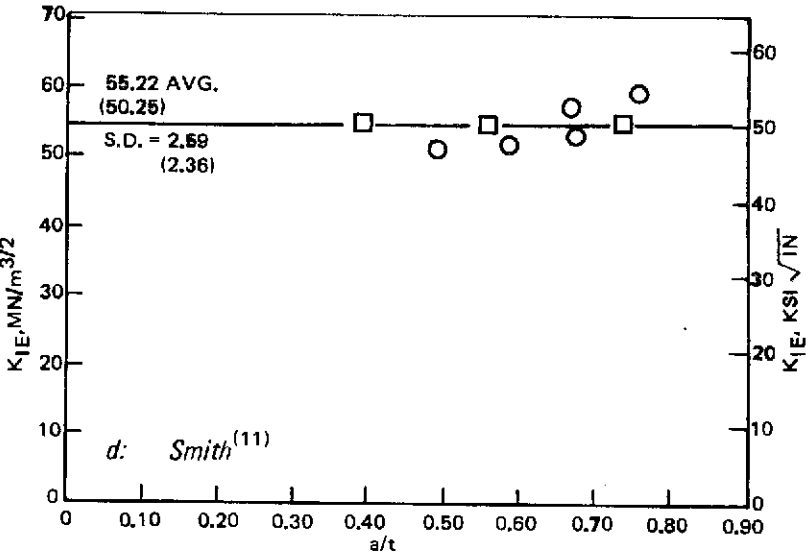
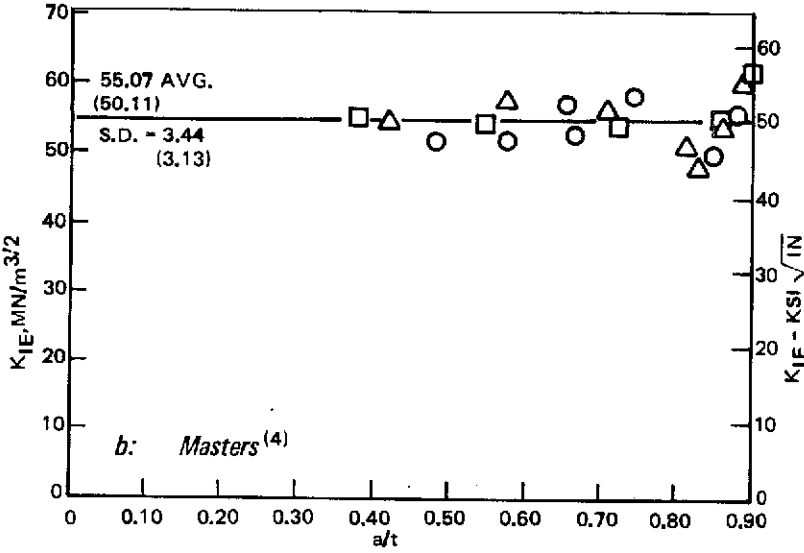
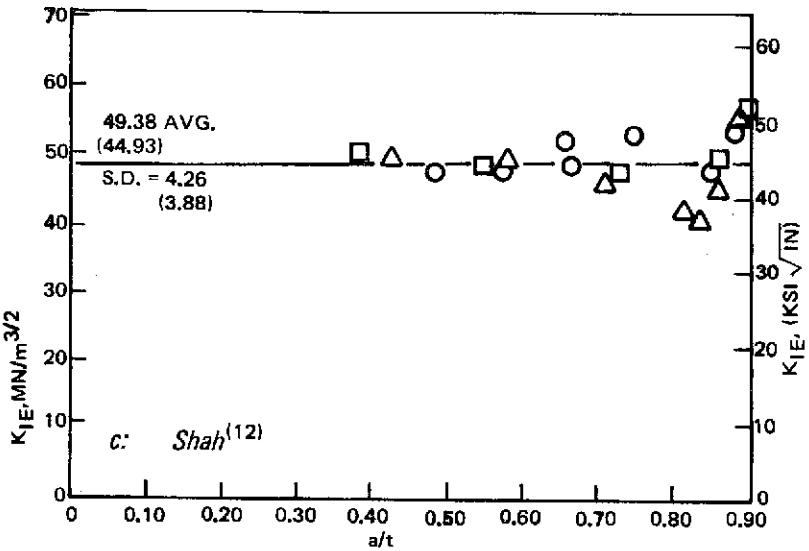
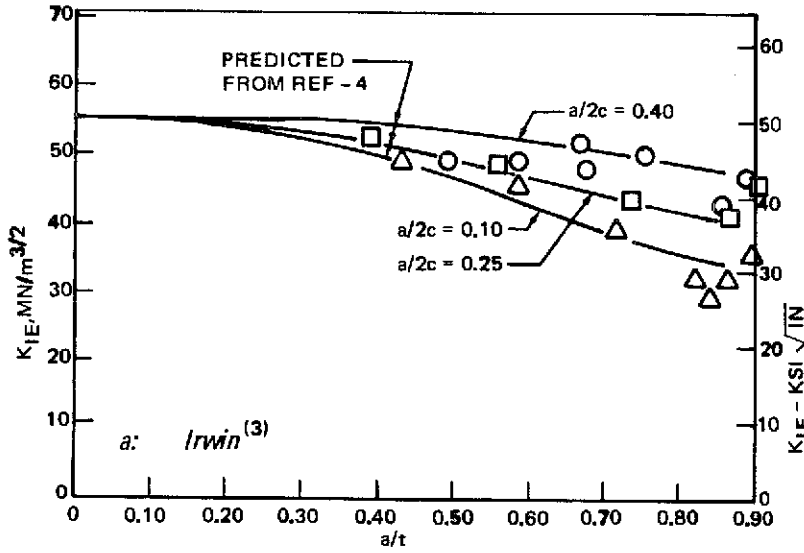


Figure 27: Comparison of Magnification Terms, 2219-T87 Base Metal at $78^{\circ}\text{K} (-320^{\circ}\text{F})$, RT Direction (Data Taken From Ref. (4))

\triangle $a/2c \approx 0.10$	2219-T87 BASE METAL	20°K (-423°F)
\circ $a/2c \approx 0.40$	RT DIRECTION	$t = 1.588 \text{ cm (0.625 IN.)}$

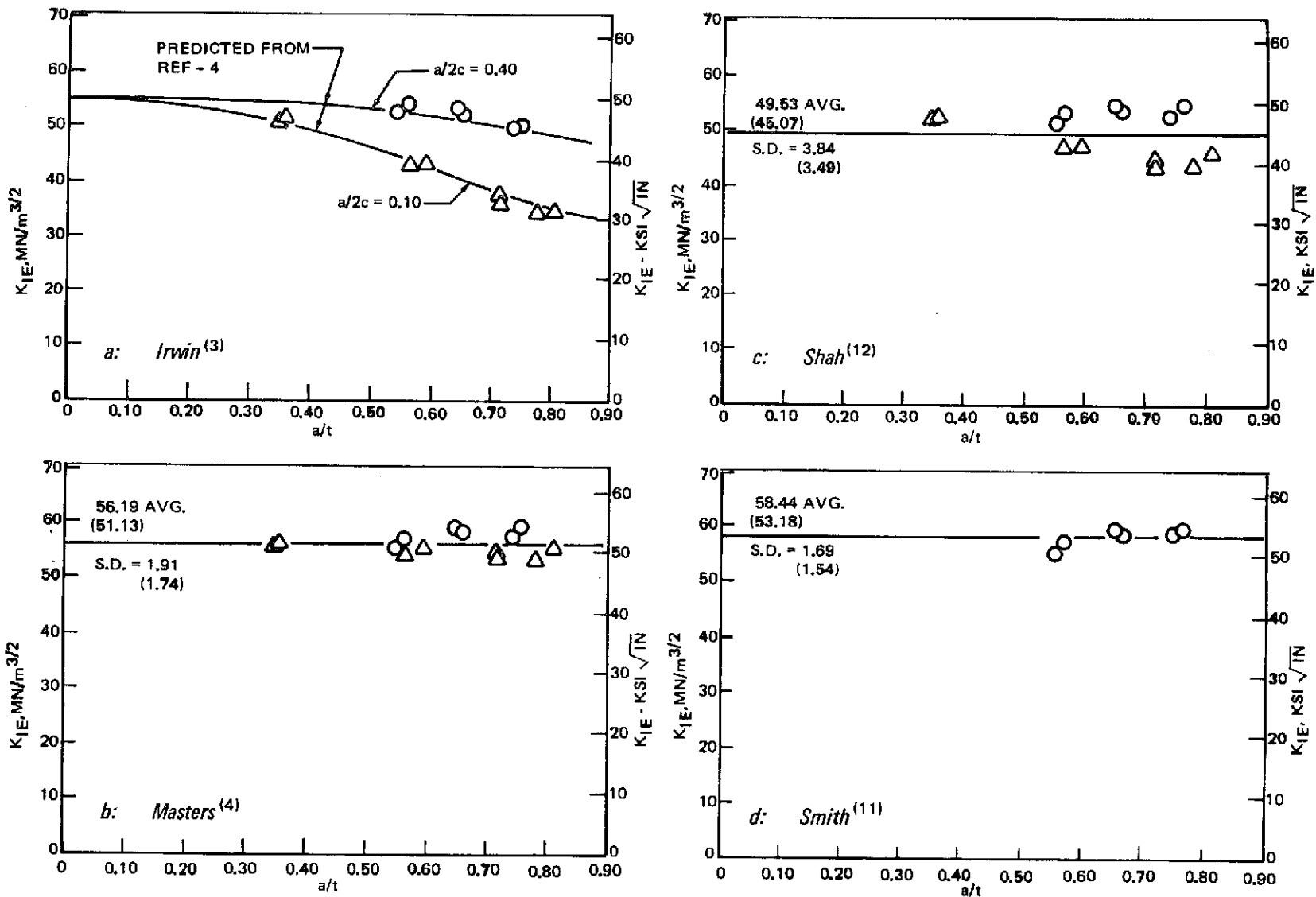


Figure 28: Comparison of Magnification Terms, 2219-T87 Base Metal at 20°K (-423°F), RT Direction (Data Taken From Ref. 4)

THICKNESS		$a/2c$ ≈ 0.25	7075-T651 ALUMINUM ROOM TEMP., WT DIRECTION
cm	(INCH)		
1.91	(0.75)	●	
1.27	(0.50)	●	
0.61	(0.20)	○	
0.38	(0.15)	○	

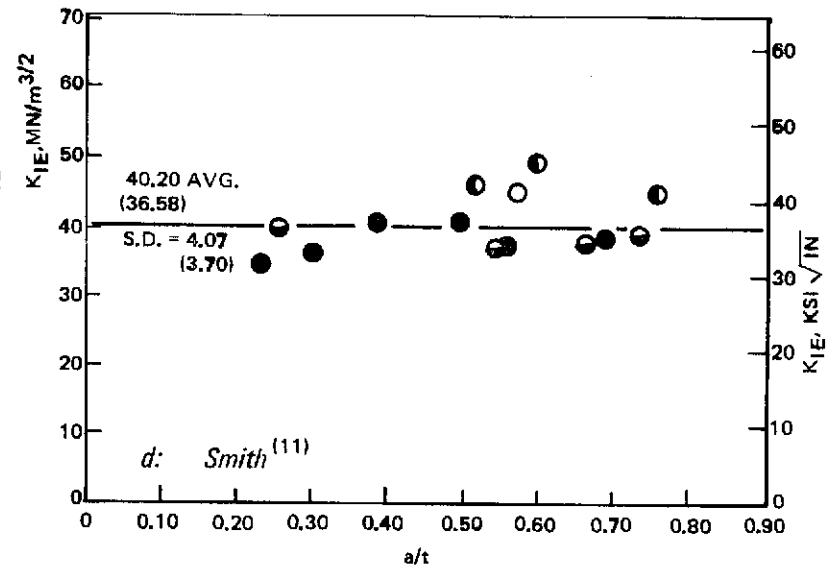
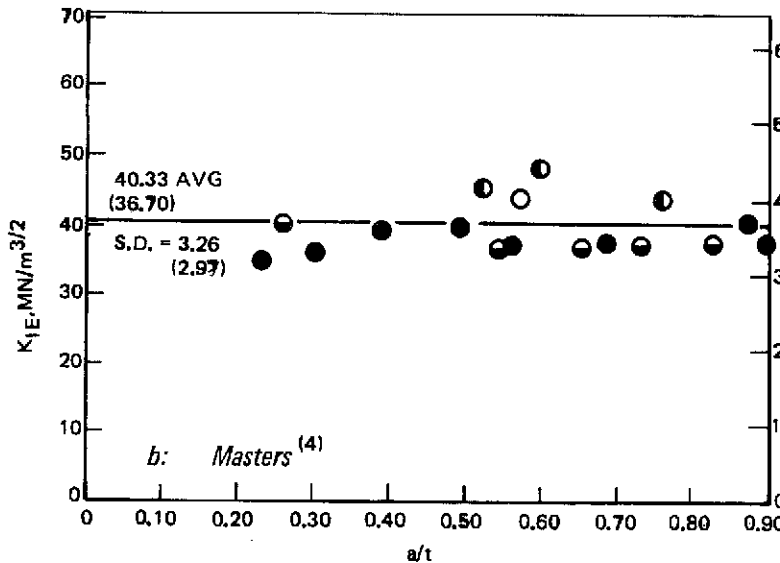
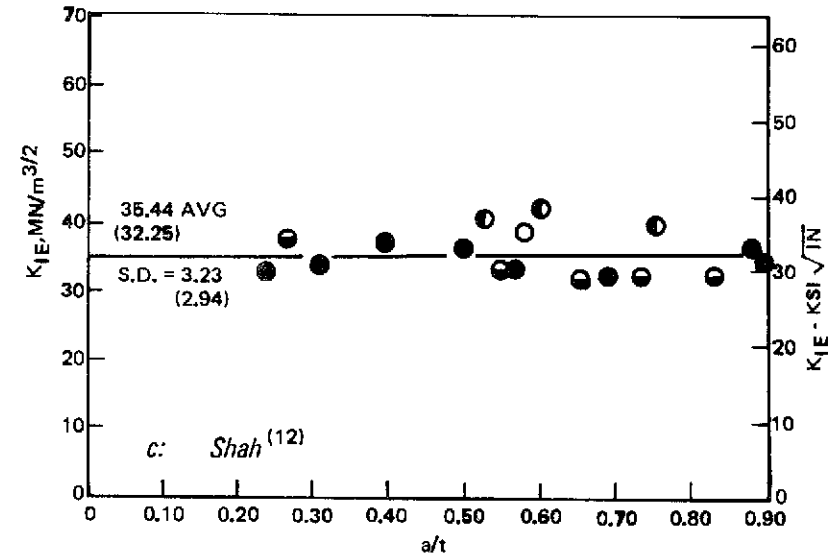
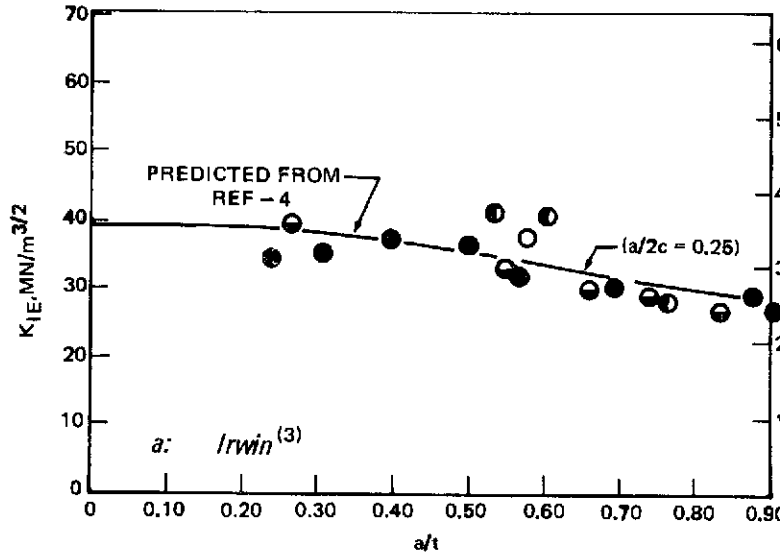


Figure 29: Comparison of Magnification Terms, 7075-T651 Aluminum at Room Temperature, WT Direction

THICKNESS cm (INCH)	a/2c ≈ 0.10	6Al-4V TITANIUM STA ROOM TEMP, RT DIRECTION
0.152 (0.060)	△	
0.318 (0.125)	▲	
0.508 (0.200)	▲	

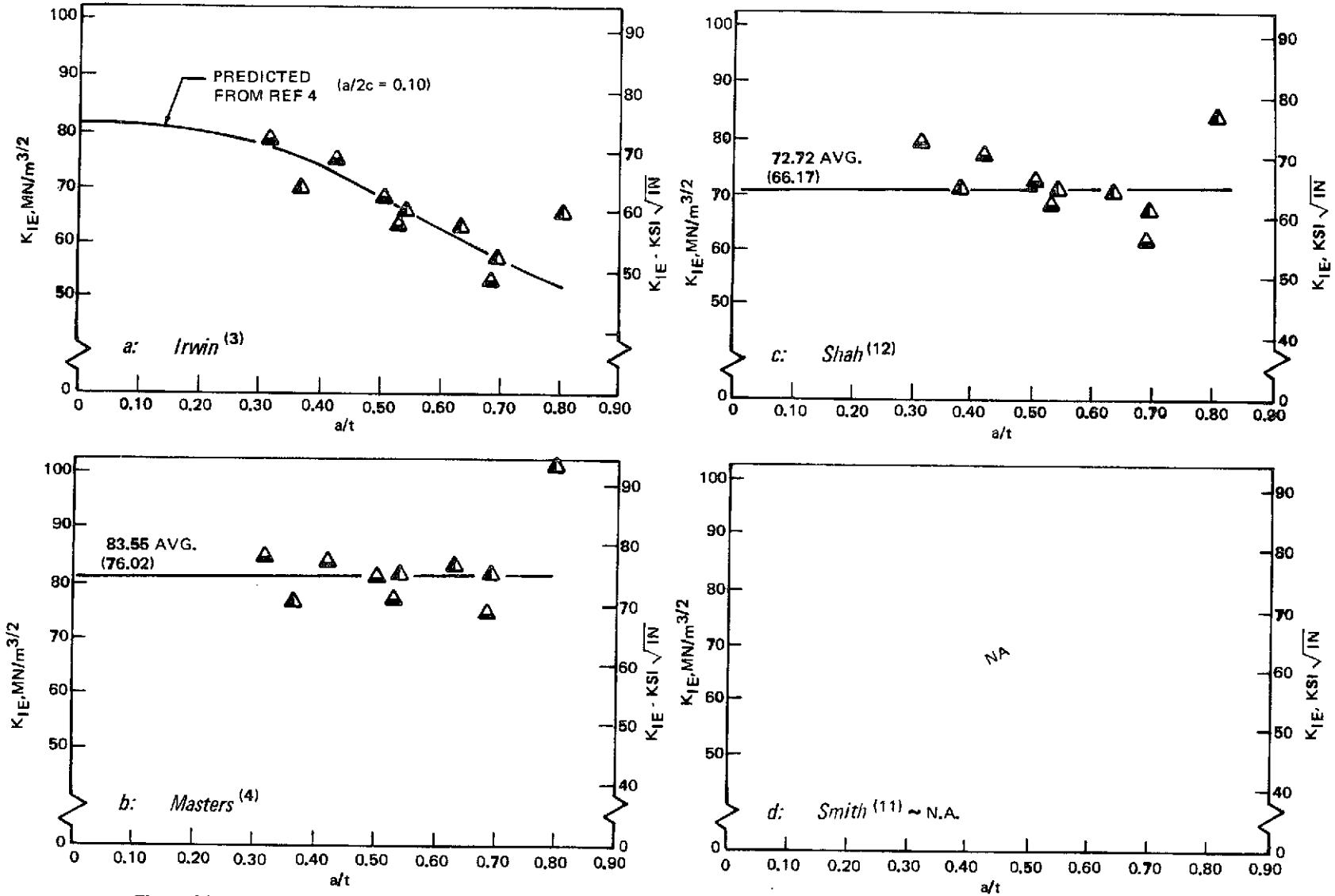


Figure 30: Comparison of Magnification Terms, 6Al-4V Titanium STA at Room Temperature, RT Direction, a/2c = 0.10

THICKNESS cm (INCH)	a/2c ≈ 0.25	6Al-4V TITANIUM STA ROOM TEMP, RT DIRECTION
0.318 (0.125)	□	
0.508 (0.200)	■	

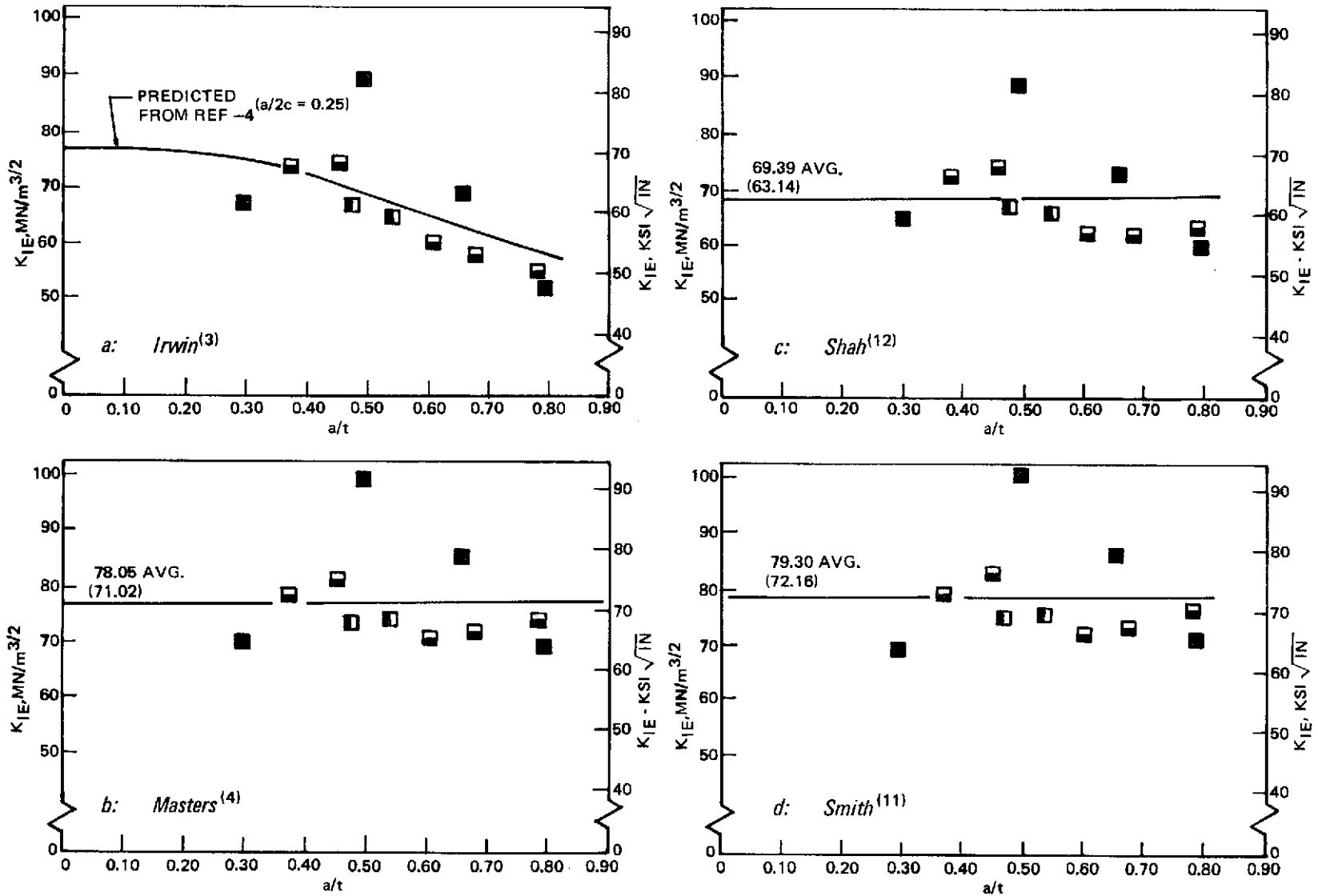


Figure 31: Comparison of Magnification Terms, 6Al-4V Titanium STA at Room Temperature, RT Direction, a/2c = 0.25

THICKNESS cm (INCH)	a/2c ≈ 0.40	6Al-4V TITANIUM STA ROOM TEMP, RT DIRECTION
0.318 (0.125) 0.508 (0.200)	● ●	

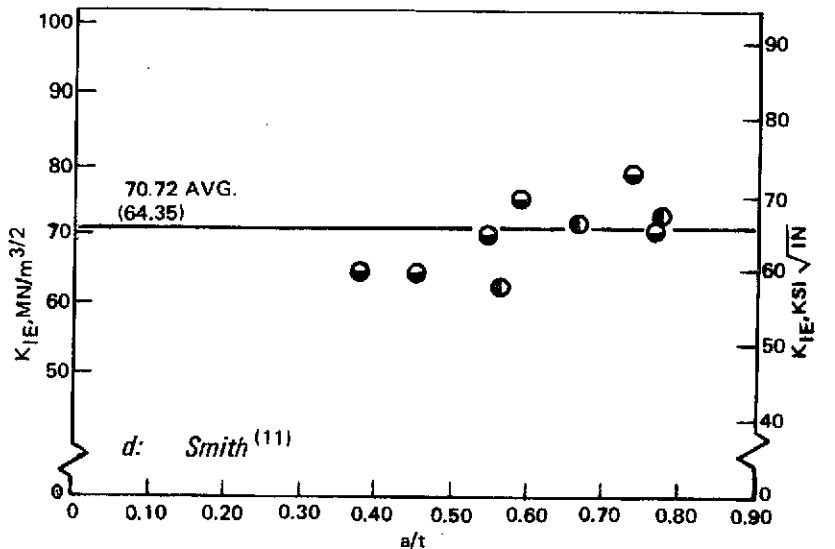
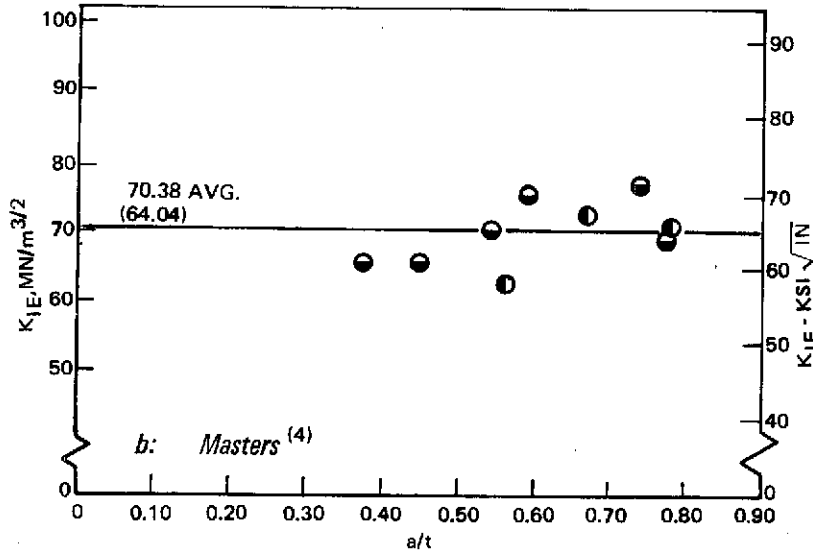
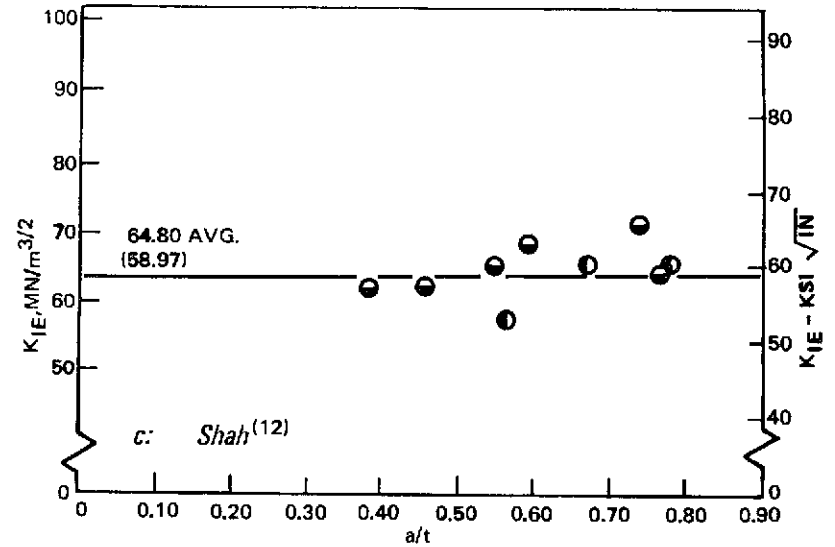
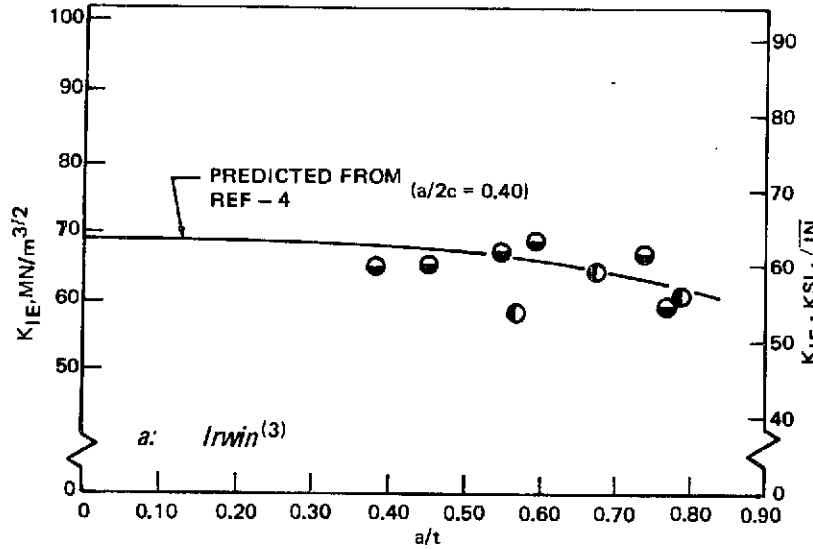


Figure 32: Comparison of Magnification Terms, 6Al-4V Titanium STA at Room Temperature, RT Direction; a/2c = 0.40

1-2

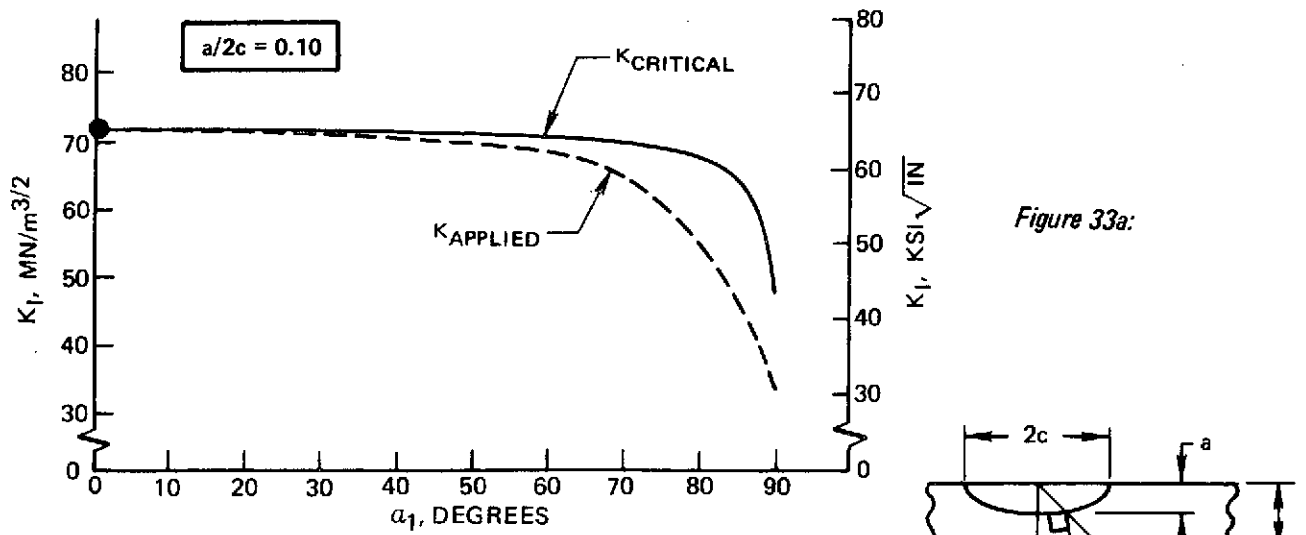


Figure 33a:

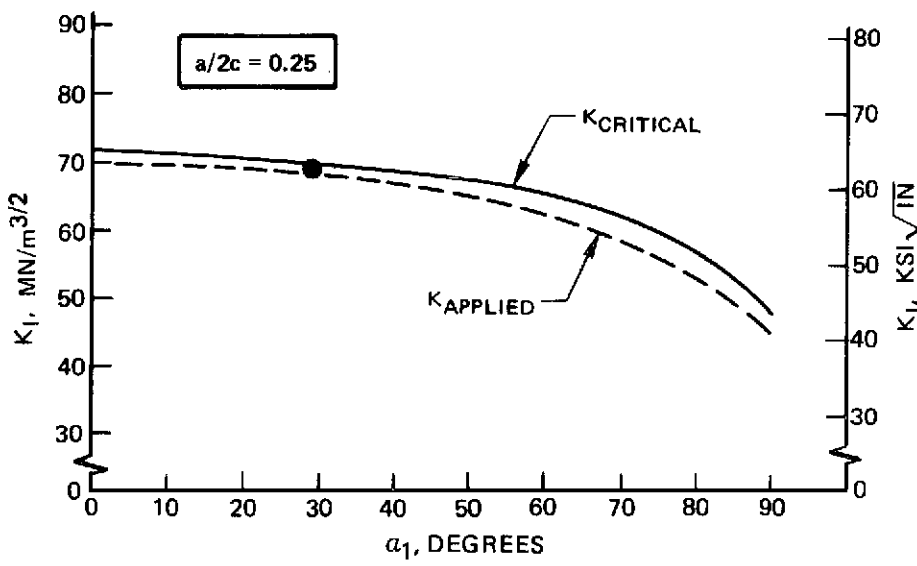


Figure 33b:

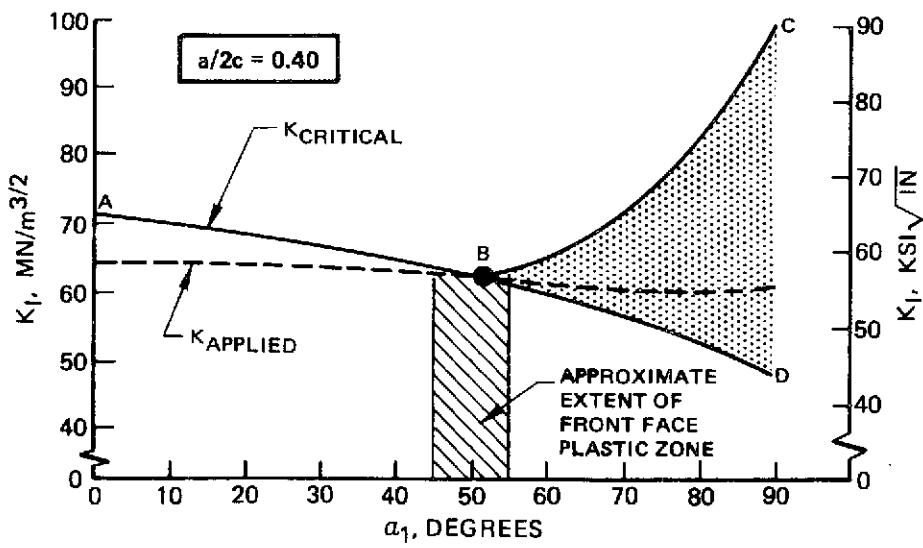


Figure 33c:

Figure 33: Variation of Applied and Critical Stress Intensity Around the Periphery of a Surface Flaw 6Al-4V Titanium STA at Room Temperature (RT Direction)

SYMBOL	σ / σ_{ys}					THICKNESS CM (INCH)
	0.53	0.66	0.79	0.92	0.99	
○	●	◐	◑	◒	◓	0.152 (0.060)
△	▲	▴	▵	▶	▷	0.315 (0.124)
□	■	◼	◽	◾	◿	0.538 (0.212)

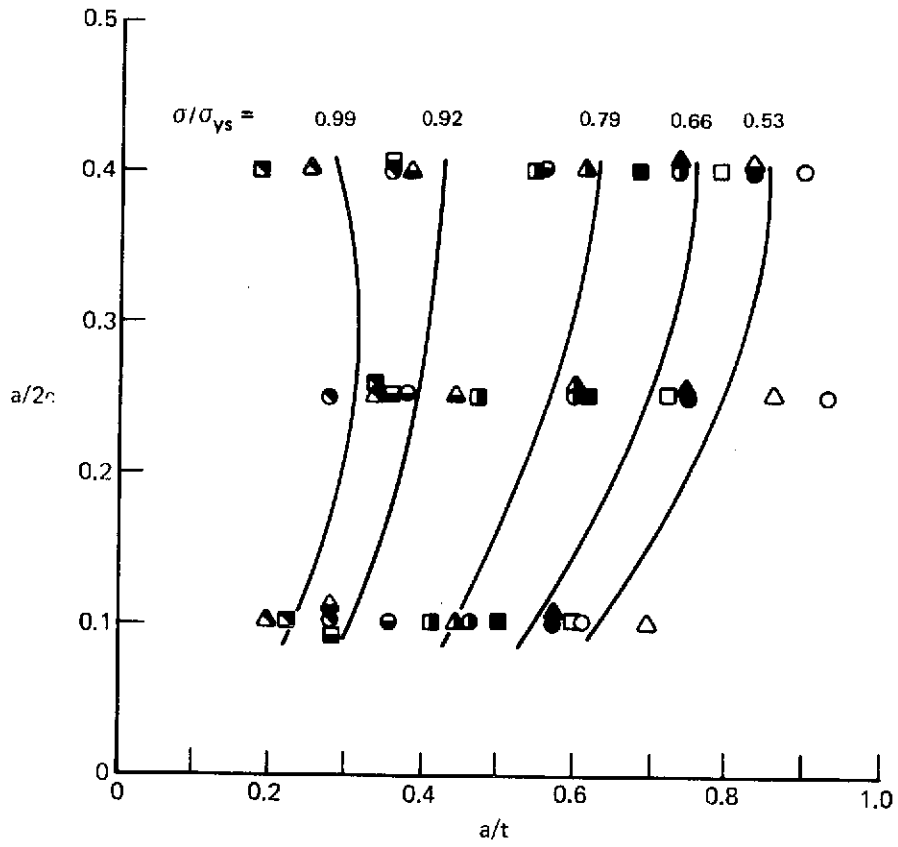


Figure 34: Dimpling Thresholds for 6Al-4V STA Titanium at Room Temperature (RT Direction)

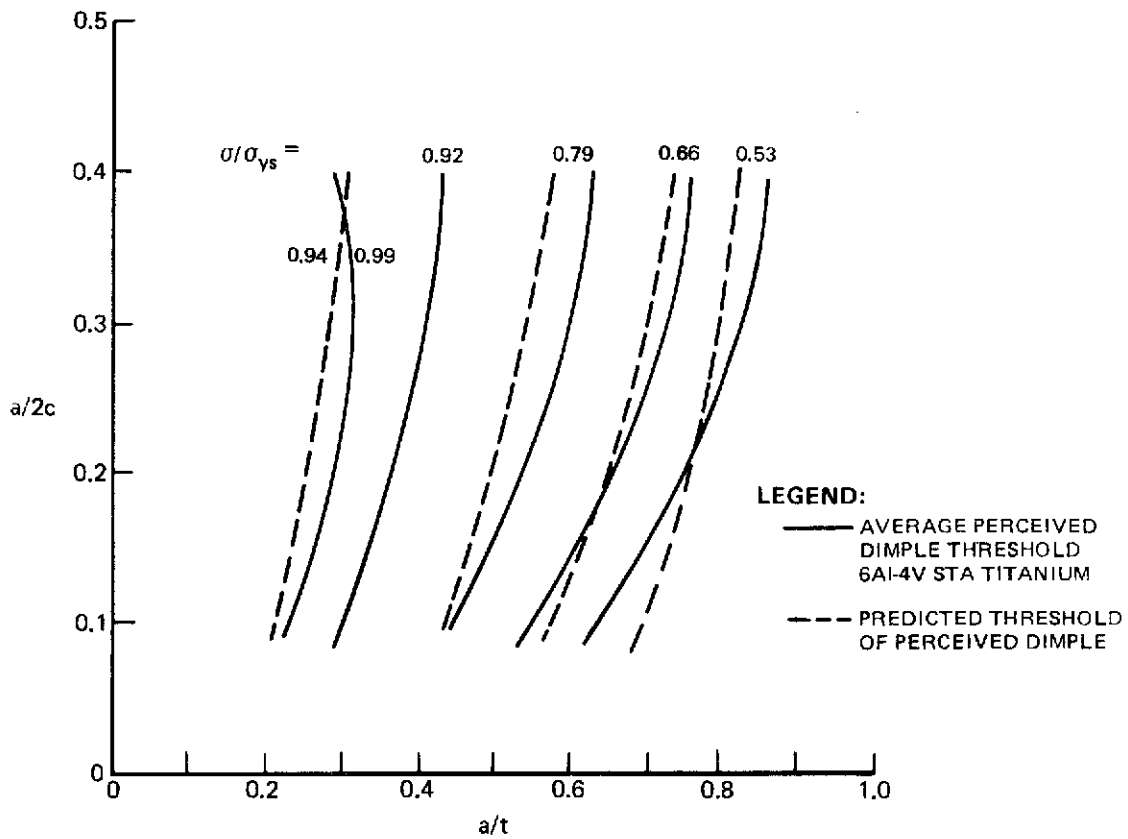


Figure 35: Comparison of Experimental and Theoretical Dimpling Threshold for 6Al-4V STA Titanium at Room Temperature RT Direction

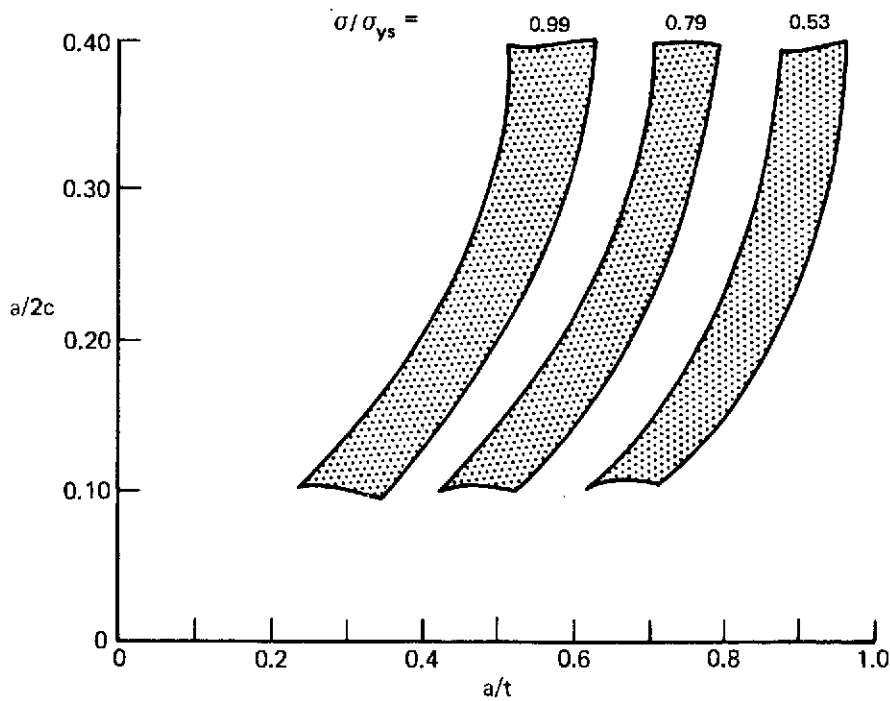


Figure 36: 2219-T87 Aluminum Dimpling Threshold at 78K (-320F), WT Direction

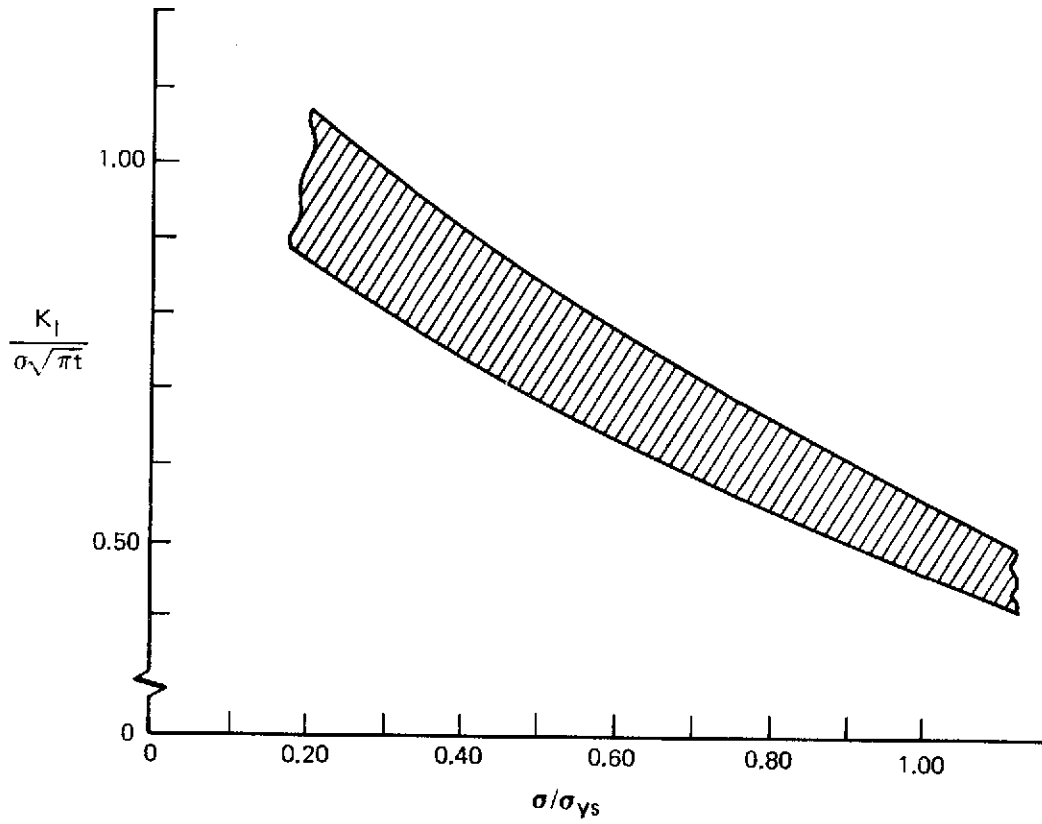


Figure 37: 6Al-4V STA Titanium Dimple Threshold at Room Temperature (RT Direction)

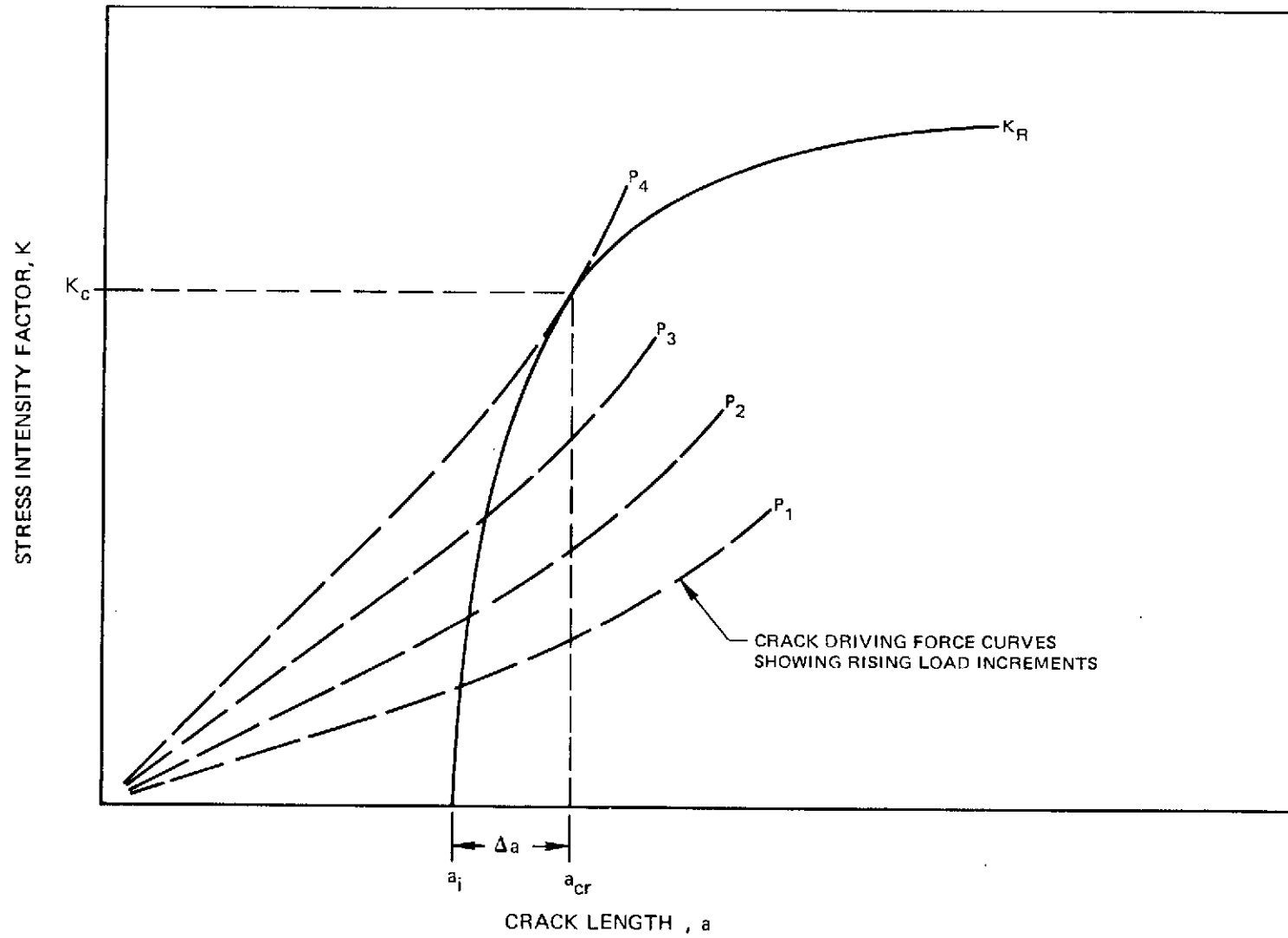


Figure 38: Crack-Growth-Resistance Curve and Crack Driving Force Curves for Load Controlled Test – Schematic

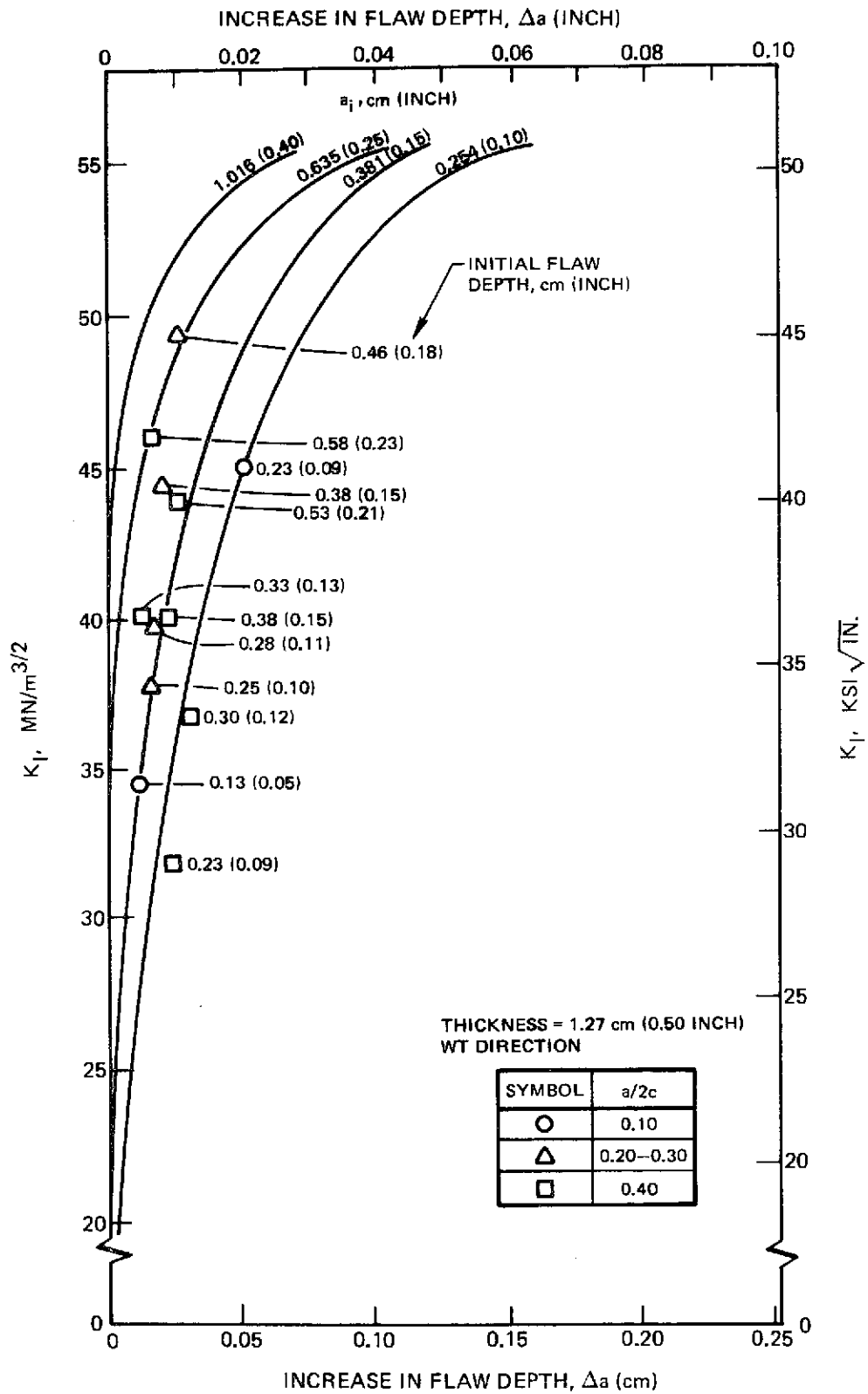


Figure 39: Stable Flaw Growth Measurements for 2219-T87 Base Metal at Room Temperature

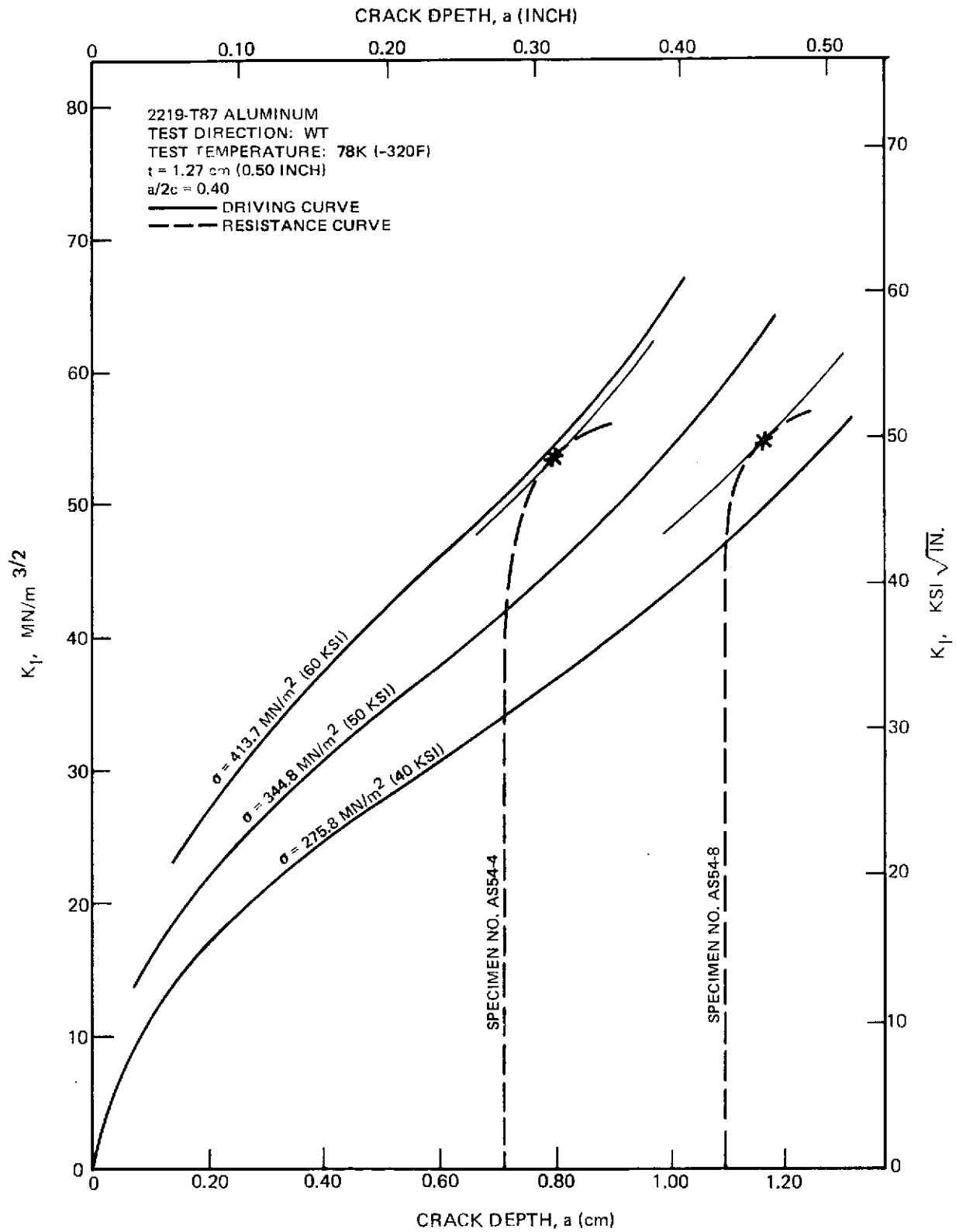


Figure 40: Crack Growth-Resistance and -Driving Curves for 2219-T87 Base Metal ($a/2c = 0.40$)

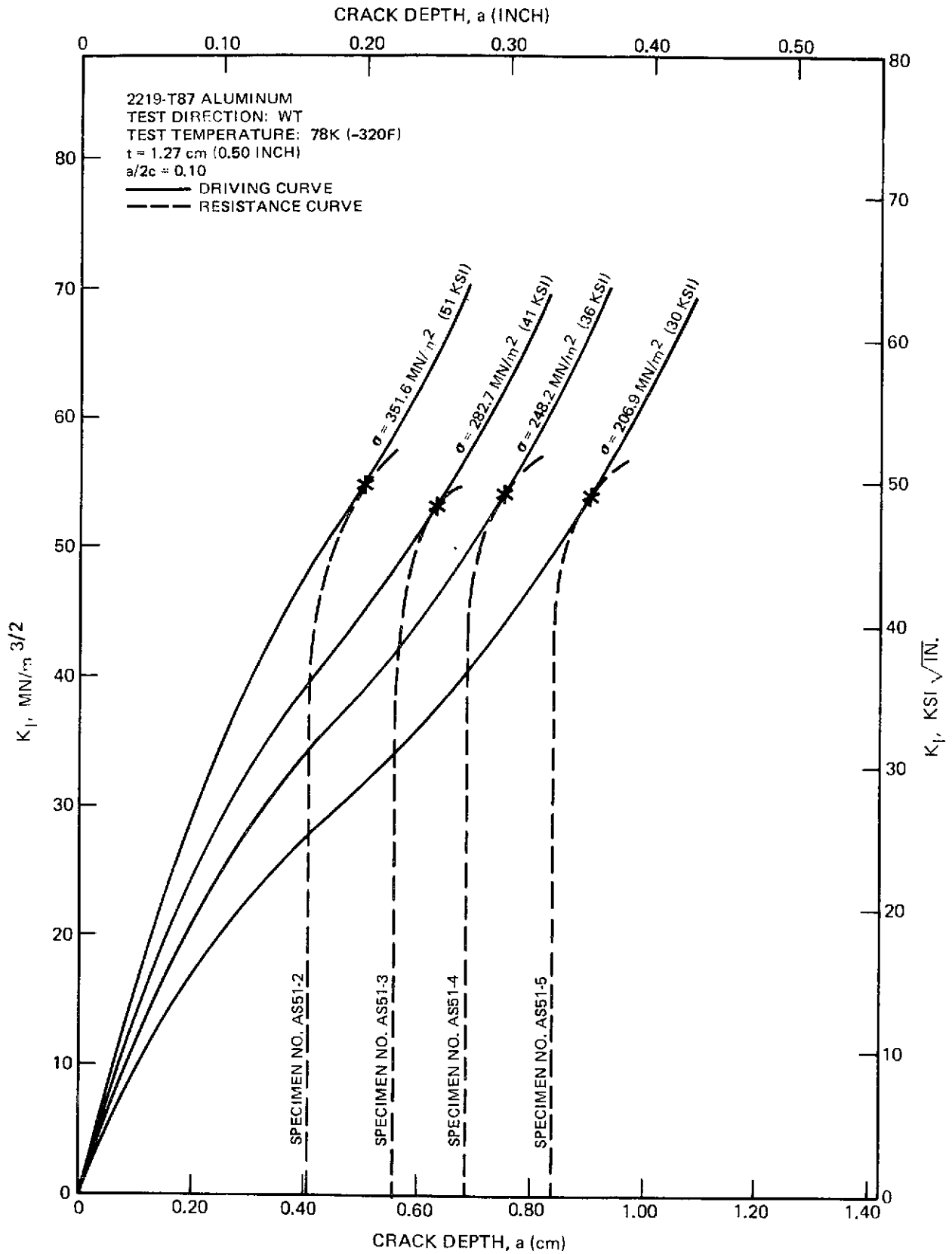


Figure 41: Crack Growth-Resistance and -Driving Curves for 2219-T87 Base Metal ($a/2c = 0.10$)

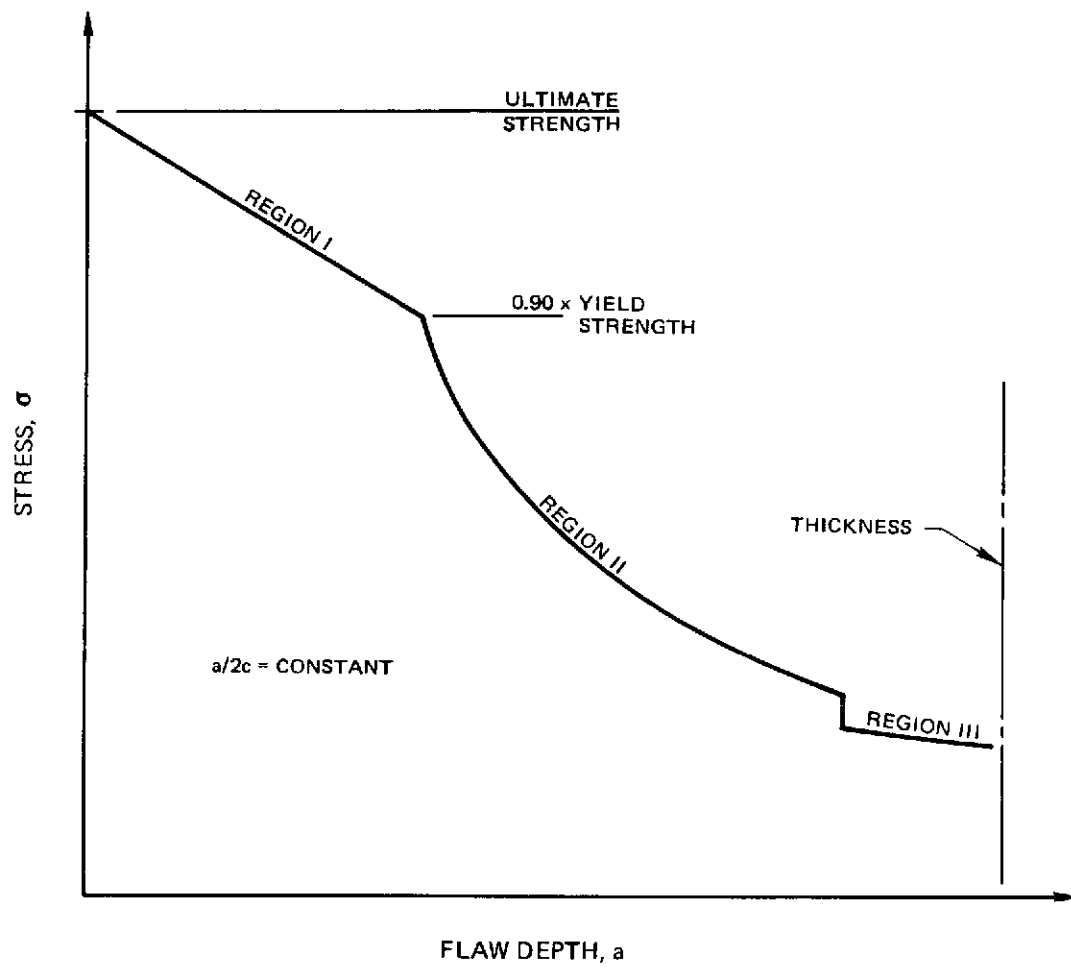


Figure 42: Generalized Stress Versus Flaw Depth Relationship for Static Fracture

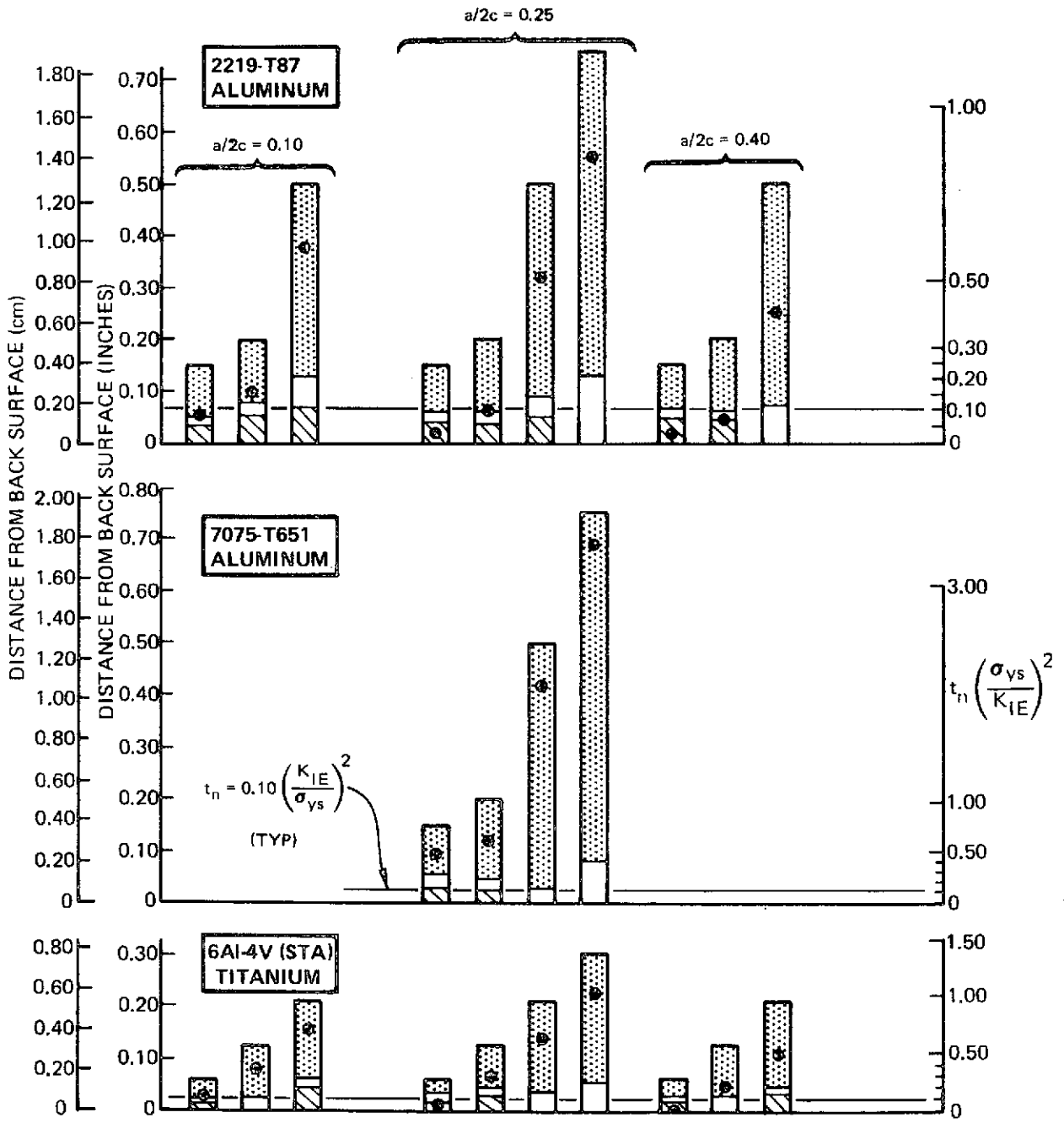
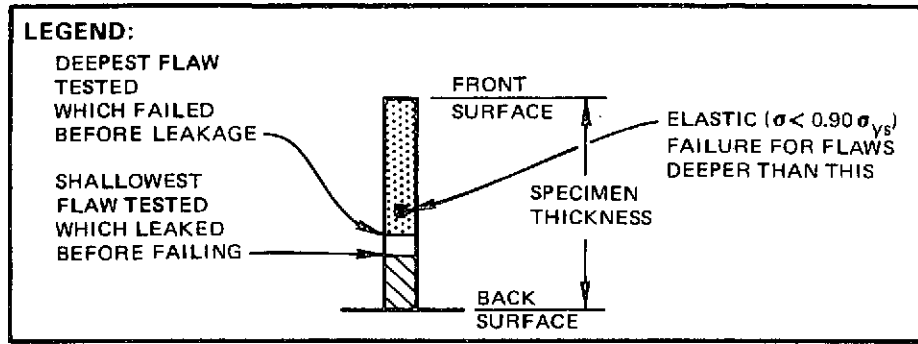


Figure 43: Summary of Static Fracture Test Results

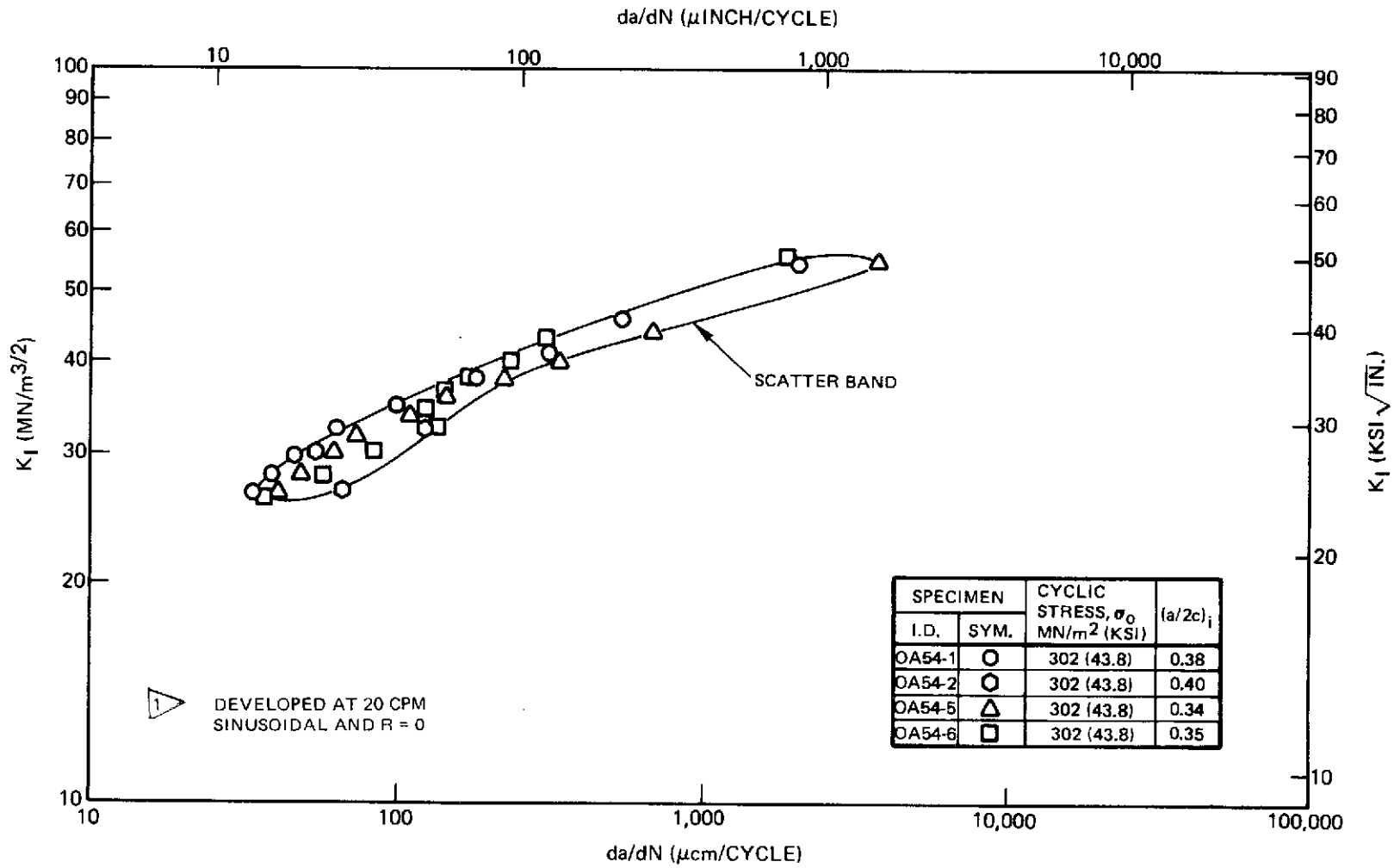


Figure 44: Cyclic Crack Growth Rates for 1.27 cm (0.50 Inch) Thick 2219-T87 Aluminum (WT Direction) at 78°K (-320°F) with $\sigma_0 = 0.67 \sigma_{ys}$ and $(a/2c)_i \cong 0.37$

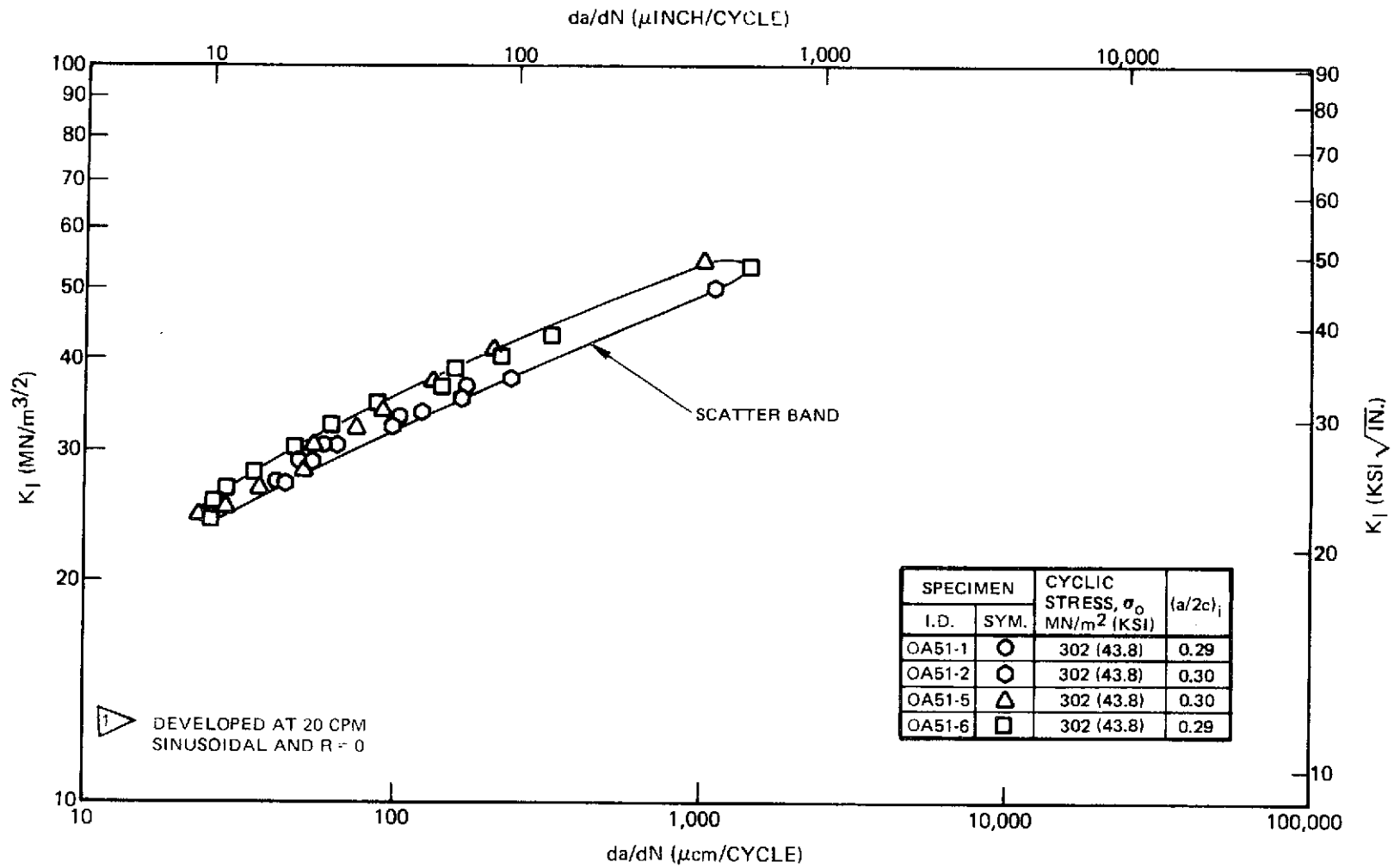


Figure 45: Cyclic Crack Growth Rates for 1.27 cm (0.50 Inch) Thick 2219-T87 Aluminum (WT Direction) at 78°K (-320°F) with $\sigma_0 = 0.67 \sigma_{YS}$ and $(a/2c)_i \cong 0.30$

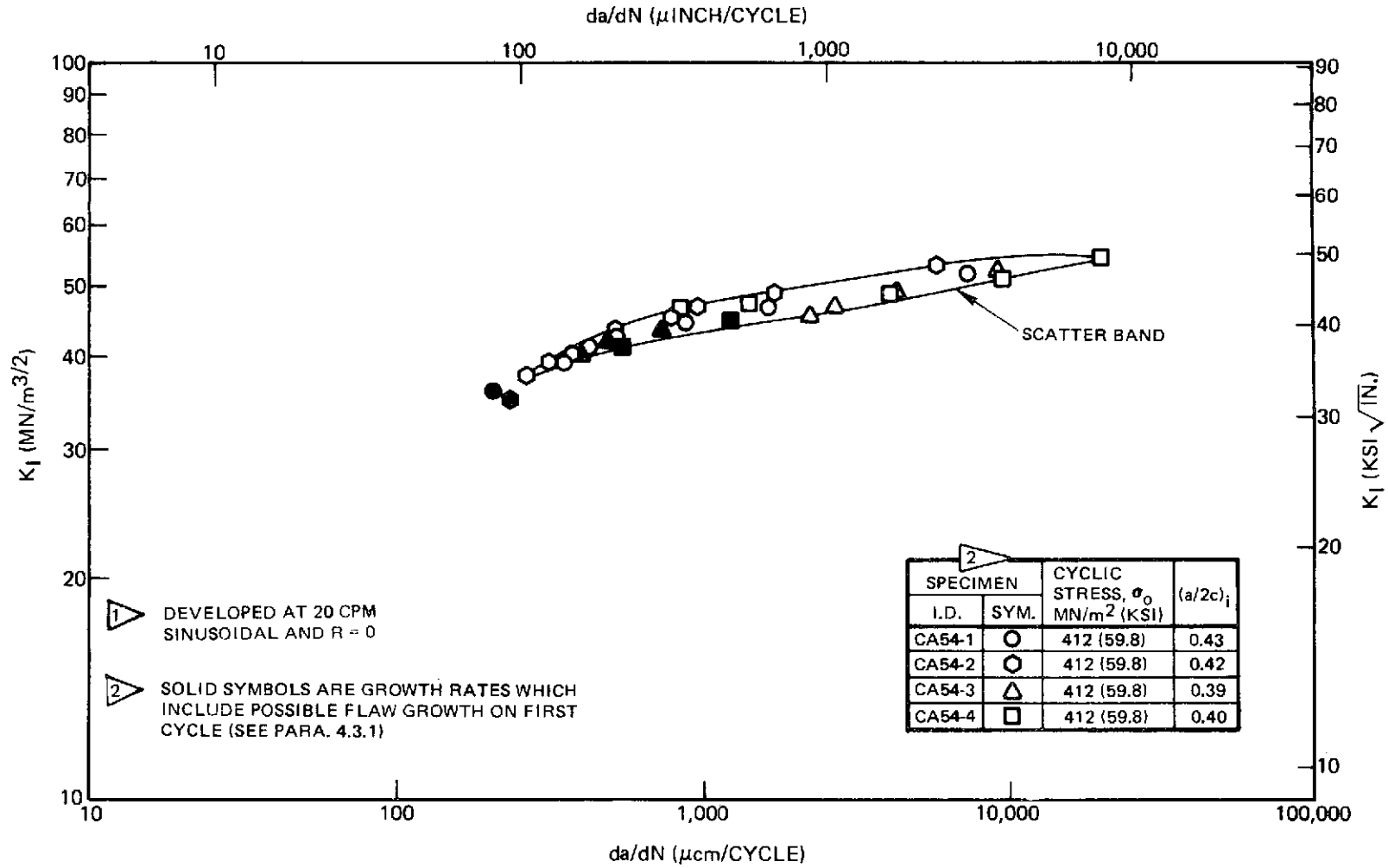
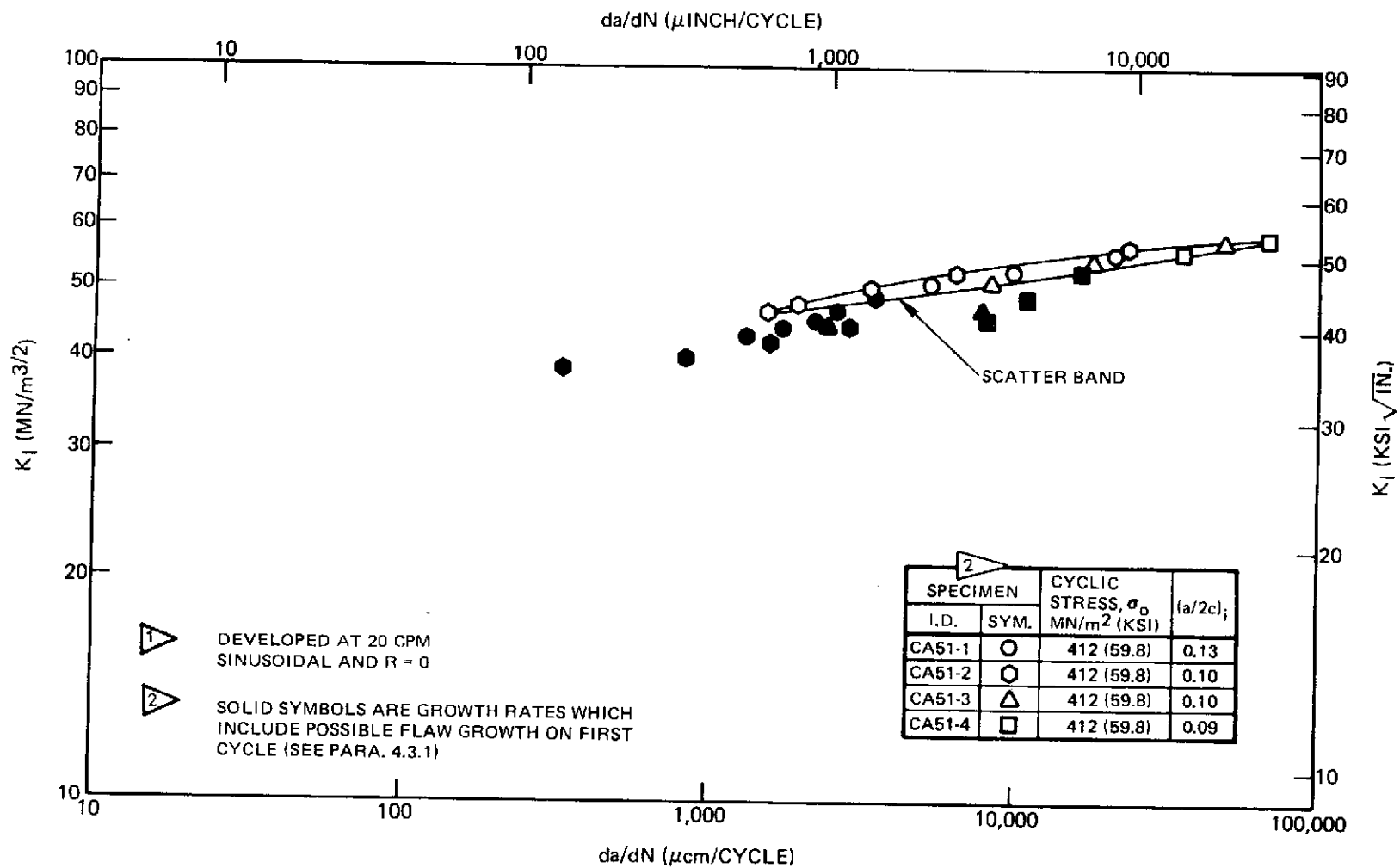
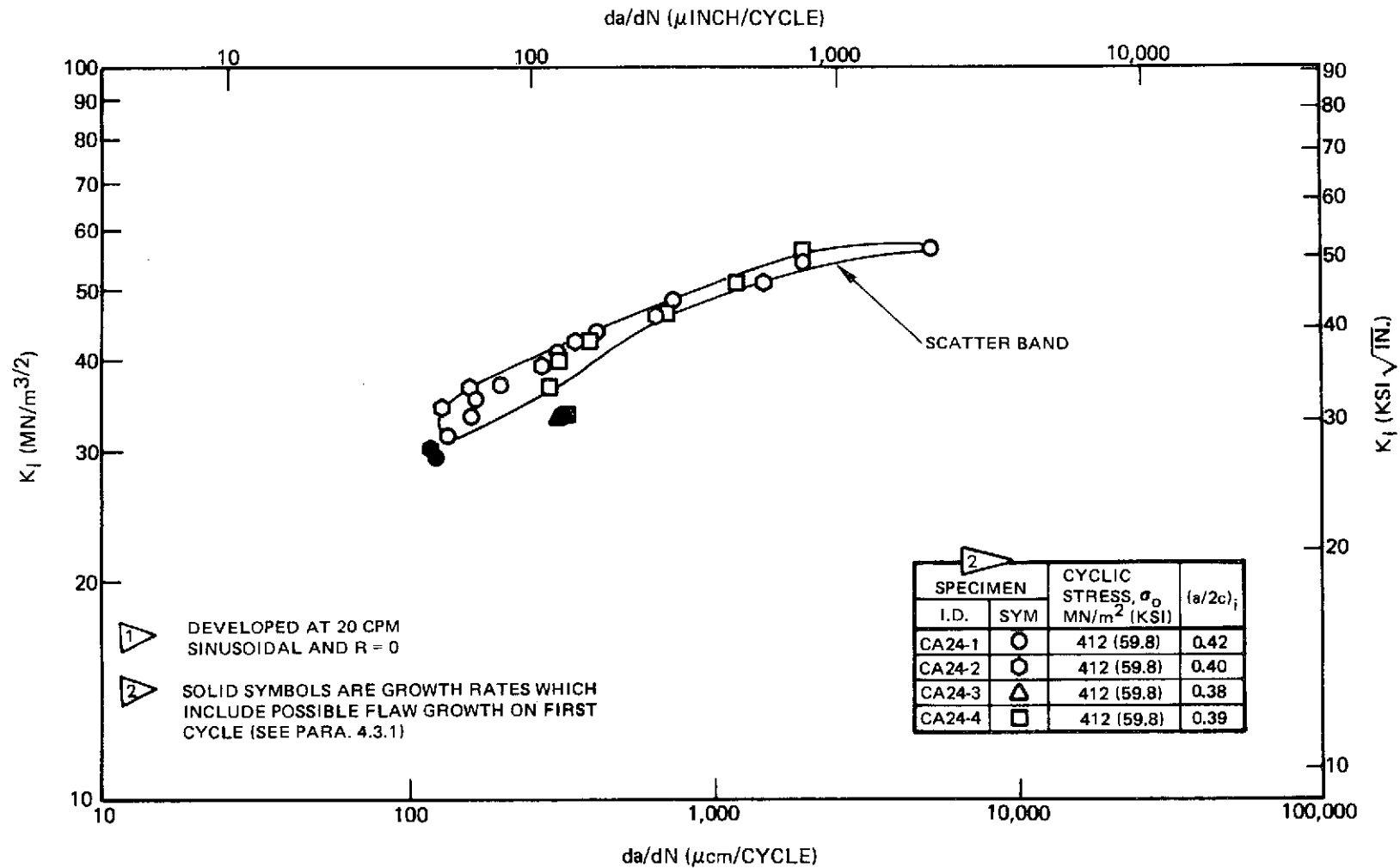


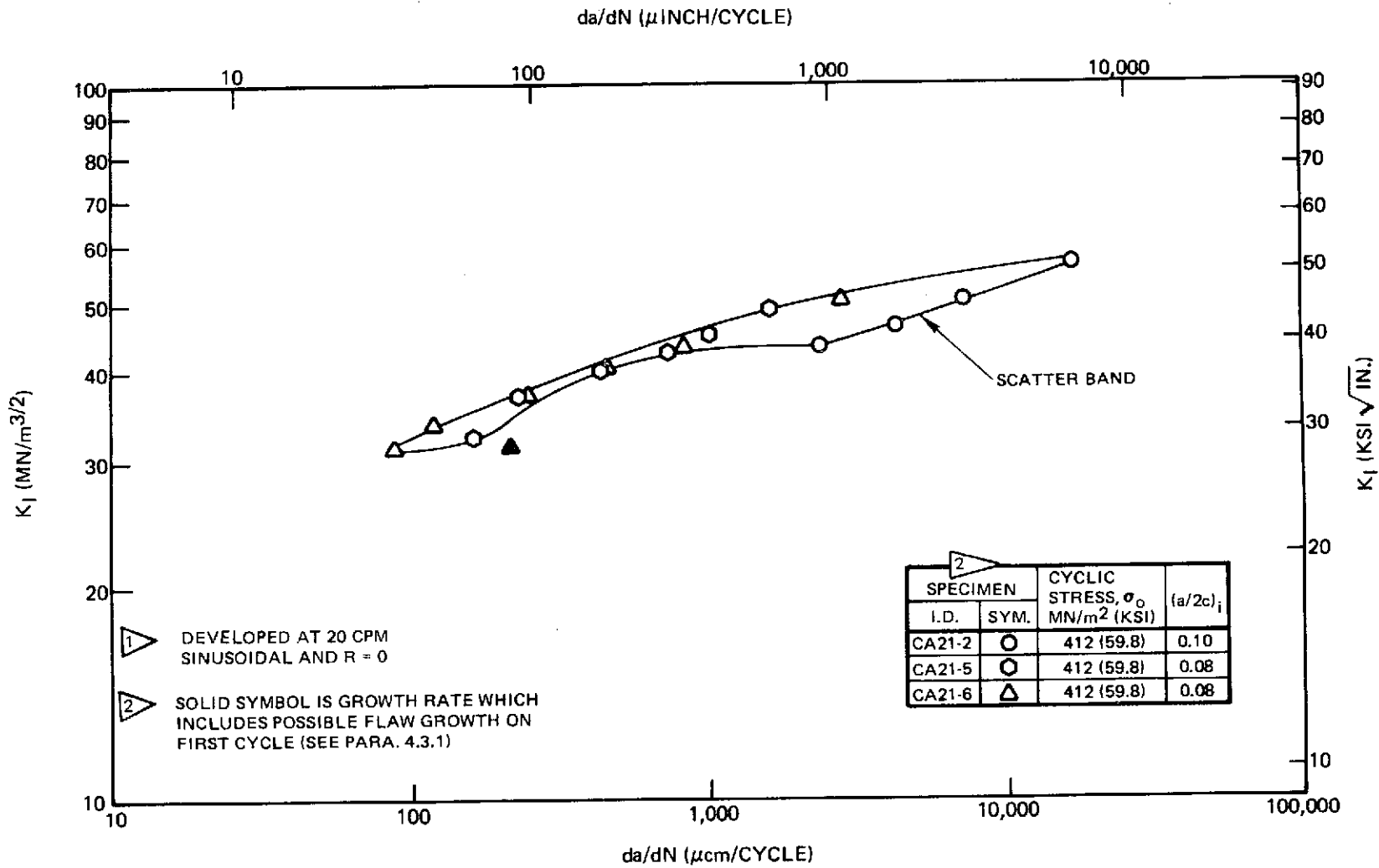
Figure 46: Cyclic Crack Growth Rates for 1.27 cm (0.50 Inch) Thick 2219-T87 Aluminum (WT Direction) at 78°K (-320°F) with $\sigma_0 = 0.91 \sigma_{ys}$ and $(a/2c)_i \cong 0.41$



1
 Figure 47: Cyclic Crack Growth Rates for 1.27 cm (0.50 Inch) Thick 2219-T87 Aluminum (WT Direction) at 78°K (-320°F) with $\sigma_0 = 0.91 \sigma_{YS}$ and $(a/2c)_i \cong 0.11$



1
Figure 48: Cyclic Crack Growth Rates for 0.51 cm (0.20 Inch) Thick 2219-T87 Aluminum (WT Direction) at 78°K (-320° F) with $\sigma_o = 0.91 \sigma_{ys}$ and $(a/2c)_i \cong 0.40$



1

Figure 49: Cyclic Crack Growth Rates for 0.51 cm (0.20 Inch) Thick 2219-T87 Aluminum (WT Direction) at 78°K (-320° F) with $\sigma_o = 0.91 \sigma_{YS}$ and $(a/2c)_i \cong 0.09$

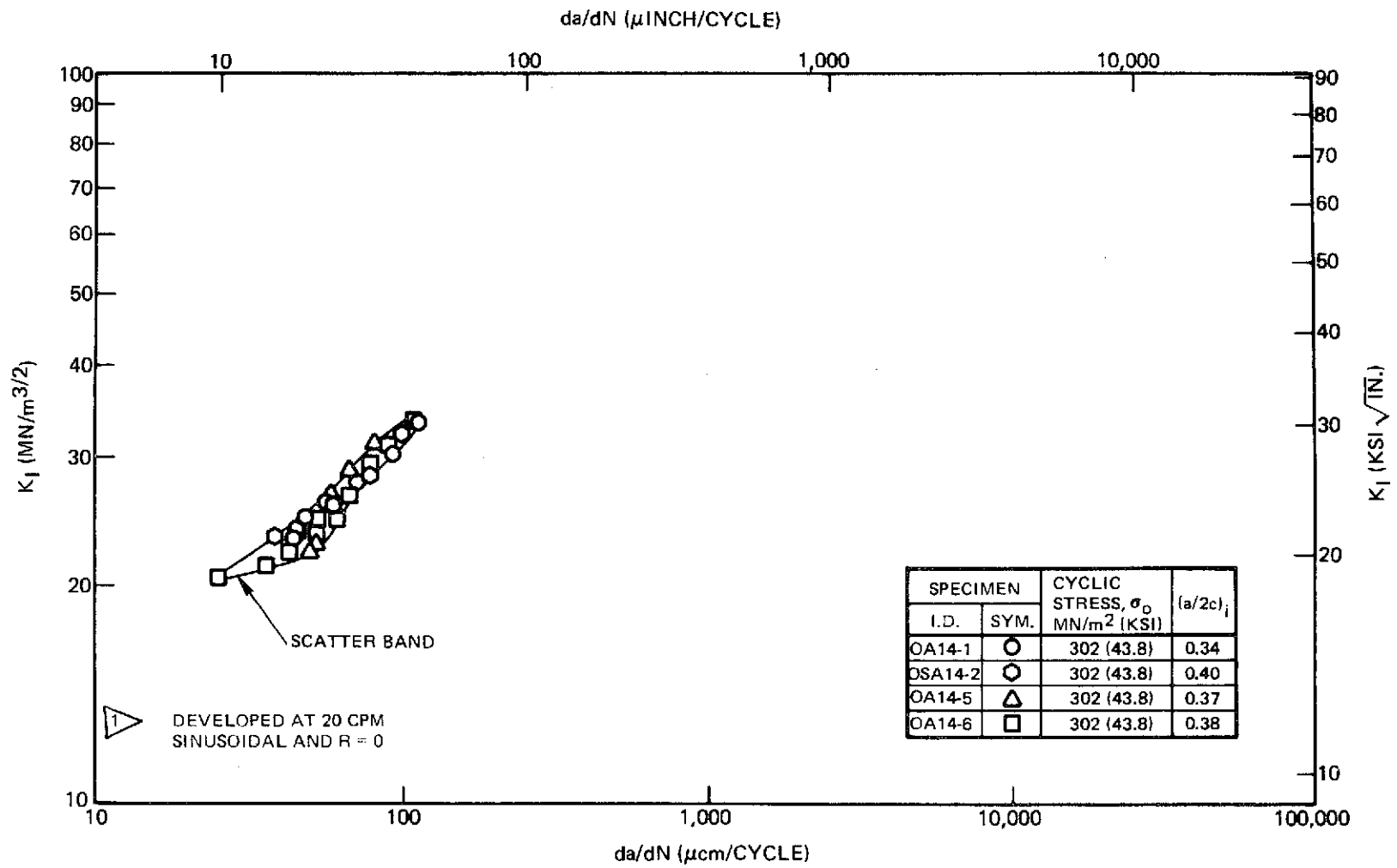


Figure 50: Cyclic Crack Growth Rates for 0.38 cm (0.15 Inch) Thick 2219-T87 Aluminum (WT Direction) at 78°K (-320° F) with $\sigma_0 = 0.67 \sigma_{YS}$ and $(1/2c)_i \cong 0.37$

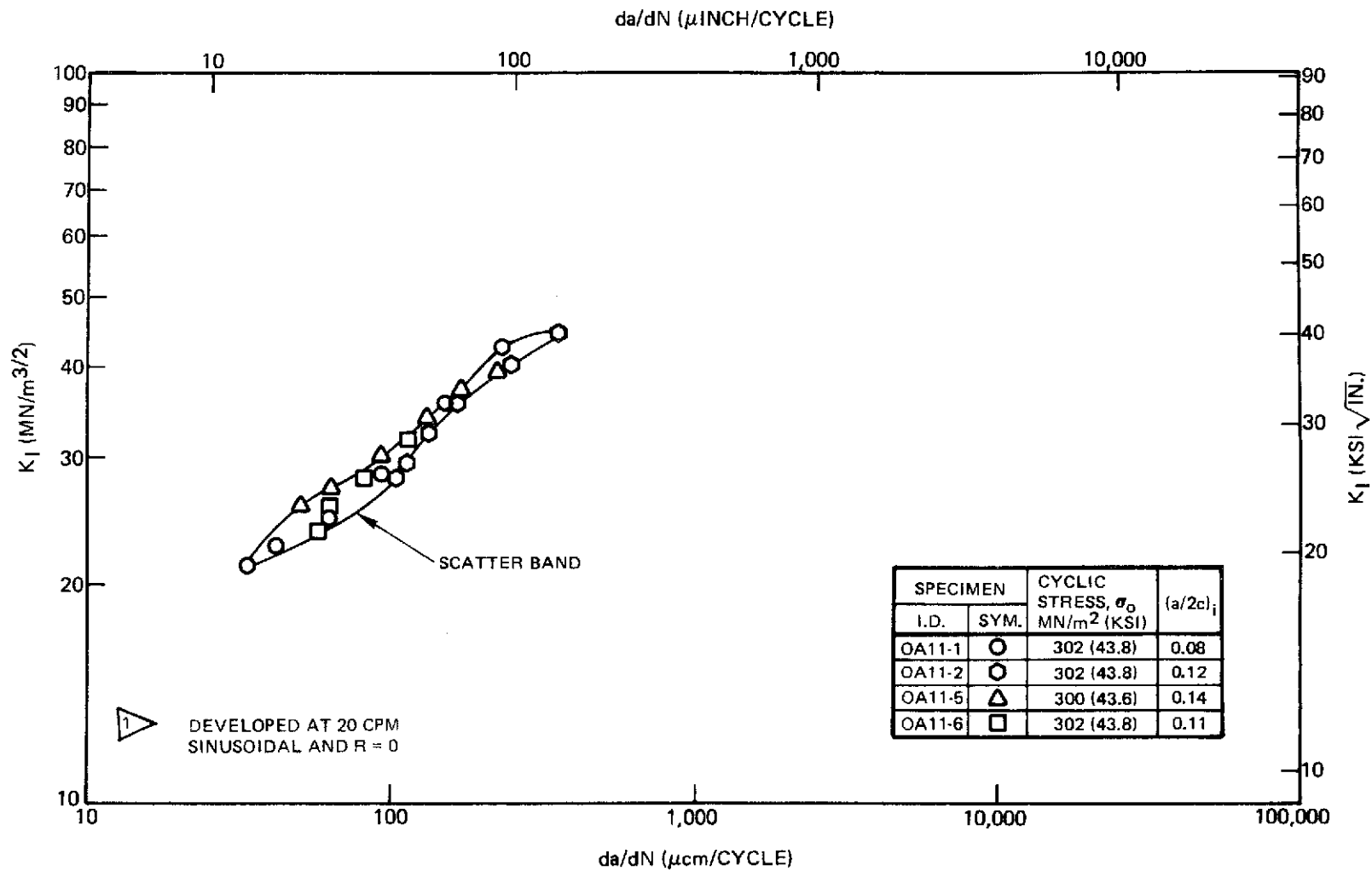
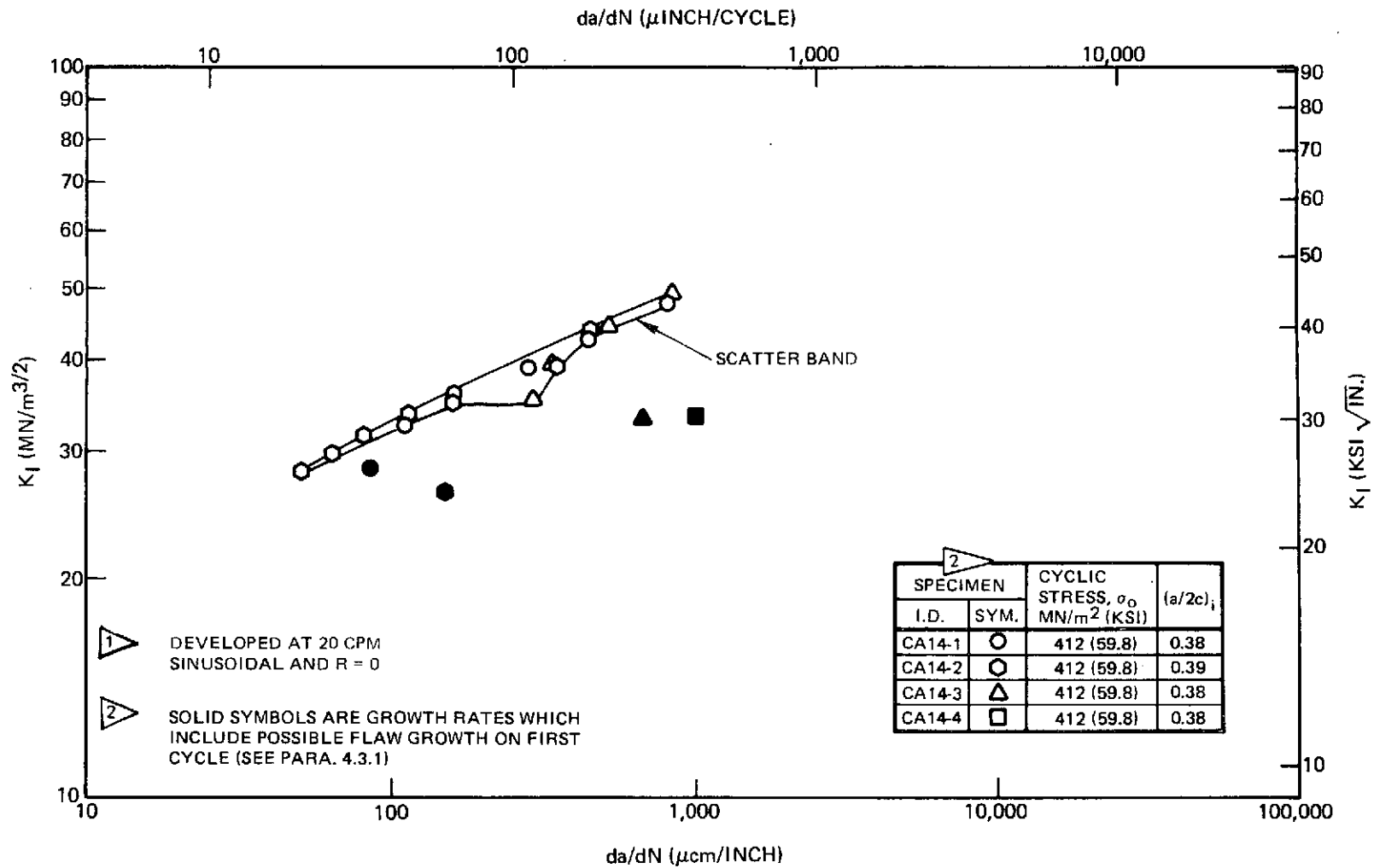
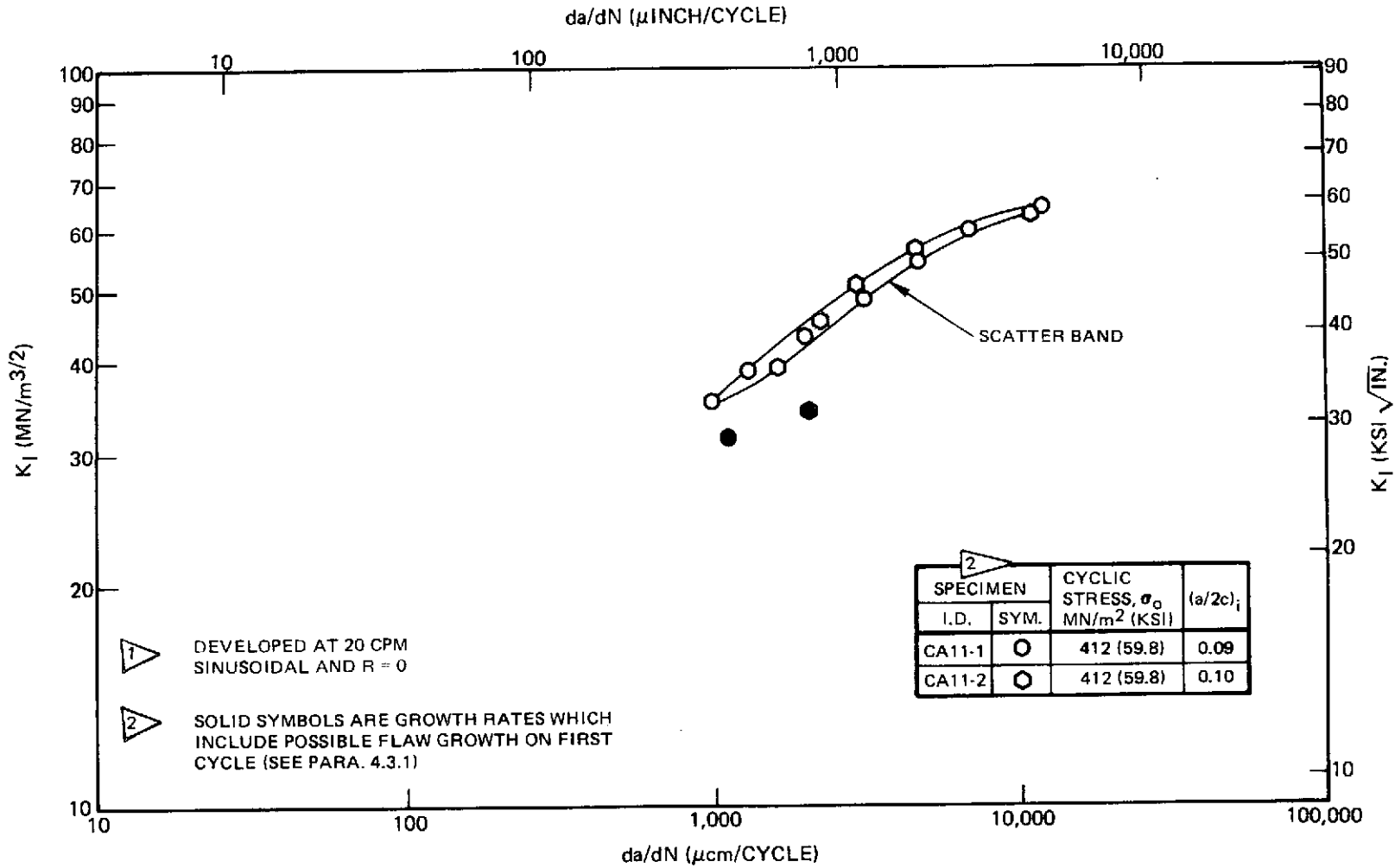


Figure 51: Cyclic Crack Growth Rates for 0.38 cm (0.15 Inch) Thick 2219-T87 Aluminum (WT Direction) at 78°K (-320°F) with $\sigma_o = 0.67 \sigma_{ys}$ and $(a/2c)_i \cong 0.11$

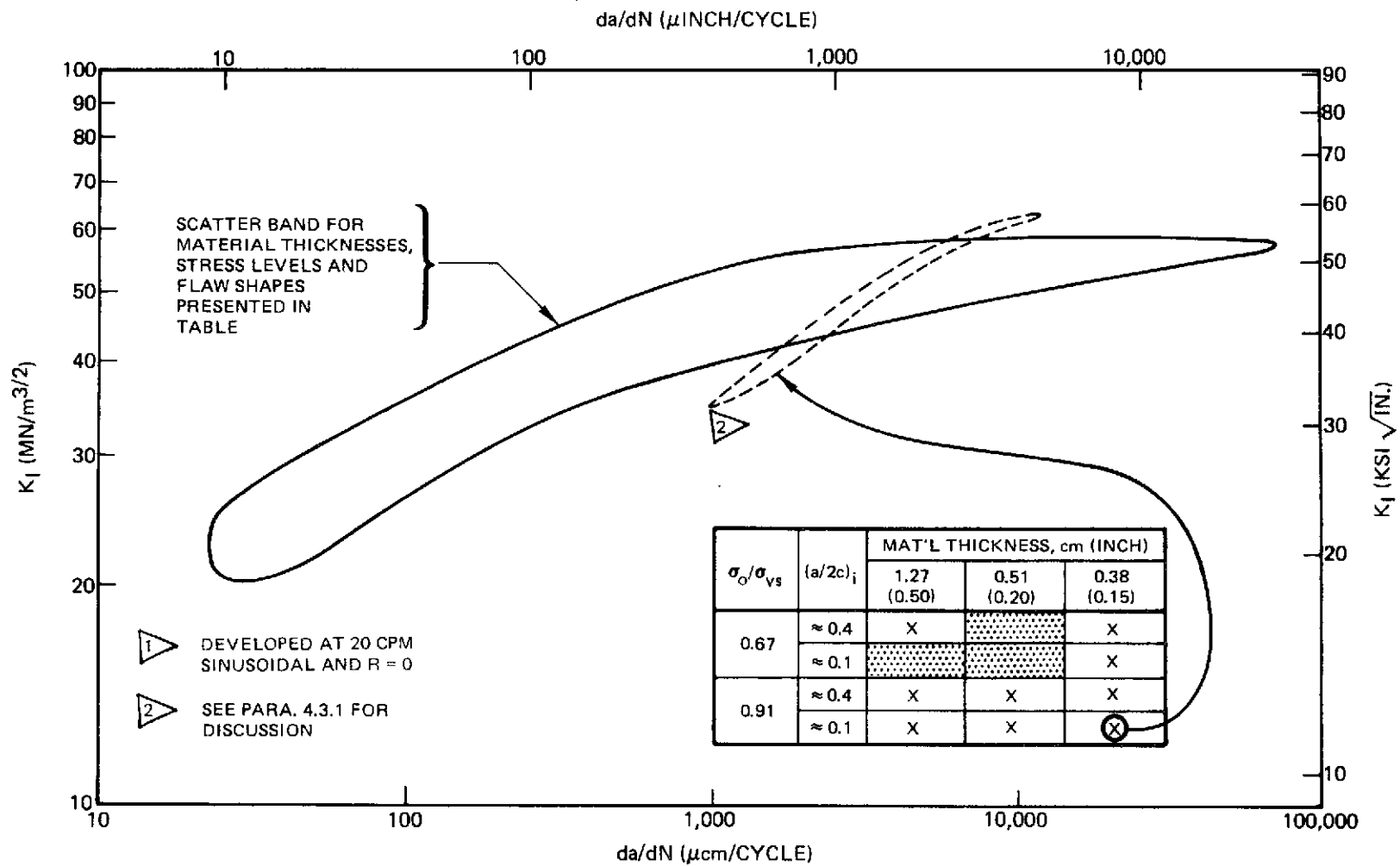


1
 Figure 52: Cyclic Crack Growth Rates for 0.38 cm (0.15 Inch) Thick 2219-T87 Aluminum (WT Direction) at 78°K (-320° F) with $\sigma_D = 0.91 \sigma_{YS}$ and $(a/2c)_i \cong 0.38$



1

Figure 53: Cyclic Crack Growth Rates for 0.38 cm (0.15 Inch) Thick 2219-T87 Aluminum (WT Direction) at 78°K (-320°F) with $\sigma_o = 0.91 \sigma_{YS}$ and $(a/2c)_i \cong 0.10$



1

Figure 54: Summary of Baseline Cyclic Crack Growth Rates for 2219-T87 Aluminum (WT Direction) at 78°K (-320°F)

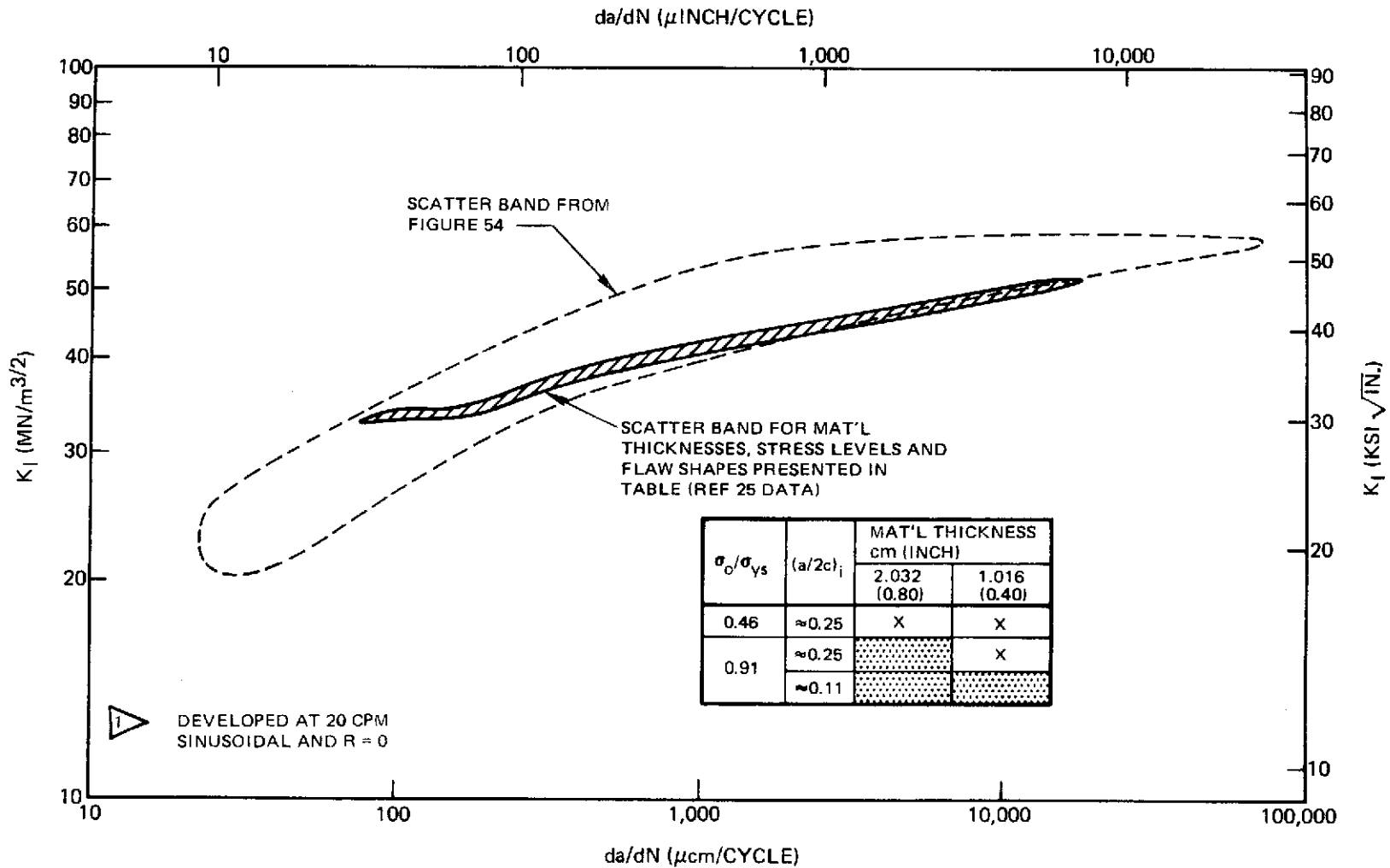


Figure 55: Comparison of 2219-T87 Aluminum (WT Direction) Fatigue Crack Growth Rate Data at 78°K (-320°F)

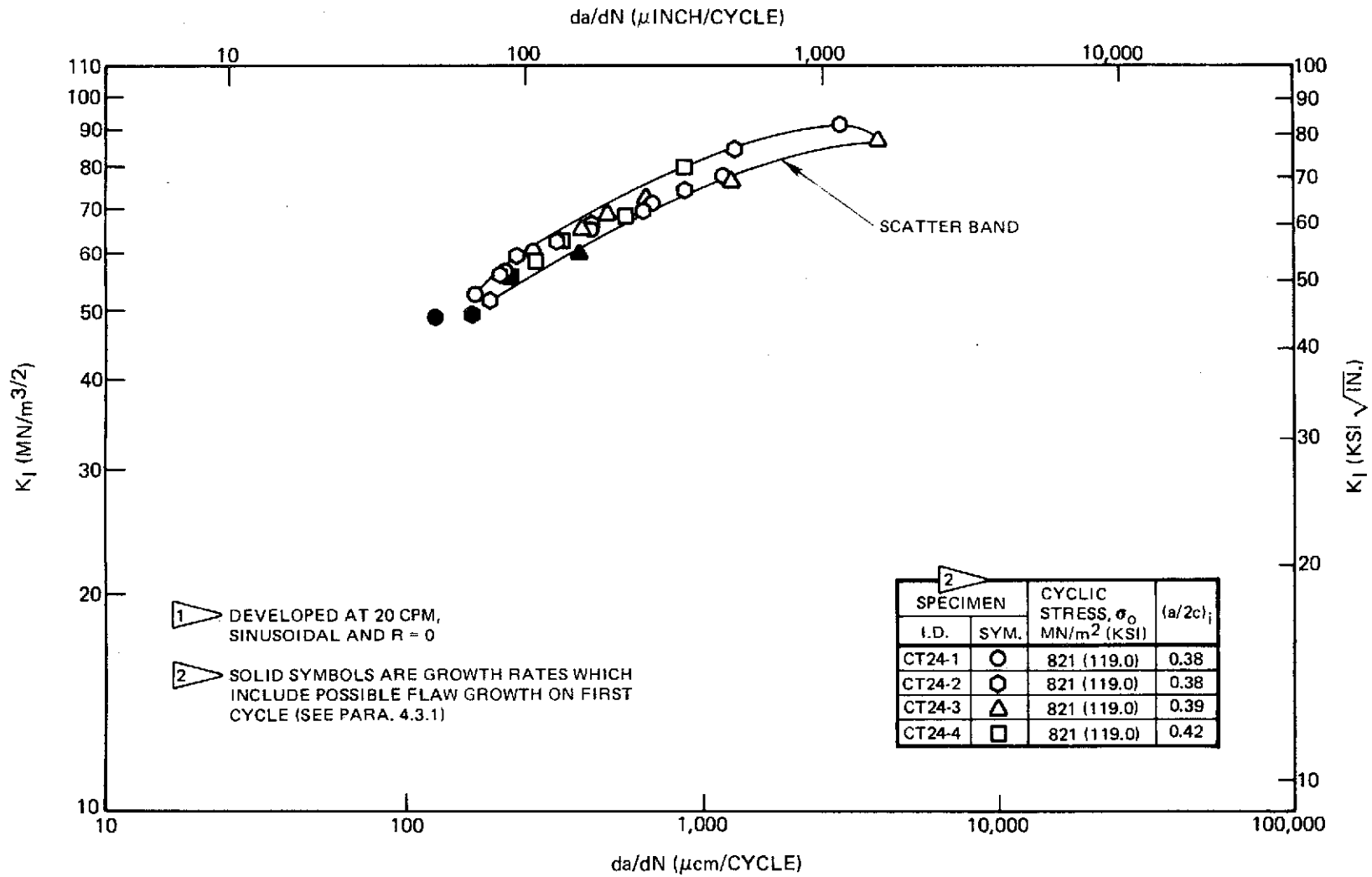


Figure 56: Cyclic Crack Growth Rates ¹ for 0.54 cm (0.21 Inch) Thick 6Al-4V STA Titanium (RT Direction) at 295°K (72° F) in Air with $\sigma_D = 0.77 \sigma_{YS}$ and (a/2c)_i \cong 0.39

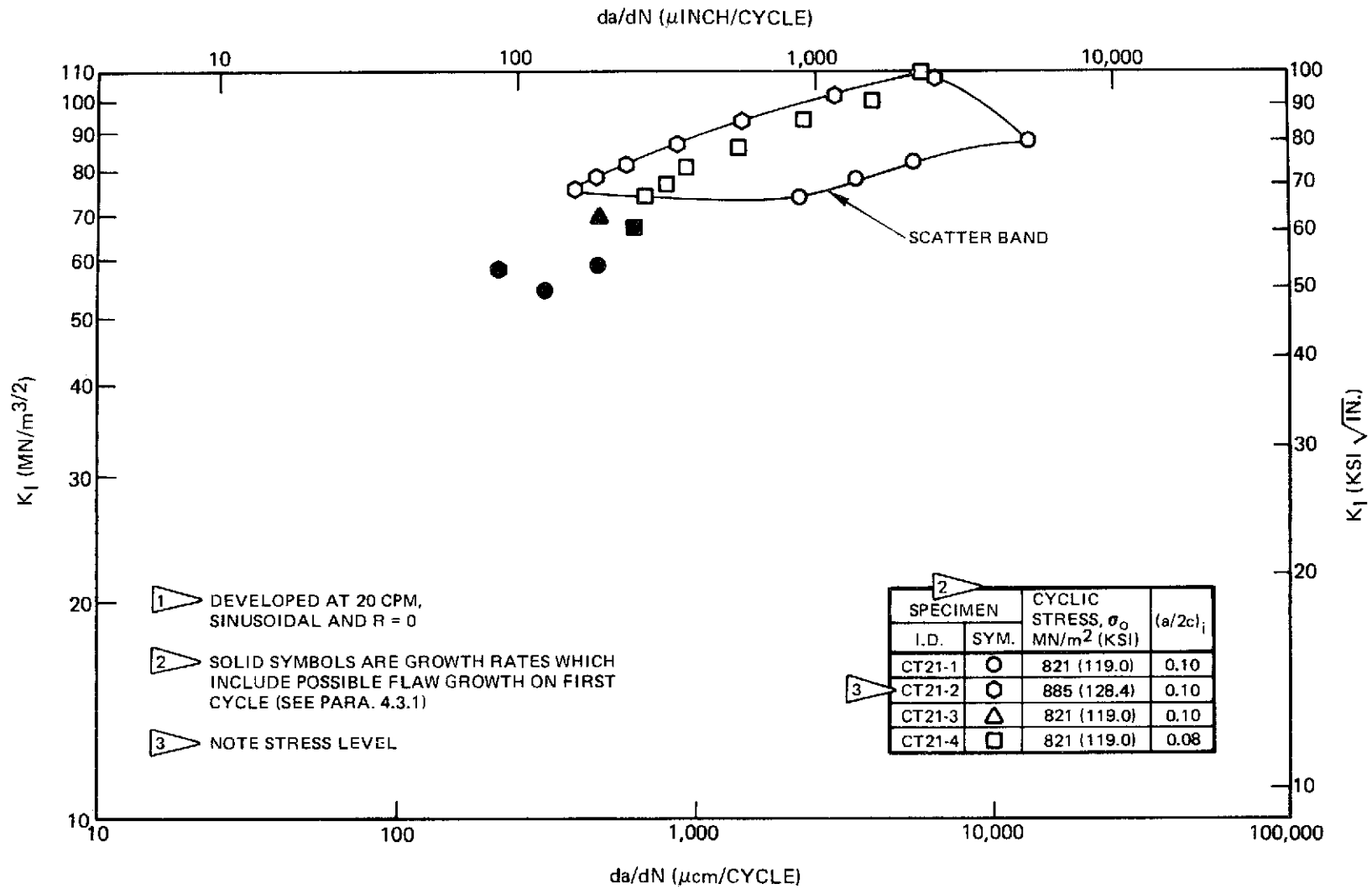


Figure 57: Cyclic Crack Growth Rates ¹ for 0.54 cm (0.21 Inch) Thick 6Al-4V STA Titanium (RT Direction) at 295°K (72° F) in Air with $\sigma_o = 0.77 \sigma_{ys}$ and $(a/2c)_i \cong 0.10$

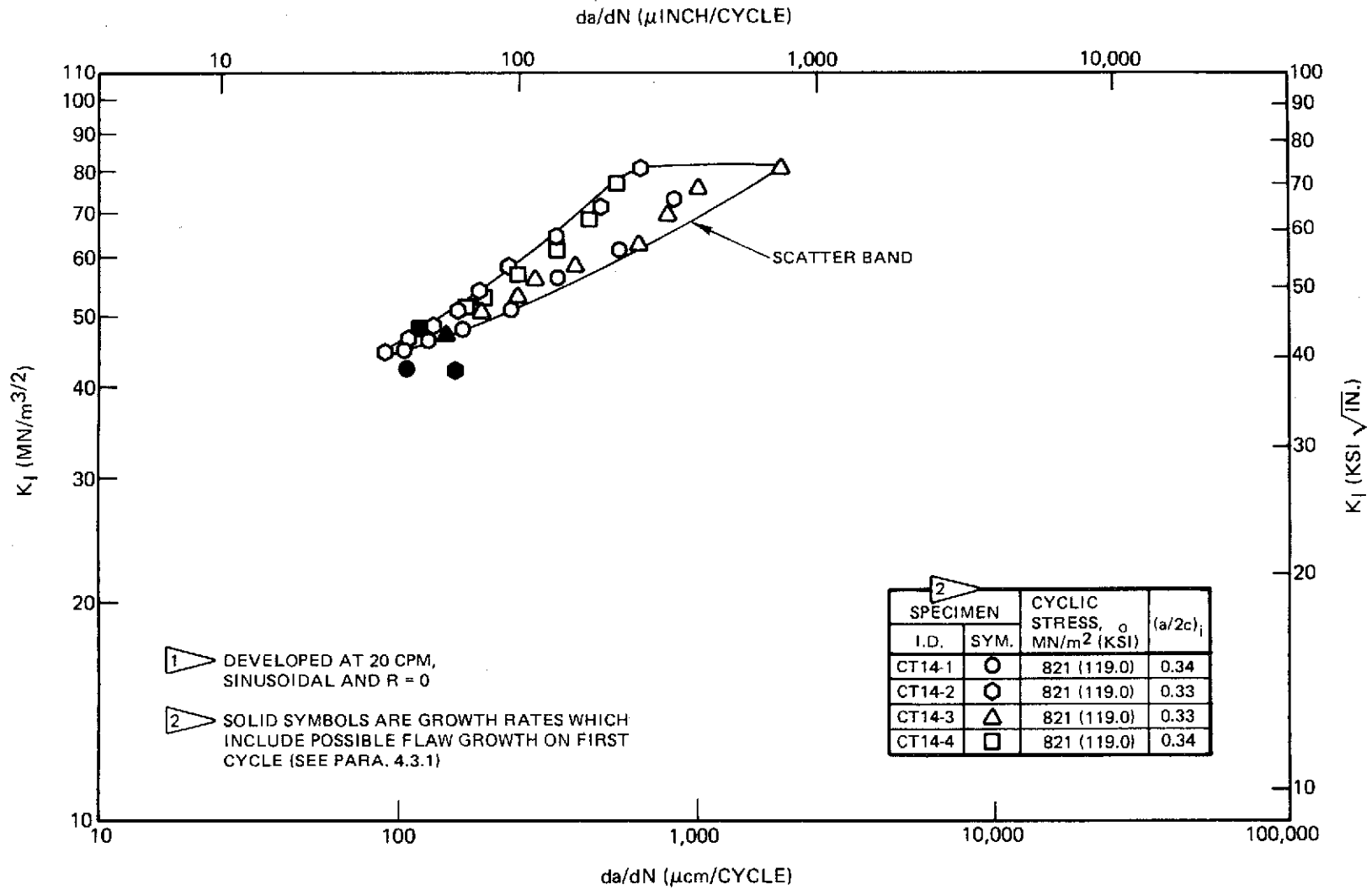


Figure 58: Cyclic Crack Growth Rates \triangle for 0.31 cm (0.12 Inch) Thick 6Al-4V STA Titanium (RT Direction) at 295°K (72° F) in Air with $\sigma_0 = 0.77 \sigma_{ys}$ and $(a/2c)_i \cong 0.34$

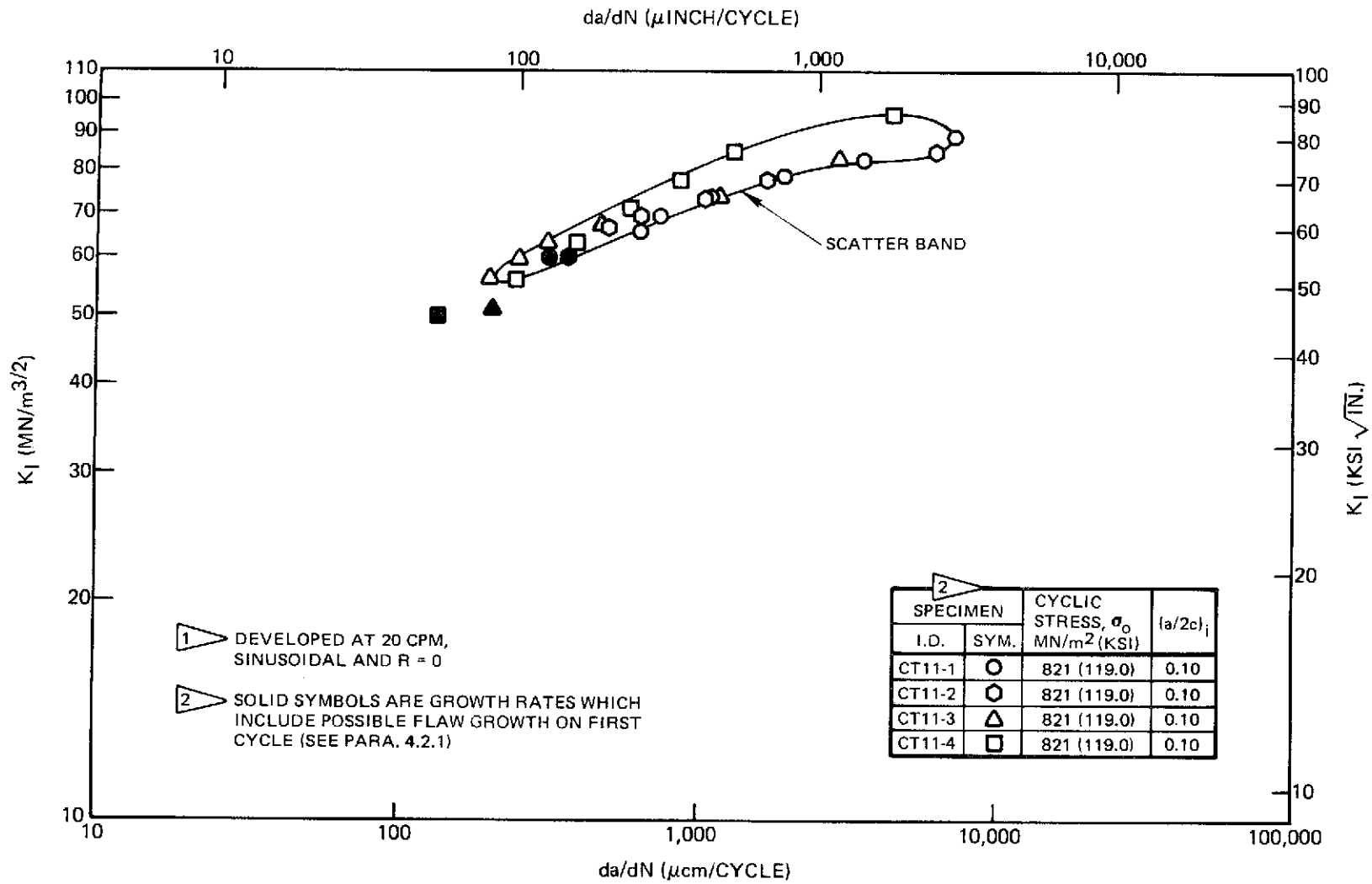


Figure 59: Cyclic Crack Growth Rates ¹ for 0.31 cm (0.12 Inch) Thick 6Al-4V STA Titanium (RT Direction) at 295°K (72° F) in Air with $\sigma_D = 0.77 \sigma_{YS}$ and $(a/2c)_i = 0.10$

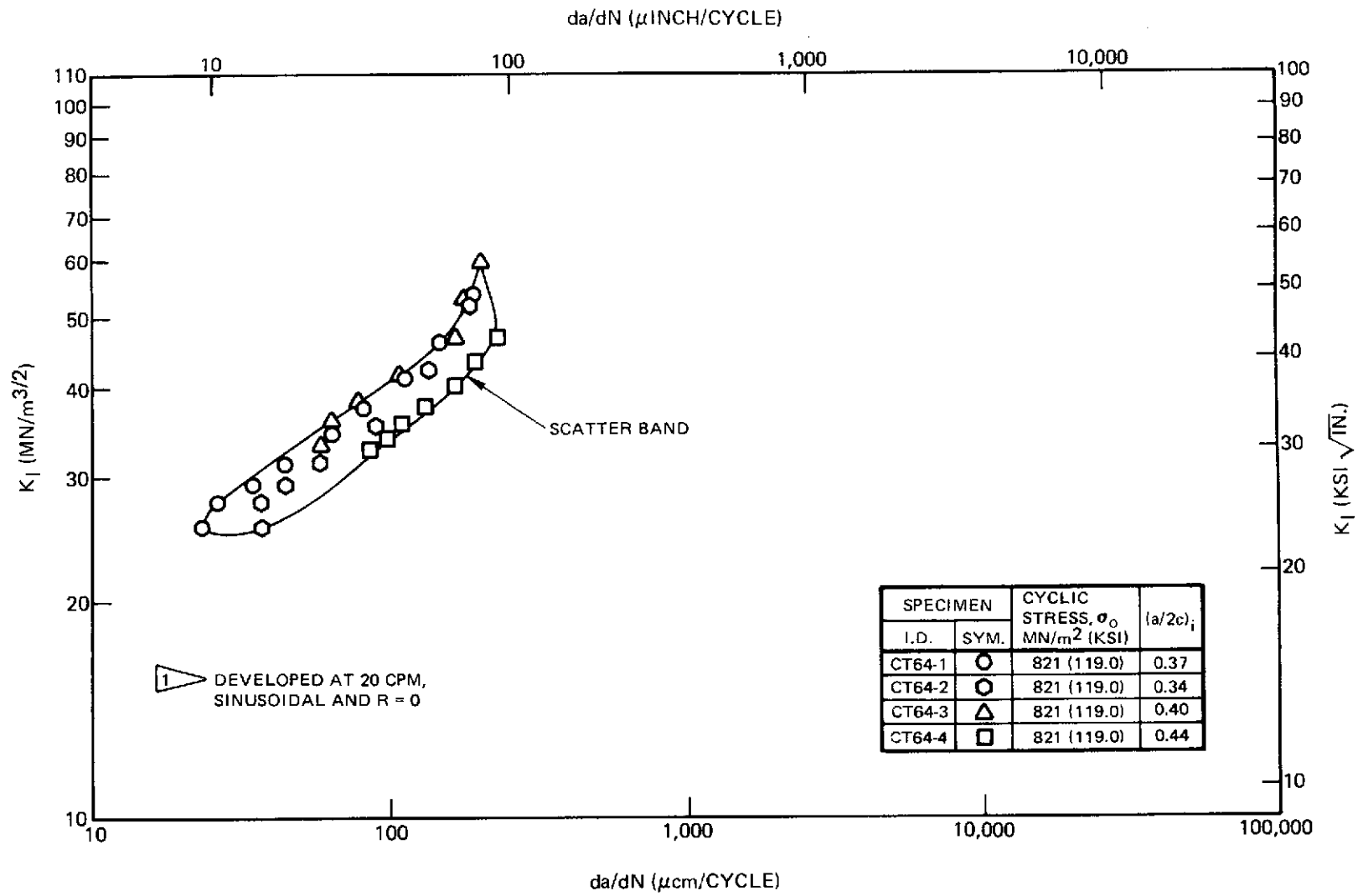



Figure 60: Cyclic Crack Growth Rates  for 0.16 cm (0.063 Inch) Thick 6Al-4V STA Titanium (RT Direction) at 295°K (72° F) in Air with $\sigma_0 = 0.77 \sigma_{YS}$ and $(a/2c)_i \cong 0.40$

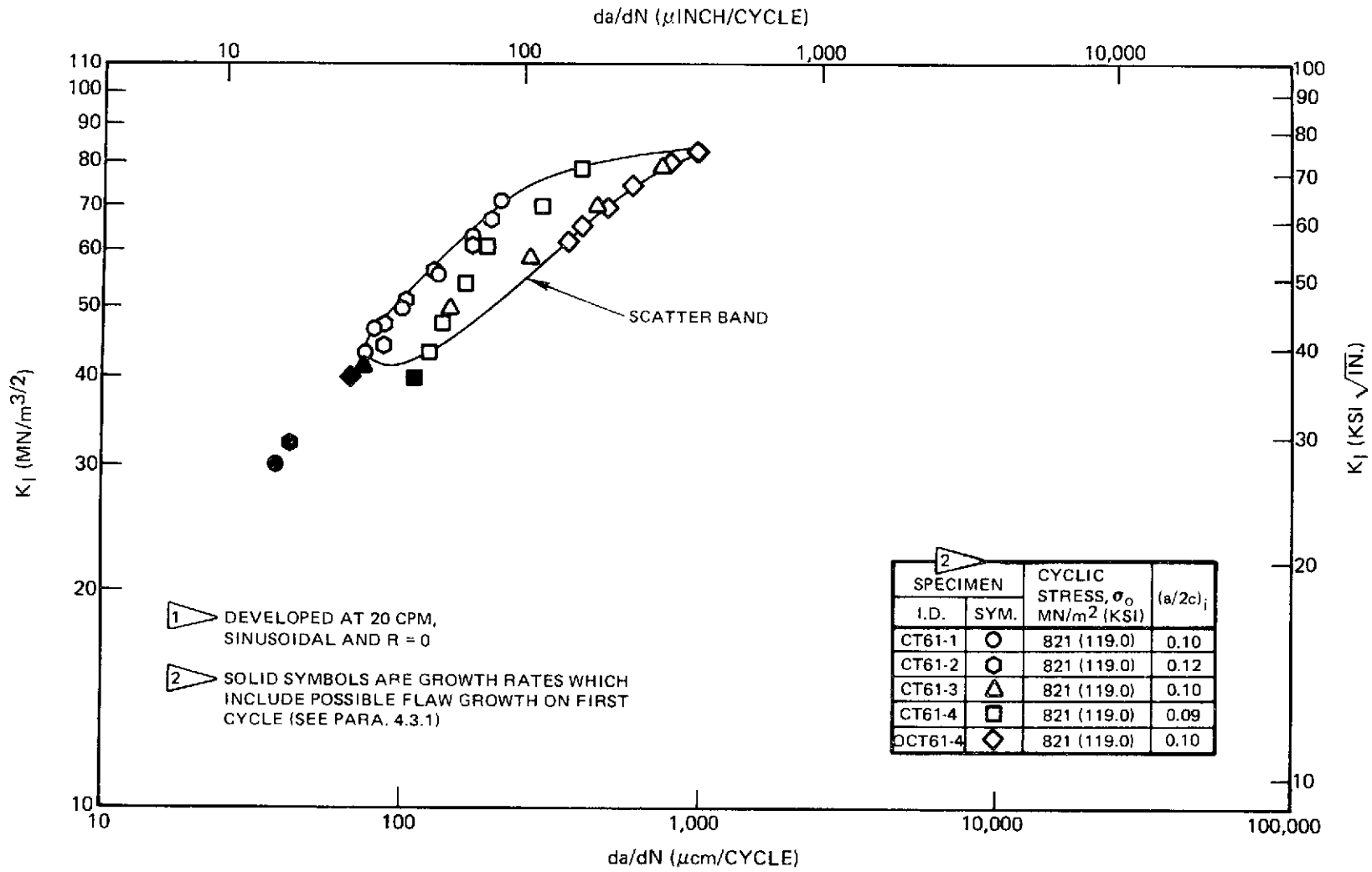


Figure 61: Cyclic Crack Growth Rates ¹ for 0.16 cm (0.063 Inch) Thick 6Al-4V STA Titanium (RT Direction) at 295°K (72° F) in Air with $\sigma_0 = 0.77 \sigma_{YS}$ and $(a/2c)_i \cong 0.10$

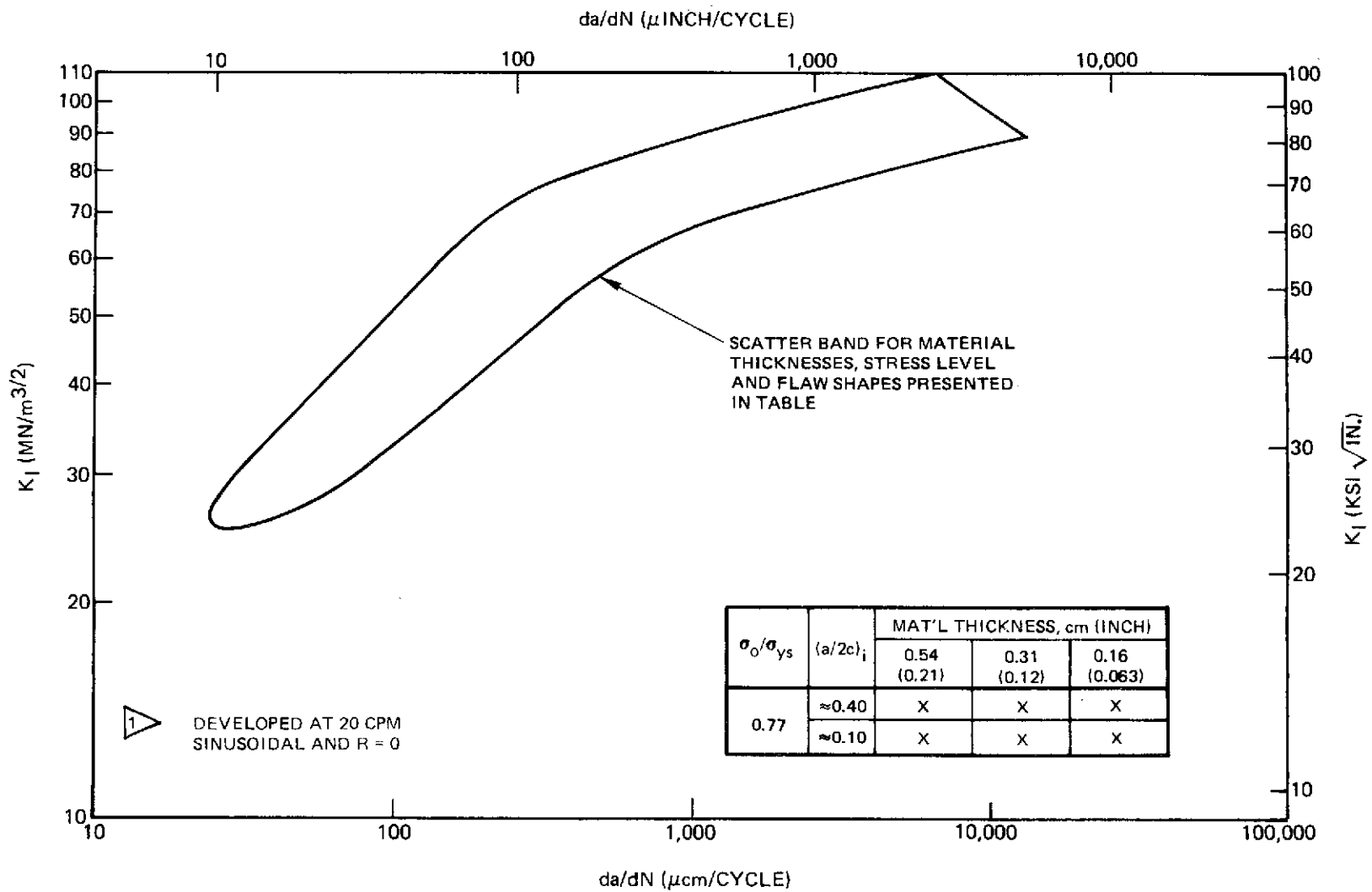


Figure 62: Summary of Baseline Cyclic Crack Growth Rates for 6Al-4V STA Titanium (RT Direction) Plate at 295°K (72°F)

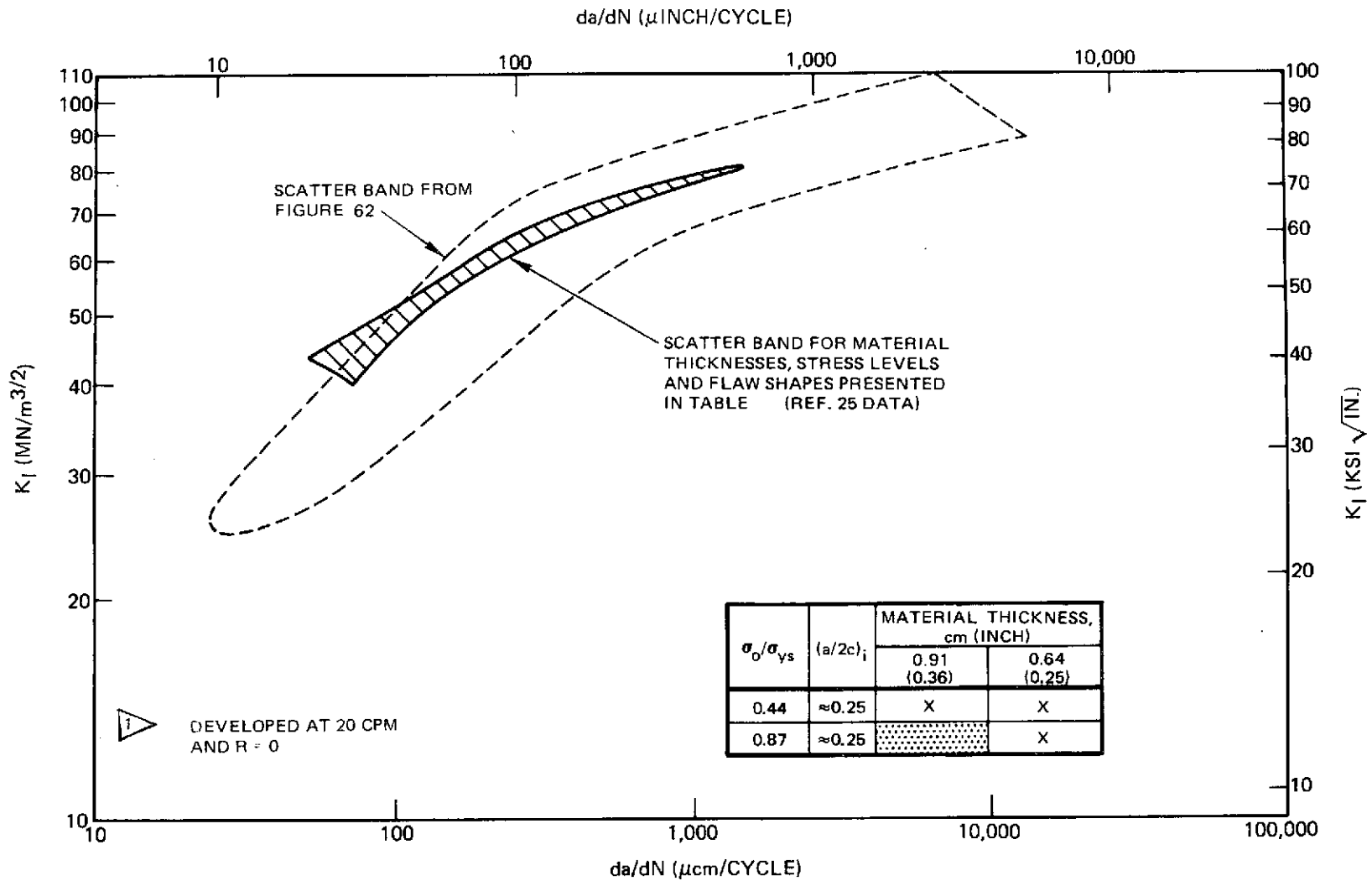


Figure 63: Comparison of 6Al-4V STA Titanium (RT Direction) Fatigue Crack Growth Rate Data at 295°K (72°F)

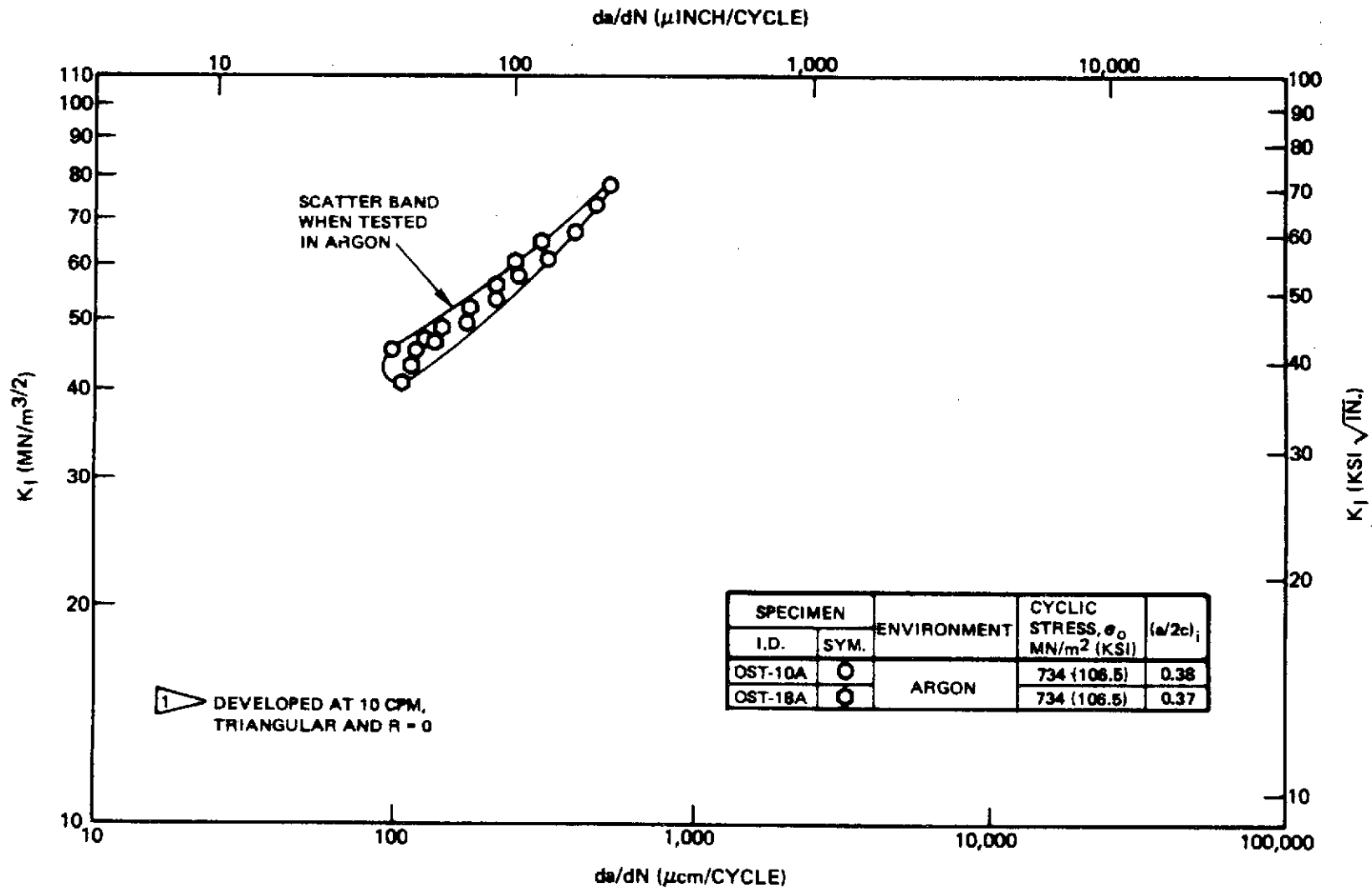


Figure 64: Cyclic Crack Growth Rates ¹ for 0.31 cm (0.12 Inch) Thick 6Al-4V STA Titanium (WT Direction) at 295°K (72° F) in Argon with $\sigma_0 = 0.68 \sigma_{ys}$ and $(a/2c)_i \cong 0.37$

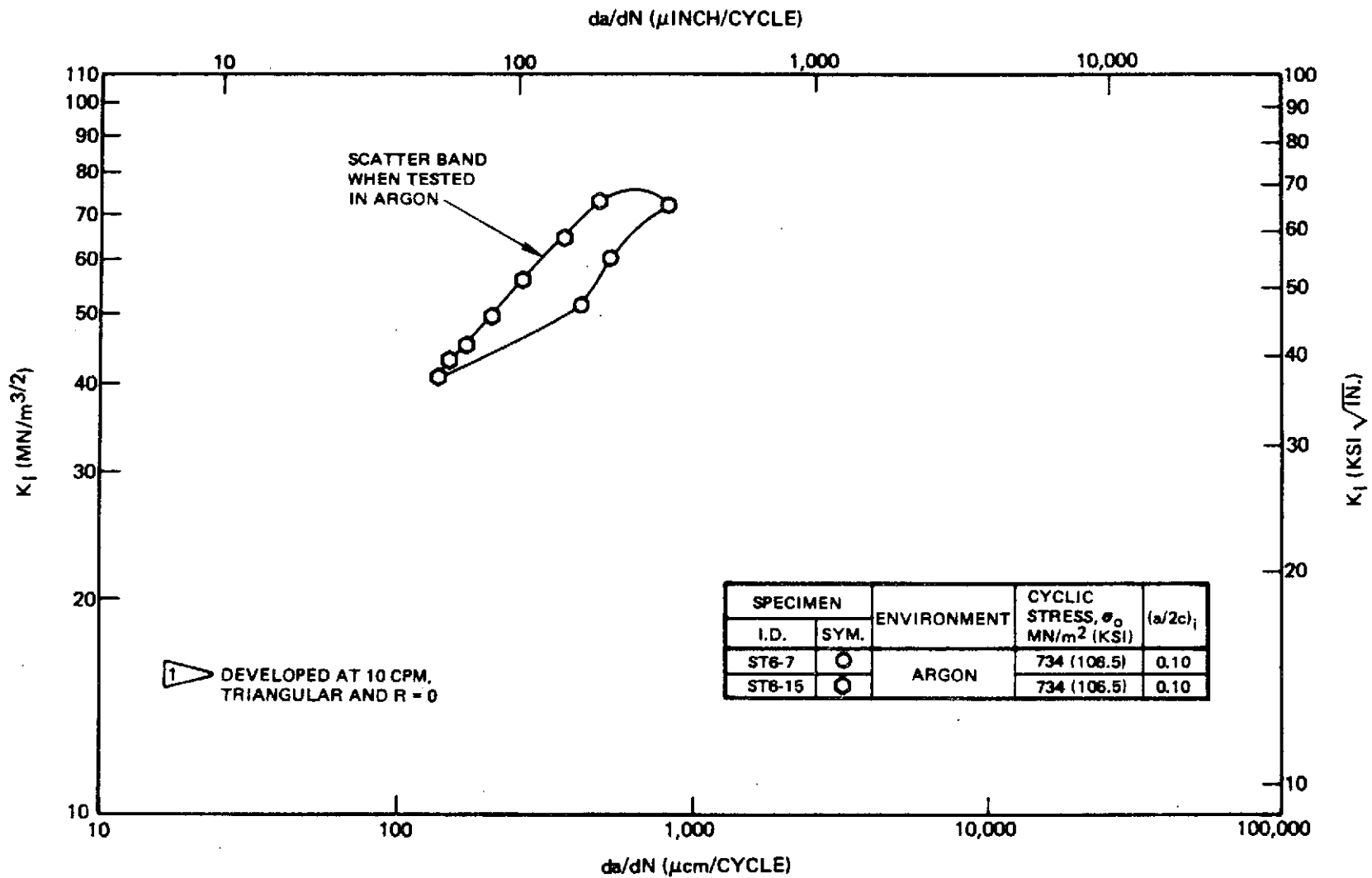


Figure 65: Cyclic Crack Growth Rates for 0.16 cm (0.063 Inch) Thick 6Al-4V STA Titanium (WT Direction) at 295°K (72° F) in Argon with $\sigma_0 = 0.68 \sigma_{YS}$ and $(a/2c)_i \cong 0.10$

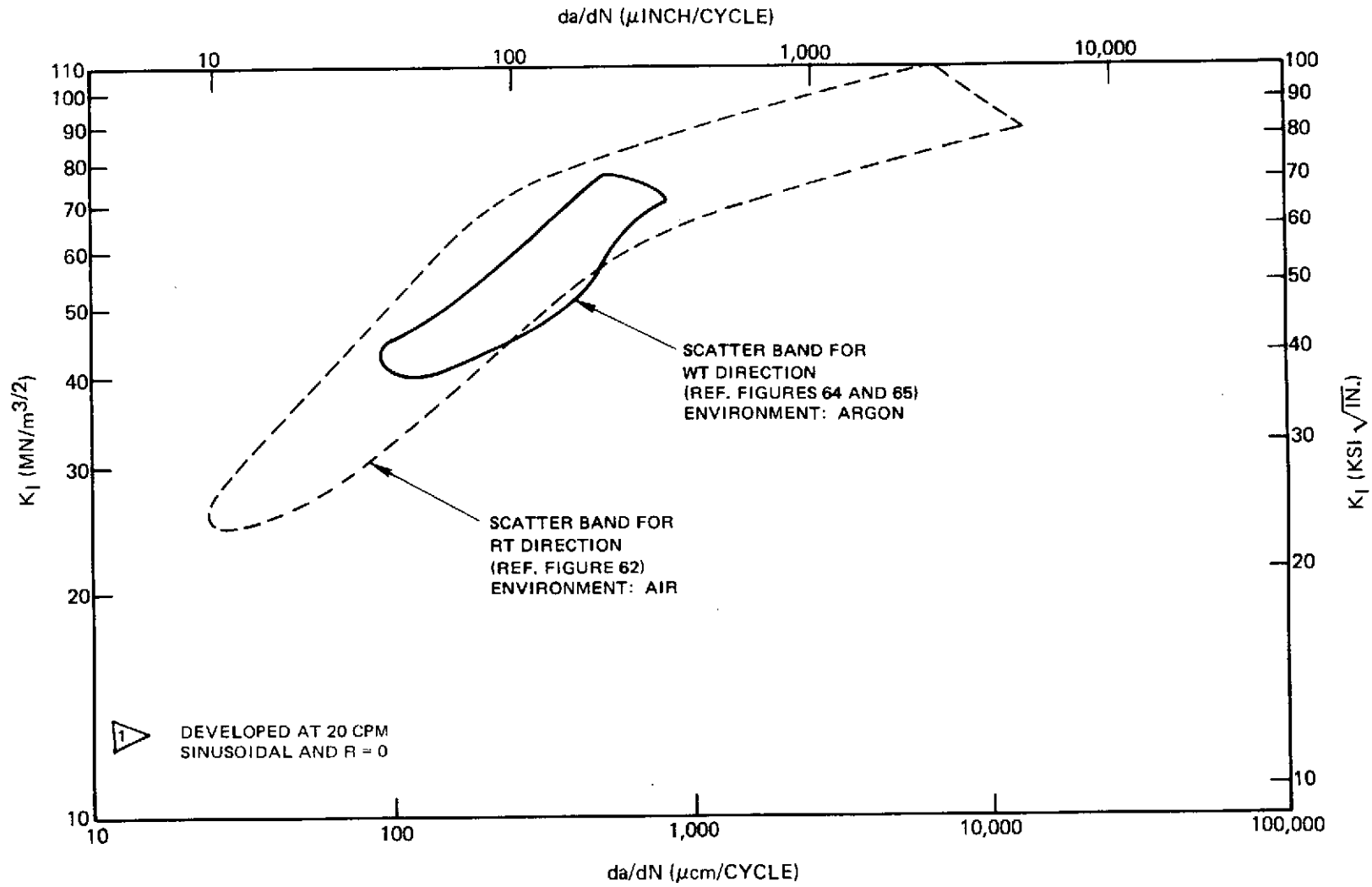


Figure 66: Effect of Crack Orientation on Fatigue Crack Growth Rate Data for 6Al-4V STA Titanium at 295°K (72°F)

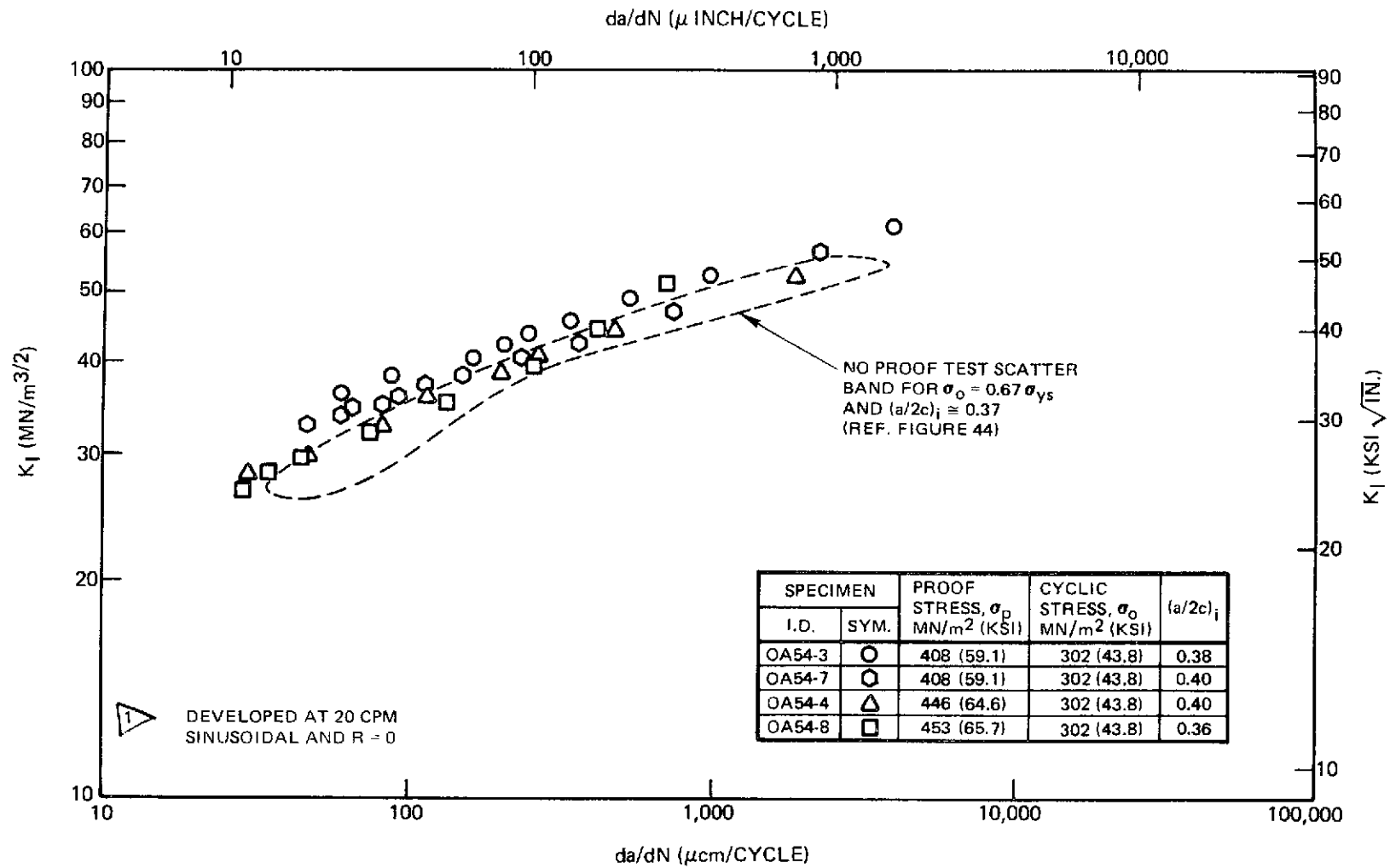


Figure 67: Cyclic Crack Growth Rates (After a Cryogenic Proof Test) for 1.27 cm (0.50 Inch) Thick 2219-T87 Aluminum (WT Direction) at 78°K (-320°F) with $\sigma_o = 0.67 \sigma_{ys}$ and $(a/2c)_i \approx 0.39$

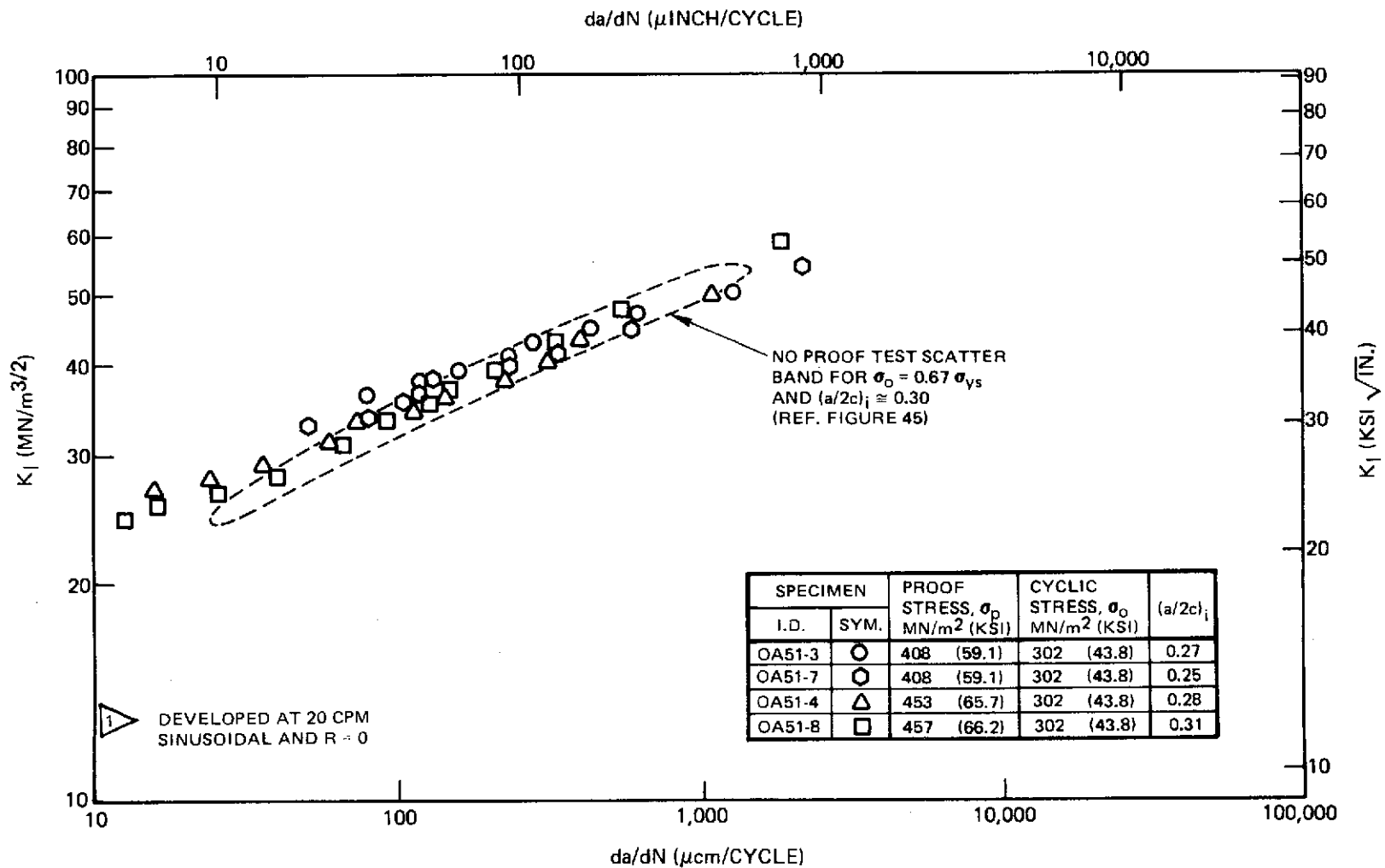


Figure 68: Cyclic Crack Growth Rates (After a Cryogenic Proof Test) for 1.27 cm (0.50 Inch) Thick 2219-T87 Aluminum (WT Direction) at 78°K (-320°F) with $\sigma_0 = 0.67 \sigma_{ys}$ and $(a/2c)_i = 0.28$

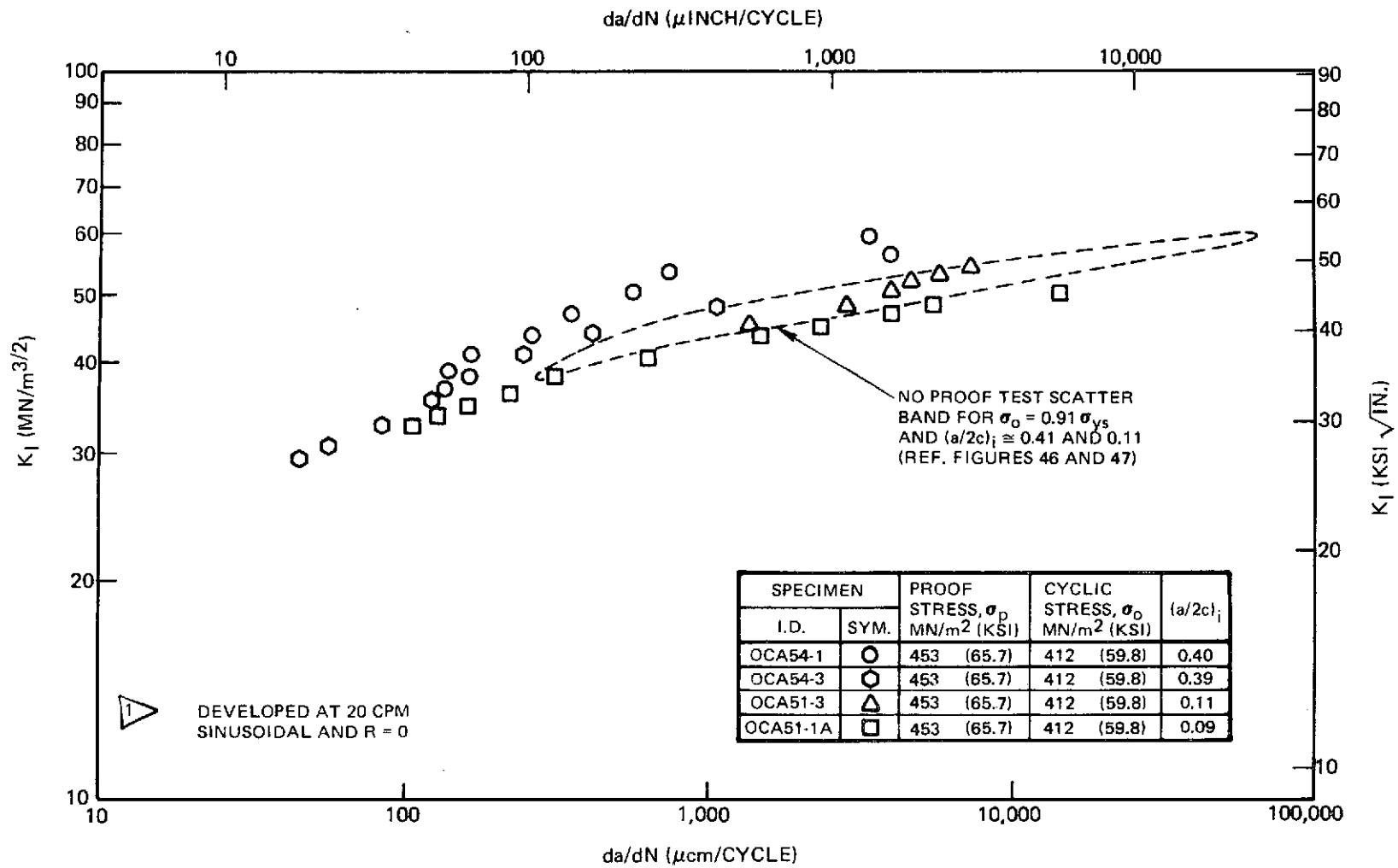
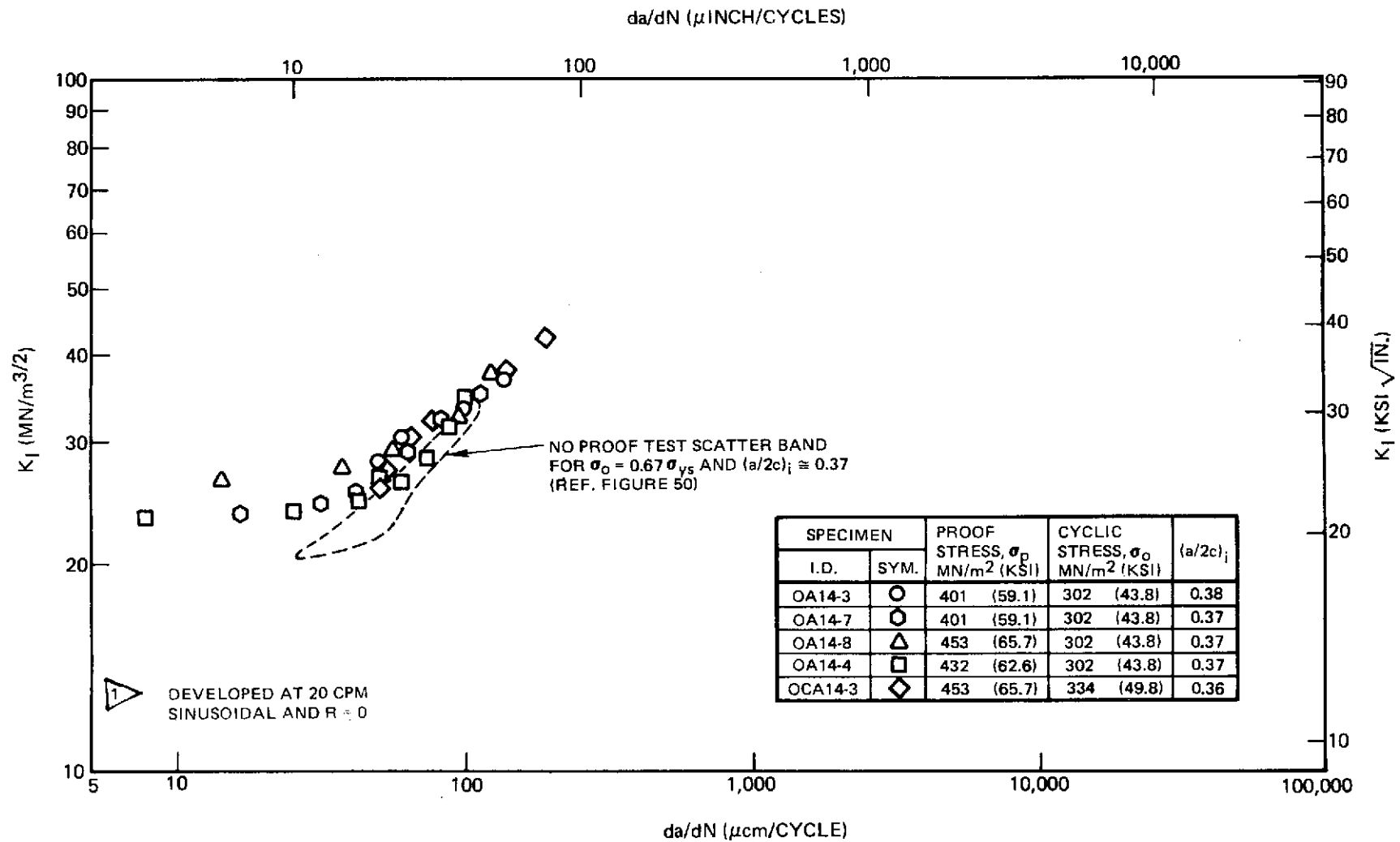


Figure 69: Cyclic Crack Growth Rates (After a Cryogenic Proof Test) for 1.27 cm (0.50 Inch) Thick 2219-T87 Aluminum (WT Direction) at 78°K (-320°F) with $\sigma_0 = 0.91 \sigma_{ys}$ and $(a/2c)_i \cong 0.40$ and 0.10



△

Figure 70: Cyclic Crack Growth Rates (After a Cryogenic Proof Test) for 0.38 cm (0.15 Inch) Thick 2219-T87 Aluminum (WT Direction) at 78°K (-320°F) with $\sigma_o \approx 0.67 \sigma_{ys}$ and $(a/2c)_i \approx 0.37$

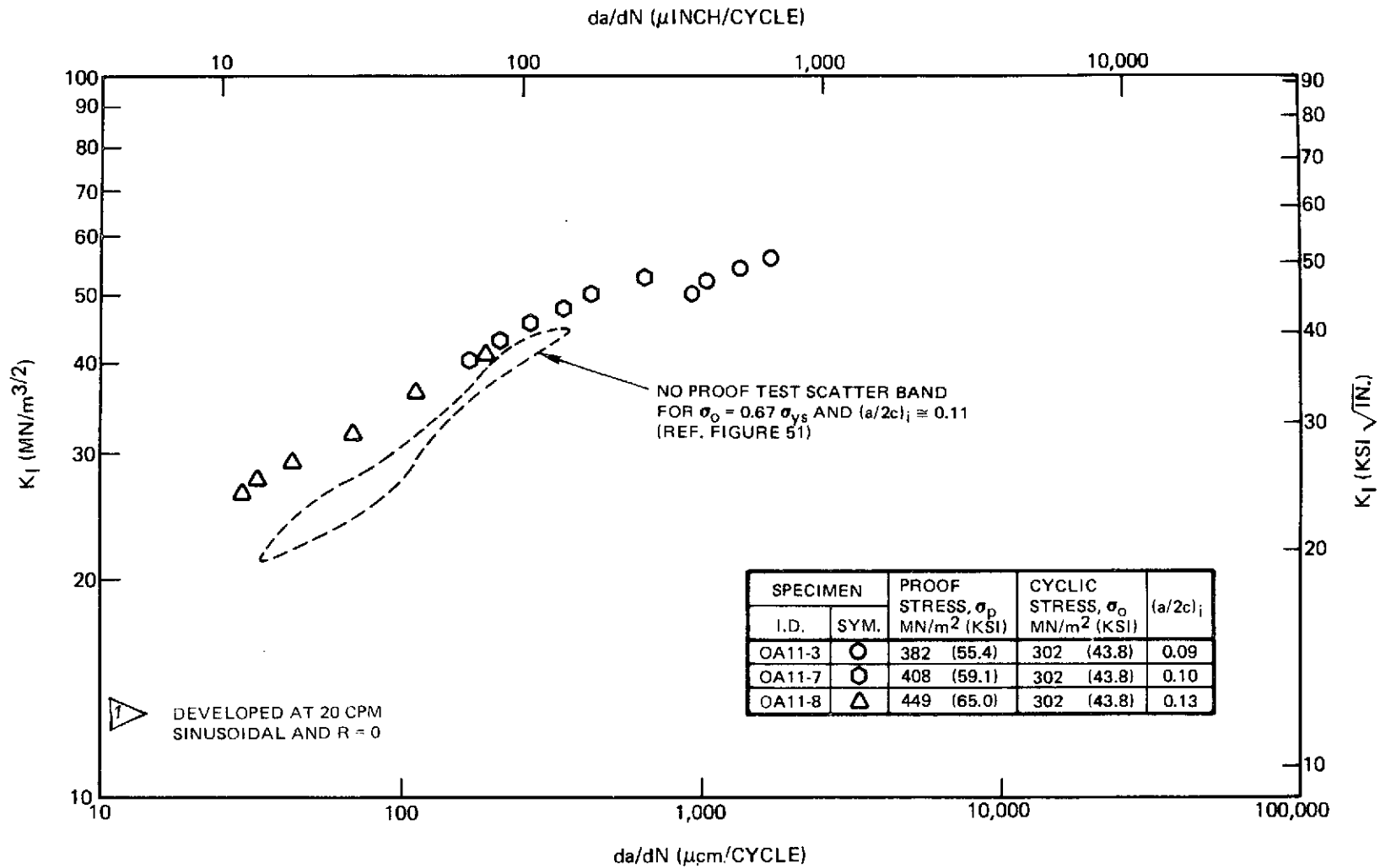


Figure 71: Cyclic Crack Growth Rates (After a Cryogenic Proof Test) for 0.38 cm (0.15 Inch) Thick 2219-T87 Aluminum (WT Direction) at 78°K (-320°F) with $\sigma_o = 0.67 \sigma_{ys}$ and $(a/2c)_i \approx 0.11$

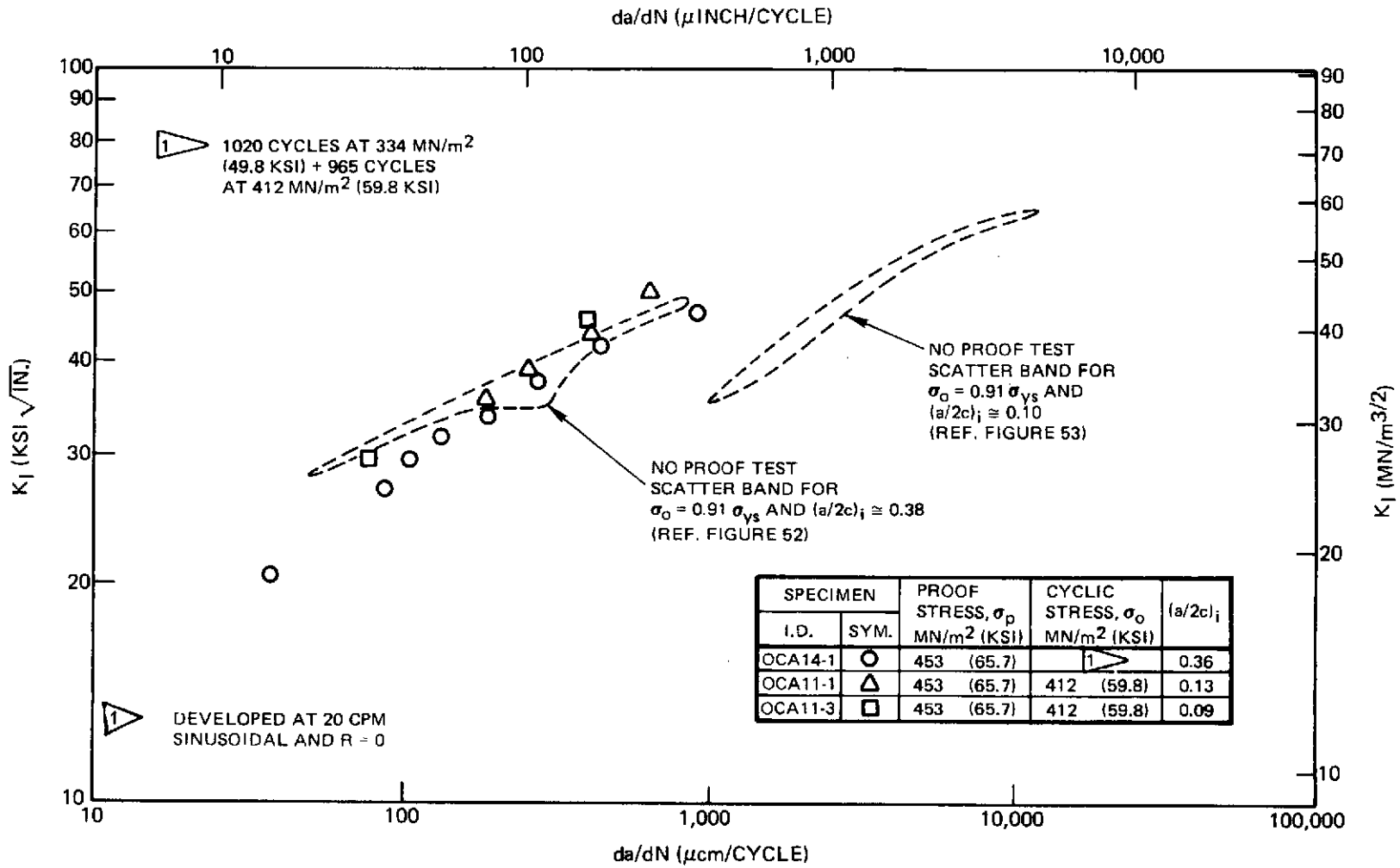


Figure 72: Cyclic Crack Growth Rates (After a Cryogenic Proof Test) for 0.38 cm (0.15 Inch) Thick 2219-T89 Aluminum (WT Direction) at 78°K (-320°F) with $\sigma_0 = 0.76 \sigma_{ys} \rightarrow 0.91 \sigma_{ys}$ and $(a/2c)_i \approx 0.11$ and 0.36

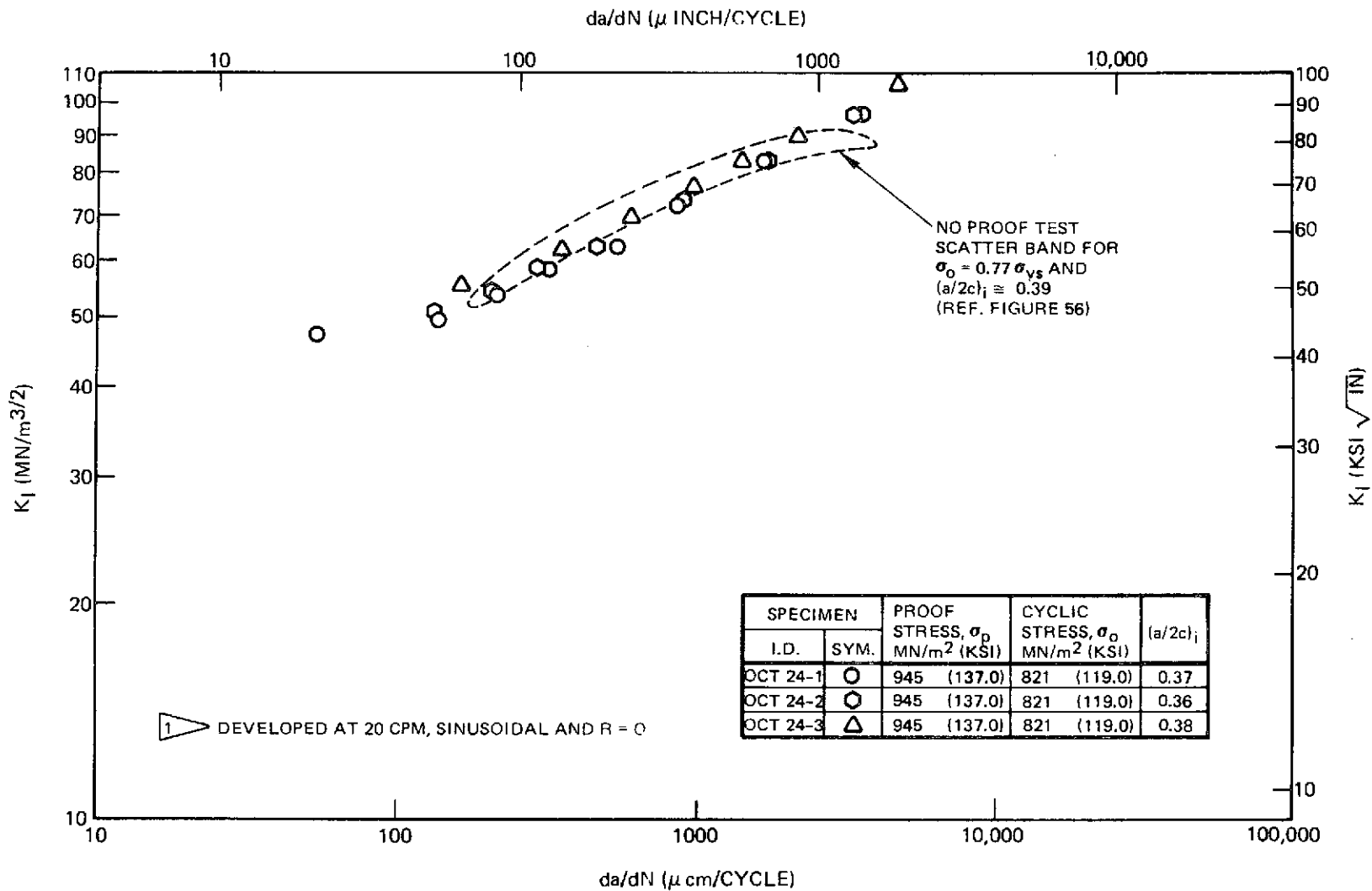


Figure 73: Cyclic Crack Growth Rates (After a Proof Test) For 0.54 cm (0.21 Inch) Thick 6Al-4V STA Titanium (RT Direction) at 295°K (72° F) in Air with $\sigma_0 = 0.77 \sigma_{ys}$ and $(a/2c)_i \approx 0.37$

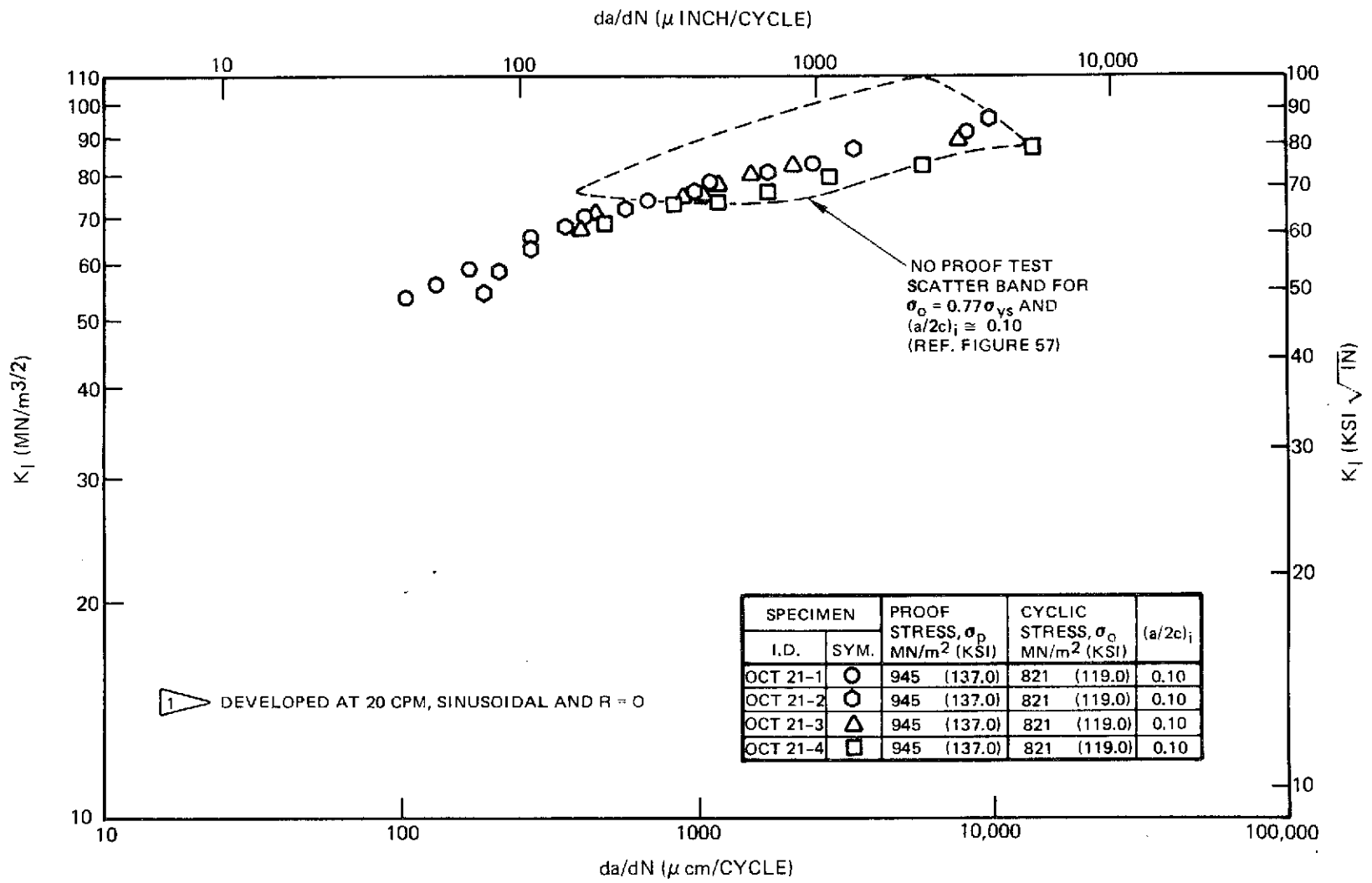


Figure 74: Cyclic Crack Growth Rates (After a Proof Test) For 0.54 cm (0.21 Inch) Thick 6Al-4V STA Titanium (RT Direction) at 295°K (72° F) in Air With $\sigma_0 = 0.77 \sigma_{YS}$ and $(a/2c)_i = 0.10$

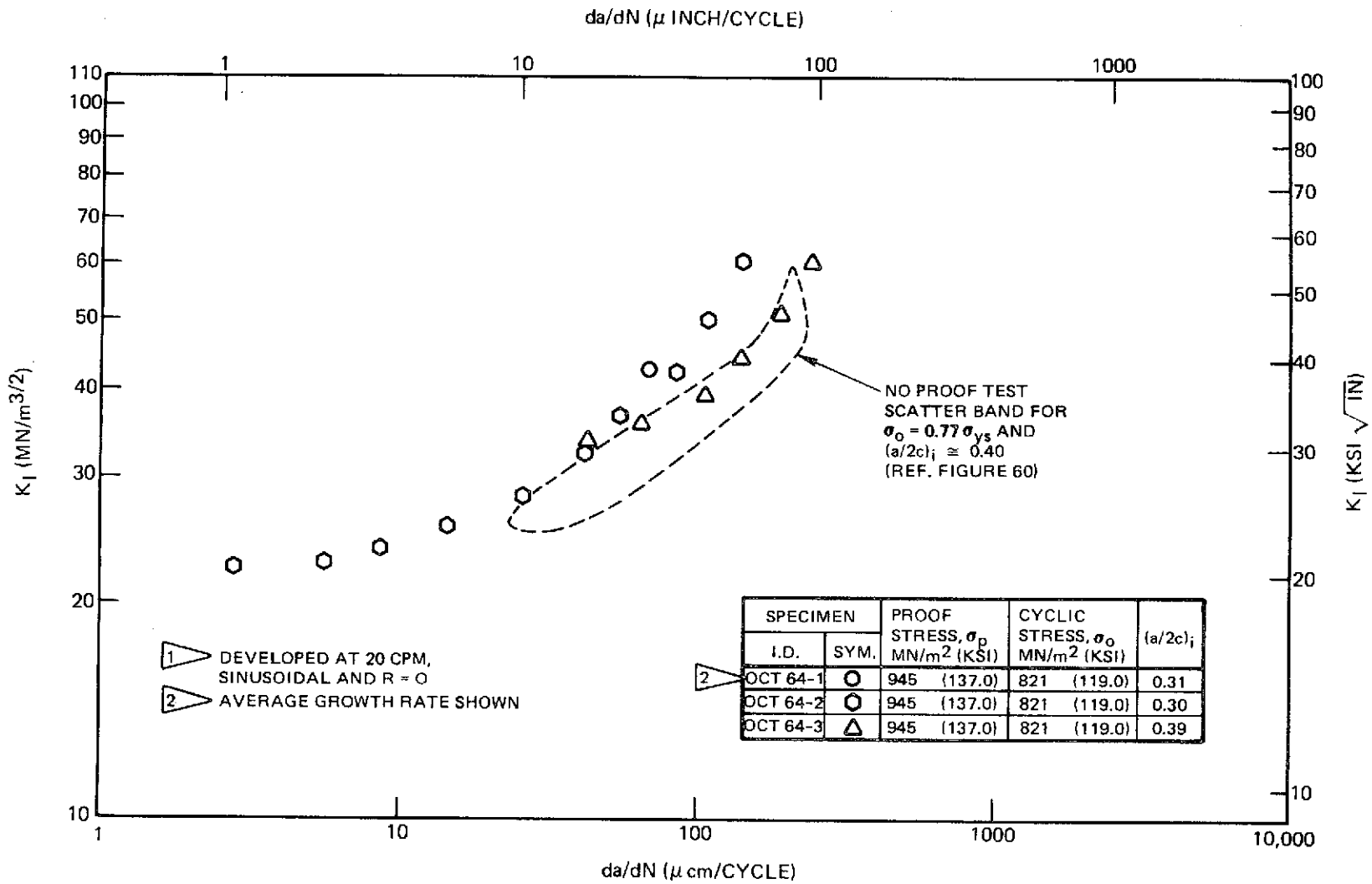


Figure 75: Cyclic Crack Growth Rates (After a Proof Test) For 0.16 cm (0.063 Inch) Thick 6Al-4V STA Titanium (RT Direction) at 295°K (72° F) in Air With $\sigma_o = 0.77 \sigma_{ys}$ and $(a/2c)_i \approx 0.33$

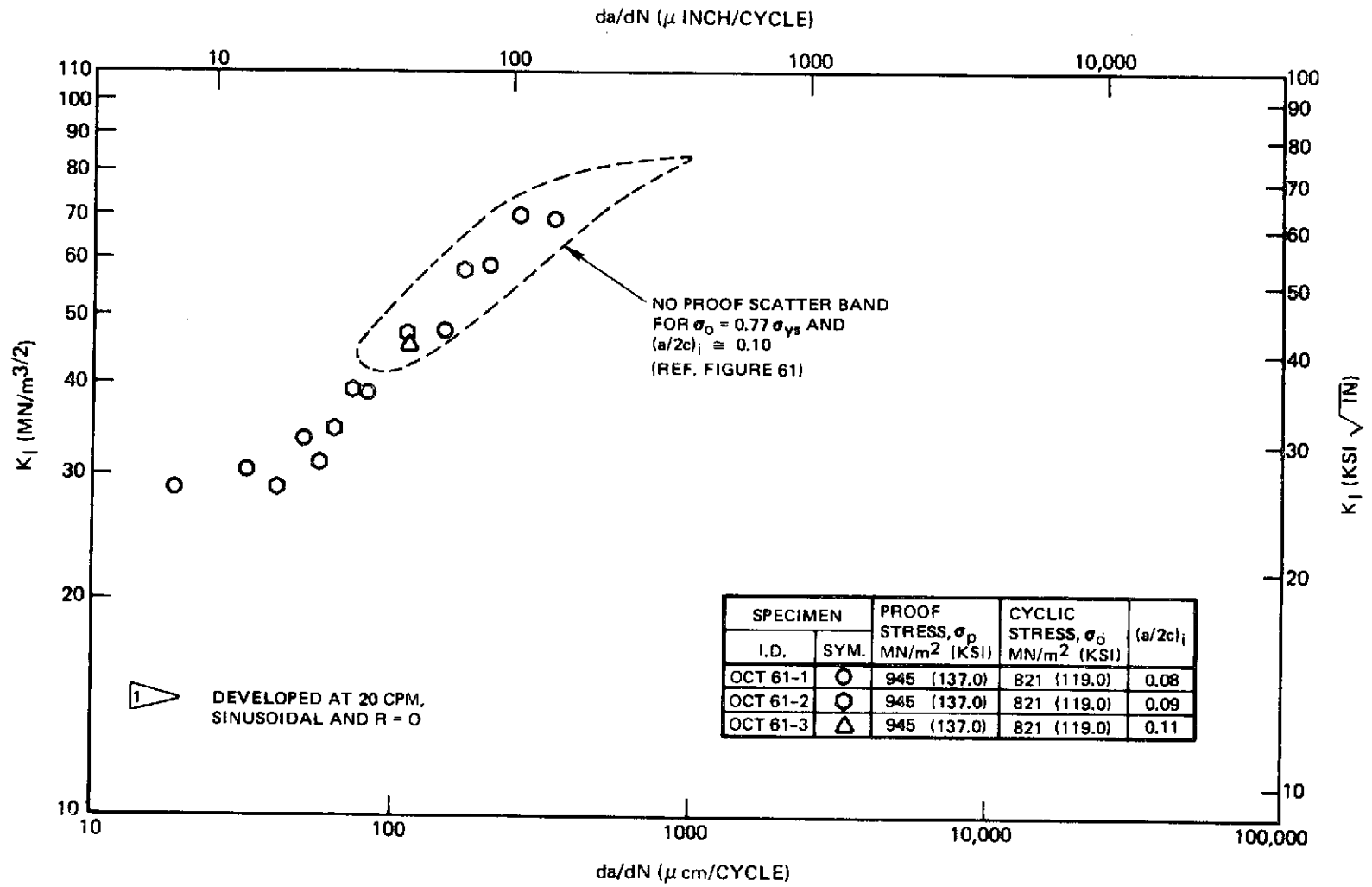


Figure 76: Cyclic Crack Growth Rates (After a Proof Test) For 0.16 cm (0.063 Inch) Thick 6Al-4V STA Titanium (RT Direction) at 295°K (72° F) in Air With $\sigma_o = 0.77 \sigma_{ys}$ and $(a/2c)_i \cong 0.09$

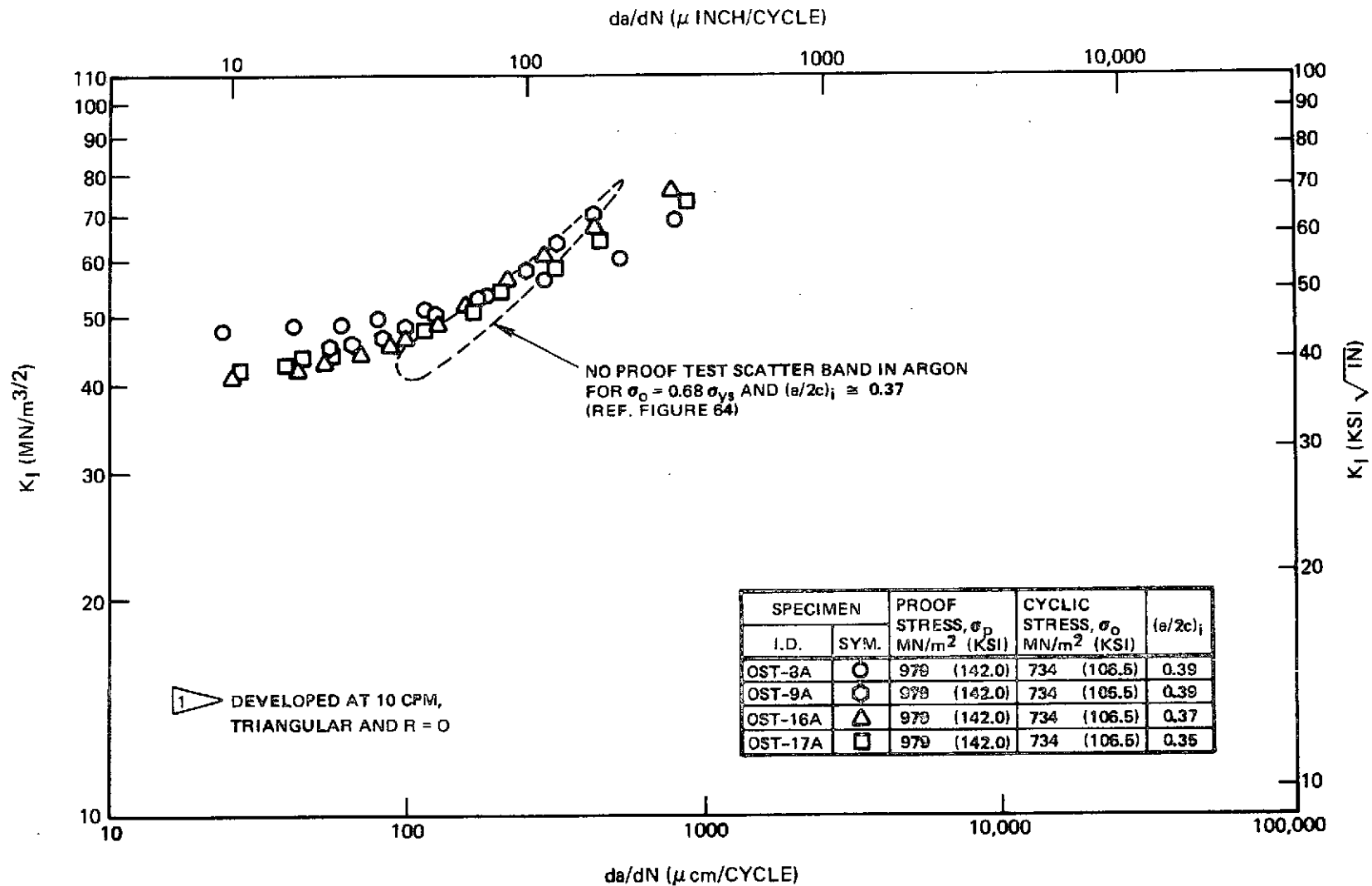


Figure 77: Cyclic Crack Growth Rates (After a Proof Test) For 0.31 cm (0.12 Inch) Thick 6Al-4V STA Titanium (WT Direction) at 295°K (72° F) in Argon With $\sigma_0 = 0.68 \sigma_{YS}$ and $(a/2c)_i \approx 0.38$

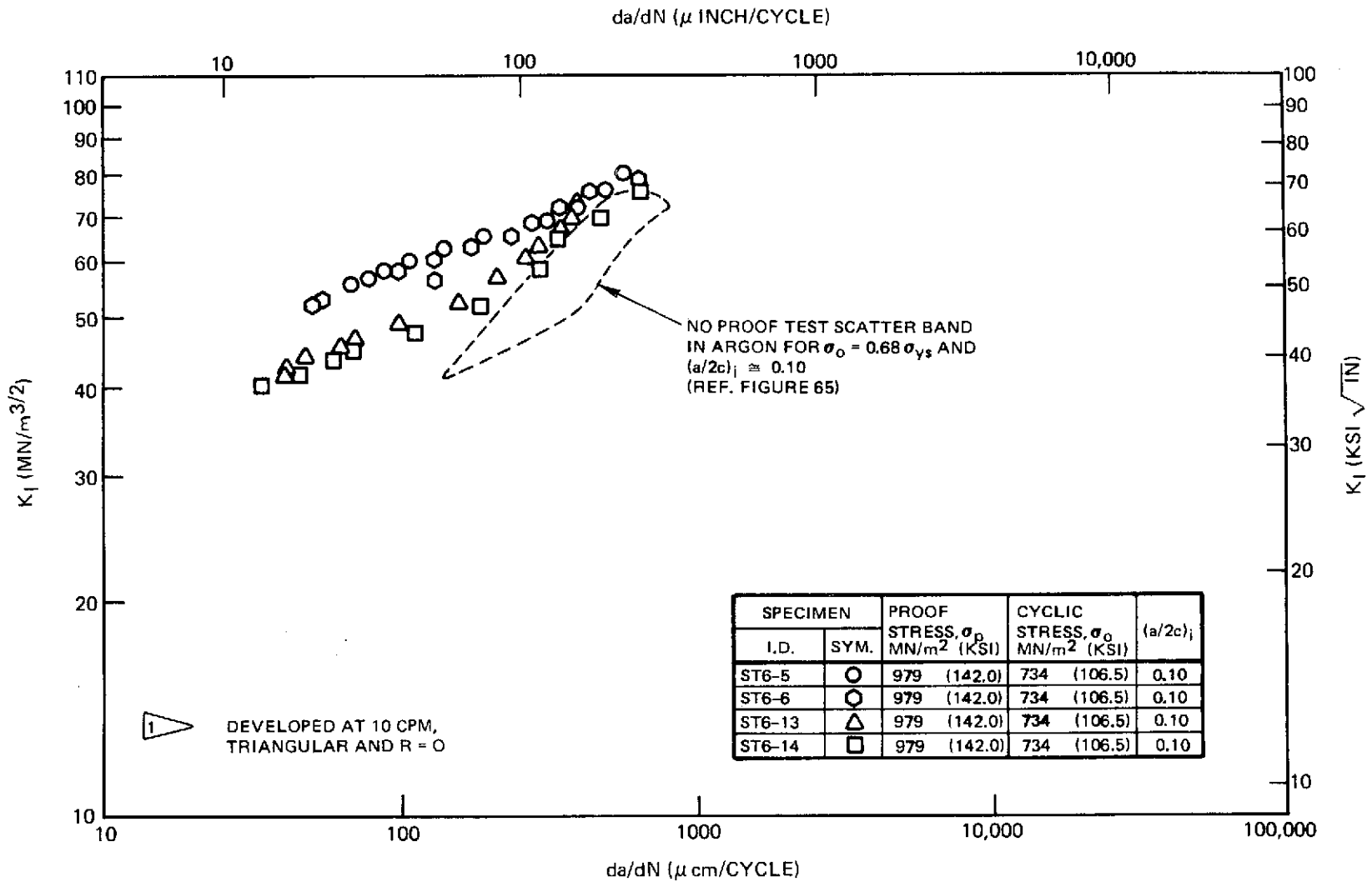


Figure 78: Cyclic Crack Growth Rates (After a Proof Test) For 0.16 cm (0.063 Inch) Thick 6Al-4V STA Titanium (WT Direction) at 295°K (72° F) in Argon With $\sigma_0 = 0.68 \sigma_{ys}$ and $(a/2c)_i = 0.10$

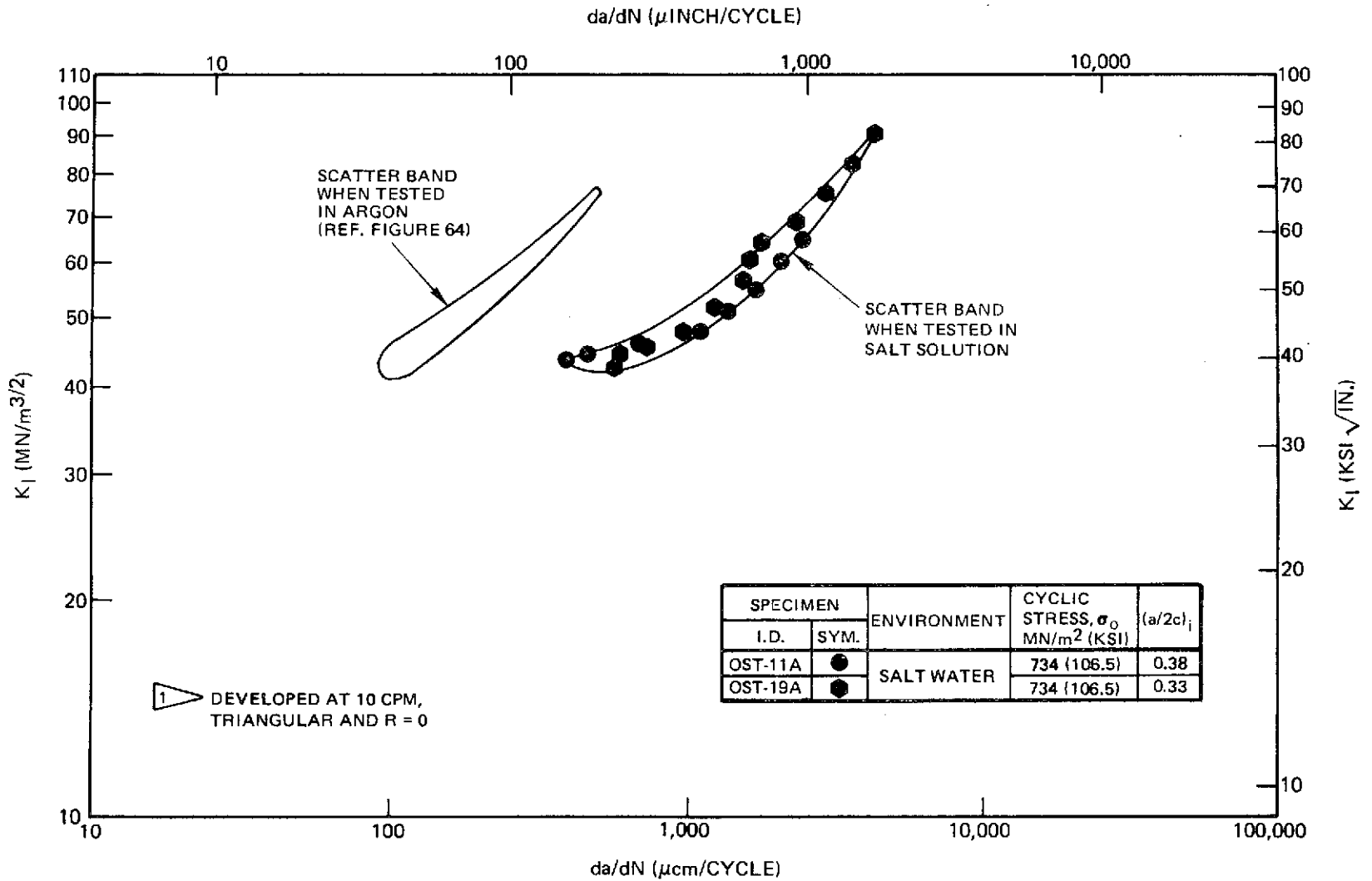


Figure 79: Cyclic Crack Growth Rates ¹ for 0.31 cm (0.12 Inch) Thick 6Al-4V STA Titanium (WT Direction) at 295°K (72° F) Salt Water with $\sigma_o = 0.68 \sigma_{ys}$ and $(a/2c)_i \cong 0.37$

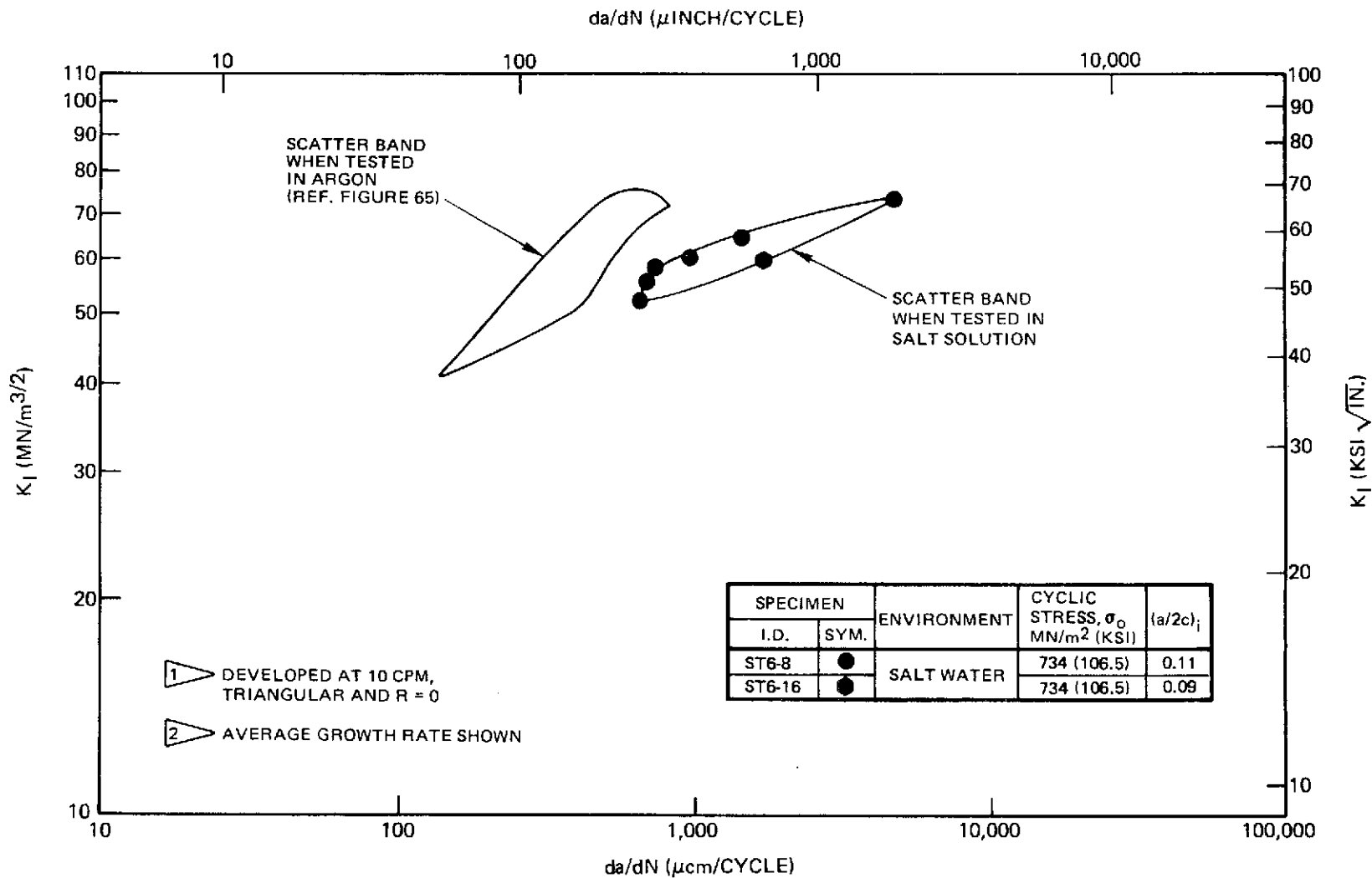


Figure 80: Cyclic Crack Growth Rates for 0.16 cm (0.063 Inch) Thick 6Al-4V STA Titanium (WT Direction) at 295°K (72° F) Salt Water with $\sigma_o = 0.68 \sigma_{YS}$ and $(a/2c)_i \cong 0.10$

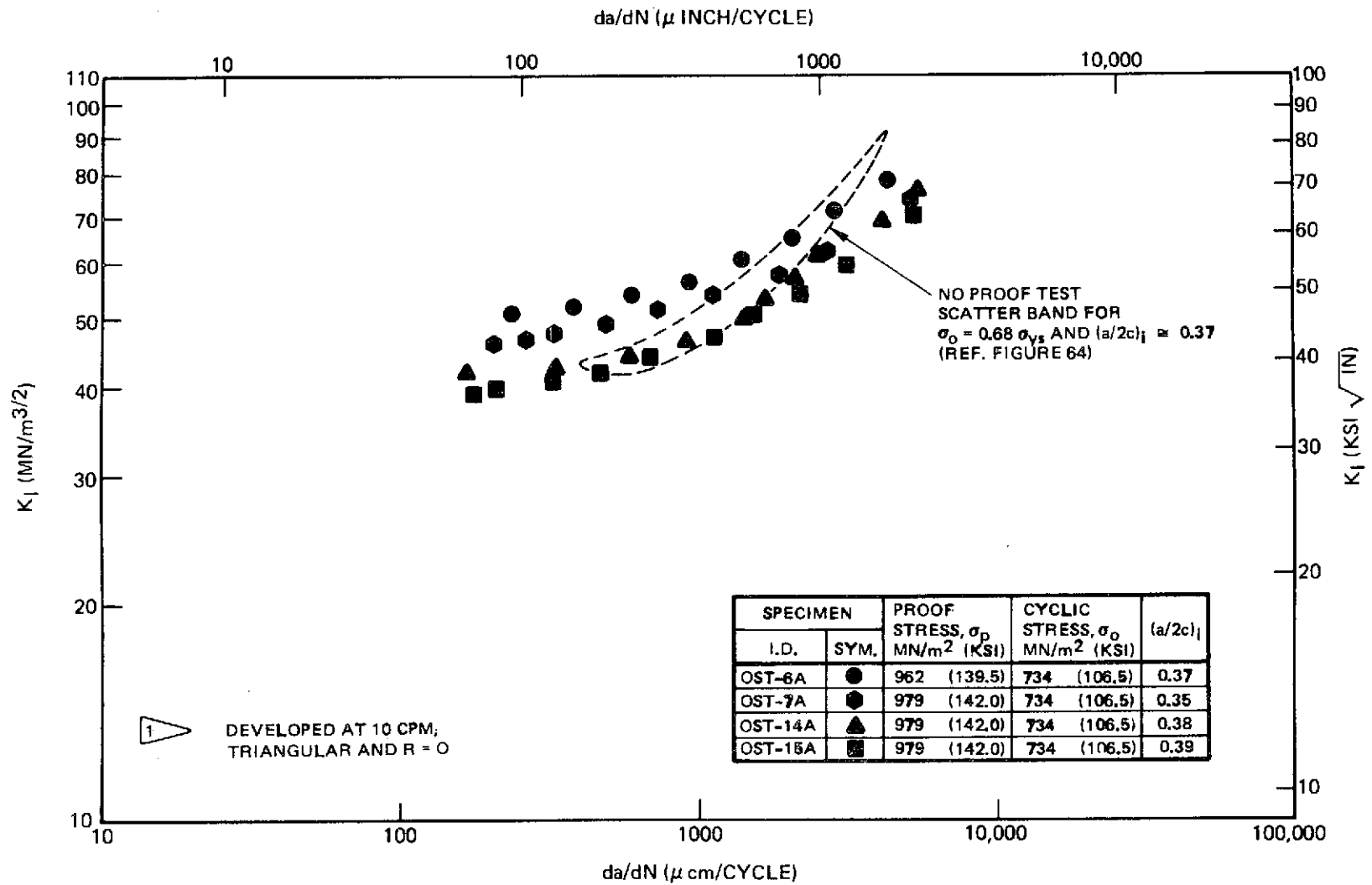


Figure 81: Cyclic Crack Growth Rates (After a Proof Test) For 0.31 cm (0.12 Inch) Thick 6Al-4V STA Titanium (WT Direction) at 295°K (72° F) in Salt Water With $\sigma_o = 0.68 \sigma_{ys}$ and $(a/2c)_i \cong 0.38$

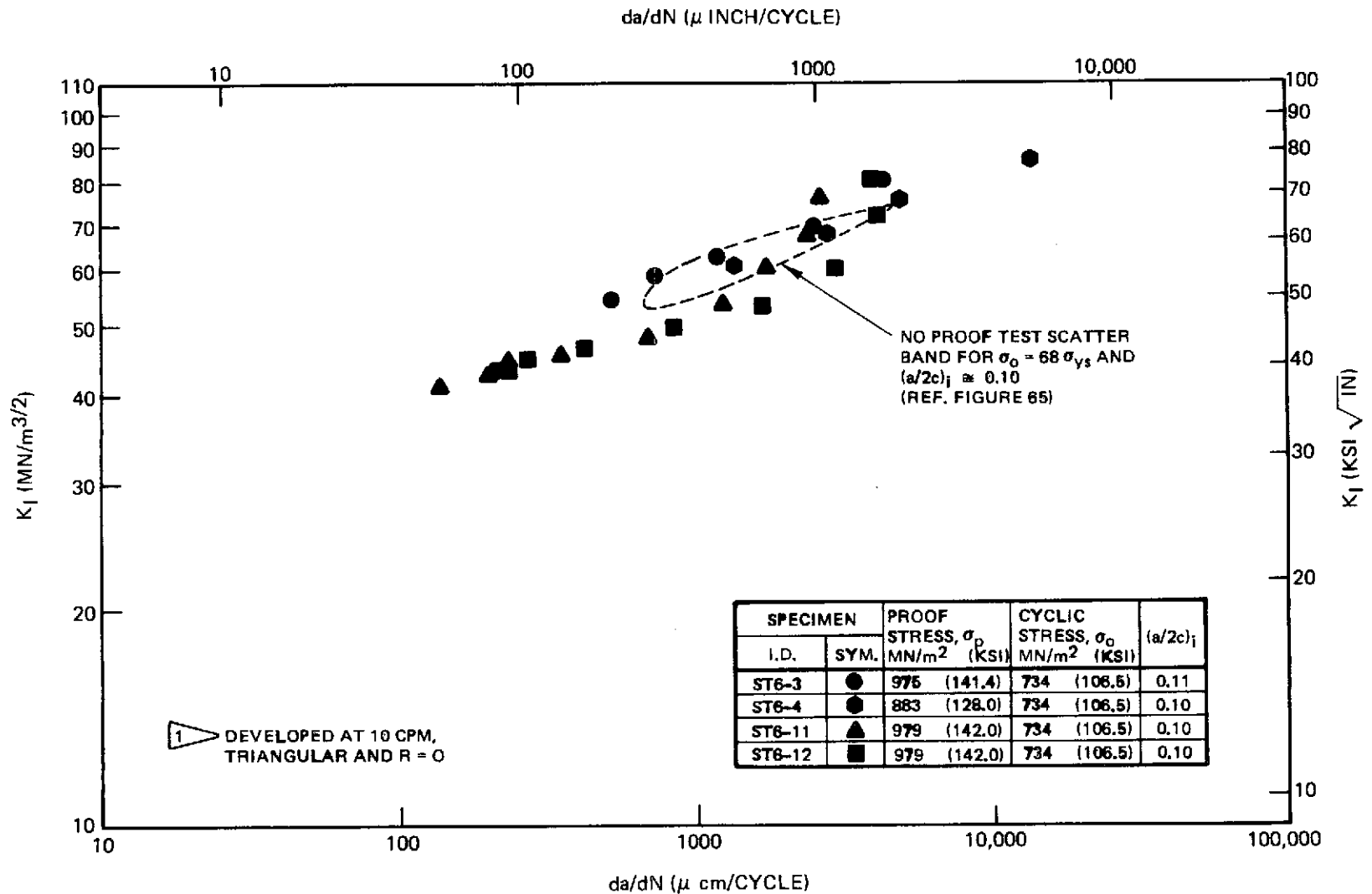


Figure 82: Cyclic Crack Growth Rates (After a Proof Test) For 0.16 cm (0.063 Inch) Thick 6Al-4V STA Titanium (WT Direction) at 295°K (72°F) in Salt Water With $\sigma_0 = 0.68 \sigma_{ys}$ and $(a/2c)_i \approx 0.10$

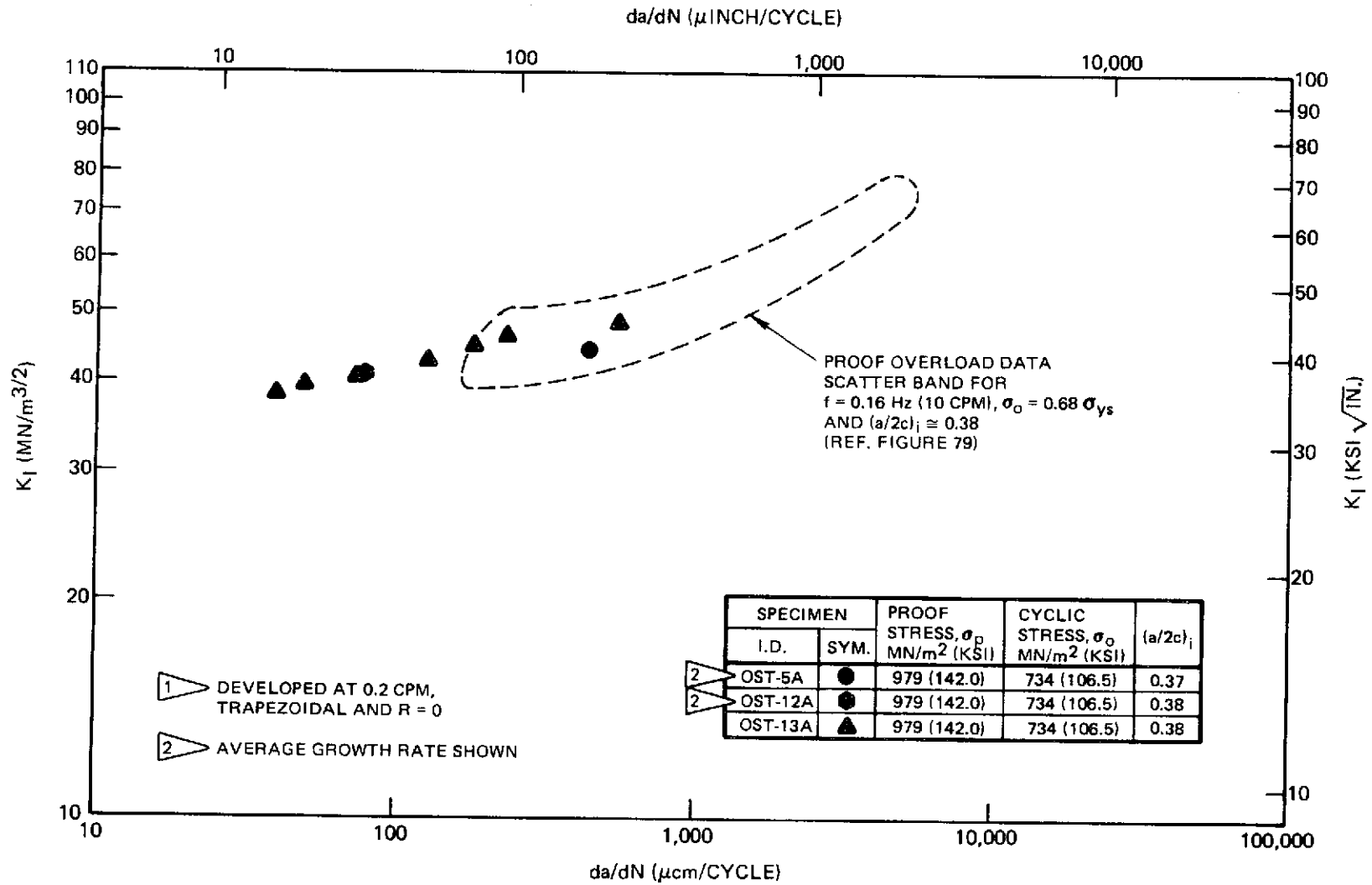


Figure 83: Cyclic Crack Growth Rates (After a Proof Test) for 0.31 cm (0.12 Inch) Thick 6Al-4V STA Titanium (WT Direction) at 295°K (72° F) in Salt Water with $\sigma_o = 0.68 \sigma_{ys}$ and $(a/2c)_i \cong 0.38$

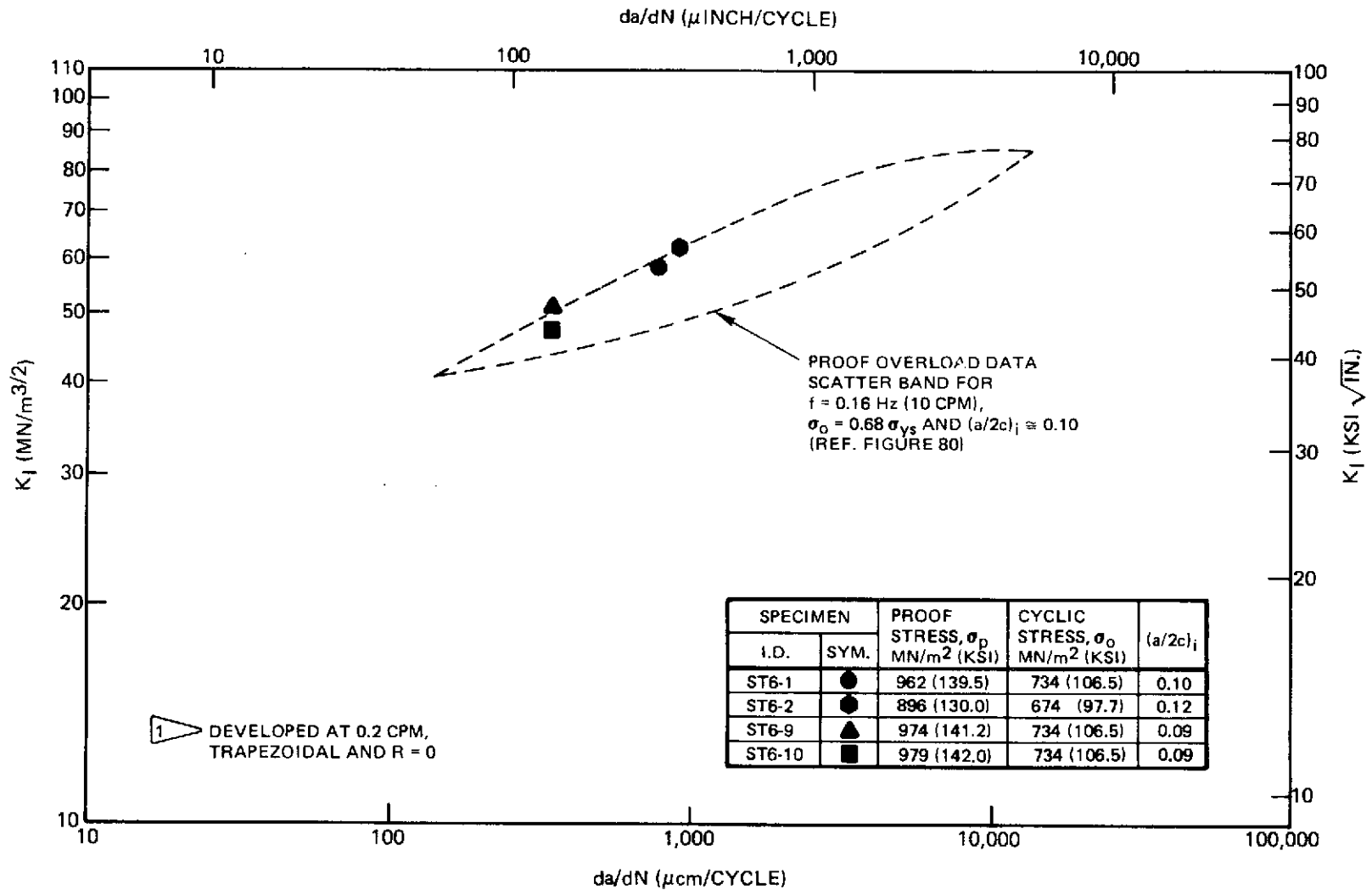


Figure 84: Cyclic Crack Growth Rates ¹ (After a Proof Test) for 0.16 cm (0.063 Inch) Thick 6Al-4V STA Titanium (WT Direction) at 295°K (72° F) in Salt Water with $\sigma_o \cong 0.68 \sigma_{ys}$ and $(a/2c)_i \cong 0.10$

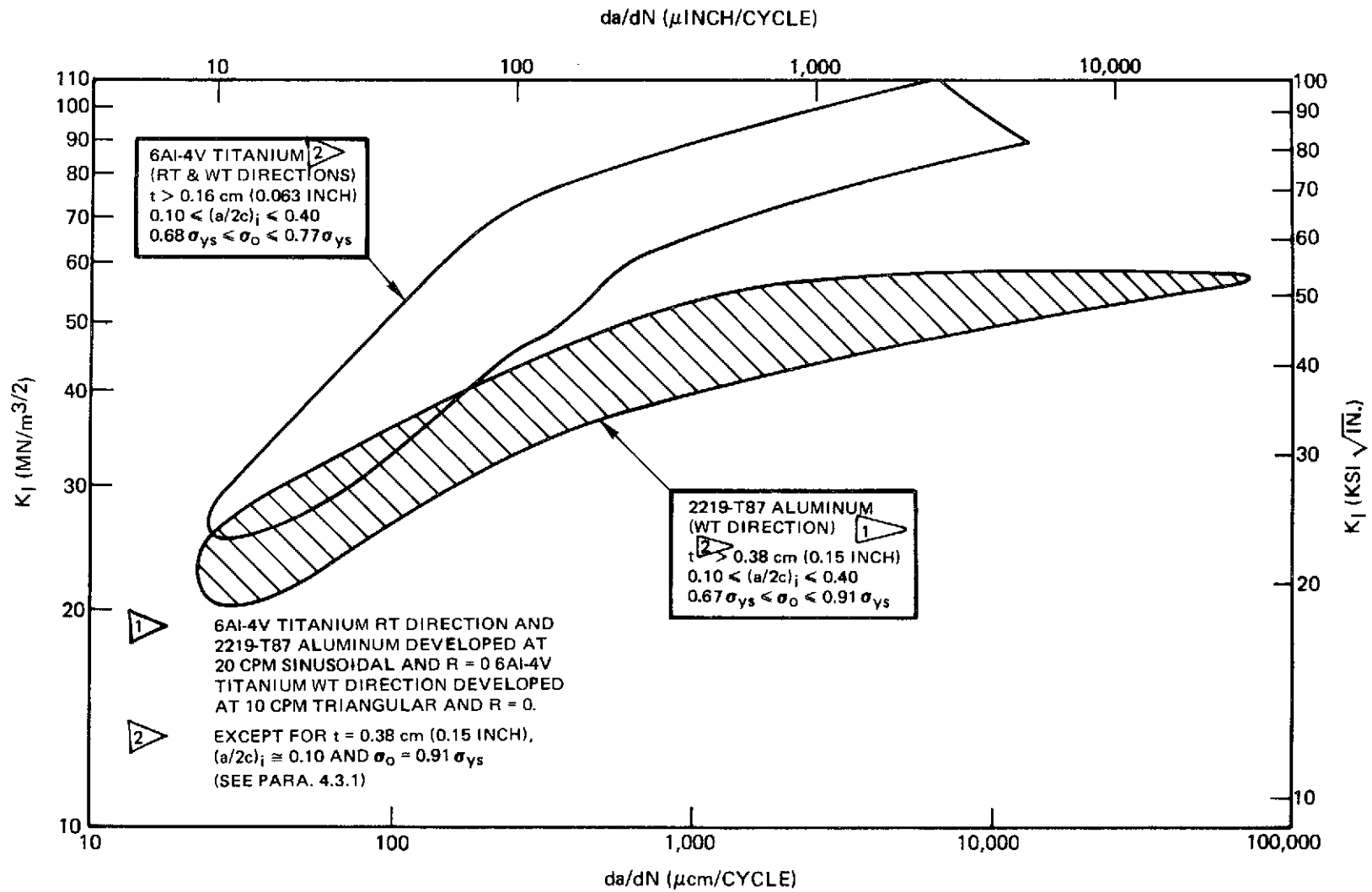


Figure 85: Summary of Baseline da/dN Developed for 2219-T87 Aluminum and 6Al-4V STA Titanium in Inert Environments

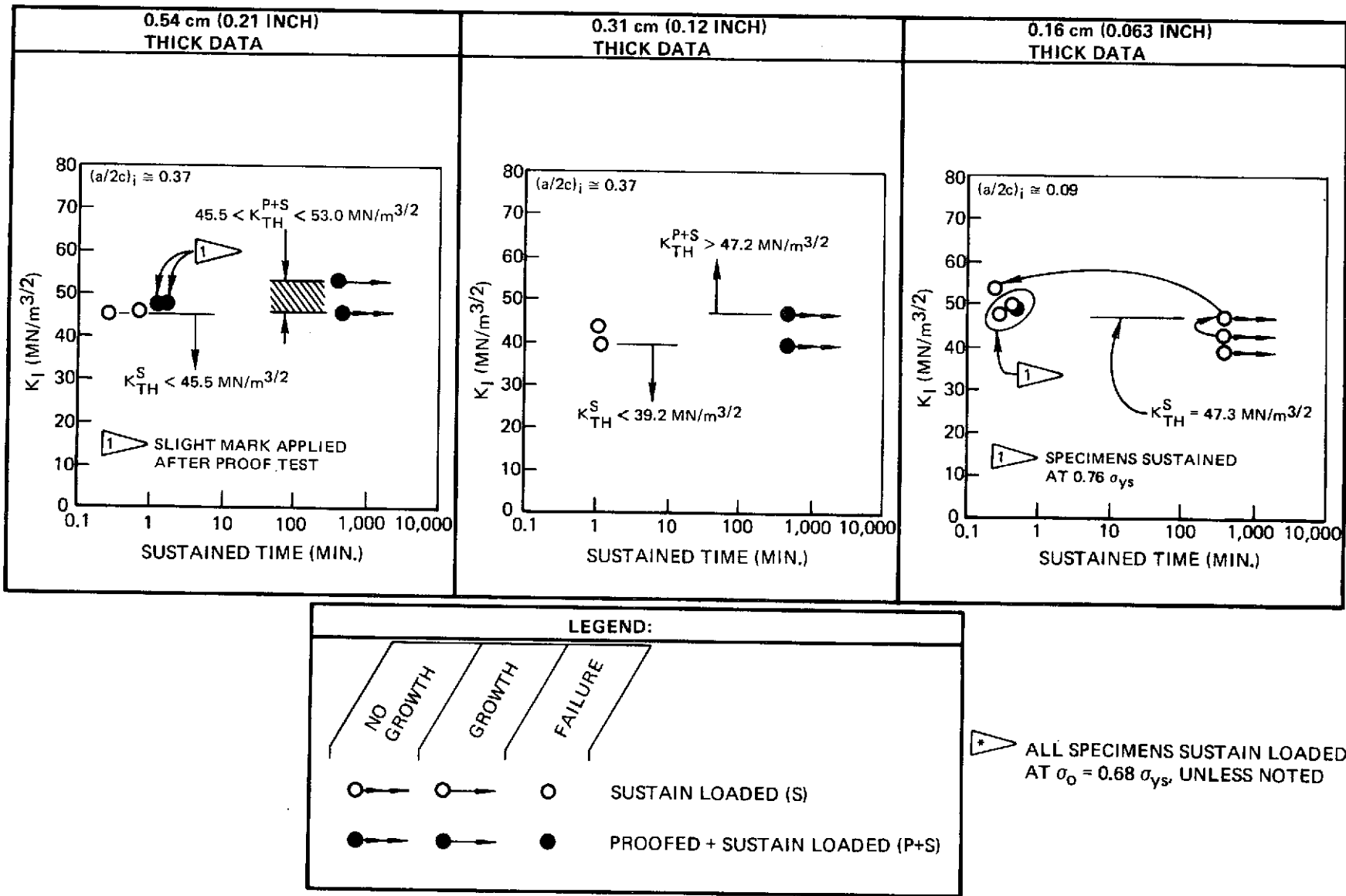


Figure 86: Summary of 6Al-4V STA Titanium (WT Direction) Sustained Load Data ^{*} in Salt Water at 295°K (72°F)

PRECEDING PAGE BLANK NOT FILMED

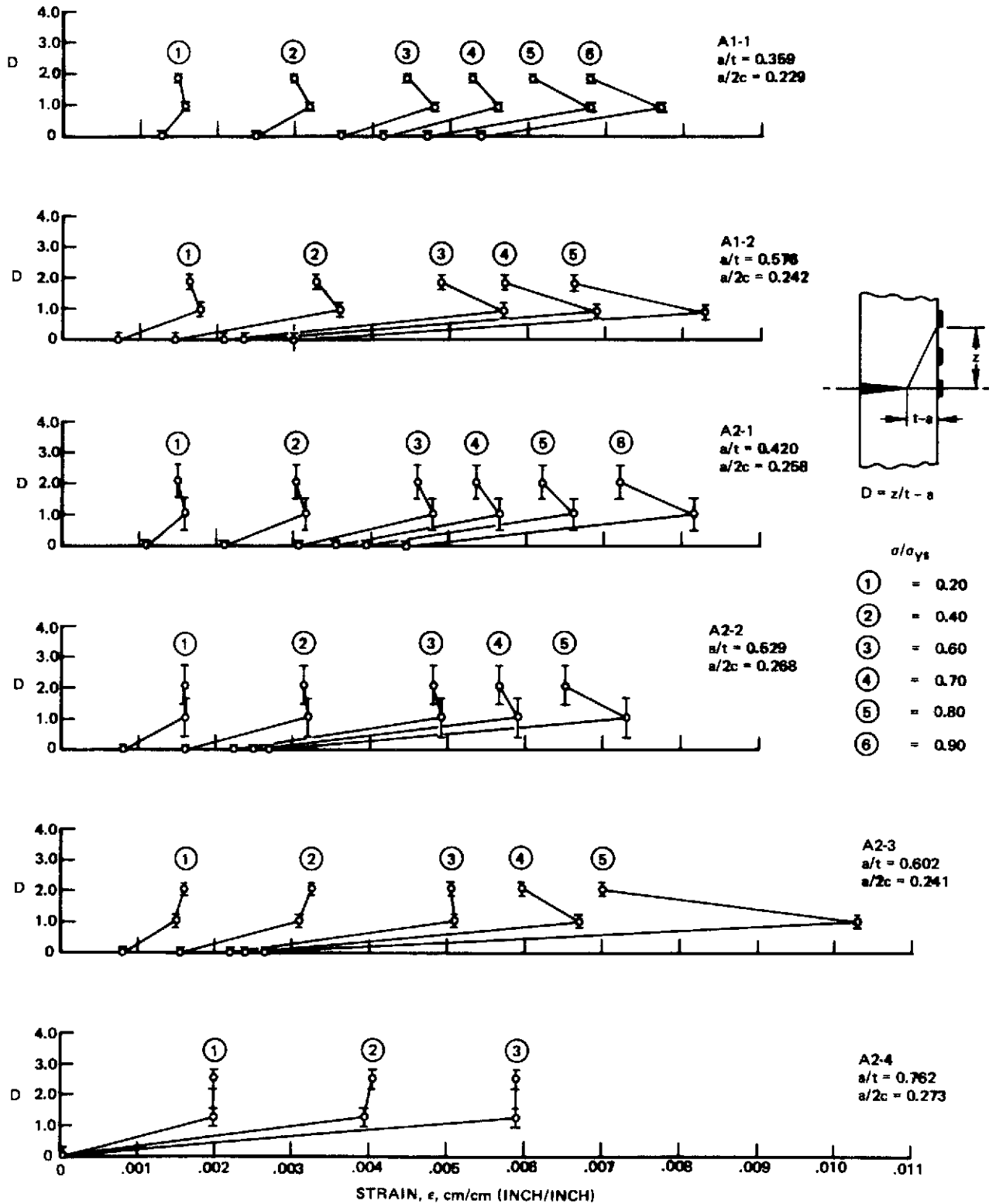


Figure A-1: Rear Surface Strain Gage Data for 0.381 cm (0.150 Inch) and 0.508 cm (0.200 Inch) Thick 7075-T651 Aluminum at Room Temperature

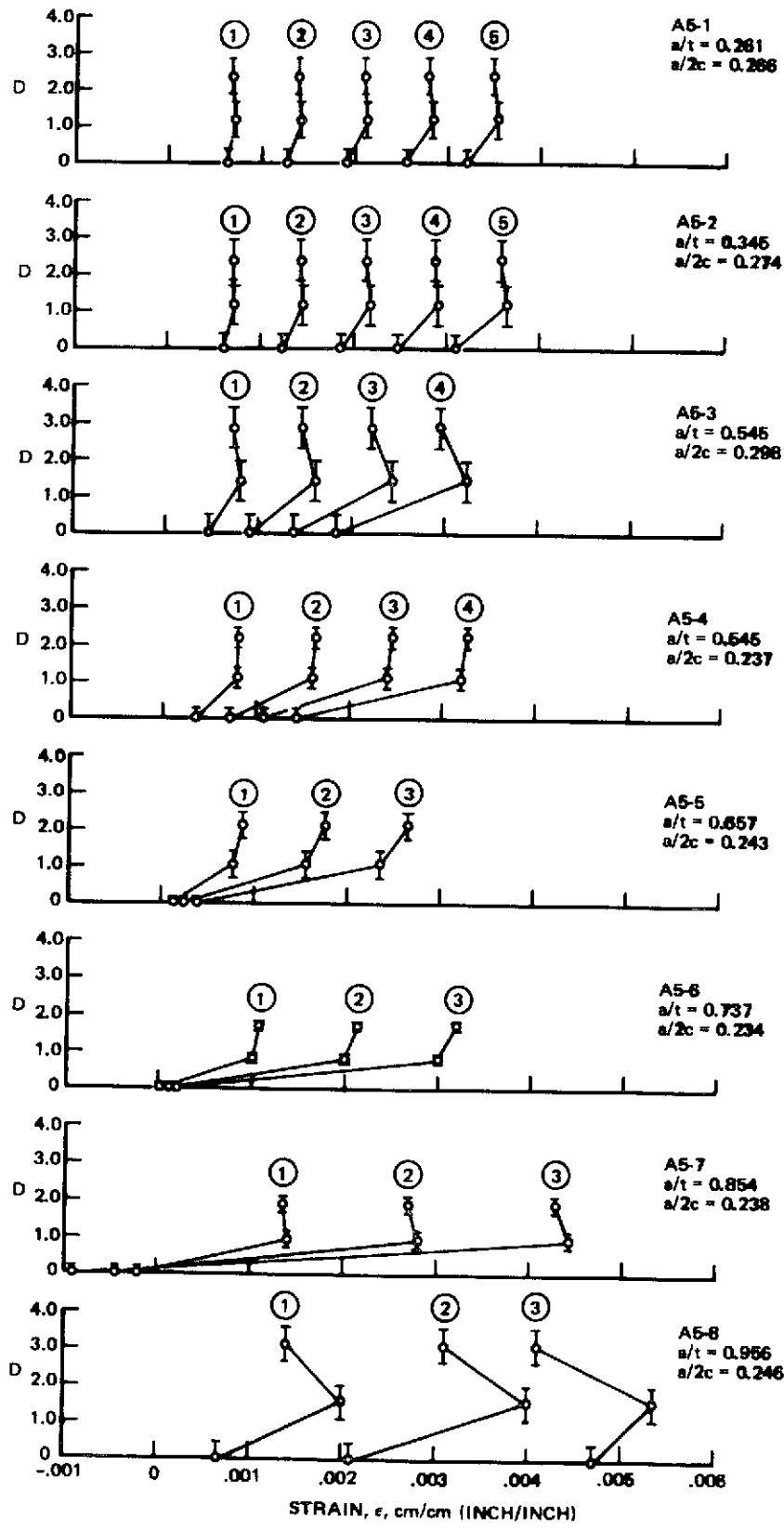


Figure A-2: Rear Surface Strain Gage Data for 1.27 cm (0.500 Inch) Thick 7075-T651 Aluminum at Room Temperature

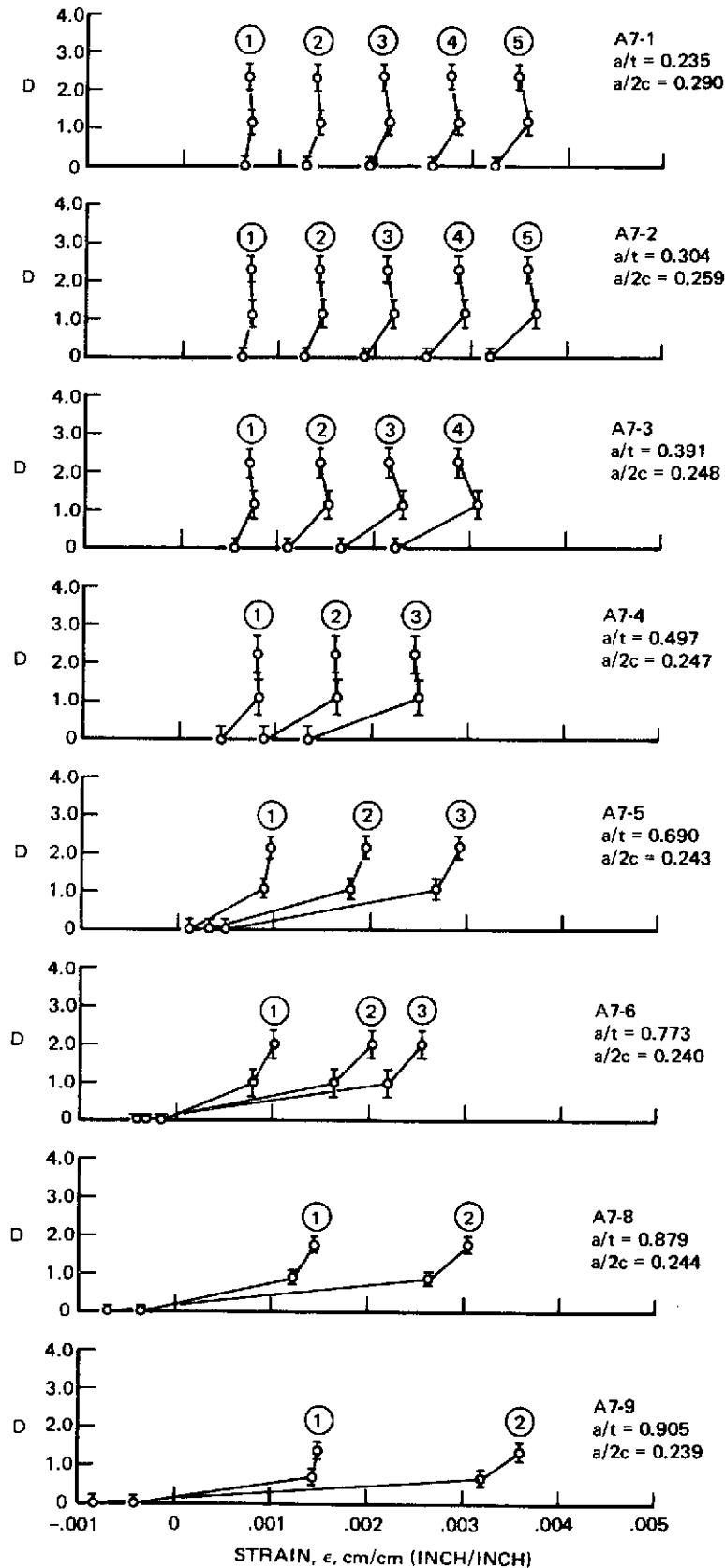


Figure A-3: Rear Surface Strain Gage Data for 1.905 cm (0.750 Inch) Thick 7075-T651 Aluminum at Room Temperature

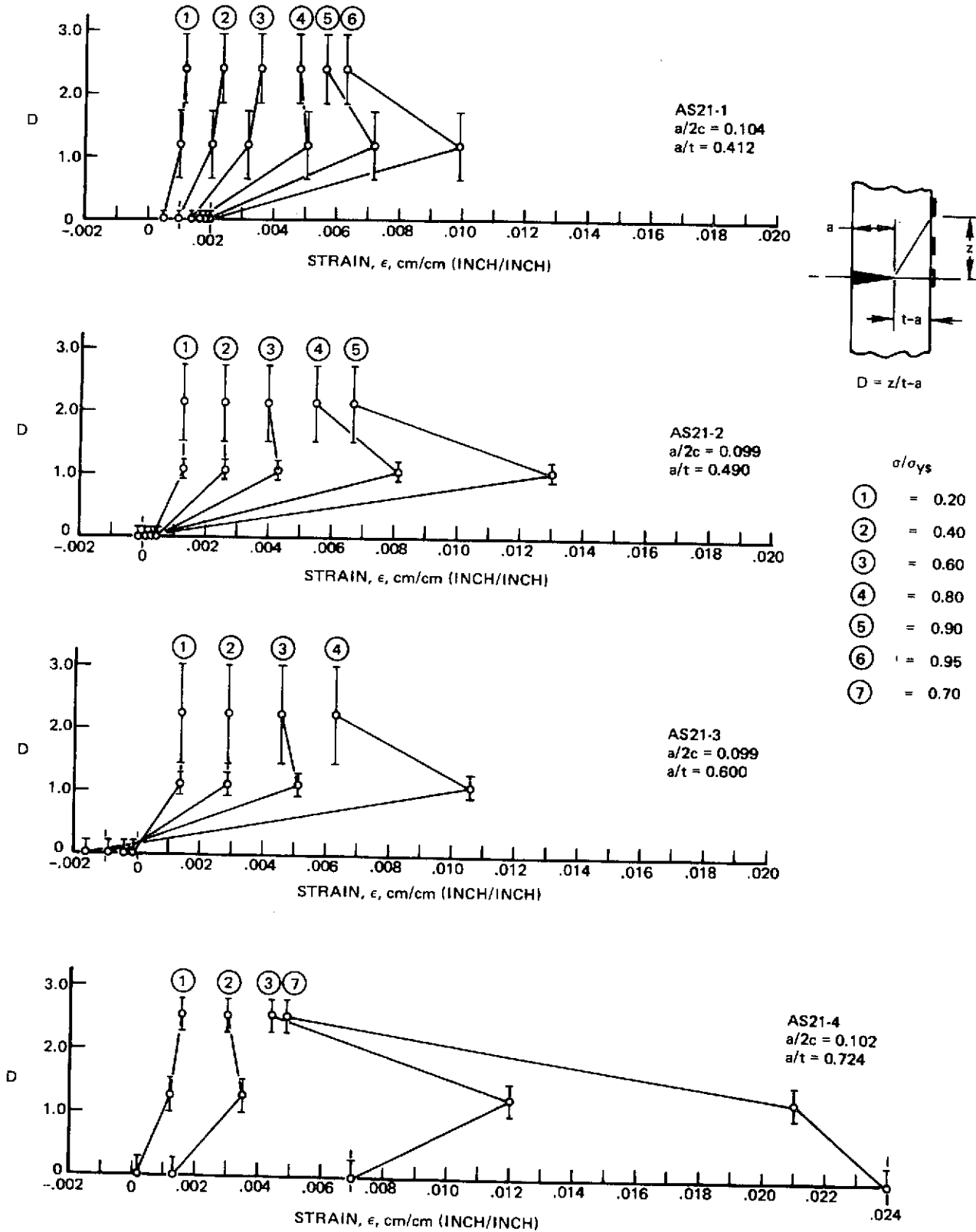


Figure A-4: Rear Surface Strain Gage Data for 0.508 cm (0.200 Inch) Thick 2219-T87 Aluminum at 78°K (-320°F)

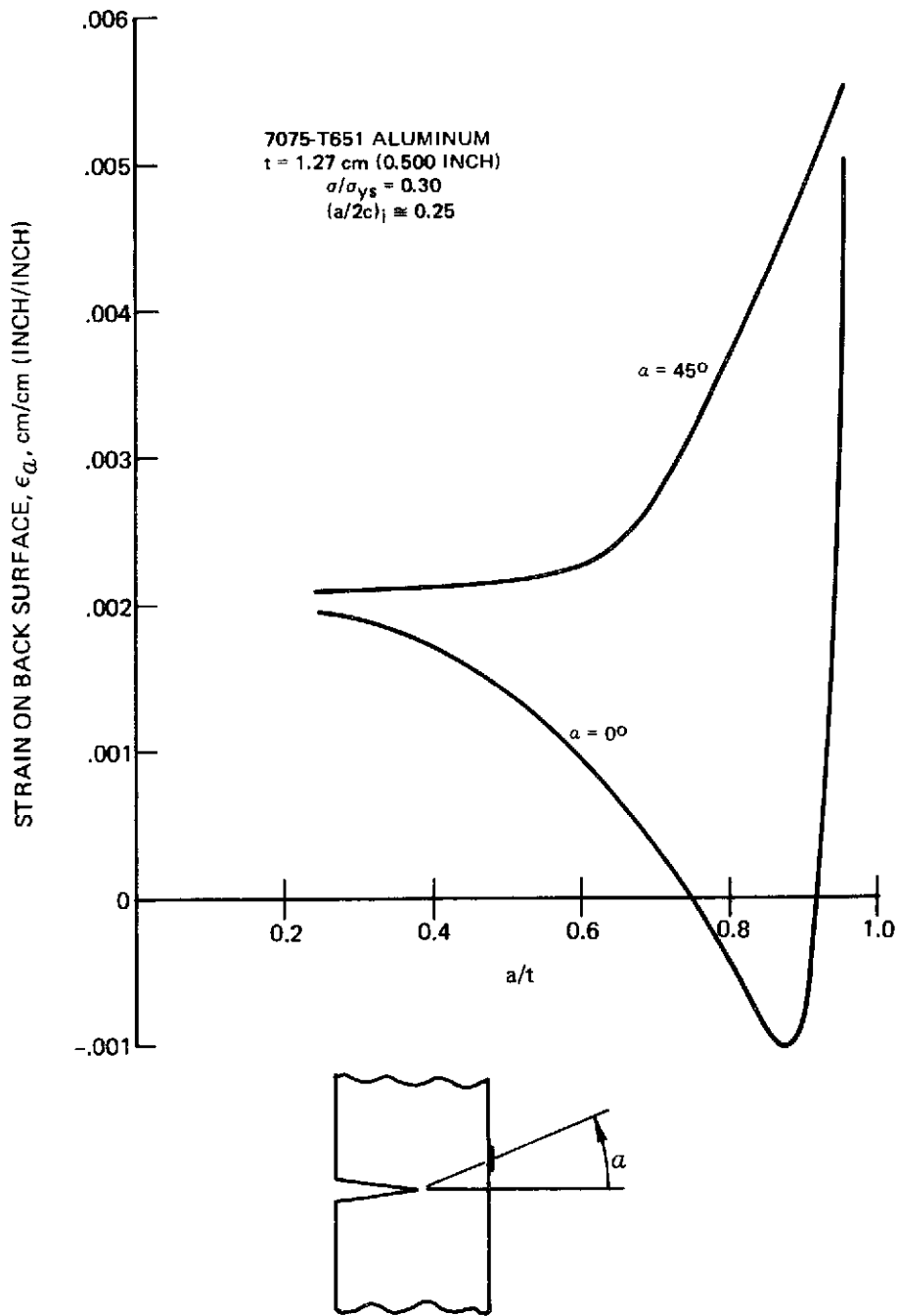


Figure A-5: Rear Surface Strain Measurements as a Function of Flaw Depth for 7075-T651 Aluminum at Room Temperature

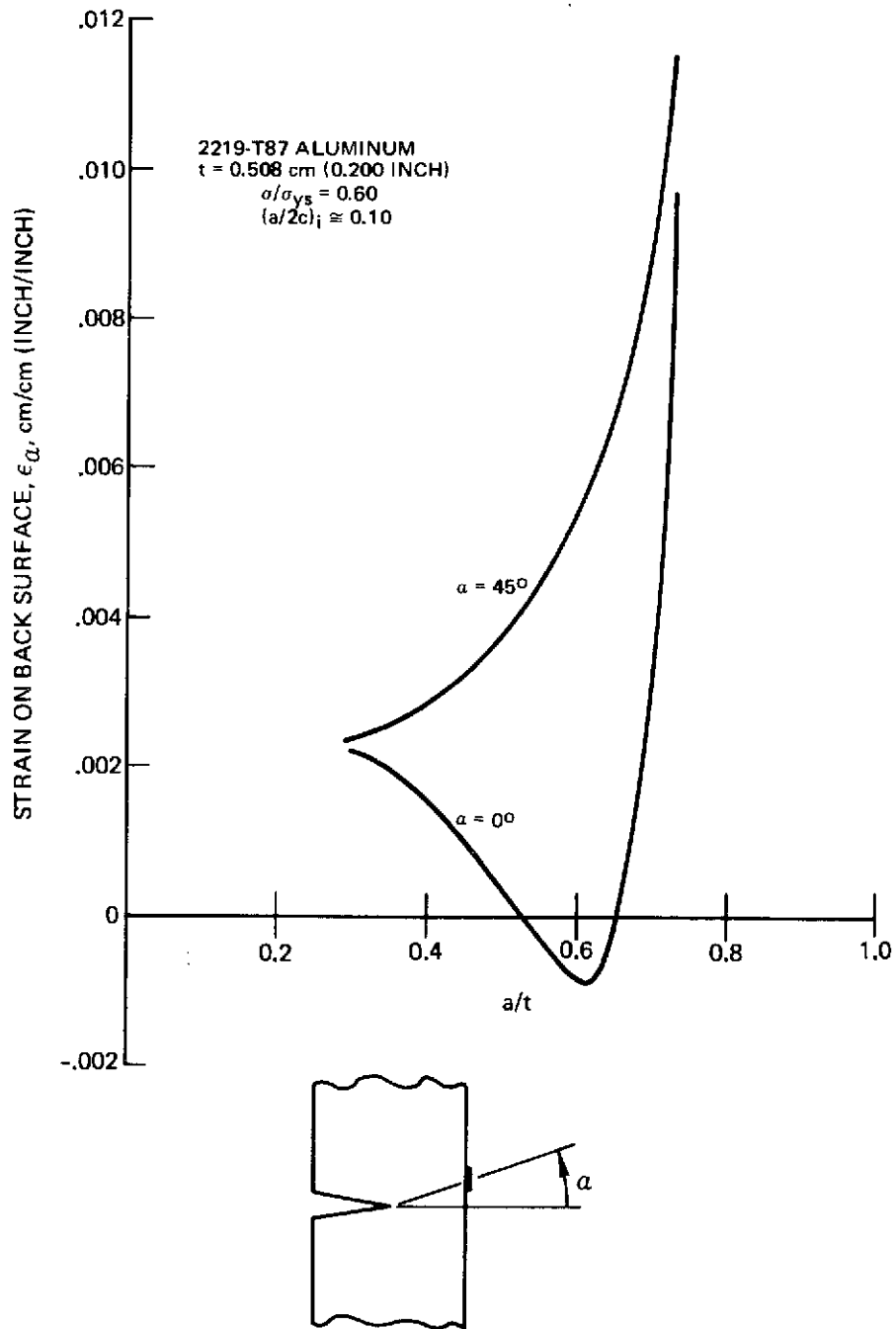


Figure A-6: Rear Surface Strain Measurement as a Function of Flaw Depth for 2219-T87 Aluminum at 78°K (-320°F)

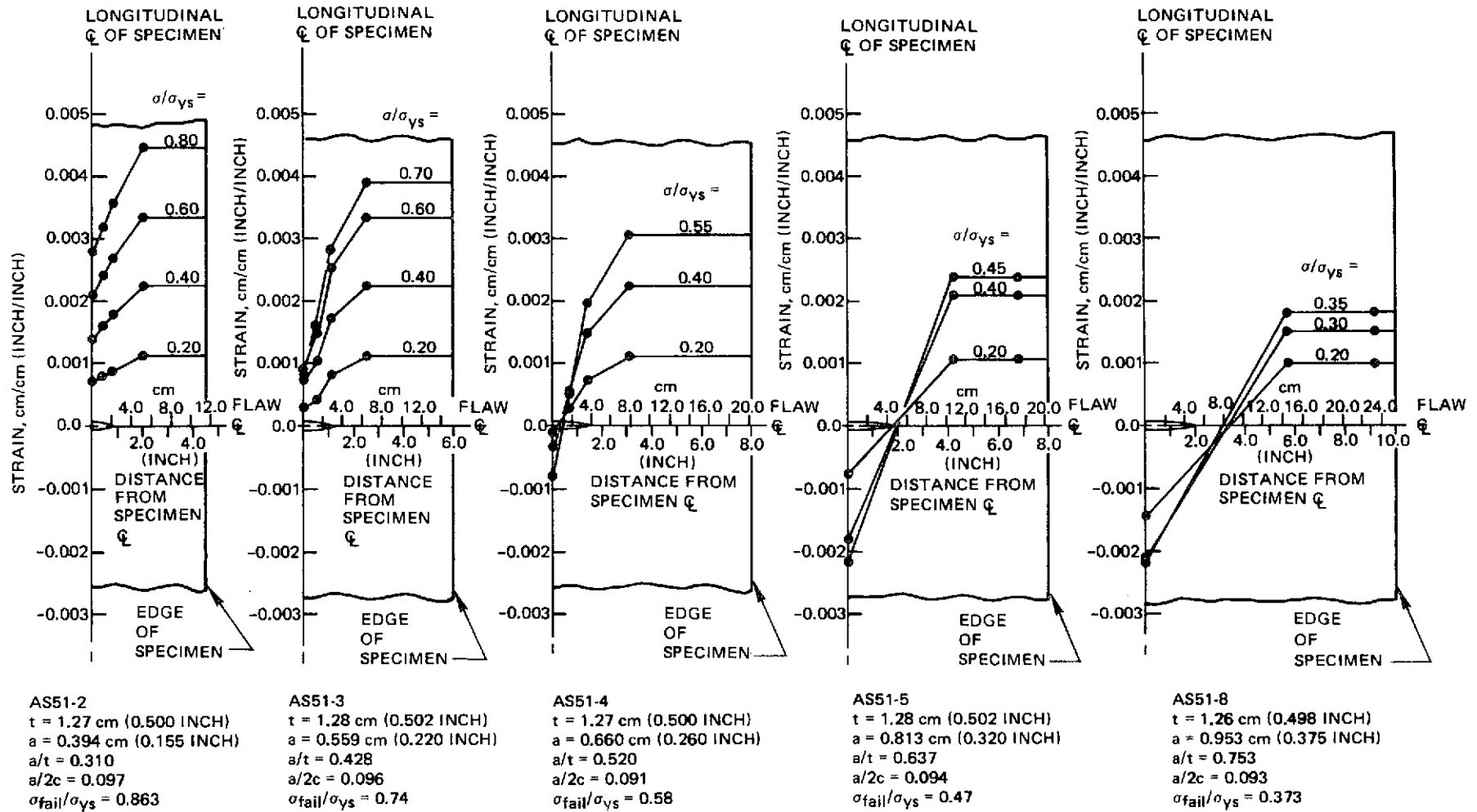


Figure A-7: Rear Surface Strain Gage Data for 1.27 cm (0.500 Inch) Thick 2219-T87 Aluminum at -320°F

PRECEDING PAGE BLANK NOT FILMED

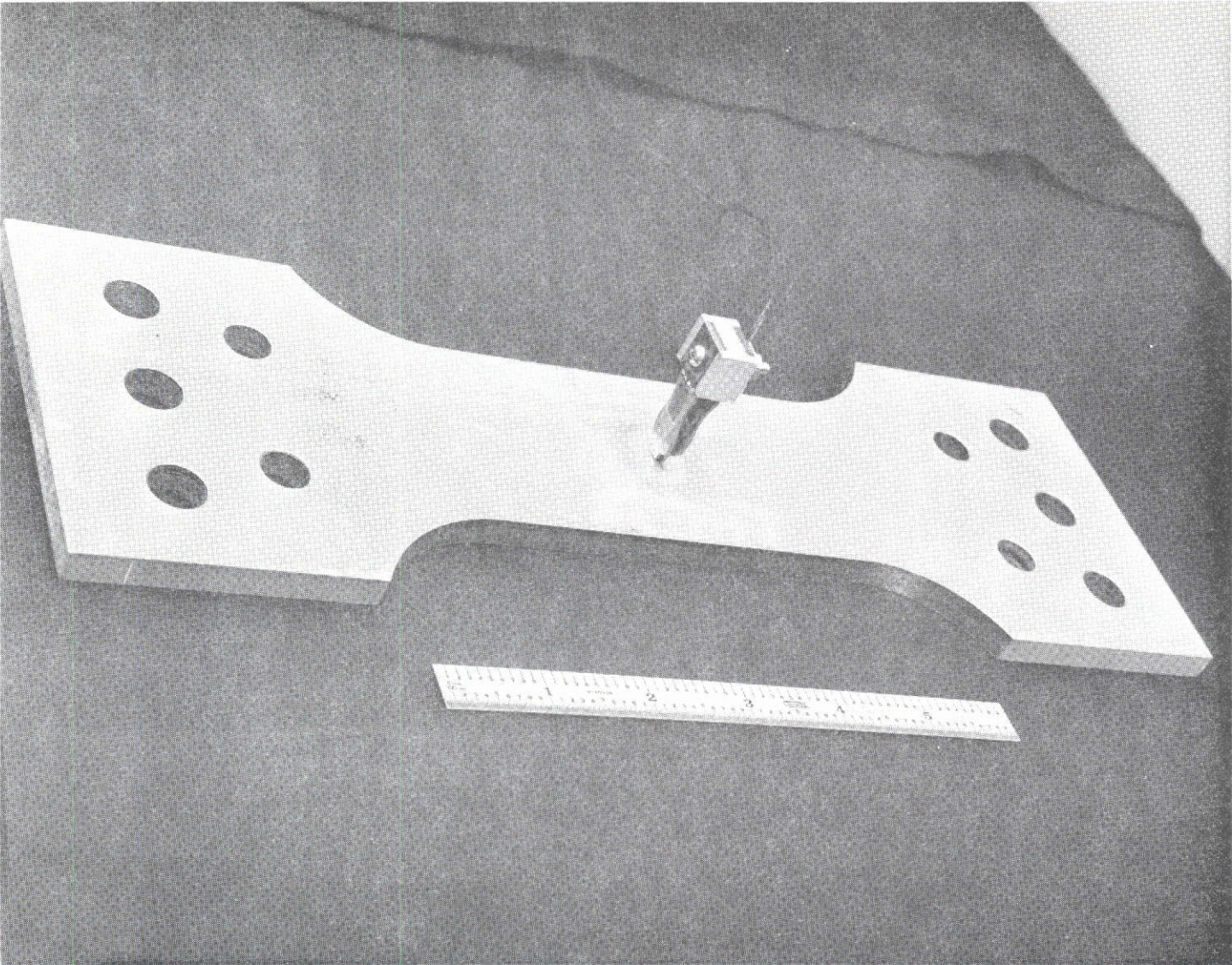


Figure B-1: EDI Clip Gage Installation

COD OBTAINED USING INTEGRAL KNIFE EDGES	SPECIMEN THICKNESS cm (INCHES)
○	0.38 (0.15)
△	0.51 (0.20)
□	1.27 (0.50)

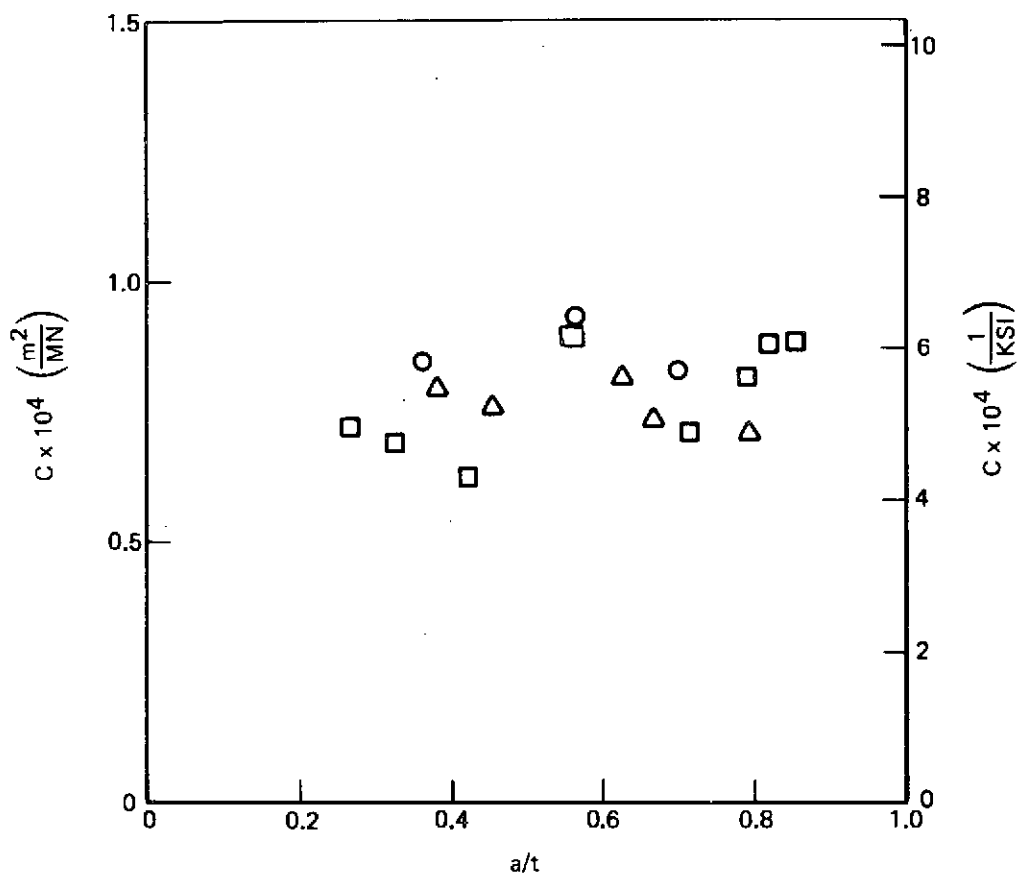


Figure B-2: Variation of C with Flaw Depth for 2219-T87 Aluminum at 78°K (-320°F) and an $(a/2c)_i \cong 0.40$

COD OBTAINED USING		SPECIMEN THICKNESS cm (INCHES)
INTEGRAL KNIFE EDGES	SPOT WELDED TABS	
△	●	0.38 (0.15)
□	▲	0.51 (0.20)
◇		1.27 (0.50)
		1.91 (0.75)

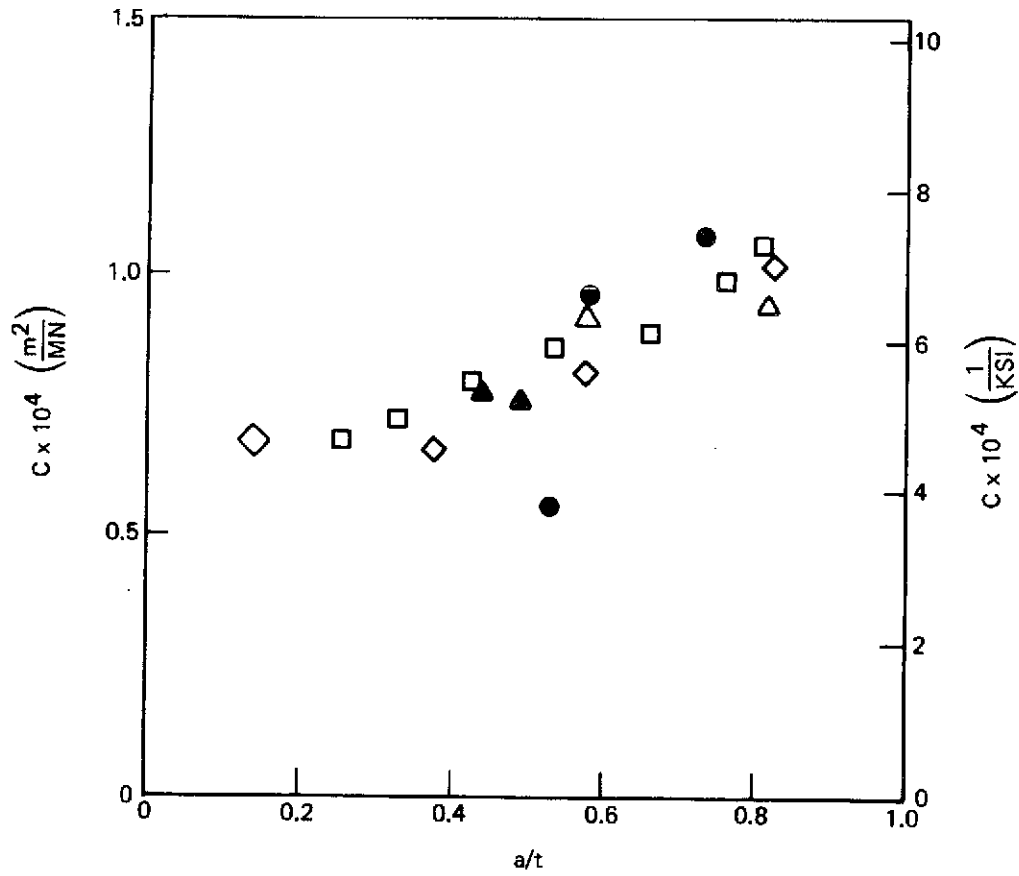


Figure B-3: Variation of C with Flaw Depth for 2219-T87 Aluminum at 78°K (-320°F) and an (a/2c)_j ≈ 0.25

COD OBTAINED USING INTEGRAL KNIFE EDGES	SPECIMEN THICKNESS cm (INCHES)
○	0.38 (0.15)
△	0.51 (0.20)
□	1.27 (0.50)

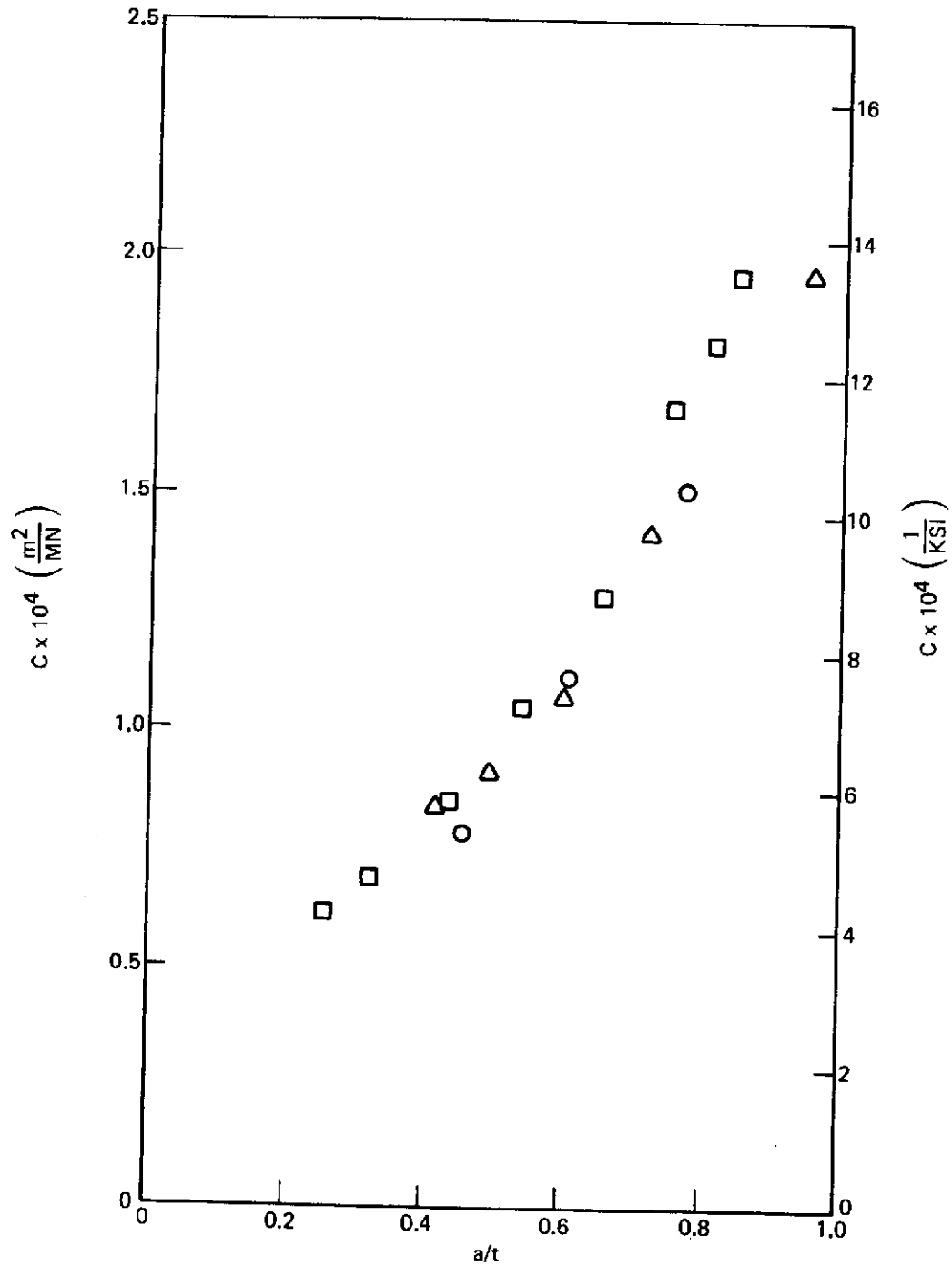


Figure B-4: Variation of C with Flaw Depth for 2219-T87 Aluminum at 78°K (-320°F) and an $(a/2c)_j \cong 0.10$

COD OBTAINED USING		SPECIMEN THICKNESS cm (INCHES)
INTEGRAL KNIFE EDGES	SPOT WELDED TABS	
○	●	0.38 (0.15)
△	▲	0.51 (0.20)
□		1.27 (0.50)
◇		1.91 (0.75)

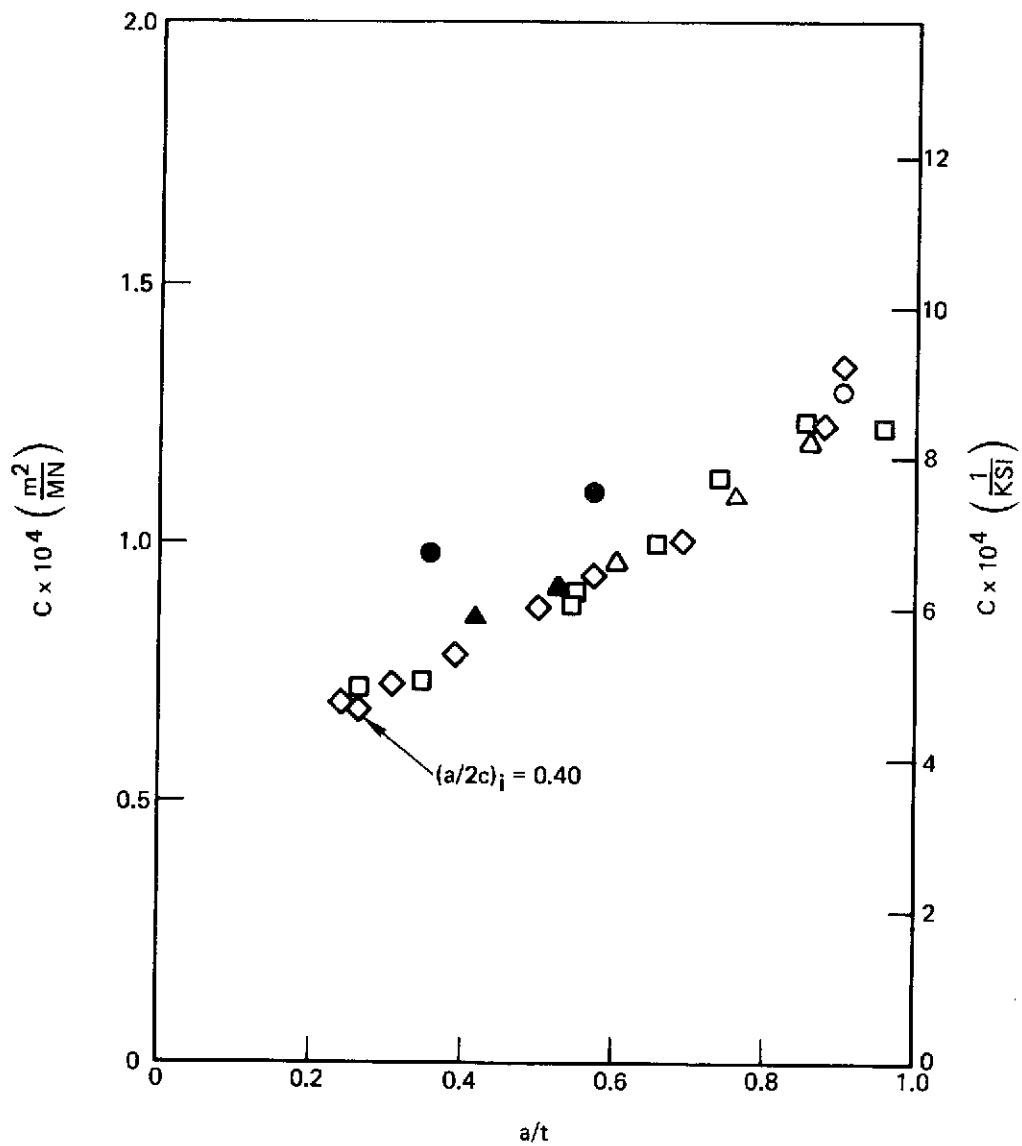


Figure B-5: Variation of C with Flaw Depth for 7075-T651 Aluminum at Room Temperature and an $(a/2c)_i \cong 0.25$

PRECEDING PAGE BLANK NOT FILMED

Table 1: Summary: NAS3-10290 Investigation of Deep Flaws in Thin Walled Tanks

MATERIAL	THICKNESS cm (INCH)	TEST TEMPERATURE °K (°F)	TEST TYPE			
			TENSILE	STATIC FRACTURE		CYCLIC SURFACE FLAWED
				SURFACE FLAWED	CENTER CRACK	
2219-T87 ALUMINUM PARENT METAL	1.588 (0.625) & 0.160 (0.063)	R.T. 78 (-320) 20 (-423)	X X X	X X X	X X X	X X X
2219 ALUMINUM WELD METAL	2.54 (1.00) & 0.318 (0.125)	R.T. 78 (-320) 20 (-423)	X X X	X X X	X X X	X X X
5Al-2.55n ELI TITANIUM PARENT METAL	0.508 (0.200) & 0.051 (0.020)	R.T. 78 (-320) 20 (-423)	X X X	X X X	X X X	X X X
5Al-2.5Sn TITANIUM WELD METAL	0.508 (0.200) & 0.051 (0.020)	R.T. 78 (-320) 20 (-423)	X X X	X X X	X X X	X X X

Table 2: Test Summary

MATERIAL	GAGE THICKNESS cm (INCH)	TENSILE TESTS	SURFACE FLAW TESTS				
			TEST TEMPERATURE °K (°F)	FLAW DEPTH TO LENGTH RATIO (a/2c)			
				STATIC FRACTURE	CYCLIC	OVERLOAD CYCLIC	OVERLOAD SUSTAINED
2219-T87 ALUMINUM PARENT METAL	0.381 (0.150)	(A)	78 (-320)	0.10, 0.25, 0.40	0.10 & 0.40	0.10 & 0.40	0.10 & 0.40
	0.508 (0.200)	—		0.10, 0.25, 0.40	—	—	—
	1.270 (0.500)	—		0.10, 0.25, 0.40	0.10 & 0.40	0.10 & 0.40	0.10 & 0.40
	1.905 (0.750)	(A)		0.25	—	—	—
6Al-4V STA TITANIUM PARENT METAL	0.076 (0.030)	(A)	R.T.	0.10, 0.25, 0.40	—	—	—
	0.152 (0.060)	—		0.10, 0.25, 0.40	0.10 & 0.40	0.10 & 0.40	0.10 & 0.40
	0.305 (0.120)	—		0.10, 0.25, 0.40	—	0.10 & 0.40	0.10 & 0.40
	0.533 (0.210)	—		0.10, 0.25, 0.40	0.10 & 0.40	0.10 & 0.40	0.10 & 0.40
7075-T651 ALUMINUM PARENT METAL	0.381 (0.150)	(B)	R.T.	0.25	—	—	—
	0.508 (0.200)	—		0.25	—	—	—
	1.270 (0.500)	—		0.25	—	—	—
	1.950 (0.750)	(B)		0.25	—	—	—

(A) – TENSILE TESTS (BOTH LONGITUDINAL & TRANSVERSE) CONDUCTED AT R.T., 78°K (-320°F) AND 20°K (-423°F)

(B) – TENSILE TESTS (BOTH LONGITUDINAL & TRANSVERSE) CONDUCTED AT R.T.

Table 3: Chemical Compositions of Materials

ELEMENT (% By Weight)	2219 ALUMINUM PLATE		7075 ALUMINUM PLATE		6Al-4V TITANIUM PLATE
	Min.	Max.	Min.	Max.	
Copper	5.80	6.80	1.20	2.00	—
Silicon	—	0.20	—	0.50	—
Manganese	0.20	0.40	—	0.30	—
Magnesium	—	0.20	2.10	2.90	—
Iron	—	0.30	—	0.70	0.120
Chromium	—	—	0.18	0.40	—
Zinc	—	0.10	5.10	6.10	—
Vanadium	0.05	0.15	—	—	4.0
Zirconium	0.10	0.25	—	—	—
Carbon	—	—	—	—	0.026
Nitrogen (ppm)	—	—	—	—	130
Oxygen (ppm)	—	—	—	—	1500
Hydrogen (ppm)	—	—	—	—	80
Titanium	0.02	0.10	—	0.20	Remainder
Aluminum	Remainder		Remainder		5.80
Other	—	—	—	0.15	—

Table 4: Tensile Properties 2219-T87 Aluminum Parent Metal

SPECIMEN NUMBER	NOMINAL THICKNESS cm (INCH)	CROSS-SECTIONAL AREA cm ² (INCH ²)	GRAIN DIRECTION L—LONGITUDINAL T—TRANSVERSE	TEST ENVIRONMENT	TEST TEMPERATURE °K (°F)	ULTIMATE STRENGTH MN/m ² (KSI)	YIELD STRENGTH MN/m ² (KSI)	PERCENT ELONGATION IN 5.08 cm (2.0 INCH) GAGE LENGTH	REDUCTION IN AREA AT FRACTURE (%)	POISSON'S RATIO	MODULUS OF ELASTICITY ~ E x 10 ⁻³ MN/m ² (~ E x 10 ⁻³ KSI)				
TA-1	1.91 (0.75)	2.406 (0.373)	L	AIR	R.T.	469.5 (68.10)	381.3 (55.30)	12.5	24.8	0.331	73.1 (10.6)				
TA-2	1.91 (0.75)	2.406 (0.373)				69.0 (10.0)									
TA-7	0.38 (0.15)	0.497 (0.077)				73.8 (10.7)									
TA-8	0.38 (0.15)	0.491 (0.076)				75.8 (11.0)									
TA-13	1.91 (0.75)	2.451 (0.380)	T			LN ₂	78 (-320)	471.6 (68.40)	374.4 (54.30)	8.0	10.4	0.336	72.4 (10.5)		
TA-14	1.91 (0.75)	2.458 (0.381)						71.0 (10.3)							
TA-19	0.38 (0.15)	0.497 (0.077)						78.6 (11.4)							
TA-20	0.38 (0.15)	0.491 (0.076)						74.5 (10.8)							
TA-3	1.91 (0.75)	2.432 (0.377)	L					LN ₂	78 (-320)	574.4 (83.30)	439.2 (63.70)	14.0	25.3	0.309	75.2 (10.9)
TA-4	1.91 (0.75)	2.451 (0.380)								79.3 (11.5)					
TA-9	0.38 (0.15)	0.491 (0.076)								80.7 (11.7)					
TA-10	0.38 (0.15)	0.491 (0.076)								82.7 (12.0)					
TA-15	1.91 (0.75)	2.465 (0.382)	T	LN ₂	78 (-320)					584.7 (84.80)	455.1 (66.00)	11.0	13.3	0.329	81.4 (11.8)
TA-16	1.91 (0.75)	2.445 (0.379)								77.2 (11.2)					
TA-21	0.38 (0.15)	0.491 (0.076)								84.8 (12.3)					
TA-22	0.38 (0.15)	0.491 (0.076)								80.7 (11.7)					
TA-5	1.91 (0.75)	2.451 (0.380)	L			LN ₂	20 (-423)			681.9 (98.90)	469.5 (68.10)	16.5	20.0	0.349	95.8 (13.9)
TA-6	1.91 (0.75)	2.471 (0.383)								100.7 (14.6)					
TA-11	0.38 (0.15)	0.497 (0.077)								92.4 (13.4)					
TA-12	0.38 (0.15)	0.490 (0.076)								—					
TA-17	1.91 (0.75)	2.413 (0.374)	T					LN ₂	20 (-423)	699.8 (101.50)	497.8 (72.20)	12.0	11.6	0.389	102.0 (14.8)
TA-18	1.91 (0.75)	2.445 (0.379)								97.9 (14.2)					
TA-23	0.38 (0.15)	0.491 (0.076)								99.3 (14.4)					
TA-24	0.38 (0.15)	0.491 (0.076)								97.9 (14.2)					

Table 5: Tensile Properties 7075-T6 Aluminum Parent Metal

SPECIMEN NUMBER	NOMINAL THICKNESS cm (INCH)	CROSS-SECTIONAL AREA cm ² (IN. ²)	GRAIN DIRECTION L—LONGITUDINAL T—TRANSVERSE	TEST ENVIRONMENT	TEST TEMPERATURE, °K (°F)	ULTIMATE STRENGTH, MN/m ² (KSI)	YIELD STRENGTH MN/m ² (KSI)	% ELONGATION IN 5.08 cm (2.00 INCH) GAGE LENGTH	REDUCTION IN AREA AT FRACTURE (%)	POISSON'S RATIO	MODULUS OF ELASTICITY E x 10 ⁻³ MN/m ² (E x 10 ⁻³ KSI)
AT-1	1.91 (0.75)	2.426 (0.376)	T	AIR	R.T.	599.2 (86.90)	520.6 (75.50)	12.2	16.5	0.327	68.3 (9.9)
AT-2	1.91 (0.75)	2.445 (0.379)				600.6 (87.10)	528.2 (76.60)	13.1	17.2	0.346	70.3 (10.2)
AT-3	0.38 (0.15)	0.484 (0.075)				621.2 (90.10)	554.4 (80.40)	9.5	12.9	0.325	75.2 (10.9)
AT-4	0.38 (0.15)	0.490 (0.076)				608.1 (88.20)	541.3 (78.50)	9.4	13.9	0.331	65.5 (9.5)
						AVG. 536.1 (77.75)					
AT-5	1.91 (0.75)	2.439 (0.378)	L	AIR	R.T.	610.9 (88.60)	553.0 (80.20)	12.4	14.4	0.315	74.5 (10.8)
AT-6	1.91 (0.75)	2.439 (0.378)				609.5 (88.40)	550.9 (79.90)	11.8	14.7	0.306	69.6 (10.1)
AT-7	0.38 (0.15)	0.497 (0.077)				609.5 (88.40)	550.2 (79.80)	9.8	11.8	0.317	65.5 (9.5)
AT-8	0.38 (0.15)	0.490 (0.076)				609.5 (88.40)	549.5 (79.70)	10.4	15.6	0.334	64.1 (9.3)

Table 6: Tensile Properties 6Al-4V STA Titanium Parent Metal

SPECIMEN NUMBER	NOMINAL THICKNESS cm (INCH)	CROSS-SECTIONAL AREA, cm ² (IN. ²)	GRAIN DIRECTION L—LONGITUDINAL T—TRANSVERSE	TEST ENVIRONMENT	TEST TEMPERATURE, °K (°F)	ULTIMATE STRENGTH, MN/m ² (KSI)	YIELD STRENGTH MN/m ² (KSI)	% ELONGATION IN 5.08 cm (2.00 INCH) GAGE LENGTH	REDUCTION IN AREA OF FRACTURE (%)	POISSON'S RATIO	MODULUS OF ELASTICITY E x 10 ⁻³ MN/m ² (E x 10 ⁻³ KSI)				
TT-1	0.64 (0.25)	0.806 (0.125)	L	AIR	R.T.	1174.2 (170.30)	1073.5 (155.70)	10.0	35.9	0.282	117.9 (17.1)				
TT-2	0.64 (0.25)	0.800 (0.124)				1174.2 (170.30)	1070.1 (155.20)	11.0	34.1	0.291	118.6 (17.2)				
TT-7	0.05 (0.02)	0.071 (0.011)				1137.0 (164.90)	1017.0 (147.50)	5.6	30.7	0.310	117.9 (17.1)				
TT-8	0.05 (0.02)	0.071 (0.011)				1143.2 (165.80)	1039.8 (150.80)	5.6	28.3	0.291	118.6 (17.2)				
TT-13	0.64 (0.25)	0.819 (0.127)	T			LN ₂	78 (-320)	1191.5 (172.80)	1117.0 (162.00)	9.0	31.2	0.290	126.2 (18.3)		
TT-14	0.64 (0.25)	0.819 (0.127)						1199.7 (174.00)	1115.6 (161.80)	10.0	36.3	0.303	129.6 (18.8)		
TT-19	0.05 (0.02)	0.071 (0.011)						1137.7 (165.00)	1049.4 (152.20)	6.0	28.9	0.306	122.0 (17.7)		
TT-21	0.05 (0.02)	0.071 (0.011)						1181.1 (171.30)	1081.1 (156.80)	5.0	23.3	0.308	124.8 (18.1)		
TT-3	0.64 (0.25)	0.819 (0.127)	L					LN ₂	78 (-320)	1758.9 (255.10)	1658.3 (240.50)	10.6	19.4	0.293	133.1 (19.3)
TT-4	0.64 (0.25)	0.819 (0.127)								1741.0 (252.50)	1659.6 (240.70)	10.6	20.3	0.291	132.4 (19.2)
TT-9	0.05 (0.02)	0.071 (0.011)								1671.3 (242.40)	1570.7 (227.80)	4.0	22.4	0.285	125.5 (18.2)
TT-10	0.05 (0.02)	0.071 (0.011)								1648.6 (239.10)	1550.0 (225.10)	3.0	21.7	0.297	124.1 (18.0)
TT-15	0.64 (0.25)	0.819 (0.127)	T	LN ₂	78 (-320)					1716.9 (249.00)	1634.8 (237.10)	5.5	22.5	0.288	133.1 (19.3)
TT-16	0.64 (0.25)	0.819 (0.127)								1730.0 (250.90)	1662.4 (241.10)	6.0	22.1	0.305	134.5 (19.5)
TT-20	0.05 (0.02)	0.071 (0.011)								1687.2 (244.70)	1612.1 (233.80)	3.0	21.7	0.301	133.8 (19.4)
TT-22	0.05 (0.02)	0.071 (0.011)								1762.4 (255.60)	1684.4 (244.30)	3.5	19.2	0.294	139.3 (20.2)
TT-5	0.64 (0.25)	0.794 (0.123)	L			LN ₂	20 (-423)			2004.4 (290.7)	1976.1 (286.6)	—	18.7	0.259	122.2 (17.72)
TT-6	0.64 (0.25)	0.813 (0.126)								2017.5 (292.6)	1978.2 (286.9)	3.0	15.9	0.264	127.9 (18.55)
TT-11	0.05 (0.02)	0.071 (0.011)								—	—	—	—	0.262	127.4 (18.48)
TT-12	0.05 (0.02)	0.077 (0.012)								1989.2 (288.5)	1923.0 (278.9)	2.4	12.8	0.261	126.5 (18.35)
TT-17	0.64 (0.25)	0.819 (0.127)	T					LN ₂	20 (-423)	1931.3 (280.1)	1909.2 (276.9)	3.0	18.0	0.290	136.7 (19.83)
TT-18	0.64 (0.25)	0.819 (0.127)								1949.2 (282.7)	—	2.2	14.6	0.232	133.1 (19.31)
TT-23	0.05 (0.02)	0.071 (0.011)								1953.4 (283.3)	1861.0 (269.9)	3.0	18.0	0.261	134.9 (19.57)
TT-24	0.05 (0.02)	0.071 (0.011)								1958.2 (284.0)	1881.0 (272.8)	1.8	—	0.253	135.7 (19.68)

Table 7: Static Fracture Data for 0.38 cm (0.15 Inch) 2219-T87 Aluminum Parent Metal (WT Direction)

SPECIMEN			TEST		FRACTURE DATA								
Number	Gage Thickness, t cm (Inch)	Gage Width, w cm (Inch)	Temperature °K (°F)	Environment	Failure Stress, σ_G MN/m ² (Ksi)	Dimpling Stress, σ_D MN/m ² (Ksi)	Breakthrough Stress, σ_B MN/m ² (Ksi)	Initial Raw Depth, a_i cm (Inch)	Initial Flaw Length, (2c) _i cm (Inch)	Initial Flaw Depth Gage Thickness, a/t	Initial Flaw Depth Initial Flaw Length, (a/2c) _i	Failure Stress Yield Stress, σ_G/σ_{ys}	Irwin's Apparent K MN/m ^{3/2} (Ksi√In)
AS14-1	0.386 (0.152)	8.89 (3.50)	78 (-320)	LN ₂	485.4 (70.4)	446.8 (64.8)	—	0.142 (0.056)	0.386 (0.152)	0.368	0.368	1.07	27.6 (25.1)
AS14-2	0.386 (0.152)	8.89 (3.50)			470.2 (68.2)	437.1 (63.4)	—	0.218 (0.086)	0.579 (0.228)	0.566	0.377	1.04	32.9 (29.9)
AS14-3	0.381 (0.150)	8.89 (3.50)			455.8 (66.1)	388.2 (56.3)	452.3 (65.6)	0.269 (0.106)	0.742 (0.292)	0.707	0.363	1.01	35.9 (32.7)
AS12-1	0.384 (0.151)	8.89 (3.50)	78 (-320)	LN ₂	470.2 (68.2)	355.1 (51.5)	—	0.203 (0.080)	0.655 (0.258)	0.530	0.310	1.04	34.3 (31.2)
AS12-2	0.381 (0.150)	8.89 (3.50)			445.4 (64.6)	400.6 (58.1)	—	0.221 (0.087)	0.914 (0.360)	0.580	0.242	0.98	36.7 (33.4)
AS12-3	0.386 (0.152)	8.89 (3.50)			425.4 (61.7)	391.6 (56.8)	424.0 (61.5)	0.284 (0.112)	1.232 (0.485)	0.737	0.231	0.94	40.0 (36.4)
AS11-1	0.378 (0.149)	8.89 (3.50)	78 (-320)	LN ₂	441.3 (64.0)	366.1 (53.1)	—	0.173 (0.068)	1.524 (0.600)	0.456	0.113	0.97	37.1 (33.8)
AS11-2	0.381 (0.150)	12.70 (5.00)			410.9 (59.6)	312.3 (45.3)	391.6 (56.8)	0.231 (0.091)	2.261 (0.890)	0.607	0.102	0.91	40.0 (36.4)
AS11-3	0.376 (0.148)	12.70 (5.00)			336.5 (48.8)	—	304.8 (44.2)	0.292 (0.115)	3.073 (1.210)	0.777	0.095	0.74	35.9 (32.7)

Table 8: Static Fracture Data for 0.51 cm (0.20 Inch) 2219-T87 Aluminum Parent Metal (WT Direction)

SPECIMEN			TEST		FRACTURE DATA								
Number	Gage Thickness, t cm (Inch)	Gage Width, w cm (Inch)	Temperature $^{\circ}$ K ($^{\circ}$ F)	Environment	Failure Stress, σ_G MN/m ² (Ksi)	Dimpling Stress, σ_D MN/m ² (Ksi)	Breakthrough Stress, σ_B MN/m ² (Ksi)	Initial Flaw Depth, a_i cm (Inch)	Initial Flaw Length, (2c) _i cm (Inch)	Initial Flaw Depth Gage Thickness, a/t	Initial Flaw Depth Initial Flaw Length, $(a/2c)_i$	Failure Stress Yield Stress, σ_G/σ_{ys}	Irwin's Apparent K MN/m ^{3/2} (Ksi \sqrt{m})
AS24-1	0.510 (0.201)	8.89 (3.50)	78 (-320)	LN ₂	476.4 (69.1)	460.2 (66.3)	—	0.196 (0.077)	0.521 (0.205)	0.383	0.378	1.05	31.5 (26.7)
AS24-2	0.510 (0.201)	8.89 (3.50)			465.4 (67.5)	437.1 (63.4)	—	0.234 (0.092)	0.648 (0.256)	0.458	0.361	1.03	34.3 (31.2)
AS24-3	0.508 (0.200)	8.89 (3.50)			447.5 (64.9)	414.4 (60.1)	—	0.320 (0.126)	0.787 (0.310)	0.630	0.406	0.99	36.5 (33.2)
AS24-4	0.510 (0.201)	8.89 (3.50)			442.0 (64.1)	403.4 (58.5)	—	0.343 (0.135)	0.902 (0.355)	0.672	0.380	0.98	38.4 (34.9)
AS24-5	0.510 (0.201)	8.89 (3.50)			416.5 (60.4)	314.4 (45.6)	410.3 (59.5)	0.406 (0.160)	1.092 (0.430)	0.796	0.372	0.92	39.6 (36.0)
AS22-1	0.516 (0.203)	8.89 (3.50)	78 (-320)	LN ₂	456.4 (66.2)	456.5 (66.2)	—	0.226 (0.089)	0.831 (0.327)	0.438	0.272	1.01	38.6 (33.5)
AS22-2	0.510 (0.201)	8.89 (3.50)			453.7 (65.8)	413.0 (59.9)	—	0.249 (0.098)	1.054 (0.415)	0.488	0.236	1.00	39.8 (36.2)
AS22-3	0.510 (0.201)	8.89 (3.50)			435.8 (63.2)	398.5 (57.8)	—	0.297 (0.117)	1.219 (0.480)	0.582	0.244	0.96	41.4 (37.7)
AS22-4	0.513 (0.202)	8.89 (3.50)			409.6 (59.4)	372.3 (54.0)	—	0.356 (0.140)	1.422 (0.560)	0.693	0.250	0.90	41.9 (38.1)
AS22-5	0.510 (0.201)	8.89 (3.50)			397.2 (57.6)	348.2 (50.5)	374.4 (54.3)	0.417 (0.164)	1.702 (0.670)	0.816	0.245	0.88	44.1 (40.1)
AS21-1	0.505 (0.199)	12.70 (5.00)	78 (-320)	LN ₂	437.8 (63.5)	399.9 (58.0)	—	0.208 (0.082)	1.956 (0.770)	0.412	0.104	0.97	40.9 (37.2)
AS21-2	0.508 (0.200)	12.70 (5.00)			413.7 (60.0)	348.2 (50.0)	—	0.249 (0.098)	2.515 (0.990)	0.490	0.099	0.91	42.0 (38.2)
AS21-3	0.508 (0.200)	12.70 (5.00)			368.2 (53.4)	302.7 (43.9)	—	0.305 (0.120)	3.073 (1.210)	0.600	0.099	0.81	40.6 (36.9)
AS21-4	0.505 (0.199)	22.86 (9.00)			335.8 (48.7)	208.9 (30.3)	329.6 (47.8)	0.366 (0.144)	3.594 (1.415)	0.724	0.012	0.74	39.9 (36.3)
AS21-5	0.505 (0.199)	22.86 (9.00)			386.8 (41.6)	113.1 (16.4)	156.5 (22.7)	0.493 (0.190)	4.420 (1.740)	0.955	0.109	0.63	38.6 (35.1)

Table 9: Static Fracture Data for 1.27 cm (0.50 Inch) 2219-T87 Aluminum Parent Metal (WT Direction)

SPECIMEN			TEST		FRACTURE DATA								
Number	Gage Thickness, t cm (Inch)	Gage Width, w cm (Inch)	Temperature °K (°F)	Environment	Failure Stress, σ_G MN/m ² (Ksi)	Dimpling Stress, σ_D MN/m ² (Ksi)	Breakthrough Stress, σ_B MN/m ² (Ksi)	Initial Flaw Depth, a_i cm (Inch)	Initial Flaw Length, (2c) _i cm (Inch)	Initial Flaw Depth Gage Thickness, a/t	Initial Flaw Depth Initial Flaw Length, (a/2c) _i	Failure Stress Yield Stress, σ_G/σ_{ys}	Irwin's Apparent K MN/m ^{3/2} (Ksi√In)
AS54-1	1.267 (0.499)	8.89 (3.50)	78 (-320)	LN ₂	467.5 (67.8)	454.4 (65.9)	—	0.335 (0.132)	0.813 (0.320)	0.265	0.412	1.03	38.8 (35.3)
AS54-2	1.270 (0.500)	8.89 (3.50)			449.6 (65.2)	442.7 (64.2)	—	0.417 (0.164)	1.041 (0.410)	0.328	0.400	0.99	42.2 (38.4)
AS54-3	1.278 (0.503)	8.89 (3.50)			435.1 (63.1)	431.6 (62.6)	—	0.541 (0.213)	1.397 (0.550)	0.423	0.387	0.96	47.0 (42.8)
AS54-4	1.270 (0.500)	8.89 (3.50)			398.5 (57.8)	395.8 (57.4)	—	0.716 (0.282)	1.803 (0.710)	0.564	0.397	0.88	48.6 (44.2)
AS54-5	1.272 (0.501)	12.70 (5.00)			355.8 (51.6)	—	—	0.914 (0.360)	2.388 (0.940)	0.719	0.383	0.79	49.3 (44.9)
AS54-6	1.275 (0.502)	12.70 (5.00)			333.7 (48.4)	324.8 (47.1)	—	1.016 (0.400)	2.767 (1.090)	0.797	0.367	0.74	49.5 (45.0)
AS54-7	1.270 (0.500)	12.70 (5.00)			322.0 (46.7)	—	—	1.041 (0.410)	2.845 (1.120)	0.820	0.366	0.71	48.2 (43.9)
AS54-8	1.272 (0.501)	12.70 (5.00)			315.1 (45.7)	244.1 (35.4)	—	1.092 (0.430)	2.972 (1.170)	0.858	0.368	0.70	48.2 (43.9)
AS52-1	1.272 (0.501)	8.89 (3.50)	R.T.	AIR	387.5 (56.2)	—	—	0.325 (0.128)	1.227 (0.483)	0.255	0.265	1.03	37.8 (34.4)
AS52-2	1.270 (0.500)	8.89 (3.50)			371.0 (53.8)	—	—	0.417 (0.164)	1.626 (0.640)	0.328	0.266	0.99	41.3 (37.6)
AS52-3	1.270 (0.500)	12.70 (5.00)			353.7 (51.3)	—	—	0.541 (0.213)	2.248 (0.885)	0.426	0.241	0.94	45.4 (41.3)
AS52-4	1.272 (0.501)	12.70 (5.00)			327.5 (47.5)	—	—	0.678 (0.267)	2.827 (1.113)	0.533	0.240	0.87	46.6 (42.4)
AS52-5	1.270 (0.500)	22.86 (9.00)	78 (-320)	LN ₂	322.7 (46.8)	298.6 (43.3)	—	0.846 (0.333)	3.480 (1.370)	0.666	0.243	0.71	50.0 (45.5)
AS52-6	1.272 (0.501)	22.86 (9.00)			284.8 (41.3)	252.4 (36.6)	—	0.970 (0.382)	4.064 (1.600)	0.762	0.239	0.63	47.1 (42.9)
AS52-7	1.260 (0.496)	22.83 (8.99)			269.6 (39.1)	228.9 (33.2)	—	1.021 (0.402)	4.369 (1.720)	0.810	0.234	0.60	45.8 (41.7)
AS52-8	1.280 (0.504)	22.86 (9.00)			257.2 (37.3)	148.2 (21.5)	244.1 (35.4)	1.143 (0.450)	4.666 (1.837)	0.893	0.245	0.57	45.6 (41.5)

Table 9: (Continued)

SPECIMEN			TEST		FRACTURE DATA								
Number	Gage Thickness, t cm (Inch)	Gage Width, w cm (Inch)	Temperature σ_K ($^{\circ}F$)	Environment	Failure Stress, σ_G MN/m ² (Ksi)	Dimpling Stress, σ_D MN/m ² (Ksi)	Breakthrough Stress, σ_B MN/m ² (Ksi)	Initial Flaw Depth, a_i cm (Inch)	Initial Flaw Length, (2c) _i cm (Inch)	Initial Flaw Depth Gage Thickness, a/t	Initial Flaw Depth Initial Flaw Length, (a/2c) _i	Failure Stress Yield Stress, σ_G/σ_{ys}	Irwin's Apparent K MN/m ^{3/2} (Ksi \sqrt{In})
AS51-1	1.270 (0.500)	12.70 (5.00)			439.9 (63.8)	432.3 (62.7)	—	0.328 (0.129)	3.023 (1.190)	0.268	0.108	0.97	51.3 (46.7)
AS51-2	1.270 (0.500)	22.88 (9.00)			390.9 (56.7)	364.7 (52.9)	—	0.403 (0.160)	2.948 (1.160)	0.320	0.100	0.86	50.1 (46.6)
AS51-3	1.275 (0.502)	30.48 (12.00)			335.8 (48.7)	—	—	0.559 (0.220)	5.664 (2.230)	0.438	0.099	0.74	49.5 (46.0)
AS51-4	1.270 (0.500)	40.64 (16.00)	78 (-320)	LN ₂	234.8 (38.4)	233.4 (38.2)	—	0.686 (0.270)	7.239 (2.850)	0.540	0.098	0.68	42.4 (38.6)
AS51-5	1.275 (0.502)	40.64 (16.00)			214.4 (31.1)	(A)	—	0.838 (0.330)	8.687 (3.420)	0.657	0.085	0.47	37.5 (34.1)
AS51-6	1.272 (0.501)	50.80 (20.00)			151.7 (22.0)	(A)	144.8 (21.0)	1.090 (0.425)	11.735 (4.620)	0.848	0.092	0.33	29.9 (27.2)
AS51-7	1.232 (0.497)	50.77 (19.99)			153.8 (22.3)	(A)	151.0 (21.9)	1.029 (0.405)	11.074 (4.360)	0.815	0.093	0.34	29.6 (23.9)
AS51-8	1.265 (0.498)	50.80 (20.00)			168.9 (24.5)	(A)	168.9 (24.5)	0.953 (0.375)	10.668 (4.200)	0.753	0.089	0.37	31.4 (28.6)

(A) LOADED TWICE

1  NO STRAIN GAGE TO DETECT DIMPLING

Table 10: Static Fracture Data for 1.91 cm (0.75 Inch) 2219-T87 Aluminum Parent Metal (WT Direction)

SPECIMEN			TEST		FRACTURE DATA									
Number	Gage Thickness, t cm (Inch)	Gage Width, w cm (Inch)	Temperature °K (°F)	Environment	Failure Stress, σ_G MN/m ² (Ksi)	Dimpling Stress, σ_D MN/m ² (Ksi)	Breakthrough Stress, σ_B MN/m ² (Ksi)	Initial Flaw Depth, a_i cm (Inch)	Initial Flaw Length, $(2c)_i$ cm (Inch)	$\frac{\text{Initial Flaw Depth}}{\text{Gage Thickness}}, a/t$	$\frac{\text{Initial Flaw Depth}}{\text{Initial Flaw Length}}, (a/2c)_i$	$\frac{\text{Failure Stress}}{\text{Yield Stress}}, \sigma_G/\sigma_{ys}$	Irwin's Apparent K MN/m ^{3/2} (Ksi√In)	
AS72-1	1.910 (0.752)	8.89 (3.50)	R.T.	AIR	388.2 (56.3)	—	—	0.310 (0.122)	1.219 (0.480)	0.162	0.254	1.04	37.5 (34.1)	
AS72-2	1.910 (0.752)	12.70 (5.00)	78 (-320)	LN ₂	396.8 (57.4)	—	—	0.716 (0.282)	2.807 (1.105)	0.376	0.256	0.87	56.8 (51.7)	
AS72-3	1.908 (0.751)	22.83 (8.99)			300.6 (43.6)	(A)	—	—	1.092 (0.430)	4.674 (1.840)	0.573	0.234	0.73	53.3 (48.5)
AS72-4	1.902 (0.749)	30.48 (12.00)			213.7 (31.0)	182.7 (26.5)	—	—	1.575 (0.620)	6.655 (2.620)	0.828	0.237	0.47	44.5 (40.5)

(A) NO STRAIN GAGE FOR DIMPLE DETECTION

Table 11: Static Fracture Data for 7075-T651 Aluminum Parent Metal (WT Direction)

SPECIMEN			TEST		FRACTURE DATA								
Number	Gage Thickness, t cm (Inch)	Gage Width, w cm (Inch)	Temperature °K (°F)	Environment	Failure Stress, σ_G MN/m ² (Ksi)	Dimpling Stress, σ_D MN/m ² (Ksi)	Breakthrough Stress, σ_B MN/m ² (Ksi)	Initial Flaw Depth, a_i cm (Inch)	Initial Flaw Length, (2c) _i cm (Inch)	Initial Flaw Depth Gage Thickness, a/t	Initial Flaw Depth Initial Flaw Length, (a/2c) _i	Failure Stress Yield Stress, σ_G/σ_{ys}	Irwin's Apparent K MN/m ^{3/2} (Ksi√in)
A1-1	0.389 (0.153)	8.86 (3.49)	R.T.	AIR	516.4 (74.9)	—	—	0.140 (0.055)	0.610 (0.240)	0.359	0.229	0.96	34.3 (31.2)
A1-2	0.384 (0.151)	8.86 (3.49)			469.5 (68.1)	468.9 (68.0)	—	0.221 (0.087)	0.914 (0.360)	0.576	0.242	0.88	38.0 (34.8)
A1-3	0.366 (0.144)	8.86 (3.49)			344.1 (49.9)	268.9 (39.0)	335.8 (48.7)	0.330 (0.130)	1.257 (0.495)	0.903	0.263	0.64	32.4 (29.5)
A2-1	0.508 (0.200)	8.86 (3.49)	R.T.	AIR	505.4 (73.3)	495.8 (71.9)	—	0.213 (0.084)	0.826 (0.325)	0.420	0.258	0.94	39.9 (36.3)
A2-2	0.526 (0.204)	8.86 (3.49)			471.6 (68.4)	462.7 (67.1)	—	0.274 (0.108)	1.024 (0.403)	0.529	0.268	0.88	41.3 (37.6)
A2-3	0.498 (0.196)	8.86 (3.49)			437.8 (63.5)	392.3 (56.9)	—	0.300 (0.118)	1.245 (0.490)	0.602	0.241	0.82	41.1 (37.4)
A2-4	0.513 (0.202)	8.86 (3.49)			348.2 (50.5)	—	—	0.391 (0.154)	1.435 (0.565)	0.762	0.273	0.65	35.3 (32.1)
A2-5	0.511 (0.201)	8.86 (3.49)			311.7 (45.2)	226.8 (32.9)	296.5 (43.0)	0.442 (0.174)	1.727 (0.680)	0.866	0.256	0.58	34.0 (30.9)
A5-1	1.257 (0.495)	8.86 (3.49)	R.T.	AIR	418.5 (60.7)	—	—	0.328 (0.129)	1.232 (0.485)	0.261	0.266	0.78	39.7 (36.1)
A5-3	1.257 (0.495)	12.67 (4.99)			261.3 (37.9)	—	—	0.686 (0.270)	2.299 (0.905)	0.545	0.298	0.49	33.6 (30.6)
A5-5	1.275 (0.502)	12.70 (5.00)			202.0 (29.3)	—	—	0.838 (0.330)	3.454 (1.360)	0.657	0.243	0.38	30.3 (27.6)
A5-6	1.293 (0.509)	22.89 (9.01)			181.3 (26.3)	—	—	0.953 (0.375)	4.064 (1.600)	0.737	0.234	0.34	29.3 (26.6)
A5-7	1.255 (0.494)	22.89 (9.01)			184.1 (23.7)	—	—	1.041 (0.410)	4.369 (1.720)	0.854	0.238	0.30	27.4 (24.9)
A5-8	1.275 (0.502)	22.89 (9.01)			150.3 (21.8)	—	—	1.194 (0.470)	4.851 (1.910)	0.956	0.246	0.28	26.7 (24.3)
A5-2	1.280 (0.504)	12.70 (5.00)			381.3 (55.3)	—	—	0.442 (0.174)	1.613 (0.635)	0.345	0.274	0.71	41.3 (37.6)
A5-4	1.283 (0.505)	12.70 (5.00)			254.4 (36.9)	—	—	0.699 (0.275)	2.946 (1.160)	0.545	0.237	0.47	37.3 (33.9)

164

LOADING DISCONTINUED AT POP-IN, FLAW DIMENSIONS ARE FOR INITIAL CONDITIONS



Table 11: (Continued)

SPECIMEN			TEST		FRACTURE DATA								
Number	Gage Thickness, t cm (Inch)	Gage Width, w cm (Inch)	Temperature °K (°F)	Environment	Failure Stress, σ_G MN/m ² (Ksi)	Dimpling Stress, σ_D MN/m ² (Ksi)	Breakthrough Stress, σ_B MN/m ² (Ksi)	Initial Raw Depth, a_i cm (Inch)	Initial Flaw Length, (2c) _i cm (Inch)	Initial Flaw Depth Gage Thickness, a/t	Initial Flaw Depth Initial Flaw Length, (a/2c) _i	Failure Stress Yield Stress, σ_G/σ_{ys}	Irwin's Apparent K MN/m ^{3/2} (Ksi√In)
A7-1	1.920 (0.756)	6.86 (2.70)	R.T.	AIR	326.1 (47.3)			0.452 (0.178)	1.557 (0.613)	0.235	0.290	0.61	34.7 (31.6)
A7-2	1.905 (0.750)	8.86 (3.49)			284.1 (41.2)			0.579 (0.228)	2.235 (0.880)	0.304	0.259	0.53	35.2 (32.0)
A7-3	1.910 (0.752)	12.70 (5.00)			268.2 (38.9)			0.747 (0.294)	3.010 (1.185)	0.391	0.248	0.50	38.1 (34.7)
A7-4	0.915 (0.754)	22.89 (9.01)			228.2 (33.1)			0.953 (0.375)	3.861 (1.520)	0.497	0.247	0.43	36.5 (33.2)
A7-5	1.918 (0.755)	22.89 (9.01)			188.2 (27.3)			1.080 (0.425)	4.572 (1.800)	0.563	0.236	0.35	32.3 (29.4)
A7-6	1.915 (0.754)	22.89 (9.01)			161.3 (23.4)			1.321 (0.520)	5.436 (2.140)	0.690	0.243	0.30	30.3 (27.6)
A7-7	1.905 (0.750)	30.48 (12.00)			154.4 (22.4)			1.473 (0.580)	6.147 (2.420)	0.773	0.240	0.29	30.7 (27.9)
A7-8	1.908 (0.751)	30.48 (12.00)			137.9 (20.0)			1.676 (0.660)	6.883 (2.710)	0.879	0.244	0.26	29.1 (26.5)
A7-9	1.897 (0.747)	30.48 (12.00)			124.8 (18.1)			1.717 (0.676)	7.188 (2.830)	0.905	0.239	0.23	26.8 (24.4)

Table 12: Static Fracture Data for 0.08 cm (0.03 Inch) and 0.15 cm (0.06 Inch) 6Al-4V STA Titanium Parent Metal (RT Direction)

SPECIMEN			TEST		FRACTURE DATA								
Number	Gage Thickness, t cm (Inch)	Gage Width, w cm (Inch)	Temperature °K (°F)	Environment	Failure Stress, σ_G MN/m ² (Ksi)	Dimpling Stress, σ_D MN/m ² (Ksi)	Breakthrough Stress, σ_B MN/m ² (Ksi)	Initial Raw Depth, a_i cm (Inch)	Initial Flaw Length, (2c) _i cm (Inch)	Initial Flaw Depth Gage Thickness, a/t	Initial Flaw Depth Initial Flaw Length, (a/2c) _i	Failure Stress Yield Stress, σ_G/σ_{ys}	Irwin's Apparent K MN/m ^{3/2} (Ksi√In)
TS34-1	0.0838 (0.0330)	1.91 (0.75)	R.T.	AIR	1113.5 (161.5)	1037.7 (150.5)	—	0.041 (0.016)	0.107 (0.042)	0.485	0.381	1.06	33.4 (30.4)
TS34-2	0.0833 (0.0328)	1.91 (0.75)			1028.7 (149.2)	876.4 (127.1)	1023.9 (148.5)	0.061 (0.024)	0.147 (0.058)	0.732	0.414	0.98	36.3 (33.0)
TS32-1	0.0843 (0.0332)	1.91 (0.75)	R.T.	AIR	1090.7 (158.2)	964.6 (139.9)	—	0.041 (0.016)	0.104 (0.041)	0.482	0.390	1.04	32.4 (29.5)
TS32-2	0.0838 (0.0330)	1.91 (0.75)			1020.5 (148.0)	952.9 (138.2)	1010.1 (146.5)	0.056 (0.022)	0.244 (0.096)	0.667	0.229	0.97	42.9 (39.0)
TS31-1	0.0831 (0.0327)	1.91 (0.75)	R.T.	AIR	1059.8 (153.7)	857.7 (124.4)	—	0.046 (0.018)	0.259 (0.102)	0.550	0.176	1.01	43.1 (39.2)
TS31-2	0.0864 (0.0340)	3.81 (1.50)			912.9 (132.4)	603.3 (87.5)	890.8 (129.2)	0.058 (0.023)	0.632 (0.249)	0.676	0.092	0.87	44.7 (40.7)
TS64-1	0.1537 (0.0605)	1.91 (0.75)	R.T.	AIR	1171.5 (169.9)	1061.8 (154.0)	—	0.041 (0.016)	0.104 (0.041)	0.264	0.390	1.12	34.7 (31.6)
TS64-2	0.1552 (0.0611)	1.91 (0.75)			1069.4 (155.1)	990.8 (143.7)	—	0.079 (0.031)	0.203 (0.080)	0.507	0.388	1.02	44.3 (40.3)
TS64-3	0.1544 (0.0608)	1.91 (0.75)			962.5 (139.6)	795.7 (115.4)	962.5 (139.6)	0.117 (0.046)	0.333 (0.131)	0.757	0.351	0.92	50.1 (45.6)
TS62-1	0.1542 (0.0607)	1.91 (0.75)	R.T.	AIR	1090.8 (158.2)	1014.3 (147.1)	—	0.049 (0.019)	0.165 (0.065)	0.313	0.292	1.04	39.7 (36.1)
TS62-2	0.1544 (0.0608)	1.91 (0.75)			1039.8 (150.8)	915.7 (132.8)	—	0.071 (0.028)	0.320 (0.126)	0.461	0.222	0.99	49.9 (45.4)
TS62-3	0.1633 (0.0643)	3.81 (1.50)			988.1 (143.3)	724.0 (105.0)	965.3 (140.0)	0.114 (0.045)	0.452 (0.178)	0.700	0.253	0.94	57.4 (52.2)
TS61-1	0.1544 (0.0612)	1.91 (0.75)	R.T.	AIR	1143.9 (165.9)	1053.6 (152.8)	—	0.041 (0.016)	0.267 (0.105)	0.261	0.152	1.09	45.1 (41.0)
TS61-2	0.1577 (0.0621)	3.81 (1.50)			946.7 (137.3)	741.2 (107.5)	—	0.081 (0.032)	0.780 (0.307)	0.515	0.104	0.90	54.4 (49.5)
TS61-3	0.1562 (0.0615)	7.62 (3.00)			809.5 (117.4)	450.9 (65.4)	795.7 (115.4)	0.109 (0.043)	1.156 (0.455)	0.699	0.095	0.77	53.3 (48.5)

Table 13: Static Fracture Data for 0.31 cm (0.12 Inch) 6Al-4V STA Titanium Parent Metal (RT Direction)

SPECIMEN			TEST		FRACTURE DATA								
Number	Gage Thickness, t cm (Inch)	Gage Width, w cm (Inch)	Temperature °K (°F)	Environment	Failure Stress, σ_G MN/m ² (Ksi)	Dimpling Stress, σ_D MN/m ² (Ksi)	Breakthrough Stress, σ_B MN/m ² (Ksi)	Initial Raw Depth, a_i cm (Inch)	Initial Flaw Length, (2c) _i cm (Inch)	Initial Flaw Depth Gage Thickness, a/t	Initial Flaw Depth Initial Flaw Length, (a/2c) _i	Failure Stress Yield Stress, σ_G/σ_{ys}	Irwin's Apparent K MN/m ^{3/2} (Ksi√In)
TS14-1	0.307 (0.121)	1.91 (0.75)	R.T.	AIR	1034.3 (150.0)	946.0 (137.2)	—	0.130 (0.051)	0.297 (0.117)	0.421	0.429	0.98	52.3 (47.6)
TS14-2	0.307 (0.121)	1.91 (0.75)			973.6 (141.2)	973.6 (141.2)	—	0.155 (0.061)	0.414 (0.163)	0.504	0.374	0.93	56.9 (51.8)
TS14-3	0.300 (0.118)	3.81 (1.50)			957.7 (138.9)	882.6 (128.0)	—	0.170 (0.067)	0.475 (0.187)	0.568	0.358	0.91	59.7 (54.3)
TS14-4	0.320 (0.126)	3.81 (1.50)			932.2 (135.2)	731.6 (106.1)	—	0.216 (0.085)	0.601 (0.237)	0.675	0.359	0.88	65.3 (59.4)
TS14-5	0.310 (0.122)	3.81 (1.50)			837.1 (121.4)	631.6 (91.6)	—	0.244 (0.096)	0.681 (0.268)	0.787	0.358	0.80	61.7 (56.1)
TS12-1	0.310 (0.122)	3.81 (1.50)	R.T.	AIR	1045.3 (151.6)	1011.5 (146.7)	—	0.114 (0.045)	0.457 (0.180)	0.369	0.250	1.00	61.4 (55.9)
TS12-2	0.315 (0.124)	3.81 (1.50)			1007.4 (146.1)	968.1 (140.4)	—	0.150 (0.059)	0.610 (0.240)	0.476	0.246	0.96	67.8 (61.7)
TS12-3	0.305 (0.120)	3.81 (1.50)			934.3 (135.5)	875.0 (126.9)	—	0.165 (0.065)	0.686 (0.270)	0.542	0.241	0.89	65.7 (59.8)
TS12-4	0.300 (0.118)	5.08 (2.00)			839.1 (121.7)	815.7 (118.3)	833.6 (120.9)	0.208 (0.082)	0.889 (0.350)	0.695	0.234	0.80	65.9 (60.0)
TS12-5	0.300 (0.118)	5.08 (2.00)			755.7 (109.6)	637.8 (92.5)	715.0 (103.7)	0.241 (0.095)	1.041 (0.410)	0.805	0.232	0.72	63.4 (57.7)
TS11-1	0.318 (0.125)	5.08 (2.00)	R.T.	AIR	1012.2 (146.8)	895.0 (129.8)	—	0.117 (0.046)	1.156 (0.455)	0.368	0.101	0.96	71.0 (64.6)
TS11-2	0.306 (0.120)	7.62 (3.00)			830.8 (120.5)	—	—	0.165 (0.065)	1.651 (0.650)	0.542	0.100	0.79	66.9 (60.9)
TS11-3	0.320 (0.126)	10.16 (4.00)			729.5 (105.8)	610.9 (88.6)	—	0.203 (0.080)	1.829 (0.720)	0.635	0.111	0.69	63.5 (57.8)
TS11-4	0.318 (0.125)	10.16 (4.00)			639.9 (92.8)	464.7 (67.4)	—	0.221 (0.087)	2.261 (0.890)	0.696	0.098	0.61	58.2 (53.0)
TS11-5	0.318 (0.125)	12.70 (5.00)			673.6 (97.7)	426.1 (61.8)	—	0.257 (0.101)	2.565 (1.010)	0.808	0.100	0.64	66.2 (60.2)

Table 14: Static Fracture Data for 0.53 cm (0.21 Inch) 6Al-4V STA Titanium Parent Metal (RT Direction)

SPECIMEN			TEST		FRACTURE DATA									
Number	Gage Thickness, t cm (Inch)	Gage Width, w cm (Inch)	Temperature °K (°F)	Environment	Failure Stress, σ_G MN/m ² (Ksi)	Dimpling Stress, σ_D MN/m ² (Ksi)	Breakthrough Stress, σ_B MN/m ² (Ksi)	Initial Raw Depth, a_i cm (Inch)	Initial Flaw Length, (2c) _i cm (Inch)	$\frac{\text{Initial Flaw Depth}}{\text{Gage Thickness}}, a/t$	$\frac{\text{Initial Flaw Depth}}{\text{Initial Flaw Length}}, (a/2c)_i$	$\frac{\text{Failure Stress}}{\text{Yield Stress}}, \sigma_G/\sigma_{ys}$	Irwin's Apparent K MN/m ^{3/2} (Ksi√m)	
TS24-1	0.541 (0.213)	5.08 (2.00)	R.T.	AIR	1003.9 (145.6)	982.5 (142.5)	—	0.170 (0.067)	0.417 (0.164)	0.315	0.409	0.96	59.3 (54.0)	
TS24-2	0.541 (0.213)	5.08 (2.00)			981.8 (142.4)	955.6 (138.6)	—	0.206 (0.081)	0.549 (0.216)	0.380	0.375	0.93	66.2 (60.2)	
TS24-3	0.541 (0.213)	5.08 (2.00)			952.2 (138.1)	908.1 (131.7)	—	0.246 (0.097)	0.587 (0.231)	0.455	0.420	0.91	66.5 (60.5)	
TS24-4	0.546 (0.215)	5.08 (2.00)			857.7 (124.4)	839.8 (121.8)	—	0.300 (0.118)	0.787 (0.310)	0.549	0.381	0.82	68.5 (62.3)	
TS24-5	0.533 (0.210)	5.08 (2.00)			813.6 (118.0)	753.6 (109.3)	—	0.318 (0.125)	0.947 (0.373)	0.595	0.335	0.77	70.1 (63.8)	
TS24-6	0.533 (0.210)	7.62 (3.00)			744.6 (108.0)	676.4 (98.1)	—	0.396 (0.156)	1.085 (0.427)	0.743	0.365	0.71	68.8 (62.6)	
TS24-7	0.533 (0.210)	7.62 (3.00)			647.4 (93.9)	566.8 (82.2)	—	0.417 (0.164)	1.151 (0.453)	0.781	0.362	0.62	61.1 (55.8)	
TS24-8	0.533 (0.210)	7.62 (3.00)			730.9 (106.0)	484.0 (70.2)	712.9 (103.4)	—	0.447 (0.176)	1.227 (0.483)	0.838	0.364	0.70	71.8 (65.3)
TS22-1	0.536 (0.211)	5.08 (2.00)	R.T.	AIR	1040.5 (150.9)	1027.4 (149.0)	—	0.160 (0.063)	0.622 (0.245)	0.299	0.257	0.99	71.8 (65.3)	
TS22-2	0.541 (0.213)	5.08 (2.00)			952.9 (138.2)	926.7 (134.4)	—	0.203 (0.080)	0.851 (0.335)	0.376	0.239	0.91	74.7 (68.0)	
TS22-3	0.546 (0.215)	5.08 (2.00)			880.5 (127.7)	840.5 (121.9)	—	0.249 (0.098)	1.029 (0.405)	0.456	0.242	0.84	76.4 (68.6)	
TS22-4	0.536 (0.211)	7.62 (3.00)			644.0 (93.4)	—	—	0.325 (0.128)	1.296 (0.510)	0.607	0.251	0.61	60.8 (56.3)	
TS22-5	0.536 (0.211)	7.62 (3.00)			586.8 (85.1)	—	—	0.366 (0.144)	1.473 (0.580)	0.682	0.248	0.56	58.6 (53.3)	
TS22-6	0.536 (0.211)	7.62 (3.00)			668.1 (96.9)	479.2 (69.5)	663.3 (96.2)	—	0.406 (0.160)	1.740 (0.685)	0.758	0.234	0.64	72.0 (65.5)
TS22-7	0.544 (0.214)	10.16 (4.00)			508.9 (73.8)	492.3 (71.4)	—	0.427 (0.168)	1.842 (0.725)	0.785	0.232	0.48	55.6 (50.6)	
TS22-8	0.544 (0.214)	10.16 (4.00)			529.6 (76.8)	431.6 (62.6)	△	0.442 (0.174)	1.880 (0.740)	0.813	0.235	0.50	58.7 (53.4)	

△ POSSIBLE BREAKTHROUGH AT 529.6 MN/m² (76.8 KSI)

Table 14: (Continued)

SPECIMEN			TEST		FRACTURE DATA									
Number	Gage Thickness, t cm (Inch)	Gage Width, w cm (Inch)	Temperature °K (°F)	Environment	Failure Stress, σ_G MN/m ² (Ksi)	Dimpling Stress, σ_D MN/m ² (Ksi)	Breakthrough Stress, σ_B MN/m ² (Ksi)	Initial Flaw Depth, a_i cm (Inch)	Initial Flaw Length, (2c) _i cm (Inch)	Initial Flaw Depth Gage Thickness, a/t	Initial Flaw Depth Initial Flaw Length, (a/2c) _i	Failure Stress Yield Stress, σ_G/σ_{ys}	Irwin's Apparent K MN/m ^{3/2} (Ksi√in)	
TS21-1	0.538 (0.212)	6.58 (2.59)	957.0 (138.8)	R.T.	AIR	922.6 (133.8)	—	0.170 (0.067)	1.588 (0.625)	0.316	0.107	0.91	79.5 (72.3)	
TS21-2	0.546 (0.215)	10.16 (4.00)	799.8 (116.0)			799.8 (116.0)	—	0.231 (0.091)	2.286 (0.900)	0.423	0.101	0.76	75.8 (69.0)	
TS21-3	0.536 (0.211)	12.70 (5.00)	683.3 (99.1)			683.3 (99.1)	—	0.272 (0.107)	2.616 (1.030)	0.507	0.104	0.65	68.9 (62.7)	
TS21-4	0.536 (0.211)	12.70 (5.00)	614.3 (89.1)			—	—	0.284 (0.112)	3.175 (1.250)	0.531	0.090	0.58	63.7 (58.0)	
TS21-5	0.536 (0.211)	20.35 (8.01)	466.1 (67.6)			—	—	0.368 (0.145)	3.785 (1.490)	0.850	0.097	0.44	53.7 (48.9)	
TS21-6	0.566 (0.223)	20.29 (7.99)	457.1 (66.3)			—	—	430.2 (62.4)	0.422 (0.166)	4.293 (1.690)	0.744	0.098	0.44	56.4 (51.3)
TS21-7	0.549 (0.216)	20.40 (8.03)	362.7 (52.6)			—	—	339.2 (49.2)	0.432 (0.170)	4.572 (1.800)	0.787	0.094	0.35	45.1 (41.0)
TS21-8	0.554 (0.218)	20.29 (7.99)	343.4 (49.8)			—	—	297.2 (43.1)	0.483 (0.190)	4.978 (1.960)	0.872	0.097	0.33	44.9 (40.9)

Table 15: Static Fracture Data for 0.76 cm (0.30 Inch) 6Al-4V STA Titanium Parent Metal (RT Direction)

SPECIMEN			TEST		FRACTURE DATA								
Number	Gage Thickness, t cm (Inch)	Gage Width, w cm (Inch)	Temperature °K (°F)	Environment	Failure Stress, σ_G MN/m ² (Ksi)	Dimpling Stress, σ_D MN/m ² (Ksi)	Breakthrough Stress, σ_B MN/m ² (Ksi)	Initial Flaw Depth, a_i cm (Inch)	Initial Flaw Length, (2c) _i cm (Inch)	Initial Flaw Depth Gage Thickness, a/t	Initial Flaw Depth Initial Flaw Length, (a/2c) _i	Failure Stress Yield Stress, σ_G/σ_{ys}	Irwin's Apparent K MN/m ^{3/2} (Ksi√In)
TS3-1	0.765 (0.301)	7.62 (3.00)	R.T.	AIR	845.3 (122.6)	—	—	0.229 (0.090)	0.894 (0.352)	0.299	0.256	0.80	67.9 (61.8)
TS3-2	0.767 (0.302)	7.62 (3.00)			865.3 (125.5)	834.3 (121.0)	—	0.381 (0.150)	1.524 (0.600)	0.497	0.260	0.82	90.6 (82.4)
TS3-3	0.767 (0.302)	10.16 (4.00)			587.5 (85.2)	584.0 (84.7)	—	0.508 (0.200)	2.108 (0.830)	0.662	0.241	0.56	69.7 (63.4)
TS3-4	0.777 (0.306)	12.70 (5.00)			407.5 (59.1)	407.5 (59.1)	—	0.620 (0.244)	2.515 (0.990)	0.797	0.246	0.39	52.4 (47.7)

Table 16: 2219-T87 Aluminum Cyclic Flaw Growth Data at 78°K (-320°F); t = 1.27 cm (0.50 Inch),
 $\sigma_0 = 0.67 \sigma_{YS}$ and $(a/2c)_i \cong 0.37$

SPECIMEN NUMBER	THICKNESS, t cm (INCH)	WIDTH, W cm (INCH)	TEST CONDITIONS AT	GROSS STRESS, G MN/m ² (KSI)	FLAW DEPTH, a cm (INCH)	FLAW WIDTH, 2c cm (INCH)	a/2c	a/t	TEST ENVIRONMENT	IRWIN K _I MN/m ^{3/2} (KSI √IN)	K _I WITH M _K MN/m ^{3/2} (KSI √IN)	REMARKS
OA54-1	1.280 (0.504)	12.70 (5.00)	1	302.0 (43.8)	0.338 (0.133)	0.894 (0.352)	0.38	0.26	LN ₂	25.4 (23.1)	25.8 (23.5)	TEST TERMINATED IMMED. PRIOR TO FAILURE AT 4960 CYCLES; SPECIMEN THEN FAILED AT R.T.
			4		1.016 (0.400)	3.429 (1.350)	0.30	0.79		48.1 (43.8)	60.7 (55.2)	
			5		267.5 (38.8)	1.016 (0.400)	3.429 (1.350)	0.30	0.79	AIR	42.9 (39.0)	
OA54-2	1.270 (0.500)	12.70 (5.00)	1	302.0 (43.8)	0.356 (0.140)	0.902 (0.355)	0.39	0.28	LN ₂	25.5 (23.2)	26.0 (23.7)	2 FLAW SIZE AFTER 766 CYCLES 3 SPECIMEN OVERLOAD ON 767TH CYCLE; FLAW SIZE AT 768TH CYCLE. SPECIMEN CYCLED FOR 2236 CYCLES AND THEN OVERLOADED TO FAILURE ON 2237TH CYCLE
			2		0.406 (0.160)	0.998 (0.393)	0.41	0.32		26.9 (24.5)	27.4 (24.9)	
			3		0.422 (0.166)	1.130 (0.445)	0.37	0.33		28.5 (25.9)	29.2 (26.6)	
			4		0.551 (0.217)	1.524 (0.600)	0.36	0.43		33.0 (30.0)	34.2 (31.1)	
			5		0.551 (0.217)	1.524 (0.600)	0.36	0.43		—	—	
OA54-5	1.270 (0.500)	12.70 (5.00)	1	302.0 (43.8)	0.312 (0.123)	0.914 (0.360)	0.34	0.25	LN ₂	25.4 (23.1)	25.9 (23.6)	TEST TERMINATED IMMEDIATELY PRIOR TO FAILURE AT 4640 CYCLES; SPECIMEN THEN FAILED AT R.T.
			4		1.143 (0.450)	3.353 (1.320)	0.34	0.90		48.6 (44.2)	—	
			5		257.2 (37.3)	1.143 (0.350)	3.353 (1.320)	0.34	0.90	AIR	41.4 (37.7)	
OA54-6	1.270 (0.500)	12.70 (5.00)	1	302.0 (43.8)	0.315 (0.124)	0.894 (0.352)	0.35	0.25	LN ₂	25.2 (22.9)	25.6 (23.3)	2 FLAW SIZE AFTER 3758 CYCLES 3 FLAW SIZE AFTER MARKING. SPECIMEN TEST TERMINATED IMMED. PRIOR TO FAILURE AT 4803 CYCLES; SPECIMEN THEN FAILED AT R.T.
			2		0.599 (0.236)	1.524 (0.600)	0.39	0.47		33.2 (30.2)	34.2 (31.1)	
			3		0.610 (0.240)	1.524 (0.600)	0.40	0.48		33.2 (30.2)	34.2 (31.1)	
			4		1.118 (0.440)	3.759 (1.480)	0.30	0.88		50.4 (45.9)	—	
			5		1.118 (0.440)	3.759 (1.480)	0.30	0.88	AIR	—	—	

1 INITIAL CYCLIC CONDITIONS
 4 TERMINATION OF CYCLIC TEST
 5 FAILURE

Table 17: 2219-T87 Aluminum Cyclic Flow Growth Data at 78°K (-320°F); t = 1.27 cm (0.50 Inch),
 $\sigma_0 = 0.67 \sigma_{ys}$ and $(a/2c)_i \cong 0.30$

SPECIMEN NUMBER	THICKNESS, t cm (INCH)	WIDTH, W cm (INCH)	TEST CONDITIONS AT	GROSS STRESS, G MN/m ² (KSI)	FLAW DEPTH, a cm (INCH)	FLAW WIDTH, 2c cm (INCH)	a/2c	a/t	TEST ENVIRONMENT	IRWIN K _I MN/m ^{3/2} (KSI √IN)	K _I WITH M _K MN/m ^{3/2} (KSI √IN)	REMARKS
OA51-1	1.28 (0.502)	20.32 (8.00)	1	302.0 (43.8)	0.290 (0.114)	0.991 (0.390)	0.29	0.23	LN ₂	25.8 (23.5)	26.4 (24.0)	SPECIMEN CYCLED FOR 4604 CYCLES; THEN FAILED AT R.T.—SPECIMEN DELAMINATED AT R.T.
			2		0.660 (0.260)	1.880 (0.740)	0.35	0.52		36.5 (33.2)	38.7 (35.2)	
			3	358.5 (52.0)	0.660 (0.260)	1.880 (0.740)	0.35	0.52	AIR	44.6 (40.6)	47.4 (43.1)	
OA51-2	1.27 (0.501)	20.32 (8.00)	1	302.0 (43.8)	0.290 (0.114)	0.978 (0.385)	0.30	0.23	LN ₂	25.7 (23.4)	26.3 (23.9)	TEST TERMINATED IMMED. PRIOR TO FAILURE AT 3864 CYCLES; THEN FAILED AT R.T.
			2		1.067 (0.420)	3.429 (1.350)	0.31	0.84		48.5 (44.1)	61.7 (56.1)	
			3	276.5 (40.1)	1.067 (0.420)	3.429 (1.350)	0.31	0.84	AIR	44.7 (40.7)	56.8 (51.7)	
OA51-5	1.29 (0.502)	20.32 (8.00)	1	302.0 (43.8)	0.241 (0.093)	0.813 (0.325)	0.30	0.19	LN ₂	23.4 (21.4)	23.7 (21.7)	TEST TERMINATED IMMED. PRIOR TO FAILURE AT 6617 CYCLES; THEN FAILED AT R.T.
			2		0.965 (0.380)	3.734 (1.470)	0.26	0.76		48.9 (44.5)	63.0 (57.3)	
			3	273.7 (39.7)	0.965 (0.380)	3.734 (1.470)	0.26	0.76	AIR	44.6 (40.6)	57.5 (52.3)	
OA51-6	1.28 (0.502)	20.32 (8.00)	1	302.0 (43.8)	0.236 (0.093)	0.826 (0.325)	0.29	0.19	LN ₂	23.5 (21.4)	23.8 (21.7)	TEST TERMINATED IMMED. PRIOR TO FAILURE AT 6617 CYCLES; THEN FAILED AT RT
			2		0.965 (0.380)	3.734 (1.470)	0.26	0.76		48.9 (44.5)	63.0 (57.3)	
			3	273.7 (39.7)	0.965 (0.380)	3.734 (1.470)	0.26	0.76	AIR	44.6 (40.6)	57.5 (52.3)	

1 INITIAL CYCLIC CONDITIONS
 2 TERMINATION OF CYCLIC TEST
 3 FAILURE

Table 18: 2219-T87 Aluminum Cyclic Flaw Growth Data at 78°K (-320°F); t = 1.27 cm (0.50 Inch), $\sigma_0 = 0.91 \sigma_{YS}$ and $(a/2c)_i \cong 0.41$

SPECIMEN NUMBER	THICKNESS, t cm (INCH)	WIDTH, W cm (INCH)	TEST CONDITIONS AT	GROSS STRESS, G MN/m ² (KSI)	FLAW DEPTH, a cm (INCH)	FLAW WIDTH, 2c cm (INCH)	a/2c	a/t	TEST ENVIRONMENT	IRWIN K _I MN/m ^{3/2} (KSI √IN)	K _I WITH M _K MN/m ^{3/2} (KSI √IN)	REMARKS
CA54-1	1.27 (0.499)	11.46 (4.51)	1	412.3 (59.8)	0.335 (0.132)	0.787 (0.310)	0.43	0.27	LN ₂	33.4 (30.4)	33.7 (30.7)	SPECIMEN DIMPLED AFTER 421 CYCLES AND FAILED ON 735TH CYCLE IN LN ₂
			2		0.422 (0.166)	1.003 (0.395)	0.42	0.33		37.7 (34.3)	38.2 (34.8)	
			3		0.432 (0.170)	1.016 (0.400)	0.43	0.34		37.9 (34.5)	38.5 (35.0)	
			4		0.754 (0.297)	1.956 (0.770)	0.39	0.60		52.4 (47.7)	55.6 (50.6)	
			5									
CA54-2	1.28 (0.504)	11.46 (4.51)	1	412.3 (59.8)	0.333 (0.131)	0.787 (0.310)	0.42	0.26	LN ₂	33.4 (30.4)	33.7 (30.7)	SPECIMEN DIMPLED AFTER 380 CYCLES AND TEST TERMINATED IMMED. PRIOR TO FAILURE AT 834 CYCLES; SPECIMEN THEN FAILED IN LN ₂
			2		0.422 (0.166)	0.927 (0.365)	0.46	0.33		36.3 (33.0)	36.6 (33.3)	
			3		0.429 (0.169)	0.940 (0.370)	0.46	0.34		36.5 (33.2)	36.8 (33.5)	
			4		0.762 (0.300)	2.023 (0.800)	0.38	0.60		53.3 (48.5)	57.0 (51.9)	
			5	412.3 (59.8)	0.762 (0.300)	2.023 (0.800)	0.38	0.60		53.3 (48.5)	57.0 (51.9)	
CA54-3	1.28 (0.504)	11.43 (4.50)	1	412.3 (59.8)	0.411 (0.162)	1.059 (0.417)	0.39	0.32	LN ₂	38.6 (35.1)	39.5 (35.9)	SPECIMEN DIMPLED AFTER 220 CYCLES AND TEST TERMINATED IMMED. PRIOR TO FAILURE AT 251 CYCLES; SPECIMEN THEN FAILED IN LN ₂
			2		0.521 (0.205)	1.346 (0.530)	0.39	0.41		43.5 (39.6)	44.5 (40.5)	
			3		0.528 (0.208)	1.359 (0.535)	0.39	0.41		43.7 (39.8)	44.7 (40.7)	
			4		0.673 (0.265)	1.905 (0.750)	0.35	0.53		51.4 (46.8)	54.6 (49.7)	
			5	413.7 (60.0)	0.673 (0.265)	1.905 (0.750)	0.35	0.53		51.5 (46.9)	54.8 (49.9)	
CA54-4	1.27 (0.501)	11.43 (4.50)	1	412.3 (59.8)	0.422 (0.166)	1.067 (0.420)	0.40	0.33	LN ₂	38.8 (35.3)	39.6 (36.0)	SPECIMEN DIMPLED AFTER 150 CYCLES AND TEST TERMINATED IMMED. PRIOR TO FAILURE AT 189 CYCLES; SPECIMEN THEN FAILED IN LN ₂
			2		0.518 (0.204)	1.422 (0.560)	0.36	0.41		44.5 (40.5)	45.9 (41.8)	
			3		0.528 (0.208)	1.448 (0.570)	0.37	0.42		44.9 (40.9)	46.4 (42.2)	
			4		0.711 (0.280)	2.007 (0.790)	0.35	0.56		52.8 (48.0)	56.6 (51.5)	
			5	399.2 (57.9)	0.711 (0.280)	2.007 (0.790)	0.35	0.56		50.9 (46.3)	54.6 (49.7)	

- 1 INITIAL CYCLIC CONDITIONS
- 2 DIMPLING OCCURRED
- 3 RE-START OF CYCLIC TEST AFTER DIMPLING AND MARKING
- 4 TERMINATION OF CYCLIC TEST
- 5 FAILURE

Table 19: 2219-T87 Aluminum Cyclic Flaw Growth Data at 78°K (-320°F);
 $t = 1.27 \text{ cm (0.50 inch)}$, $\sigma_0 = 0.91\sigma_{ys}$ and $(a/2c)_i \cong 0.11$

SPECIMEN NUMBER	THICKNESS, t cm (INCH)	WIDTH, W cm (INCH)	TEST CONDITIONS AT	GROSS STRESS, G MN/m ² (KSI)	FLAW DEPTH, a cm (INCH)	FLAW WIDTH, 2c cm (INCH)	a/2c	a/t	TEST ENVIRONMENT	IRWIN K _I MN/m ^{3/2} (KSI√IN)	K _I WITH M _K MN/m ^{3/2} (KSI√IN)	REMARKS
CA51-1	1.28 (0.502)	20.32 (8.00)	1	412.3 (59.8)	0.259 (0.102)	2.007 (0.790)	0.13	0.20	LN ₂	41.3 (37.6)	42.5 (38.7)	SPECIMEN DIMPLED AFTER 53 CYCLES AND TEST TERMINATED IMMEDIATELY PRIOR TO FAILURE AT 72 CYCLES; SPECIMEN THEN FAILED IN LN ₂
			2		0.386 (0.152)	2.007 (0.790)	0.19	0.30		47.0 (42.8)	50.0 (45.5)	
			3		0.399 (0.157)	2.007 (0.790)	0.20	0.31		47.5 (43.2)	50.4 (45.9)	
			4		0.635 (0.250)	2.184 (0.860)	0.29	0.50		53.7 (48.9)	58.4 (53.1)	
			5		410.3 (59.5)	0.635 (0.250)	2.184 (0.860)	0.29		0.50	53.4 (48.6)	
CA51-2	1.28 (0.502)	20.32 (8.00)	1	412.3 (59.8)	0.201 (0.079)	2.032 (0.800)	0.10	0.16	LN ₂	37.6 (34.2)	38.5 (35.0)	SPECIMEN DIMPLED AFTER 97 CYCLES AND TEST TERMINATED IMMEDIATELY PRIOR TO FAILURE AT 155 CYCLES; SPECIMEN THEN FAILED IN LN ₂ .
			2		0.305 (0.120)	2.032 (0.800)	0.15	0.24		43.9 (39.9)	45.7 (41.6)	
			3		0.310 (0.122)	2.032 (0.800)	0.15	0.24		44.1 (40.1)	46.0 (41.9)	
			4		0.660 (0.260)	2.286 (0.900)	0.29	0.52		55.0 (50.0)	60.2 (54.8)	
			5		401.3 (58.2)	0.660 (0.260)	2.286 (0.900)	0.29		0.52	53.3 (48.5)	
CA51-3	1.25 (0.492)	20.32 (8.00)	1	412.3 (59.8)	0.259 (0.102)	2.667 (1.050)	0.10	0.21	LN ₂	42.8 (38.9)	44.2 (40.2)	SPECIMEN DIMPLED AFTER 11 CYCLES AND TEST TERMINATED IMMEDIATELY PRIOR TO FAILURE AT 22 CYCLES; SPECIMEN THEN FAILED IN LN ₂ .
			2		0.312 (0.123)	2.667 (1.050)	0.12	0.25		45.9 (41.8)	48.4 (44.0)	
			3		0.325 (0.128)	2.667 (1.050)	0.12	0.26		46.6 (42.4)	49.2 (44.8)	
			4		0.533 (0.210)	2.667 (1.050)	0.20	0.43		54.8 (49.9)	60.2 (54.8)	
			5		410.9 (59.6)	0.533 (0.210)	2.667 (1.050)	0.20		0.43	54.6 (49.7)	
CA51-4	1.28 (0.502)	20.32 (8.00)	1	412.3 (59.8)	0.254 (0.100)	2.692 (1.060)	0.09	0.20	LN ₂	42.4 (38.6)	43.7 (39.8)	SPECIMEN DIMPLED AFTER 14 CYCLES AND TEST TERMINATED IMMEDIATELY PRIOR TO FAILURE AT 16 CYCLES; SPECIMEN THEN FAILED AT LN ₂ .
			2		0.417 (0.164)	2.692 (1.060)	0.16	0.33		51.0 (46.4)	54.8 (49.9)	
			3		0.430 (0.169)	2.692 (1.060)	0.16	0.34		51.4 (46.8)	55.5 (50.5)	
			4		0.533 (0.210)	2.692 (1.060)	0.20	0.42		55.0 (50.0)	60.1 (54.7)	
			5		411.6 (59.7)	0.533 (0.210)	2.692 (1.060)	0.20		0.42	54.8 (49.9)	

1 ▽ INITIAL CYCLIC CONDITIONS
 2 ▽ DIMPLING OCCURRED
 3 ▽ RESTART OF CYCLIC TEST AFTER DIMPLING AND MARKING

4 ▽ TERMINATION OF CYCLIC TEST
 5 ▽ FAILURE

Table 20: 2219-T87 Aluminum Cyclic Flow Growth Data at 78°K (-320°F); $t = 0.51$ cm (0.20 Inch),
 $\sigma_0 = 0.91 \sigma_{ys}$ and $(a/2c)_i \cong 0.40$

SPECIMEN NUMBER	THICKNESS, t cm (INCH)	WIDTH, W cm (INCH)	TEST CONDITIONS AT	GROSS STRESS, G MN/m ² (KSI)	FLAW DEPTH, a cm (INCH)	FLAW WIDTH, $2c$ cm (INCH)	$a/2c$	a/t	TEST ENVIRONMENT	IRWIN K_I MN/m ^{3/2} (KSI \sqrt{IN})	K_I WITH M/K MN/m ^{3/2} (KSI \sqrt{IN})	REMARKS
CA24-1	0.516 (0.203)	8.89 (3.50)	1	412.3 (59.8)	0.221 (0.087)	0.564 (0.222)	0.41	0.45	LN ₂	28.1 (25.6)	28.9 (26.3)	SPECIMEN DIMPLED AFTER 186 CYCLES AND TEST TERMINATED AT FLAW BREAKTHROUGH AT 906 CYCLES; SPECIMEN THEN FAILED IN LN ₂
			2		0.244 (0.096)	0.610 (0.240)	0.43	0.50		29.3 (26.7)	30.1 (27.4)	
			3		0.259 (0.102)	0.640 (0.252)	0.43	0.53		30.0 (27.3)	30.9 (28.1)	
			4		$a = t$	1.143 (0.450)	0.45	1.00		40.2 (36.6)	—	
			5		$a = t$	1.143 (0.450)	0.45	1.00		40.0 (36.4)	—	
CA24-2	0.513 (0.202)	8.89 (3.50)	1	412.3 (59.8)	0.224 (0.088)	0.564 (0.222)	0.40	0.44	LN ₂	28.1 (25.6)	28.9 (26.3)	SPECIMEN DIMPLED AFTER 250 CYCLES AND FLAW BROKE THROUGH ON 1006TH CYCLE; SPECIMEN FAILED ON 1007TH CYCLE
			2		0.254 (0.100)	0.625 (0.246)	0.41	0.50		28.7 (27.0)	30.6 (27.8)	
			3		0.259 (0.102)	0.641 (0.252)	0.41	0.51		30.0 (27.3)	31.0 (28.2)	
			4		$a = t$	1.499 (0.590)	0.34	1.00		45.2 (41.1)	—	
			5		$a = t$	1.499 (0.590)	0.34	1.00		45.2 (41.1)	—	
CA24-3	0.500 (0.197)	8.89 (3.50)	1	412.3 (59.8)	0.274 (0.108)	0.716 (0.282)	0.38	0.55	LN ₂	31.8 (28.9)	33.3 (30.3)	SPECIMEN DIMPLED AFTER 50 CYCLES AND FAILED ON 290TH CYCLE
			2		0.290 (0.114)	0.764 (0.297)	0.38	0.58		32.5 (29.6)	34.4 (31.3)	
			3		0.305 (0.120)	0.785 (0.308)	0.39	0.61		33.2 (30.2)	35.3 (32.1)	
			4		0.483 (0.190)	1.448 (0.570)	0.35	0.96		44.5 (40.5)	—	
			5		0.483 (0.190)	1.448 (0.570)	0.35	0.96		44.5 (40.5)	—	
CA24-4	0.518 (0.204)	8.89 (3.50)	1	412.3 (59.8)	0.279 (0.110)	0.709 (0.279)	0.39	0.54	LN ₂	31.5 (28.7)	32.9 (29.9)	SPECIMEN DIMPLED AFTER 85 CYCLES AND TEST TERMINATED AT FLAW BREAKTHROUGH AT 447 CYCLES; SPECIMEN THEN FAILED IN LN ₂
			2		0.307 (0.121)	0.770 (0.303)	0.40	0.59		33.0 (30.0)	34.5 (31.4)	
			3		0.315 (0.124)	0.792 (0.312)	0.40	0.61		33.4 (30.4)	35.3 (32.1)	
			4		$a = t$	1.448 (0.570)	0.36	1.00		44.8 (40.8)	—	
			5		$a = t$	1.448 (0.570)	0.36	1.00		44.2 (40.2)	—	

1 INITIAL CYCLIC CONDITIONS
 2 DIMPLING OCCURRED
 3 RE-START OF CYCLIC TEST AFTER DIMPLING AND MARKING

4 TERMINATION OF CYCLIC TEST
 5 FAILURE

Table 21: 2219-T87 Aluminum Cyclic Flaw Growth Data at 78°K (-320°F); t = 0.51 cm (0.20 Inch), $\sigma_0 = 0.91 \sigma_{ys}$ and $(a/2c) \cong 0.09$

SPECIMEN NUMBER	THICKNESS, t cm (INCH)	WIDTH, W cm (INCH)	TEST CONDITIONS AT	GROSS STRESS, G MN/m ² (KSI)	FLAW DEPTH, a cm (INCH)	FLAW WIDTH, 2c cm (INCH)	a/2c	a/t	TEST ENVIRONMENT	IRWIN K _I MN/m ^{3/2} (KSI √IN)	K _I WITH M _K MN/m ^{3/2} (KSI √IN)	REMARKS
CA21-2	0.521 (0.205)	12.70 (5.00)	1	412.3 (59.8)	0.203 (0.080)	2.007 (0.790)	0.10	0.39	LN ₂	37.7 (34.3)	41.7 (37.9)	SPECIMEN FAILED AT 25 CYCLES
			2		0.343 (0.135)	2.007 (0.790)	0.17	0.66		45.5 (41.4)	59.2 (53.9)	
CA21-5	0.511 (0.201)	10.16 (4.00)	1	412.3 (59.8)	0.107 (0.042)	1.397 (0.550)	0.08	0.21	LN ₂	28.0 (25.5)	28.9 (26.3)	SPECIMEN DIMPLD AFTER 131 CYCLES AND TEST TERMINATED IMMED. PRIOR TO FAILURE AT 609 CYCLES; SPECIMEN THEN FAILED IN LN ₂
			2		0.127 (0.050)	1.397 (0.550)	0.09	0.25		30.1 (27.4)	31.8 (28.9)	
			3		0.130 (0.051)	1.397 (0.550)	0.09	0.25		30.3 (27.6)	32.1 (29.2)	
			4		0.394 (0.155)	1.626 (0.640)	0.24	0.77		44.8 (40.8)	59.2 (53.9)	
			5		0.394 (0.155)	1.626 (0.640)	0.24	0.77		—	—	
CA21-6	0.518 (0.204)	10.16 (4.00)	1	412.3 (59.8)	0.109 (0.043)	1.410 (0.555)	0.08	0.21	LN ₂	28.2 (25.7)	29.2 (26.6)	SPECIMEN DIMPLD AFTER 153 CYCLES AND TEST TERMINATED IMMED. PRIOR TO FAILURE AT 745 CYCLES; SPECIMEN THEN FAILED IN LN ₂
			2		0.142 (0.056)	1.410 (0.555)	0.10	0.28		31.5 (28.7)	33.6 (30.6)	
			3		0.152 (0.060)	1.410 (0.555)	0.11	0.29		32.4 (29.5)	34.8 (31.7)	
			4		0.330 (0.130)	1.524 (0.600)	0.22	0.64		42.3 (38.5)	52.3 (47.6)	
			5	414.4 (60.1)	0.330 (0.130)	1.524 (0.600)	0.22	0.64		42.5 (38.7)	52.6 (47.9)	

- 1 INITIAL CYCLIC CONDITIONS
- 2 DIMPLING OCCURRED
- 3 RE-START OF CYCLIC TEST AFTER DIMPLING AND MARKING
- 4 TERMINATION OF CYCLIC TEST
- 5 FAILURE

Table 22: 2219-T87 Aluminum Cyclic Flaw Growth Data at 78°K (-320°F); t = 0.38 cm (0.20 Inch),
 $\sigma_0 = 0.67 \sigma_{YS}$ and $(a/2c)_i \cong 0.37$

SPECIMEN NUMBER	THICKNESS, t cm (INCH)	WIDTH, W cm (INCH)	TEST CONDITIONS AT	GROSS STRESS, G MN/m ² (KSI)	FLAW DEPTH, a cm (INCH)	FLAW WIDTH, 2c cm (INCH)	a/2c	a/t	TEST ENVIRONMENT	IRWIN K _I MN/m ^{3/2} (KSI √IN)	K _I WITH M _K MN/m ^{3/2} (KSI √IN)	REMARKS
OA14-1	0.386 (0.152)	8.89 (3.50)	1	302.0 (43.8)	0.216 (0.085)	0.635 (0.250)	0.34	0.56	LN ₂	21.1 (19.2)	22.9 (20.8)	FLAW BREAKTHROUGH AT 2490 CYCLES, THEN PULLED TO FAILURE IN R. T. AIR
			2		a = t	1.016 (0.400)	0.38	1.00		27.0 (24.6)	—	
			3		a = t	1.016 (0.400)	0.38	1.00	AIR	32.1 (29.2)	—	
OSA14-2	0.378 (0.149)	8.89 (3.50)	1	302.0 (43.8)	0.254 (0.100)	0.635 (0.250)	0.40	0.67	LN ₂	21.4 (19.5)	23.0 (20.9)	FLAW BREAKTHROUGH AT 1818 CYCLES, THEN PULLED TO FAILURE IN R.T. AIR
			2		a = t	0.991 (0.390)	0.38	1.00		26.7 (24.3)	—	
			3		a = t	0.991 (0.390)	0.38	1.00	AIR	30.8 (28.0)	—	
OA14-5	0.356 (0.140)	8.89 (3.50)	1	302.0 (43.8)	0.234 (0.092)	0.577 (0.227)	0.37	0.54	LN ₂	20.4 (18.6)	21.8 (19.8)	FLAW BREAKTHROUGH AT 2026 CYCLES, THEN PULLED TO FAILURE IN R.T. AIR
			2		a = t	0.889 (0.350)	0.40	1.00		25.4 (23.1)	—	
			3		a = t	0.889 (0.350)	0.40	1.00	AIR	30.1 (27.4)	—	
OA14-6	0.384 (0.151)	8.89 (3.50)	1	302.0 (43.8)	0.196 (0.077)	0.521 (0.205)	0.38	0.51	LN ₂	19.3 (17.6)	20.2 (18.4)	FLAW BREAKTHROUGH AT 3180 CYCLES, THEN PULLED TO FAILURE IN R.T. AIR
			2		a = t	0.991 (0.390)	0.39	1.00		26.7 (24.3)	—	
			3		a = t	0.991 (0.390)	0.39	1.00	AIR	31.3 (28.5)	—	

1 INITIAL CYCLIC CONDITIONS
 2 TERMINATION OF CYCLIC TEST
 3 FAILURE

Table 23: 2219-T87 Aluminum Cyclic Flaw Growth Data at 78°K (-320°F); $t = 0.38$ cm (0.15 Inch),
 $\sigma_0 = 0.67 \sigma_{ys}$ and $(a/2c)_i \cong 0.11$

SPECIMEN NUMBER	THICKNESS, t cm (INCH)	WIDTH, w cm (INCH)	TEST CONDITIONS AT	GROSS STRESS, G MN/m ² (KSI)	FLAW DEPTH, a cm (INCH)	FLAW WIDTH, $2c$ cm (INCH)	$a/2c$	a/t	TEST ENVIRONMENT	IRWIN K_I MN/m ^{3/2} (KSI √IN)	K_I WITH M_K MN/m ^{3/2} (KSI √IN)	REMARKS
OA11-1	0.391 (0.154)	12.70 (5.00)	1	302.0 (43.8)	0.102 (0.040)	1.346 (0.530)	0.08	0.26	LN ₂	19.1 (17.4)	20.3 (18.5)	FLAW BREAKTHROUGH AT 2768 CYCLES, THEN PULLED TO FAILURE IN RT AIR.
			2		$a = t$	1.524 (0.600)	0.26	1.00		31.2 (28.4)	—	
			3		317.9 (46.1)	$a = t$	1.524 (0.600)	0.26		1.00	AIR	
OA11-2	0.363 (0.143)	12.70 (5.00)	1	302.0 (43.8)	0.165 (0.065)	1.372 (0.540)	0.12	0.46	LN ₂	23.4 (21.3)	26.8 (24.4)	FLAW BREAKTHROUGH AT 1072 CYCLES, THEN PULLED TO FAILURE IN RT AIR.
			2		$a = t$	1.549 (0.610)	0.23	1.00		30.9 (28.1)	—	
			3		319.2 (46.3)	$a = t$	1.549 (0.610)	0.23		1.00	AIR	
OA11-5	0.391 (0.154)	12.70 (5.00)	1	300.6 (43.6)	0.130 (0.051)	1.143 (0.450)	0.14	0.40	LN ₂	22.4 (20.4)	24.6 (22.4)	FLAW BREAKTHROUGH AT 2021 CYCLES, THEN PULLED TO FAILURE IN RT AIR.
			2		$a = t$	1.321 (0.520)	0.30	1.00		29.7 (27.0)	—	
			3		323.4 (46.9)	$a = t$	1.321 (0.520)	0.30		1.00	AIR	
OA11-6	0.381 (0.150)	12.70 (5.00)	1	302.0 (43.8)	0.157 (0.062)	1.168 (0.460)	0.11	0.34	LN ₂	20.9 (19.0)	22.7 (20.7)	FLAW BREAKTHROUGH AT 2150 CYCLES, THEN PULLED TO FAILURE IN RT AIR.
			2		$a = t$	1.346 (0.530)	0.28	1.00		29.9 (27.2)	—	
			3		318.5 (46.2)	$a = t$	1.346 (0.530)	0.28		1.00	AIR	



1 INITIAL CYCLIC CONDITIONS
 2 TERMINATION OF CYCLIC TEST
 3 FAILURE

Table 24: 2219-T87 Aluminum Cyclic Flow Growth Data at 78°K (-320°F); t = 0.38 cm (0.15 Inch),
 $\sigma_0 = 0.91 \sigma_{ys}$ and $(a/2c)_i \cong 0.38$

SPECIMEN NUMBER	THICKNESS, t cm (INCH)	WIDTH, W cm (INCH)	TEST CONDITIONS AT	GROSS STRESS, G MN/m ² (KSI)	FLAW DEPTH, a cm (INCH)	FLAW WIDTH, 2c cm (INCH)	a/2c	a/t	TEST ENVIRONMENT	IRWIN K _I MN/m ^{3/2} (KSI √IN)	K _I WITH M _K MN/m ^{3/2} (KSI √IN)	REMARKS
CA14-1	0.381 (0.150)	8.86 (3.49)	1	412.3 (59.8)	0.180 (0.071)	0.472 (0.186)	0.38	0.47	LN ₂	25.7 (23.4)	26.7 (24.3)	SPECIMEN DIMPLED AFTER 300 CYCLES AND TEST TERMINATED AT FLAW BREAKTHROUGH AT 936 CYCLES; SPECIMEN THEN FAILED IN LN ₂
			2		0.206 (0.081)	0.587 (0.231)	0.35	0.54		28.5 (25.9)	30.4 (27.7)	
			3		0.216 (0.085)	0.617 (0.243)	0.35	0.57		29.2 (26.6)	31.5 (28.7)	
			4		a = t	1.092 (0.430)	0.35	1.00		38.9 (35.4)	—	
			5	423.4 (61.4)	a = t	1.092 (0.430)	0.35	1.00		40.0 (36.4)	—	
CA14-2	0.378 (0.149)	8.86 (3.49)	1	412.3 (59.8)	0.173 (0.068)	0.447 (0.176)	0.39	0.46	LN ₂	25.1 (22.8)	25.8 (23.5)	SPECIMEN DIMPLED AFTER 200 CYCLES AND TEST TERMINATED AFTER 1230 CYCLES; SPECIMEN THEN FAILED IN LN ₂
			2		0.203 (0.080)	0.483 (0.190)	0.42	0.54		26.2 (23.8)	26.9 (24.5)	
			3		0.208 (0.082)	0.495 (0.195)	0.42	0.55		26.5 (24.1)	27.4 (24.9)	
			4		0.343 (0.135)	0.973 (0.383)	0.35	0.91		36.7 (33.4)	—	
			5	443.3 (64.3)	0.343 (0.135)	0.973 (0.383)	0.35	0.91		39.8 (36.2)	—	
CA14-3	0.384 (0.151)	8.89 (3.50)	1	412.3 (59.8)	0.249 (0.098)	0.648 (0.255)	0.38	0.65	LN ₂	30.1 (27.4)	32.5 (29.6)	SPECIMEN DIMPLED AFTER 15 CYCLES AND TEST TERMINATED AT FLAW BREAKTHROUGH AT 270 CYCLES; SPECIMEN THEN FAILED IN LN ₂
			2		0.259 (0.102)	0.671 (0.264)	0.39	0.68		30.7 (27.9)	33.4 (30.4)	
			3		0.267 (0.105)	0.686 (0.270)	0.39	0.70		31.1 (28.3)	33.8 (30.8)	
			4		a = t	1.143 (0.450)	0.34	1.00		39.6 (36.0)	—	
			5	419.9 (60.9)	a = t	1.143 (0.450)	0.34	1.00		40.3 (36.7)	—	
CA14-4	0.394 (0.155)	8.89 (3.50)	1	412.3 (59.8)	0.254 (0.100)	0.663 (0.261)	0.38	0.65	LN ₂	30.6 (27.8)	33.0 (30.0)	SPECIMEN DIMPLED AFTER 10 CYCLES; THEN MARKED THROUGH-THE-THICKNESS
			2		0.264 (0.104)	0.686 (0.270)	0.39	0.67		31.0 (28.2)	33.7 (30.7)	

- 1 INITIAL CYCLIC CONDITIONS
- 2 DIMPLING OCCURRED
- 3 RE-START OF CYCLIC TEST AFTER DIMPLING AND MARKING
- 4 TERMINATION OF CYCLIC TEST
- 5 FAILURE

Table 25: 2219-T87 Aluminum Cyclic Flaw Growth Data at 78°K (-320°F); t = 0.38 cm (0.15 Inch),
 $\sigma_0 = 0.91 \sigma_{ys}$ and $(a/2c)_i \cong 0.09$

SPECIMEN NUMBER	THICKNESS, t cm (INCH)	WIDTH, W cm (INCH)	TEST CONDITIONS AT	GROSS STRESS, G MN/m ² (KSI)	FLAW DEPTH, a cm (INCH)	FLAW WIDTH, 2c cm (INCH)	a/2c	a/t	TEST ENVIRONMENT	IRWIN K _I MN/m ^{3/2} (KSI √IN)	K _I WITH M _K MN/m ^{3/2} (KSI √IN)	REMARKS
CA11-1	0.381 (0.150)	12.70 (5.00)	1	412.3 (59.8)	0.114 (0.045)	1.346 (0.530)	0.09	0.30	LN ₂	28.7 (26.1)	31.0 (28.2)	SPECIMEN DIMPLD AFTER 7 CYCLES AND FLAW BROKE THROUGH ON 100TH CYCLE; SPECIMEN FAILED ON 102ND CYCLE
			2		0.122 (0.048)	1.346 (0.530)	0.09	0.32		29.7 (26.9)	32.1 (29.2)	
			3		0.135 (0.053)	1.346 (0.530)	0.10	0.35		30.7 (27.9)	33.6 (30.6)	
			4		a = t	1.651 (0.650)	0.23	1.00		44.7 (40.7)	—	
			5		a = t	1.651 (0.650)	0.23	1.00		44.7 (40.7)	—	
CA11-2	0.386 (0.152)	12.70 (5.00)	1	412.3 (59.8)	0.135 (0.053)	1.410 (0.555)	0.10	0.35	LN ₂	30.9 (28.1)	33.8 (30.8)	SPECIMEN DIMPLD AFTER 5 CYCLES AND FLAW BROKE THROUGH ON 73RD CYCLE; SPECIMEN FAILED ON 74TH CYCLE
			2		0.145 (0.057)	1.410 (0.555)	0.10	0.38		31.8 (28.9)	34.9 (31.8)	
			3		0.160 (0.063)	1.410 (0.555)	0.11	0.41		33.0 (30.0)	36.8 (33.5)	
			4		a = t	1.651 (0.650)	0.23	1.00		44.8 (40.8)	—	
			5	405.4 (58.8)	a = t	1.651 (0.650)	0.23	1.00		44.0 (40.0)	—	
CA11-3	0.376 (0.148)	12.73 (5.01)	1	412.3 (59.8)	0.173 (0.068)	2.108 (0.830)	0.08	0.46	LN ₂	35.4 (32.2)	41.3 (37.6)	SPECIMEN DIMPLD AFTER 2 CYCLES AND FAILED ON 3RD CYCLE
			2		0.241 (0.095)	2.108 (0.830)	0.11	0.64		40.4 (36.8)	54.2 (49.3)	
			3		0.254 (0.100)	2.108 (0.830)	0.12	0.68		41.3 (37.6)	56.7 (51.6)	
CA11-4	0.384 (0.151)	2.70 (5.00)	1	412.3 (59.8)	0.170 (0.067)	2.083 (0.820)	0.8	0.44	LN ₂	35.2 (32.0)	40.6 (36.9)	SPECIMEN DIMPLD AFTER 1 CYCLE AND FAILED ON 2ND CYCLE
			2		0.196 (0.077)	2.083 (0.820)	0.9	0.51		37.3 (33.9)	44.8 (40.8)	
			3	405.4 (58.4)	0.239 (0.094)	2.083 (0.820)	0.12	0.62		40.2 (36.6)	53.0 (48.2)	

- 1 INITIAL CYCLIC CONDITIONS
- 2 DIMPLING OCCURRED
- 3 RE-START OF CYCLIC TEST AFTER DIMPLING AND MARKING
- 4 TERMINATION OF CYCLIC TEST
- 5 FAILURE

Table 26: 6AL-4V STA Titanium (RT Direction) Cyclic Flaw Growth Data at 295⁰K (72⁰F); t = 0.51 cm (0.21 Inch),
 $\sigma_0 = 0.77 \sigma_{YS}$ and $(a/2c)_i \cong 0.39$

SPECIMEN NUMBER	THICKNESS, t cm (INCH)	WIDTH, W cm (INCH)	TEST CONDITIONS AT	GROSS STRESS, G MN/m ² (KSI)	FLAW DEPTH, a cm (INCH)	FLAW WIDTH, 2c cm (INCH)	a/2c	a/t	TEST ENVIRONMENT	IRWIN K _I MN/m ^{3/2} (KSI √IN)	K _I WITH M _K MN/m ^{3/2} (KSI √IN)	REMARKS
CT24-1	0.538 (0.212)	7.62 (3.00)	1	820.5 (119.0)	0.155 (0.061)	0.411 (0.162)	0.38	0.29	AIR	47.1 (42.9)	48.2 (43.9)	SPECIMEN DIMPLED AFTER 100 CYCLES AND TEST TERMINATED AT FLAW BREAKTHROUGH AT 809 CYCLES; SPECIMEN THEN FAILED AT RT.
			2		0.168 (0.066)	0.437 (0.172)	0.38	0.31		48.7 (44.3)	49.8 (45.3)	
			3		0.173 (0.068)	0.480 (0.181)	0.38	0.32		49.8 (45.3)	51.1 (46.5)	
			4		a = t	1.092 (0.430)	0.49	1.00		77.4 (70.4)	—	
			5	786.0 (114.6)	a = t	1.092 (0.430)	0.49	1.00		74.1 (67.4)	—	
CT24-2	0.543 (0.214)	7.62 (3.00)	1	820.5 (119.0)	0.152 (0.060)	0.404 (0.159)	0.38	0.28	AIR	46.7 (42.5)	47.7 (43.4)	SPECIMEN DIMPLED AFTER 176 CYCLES BUT CYCLED FOR 180 CYCLES. SPECIMEN MARKED AND TEST RE-STARTED. TEST TERMINATED AT FLAW BREAKTHROUGH AT 1017 CYCLES; SPECIMEN THEN FAILED AT RT.
			2		0.183 (0.072)	0.457 (0.180)	0.40	0.34		49.9 (45.4)	50.9 (46.3)	
			3		0.185 (0.073)	0.460 (0.181)	0.40	0.34		50.0 (45.5)	51.0 (46.4)	
			4		a = t	1.143 (0.450)	0.48	1.00		79.2 (72.1)	—	
			5	875.0 (126.9)	a = t	1.143 (0.450)	0.48	1.00		85.3 (77.6)	—	
CT24-3	0.546 (0.215)	7.62 (3.00)	1	820.5 (119.0)	0.213 (0.084)	0.549 (0.216)	0.39	0.39	AIR	54.5 (49.6)	55.8 (50.8)	SPECIMEN DIMPLED AFTER 93 CYCLES AND TEST TERMINATED AFTER 177 CYCLES; SPECIMEN THEN FAILED AT RT.
			2		0.249 (0.098)	0.699 (0.275)	0.36	0.46		61.1 (55.6)	63.7 (58.0)	
			3		0.251 (0.099)	0.704 (0.277)	0.36	0.46		61.1 (55.6)	63.5 (57.8)	
			4		0.343 (0.135)	0.520 (0.520)	0.26	0.63		80.1 (72.9)	95.2 (86.6)	
			5	810.9 (117.6)	0.343 (0.135)	1.321 (0.520)	0.26	0.63		79.1 (72.0)	94.0 (85.5)	
CT24-4	0.541 (0.213)	7.62 (3.00)	1	820.5 (119.0)	0.224 (0.088)	0.533 (0.210)	0.42	0.41	AIR	54.0 (49.1)	55.0 (50.0)	SPECIMEN DIMPLED AFTER 80 CYCLES AND TEST TERMINATED AT FLAW BREAKTHROUGH AT 559 CYCLES; SPECIMEN THEN FAILED AT RT.
			2		0.241 (0.095)	0.572 (0.225)	0.42	0.45		55.9 (50.0)	57.0 (51.9)	
			3		0.244 (0.096)	0.577 (0.227)	0.42	0.45		56.2 (51.1)	57.3 (52.1)	
			4		a = t	1.270 (0.500)	0.43	1.00		83.4 (75.9)	—	
			5	877.7 (127.3)	a = t	1.270 (0.500)	0.43	1.00		89.6 (81.5)	—	

- 1 INITIAL CYCLIC CONDITIONS
- 2 DIMPLING OCCURRED
- 3 RE-START OF CYCLIC TEST AFTER DIMPLING AND MARKING

- 4 TERMINATION OF CYCLIC TEST.
- 5 FAILURE

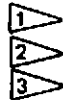
Table 27: 6AL-4V STA Titanium (RT Direction) Cyclic Flaw Growth Data at 295°K (72°F); t = 0.51 cm (0.21 Inch), $\sigma_0 = 0.77 \sigma_{ys}$ and (a/2c)_i ≈ 0.10

SPECIMEN NUMBER	THICKNESS, t cm (INCH)	WIDTH, W cm (INCH)	TEST CONDITIONS AT	GROSS STRESS, G MN/m ² (KSI)	FLAW DEPTH, a cm (INCH)	FLAW WIDTH, 2c cm (INCH)	a/2c	a/t	TEST ENVIRONMENT	IRWIN K _I MN/m ^{3/2} (KSI√IN)	K _I WITH M _K MN/m ^{3/2} (KSI√IN)	REMARKS
CT21-1	0.541 (0.213)	10.16 (4.00)	1	820.5 (119.0)	0.094 (0.037)	1.003 (0.395)	0.09	0.17	AIR	50.1 (45.6)	51.4 (46.8)	SPECIMEN DIMPLED AFTER 108 CYCLES AND TEST TERMINATED IMMEDIATELY PRIOR TO FAILURE AT 131 CYCLES; SPECIMEN THEN FAILED AT RT.
			2		0.132 (0.052)	1.003 (0.395)	0.13	0.24		57.4 (52.1)	60.0 (54.6)	
			3		0.201 (0.079)	1.003 (0.395)	0.20	0.37		65.6 (59.7)	70.7 (64.3)	
			4		0.292 (0.115)	1.397 (0.550)	0.21	0.54		78.4 (71.3)	91.3 (83.1)	
			5		0.292 (0.115)	1.397 (0.550)	0.21	0.54		83.5 (76.0)	97.4 (88.6)	
CT21-2	0.538 (0.212)	10.16 (4.00)	1	885.3 (126.4)	0.094 (0.037)	0.978 (0.385)	0.10	0.18	AIR	54.6 (49.7)	56.0 (51.0)	SPECIMEN DIMPLED AFTER 92 CYCLES AND TEST TERMINATED IMMEDIATELY PRIOR TO FAILURE AT 293 CYCLES; SPECIMEN THEN FAILED AT RT.
			2		0.114 (0.045)	0.978 (0.385)	0.12	0.21		58.9 (53.6)	60.9 (55.4)	
			3		0.183 (0.072)	0.978 (0.385)	0.19	0.34		69.2 (63.0)	70.1 (67.4)	
			4		0.381 (0.150)	1.372 (0.540)	0.28	0.71		90.0 (81.9)	110.1 (100.2)	
			5		0.381 (0.150)	1.372 (0.540)	0.28	0.71		88.6 (80.6)	108.5 (98.7)	
CT21-3	0.546 (0.215)	10.16 (4.00)	1	820.5 (119.0)	0.142 (0.056)	1.422 (0.560)	0.10	0.26	AIR	61.3 (55.8)	65.0 (59.1)	SPECIMEN DIMPLED AFTER 80 CYCLES; SPECIMEN MARKED EXCESSIVELY AND FAILED ON FIRST CYCLE OF RE-STARTED TEST.
			2		0.180 (0.071)	1.422 (0.560)	0.13	0.33		67.3 (61.2)	72.8 (66.2)	
			3		0.493 (0.194)	1.854 (0.730)	0.26	0.90		95.4 (86.8)	—	
CT21-4	0.549 (0.216)	10.16 (4.00)	1	820.5 (119.0)	0.140 (0.055)	1.422 (0.560)	0.10	0.26	AIR	60.9 (55.4)	64.3 (58.5)	SPECIMEN DIMPLED AFTER 33 CYCLES AND TEST TERMINATED IMMEDIATELY PRIOR TO FAILURE AT 162 CYCLES; SPECIMEN THEN FAILED AT RT.
			2		0.160 (0.063)	1.422 (0.560)	0.11	0.29		64.2 (58.4)	68.8 (62.6)	
			3		0.175 (0.069)	1.422 (0.560)	0.12	0.32		66.5 (60.5)	71.9 (65.4)	
			4		0.381 (0.150)	1.803 (0.710)	0.21	0.69		89.2 (81.2)	115.4 (105.0)	
			5		0.381 (0.150)	1.803 (0.710)	0.21	0.69		94.9 (86.3)	122.6 (111.6)	

- 1 INITIAL CYCLIC CONDITIONS
- 2 DIMPLING OCCURRED
- 3 RE-START OF CYCLIC TEST AFTER DIMPLING AND MARKING
- 4 TERMINATION OF CYCLIC TEST
- 5 FAILURE

Table 28: 6AL-4V STA Titanium (RT Direction) Cyclic Flow Growth Data at 295°K (72°F); $t = 0.31$ cm (0.12 Inch),
 $\sigma_0 = 0.77 \sigma_{YS}$ and $(a/2c)_i \cong 0.34$

SPECIMEN NUMBER	THICKNESS, t cm (INCH)	WIDTH, w cm (INCH)	TEST CONDITIONS AT	GROSS STRESS, G MN/m ² (KSI)	FLAW DEPTH, a cm (INCH)	FLAW WIDTH, $2c$ cm (INCH)	$a/2c$	a/t	TEST ENVIRONMENT	IRWIN K_I MN/m ^{3/2} (KSI \sqrt{IN})	K_I WITH M_K MN/m ^{3/2} (KSI \sqrt{IN})	REMARKS
CT14-1	0.310 (0.122)	5.08 (2.00)	1	820.5 (119.0)	0.104 (0.041)	0.305 (0.120)	0.34	0.34	AIR	40.2 (36.8)	41.5 (37.8)	SPECIMEN DIMPLED AFTER 84 CYCLES BUT CYCLED FOR 96 CYCLES. SPECIMEN MARKED AND TEST RE-STARTED. TEST TERMINATED AT FLAW BREAKTHROUGH AT 691 CYCLES; SPECIMEN THEN FAILED AT RT.
			2		0.114 (0.045)	0.326 (0.128)	0.35	0.37		41.7 (37.9)	43.0 (39.1)	
			3		0.117 (0.046)	0.343 (0.135)	0.34	0.38		42.6 (38.8)	44.1 (40.1)	
			4		$a = t$	0.762 (0.300)	0.41	1.00		64.5 (58.7)	—	
			5		$a = t$	0.762 (0.300)	0.41	1.00		69.2 (63.0)	—	
CT14-2	0.300 (0.118)	5.08 (2.00)	1	820.5 (119.0)	0.102 (0.040)	0.305 (0.120)	0.33	0.34	AIR	40.1 (36.5)	41.5 (37.8)	SPECIMEN DIMPLED AFTER 77 CYCLES BUT CYCLED FOR 82 CYCLES. SPECIMEN MARKED AND TEST RE-STARTED. TEST TERMINATED AT FLAW BREAKTHROUGH AT 747 CYCLES; SPECIMEN THEN FAILED AT RT.
			2		0.114 (0.045)	0.320 (0.126)	0.36	0.38		41.4 (37.7)	42.6 (38.8)	
			3		0.117 (0.046)	0.343 (0.135)	0.34	0.39		42.6 (38.8)	44.2 (40.2)	
			4		$a = t$	0.838 (0.330)	0.36	1.00		67.0 (61.0)	—	
			5		$a = t$	0.838 (0.330)	0.36	1.00		71.3 (64.9)	—	
CT14-3	0.305 (0.120)	5.08 (2.00)	1	820.5 (119.0)	0.124 (0.049)	0.381 (0.150)	0.33	0.41	AIR	44.7 (40.7)	48.6 (42.4)	SPECIMEN DIMPLED AFTER 84 CYCLES BUT CYCLED FOR 90 CYCLES. SPECIMEN MARKED AND TEST RE-STARTED. TEST TERMINATED AT FLAW BREAKTHROUGH AT 434 CYCLES; SPECIMEN THEN FAILED AT RT.
			2		0.137 (0.054)	0.406 (0.160)	0.34	0.45		46.4 (42.2)	48.6 (44.2)	
			3		0.145 (0.057)	0.432 (0.170)	0.34	0.48		47.8 (43.5)	50.4 (45.9)	
			4		$a = t$	0.762 (0.300)	0.40	1.00		64.4 (58.6)	—	
			5		$a = t$	0.762 (0.300)	0.40	1.00		64.4 (58.6)	—	
CT14-4	0.307 (0.121)	5.08 (2.00)	1	820.5 (119.0)	0.130 (0.051)	0.386 (0.152)	0.34	0.42	AIR	45.2 (41.1)	47.0 (42.8)	SPECIMEN DIMPLED AFTER 60 CYCLES BUT CYCLED FOR 64 CYCLES. SPECIMEN MARKED AND TEST RE-STARTED. TEST TERMINATED AT FLAW BREAKTHROUGH AT 605 CYCLES; SPECIMEN THEN FAILED AT RT.
			2		0.137 (0.054)	0.406 (0.160)	0.34	0.45		46.4 (42.2)	48.6 (44.2)	
			3		0.142 (0.056)	0.417 (0.164)	0.34	0.46		47.0 (42.8)	49.3 (44.9)	
			4		$a = t$	0.762 (0.300)	0.40	1.00		64.4 (58.6)	—	
			5		$a = t$	0.762 (0.300)	0.40	1.00		70.0 (63.7)	—	



1 INITIAL CYCLIC CONDITIONS

2 DIMPLING OCCURRED

3 RE-START OF CYCLIC TEST AFTER DIMPLING AND MARKING



4 TERMINATION OF CYCLIC TEST

5 FAILURE

Table 29: 6AL-4V STA Titanium (RT Direction) Cyclic Flaw Growth Data at 295⁰K (72⁰F); t = 0.31 cm (0.12 Inch), $\sigma_0 = 0.77 \sigma_{ys}$ and $(a/2c)_i \cong 0.10$

SPECIMEN NUMBER	THICKNESS, t cm (INCH)	WIDTH, W cm (INCH)	TEST CONDITIONS AT	GROSS STRESS, G MN/m ² (KSI)	FLAW DEPTH, a cm (INCH)	FLAW WIDTH, 2c cm (INCH)	a/2c	a/t	TEST ENVIRONMENT	IRWIN K _I MN/m ^{3/2} (KSI √IN)	K _I WITH M _K MN/m ^{3/2} (KSI √IN)	REMARKS
CT11-1	0.310 (0.122)	10.16 (4.00)	1	820.5 (119.0)	0.107 (0.042)	1.041 (0.410)	0.10	0.34	AIR	53.0 (48.2)	57.8 (52.6)	SPECIMEN DIMPLED AFTER 64 CYCLES AND TEST TERMINATED IMMEDIATELY PRIOR TO FAILURE AT 120 CYCLES; SPECIMEN THEN FAILED AT RT.
			2		0.127 (0.080)	1.041 (0.410)	0.12	0.41		55.7 (51.6)	63.0 (57.3)	
			3		0.132 (0.052)	1.041 (0.410)	0.13	0.43		57.5 (52.5)	64.5 (58.7)	
			4		0.213 (0.084)	1.219 (0.480)	0.18	0.69		69.6 (63.3)	92.3 (84.0)	
			5		0.213 (0.084)	1.219 (0.480)	0.18	0.69		72.5 (66.0)	98.3 (87.6)	
CT11-2	0.310 (0.122)	10.16 (4.00)	1	820.5 (119.0)	0.104 (0.041)	1.029 (0.405)	0.10	0.34	AIR	52.4 (47.7)	57.1 (52.0)	SPECIMEN DIMPLED AFTER 62 CYCLES AND TEST TERMINATED IMMEDIATELY PRIOR TO FAILURE AT 131 CYCLES; SPECIMEN THEN FAILED AT RT.
			2		0.127 (0.050)	1.029 (0.405)	0.12	0.41		55.6 (51.5)	62.9 (57.2)	
			3		0.132 (0.052)	1.029 (0.405)	0.13	0.43		57.5 (52.3)	64.5 (58.6)	
			4		0.226 (0.089)	1.143 (0.450)	0.20	0.73		69.8 (63.5)	93.8 (85.2)	
			5	0.226 (0.089)	1.143 (0.450)	0.20	0.73	71.3 (64.9)		95.7 (87.1)		
CT11-3	0.305 (0.120)	10.16 (4.00)	1	820.5 (119.0)	0.081 (0.032)	0.800 (0.315)	0.10	0.27	AIR	45.3 (42.1)	49.1 (44.7)	SPECIMEN DIMPLED AFTER 85 CYCLES AND TEST TERMINATED IMMEDIATELY PRIOR TO FAILURE AT 294 CYCLES; SPECIMEN THEN FAILED AT RT.
			2		0.089 (0.039)	0.800 (0.315)	0.12	0.33		50.0 (45.5)	54.1 (49.2)	
			3		0.104 (0.041)	0.800 (0.315)	0.13	0.34		50.9 (46.3)	55.3 (50.3)	
			4		0.216 (0.085)	1.041 (0.410)	0.21	0.71		67.5 (61.4)	88.4 (80.4)	
			5	0.216 (0.085)	1.041 (0.410)	0.21	0.71	71.2 (64.8)		93.2 (84.8)		
CT11-4	0.315 (0.124)	10.16 (4.00)	1	820.5 (119.0)	0.078 (0.031)	0.787 (0.310)	0.10	0.25	AIR	45.6 (41.5)	48.1 (43.8)	SPECIMEN DIMPLED AFTER 111 CYCLES AND TEST TERMINATED AT FLAW BREAKTHROUGH AT 411 CYCLES; SPECIMEN THEN FAILED AT RT.
			2		0.094 (0.037)	0.787 (0.310)	0.12	0.30		48.9 (44.5)	52.5 (47.8)	
			3		0.097 (0.038)	0.787 (0.310)	0.12	0.31		49.3 (44.9)	53.2 (48.4)	
			4		a = t	1.067 (0.420)	0.30	1.00		73.7 (67.1)	—	
			5	844.6 (122.5)	a = t	1.067 (0.420)	0.30	1.00		76.2 (69.3)	—	

1 INITIAL CYCLIC CONDITION
 2 DIMPLING OCCURRED
 3 RE-START OF CYCLIC TEST AFTER DIMPLING AND MARKING

4 TERMINATION OF CYCLIC TEST
 5 FAILURE

2-3

Table 30: 6AL-4V STA Titanium (RT Direction) Cyclic Flaw Growth Data at 295°K (72°F); t = 0.16 cm (0.063 Inch), $\sigma_0 = 0.77 \sigma_{ys}$ and $(a/2c)_i \cong 0.40$

SPECIMEN NUMBER	THICKNESS, t cm (INCH)	WIDTH, W cm (INCH)	TEST CONDITIONS AT	GROSS STRESS, G MN/m ² (KSI)	FLAW DEPTH, a cm (INCH)	FLAW WIDTH, 2c cm (INCH)	a/2c	a/t	TEST ENVIRONMENT	IRWIN K _I MN/m ^{3/2} (KSI √IN)	K _I WITH M _K MN/m ^{3/2} (KSI √IN)	REMARKS
CT64-1	0.160 (0.063)	3.81 (1.50)	1	820.5 (119.0)	0.048 (0.019)	0.107 (0.042)	0.45	0.30	AIR	24.2 (22.0)	24.4 (22.2)	SPECIMEN DIMPLED AFTER 83 CYCLES BUT CYCLED FOR 89 CYCLES. SPECIMEN MARKED AND TEST RE-STARTED. FLAW BREAKTHROUGH OCCURRED AT 1700 CYCLES BUT CYCLED FOR 1789 CYCLES. SPECIMEN THEN FAILED AT RT.
			2		?	?	—	—		—	—	
			3		?	?	—	—		—	—	
			4		a = t	0.401 (0.158)	0.45	1.00		46.7 (42.5)	—	
			5		a = t	0.401 (0.158)	0.45	1.00		45.8 (41.7)	—	
CT64-2	0.160 (0.063)	3.81 (1.50)	1	820.5 (119.0)	0.038 (0.015)	0.104 (0.041)	0.37	0.24	AIR	23.6 (21.5)	24.1 (21.9)	SPECIMEN DIMPLED AFTER 98 CYCLES BUT CYCLED FOR 106 CYCLES. SPECIMEN MARKED AND TEST RE-STARTED. FLAW BREAKTHROUGH OCCURRED AT 1500 CYCLES BUT CYCLED FOR 1597 CYCLES. SPECIMEN THEN FAILED AT RT.
			2		?	?	—	—		—	—	
			3		?	?	—	—		—	—	
			4		a = t	0.381 (0.150)	0.45	1.00		45.6 (41.5)	—	
			5		a = t	0.381 (0.150)	0.45	1.00		48.1 (43.8)	—	
CT64-3	0.165 (0.065)	3.81 (1.50)	1	820.5 (119.0)	0.069 (0.027)	0.178 (0.070)	0.39	0.42	AIR	31.1 (28.3)	31.9 (29.0)	SPECIMEN DIMPLED AFTER 50 CYCLES BUT CYCLED FOR 57 CYCLES. SPECIMEN MARKED AND TEST RE-STARTED. FLAW BREAKTHROUGH OCCURRED AT 740 CYCLES BUT CYCLED FOR 794 CYCLES. SPECIMEN THEN FAILED AT RT.
			2		?	?	—	—		—	—	
			3		?	?	—	—		—	—	
			4		a = t	0.419 (0.165)	0.52	1.00		47.7 (43.4)	—	
			5		a = t	0.419 (0.165)	0.52	1.00		51.0 (46.4)	—	
CT64-4	0.168 (0.066)	3.81 (1.50)	1	820.5 (119.0)	0.074 (0.029)	0.185 (0.073)	0.40	0.40	AIR	31.8 (28.9)	32.5 (29.6)	SPECIMEN DIMPLED AFTER 93 CYCLES BUT CYCLED FOR 95 CYCLES. SPECIMEN MARKED AND TEST RE-STARTED. FLAW BREAKTHROUGH OCCURRED AT 650 CYCLES BUT CYCLED FOR 787 CYCLES. SPECIMEN THEN FAILED AT RT.
			2		?	?	—	—		—	—	
			3		?	?	—	—		—	—	
			4		a = t	0.305 (0.120)	0.55	1.00		42.8 (38.9)	—	
			5		a = t	0.305 (0.120)	0.55	1.00		43.4 (39.5)	—	

1 INITIAL CYCLIC CONDITIONS
 2 DIMPLING OCCURRED
 3 RE-START OF CYCLIC TEST AFTER DIMPLING AND MARKING

4 TERMINATION OF CYCLIC TEST
 5 FAILURE

Table 31: 6AL-4V STA Titanium (RT Direction) Cyclic Flaw Growth Data at 295°K (72°F); t = 0.16 cm (0.063 Inch), $\sigma_0 = 0.77 \sigma_{ys}$ and $(a/2c)_i \cong 0.10$

SPECIMEN NUMBER	THICKNESS, t cm (INCH)	WIDTH, W cm (INCH)	TEST CONDITIONS AT	GROSS STRESS, G MN/m ² (KSI)	FLAW DEPTH, a cm (INCH)	FLAW WIDTH, 2c cm (INCH)	a/2c	a/t	TEST ENVIRONMENT	IRWIN K _I MN/m ^{3/2} (KSI √IN)	K _I WITH M _K MN/m ^{3/2} (KSI √IN)	REMARKS
CT61-1	0.155 (0.061)	5.08 (2.00)	1	820.5 (119.0)	0.030 (0.012)	0.305 (0.120)	0.10	0.20	AIR	28.4 (25.8)	29.2 (26.6)	SPECIMEN DIMPLED AFTER 134 CYCLES AND TEST TERMINATED AT FLAW BREAKTHROUGH AT 772 CYCLES. SPECIMEN THEN FAILED AT RT.
			2		0.036 (0.014)	0.305 (0.120)	0.12	0.23		30.1 (27.4)	31.4 (28.6)	
			3		0.074 (0.029)	0.305 (0.120)	0.24	0.47		37.9 (34.5)	41.8 (38.0)	
			4		a = t	0.564 (0.222)	0.28	1.00		53.0 (48.2)		
			5		a = t	0.564 (0.222)	0.28	1.00		61.8 (56.2)		
CT61-2	0.157 (0.062)	5.08 (2.00)	1	820.5 (119.0)	0.036 (0.014)	0.305 (0.120)	0.12	0.23	AIR	30.1 (27.4)	31.3 (28.5)	SPECIMEN DIMPLED AFTER 119 CYCLES BUT CYCLED FOR 120 CYCLES. SPECIMEN MARKED AND TEST RE-STARTED. FLAW BREAKTHROUGH OCCURRED AT 759 CYCLES. SPECIMEN THEN FAILED AT RT.
			2		0.041 (0.016)	0.305 (0.120)	0.13	0.26		31.8 (28.9)	33.4 (30.4)	
			3		0.076 (0.030)	0.305 (0.120)	0.25	0.49		38.2 (34.8)	42.2 (38.4)	
			4		a = t	0.508 (0.200)	0.31	1.00		51.1 (46.5)		
			5		a = t	0.508 (0.200)	0.31	1.00		59.3 (54.0)		
CT61-3	0.163 (0.064)	5.08 (2.00)	1	820.5 (119.0)	0.053 (0.021)	0.526 (0.207)	0.10	0.33	AIR	37.5 (34.1)	40.8 (37.1)	SPECIMEN DIMPLED AFTER 63 CYCLES BUT CYCLED FOR 68 CYCLES. SPECIMEN MARKED AND TEST RE-STARTED. FLAW BREAKTHROUGH OCCURRED AT 501 CYCLES. SPECIMEN THEN FAILED AT RT.
			2		0.058 (0.023)	0.526 (0.207)	0.11	0.36		38.8 (35.3)	42.5 (38.7)	
			3		0.058 (0.023)	0.526 (0.207)	0.11	0.36		38.8 (35.3)	42.5 (38.7)	
			4		a = t	0.693 (0.273)	0.23	1.00		56.8 (51.7)		
			5		a = t	0.693 (0.273)	0.23	1.00		63.6 (57.9)		
CT61-4	0.155 (0.061)	5.08 (2.00)	1	820.5 (119.0)	0.046 (0.018)	0.513 (0.202)	0.09	0.30	AIR	35.2 (32.0)	37.9 (34.5)	SPECIMEN DIMPLED AFTER 95 CYCLES AND TEST TERMINATED AT FLAW BREAKTHROUGH AT 655 CYCLES. SPECIMEN THEN FAILED AT RT.
			2		0.056 (0.022)	0.513 (0.202)	0.11	0.36		38.0 (34.6)	41.8 (38.0)	
			3		0.056 (0.022)	0.513 (0.202)	0.11	0.36		38.0 (34.6)	41.8 (38.0)	
			4		a = t	0.686 (0.270)	0.23	1.00		55.9 (50.9)		
			5		a = t	0.686 (0.270)	0.23	1.00		62.0 (56.4)		

1 INITIAL CYCLIC CONDITIONS
 2 DIMPLING OCCURRED
 3 RE-START OF CYCLIC TEST AFTER DIMPLING AND MARKING

4 TERMINATION OF CYCLIC TEST
 5 FAILURE

Table 32: 6AL-4V STA Titanium (WT Direction) Cyclic Flaw Growth Data at 295°K (72° F) in Argon and Salt Water at 10 cpm; $t = 0.31$ cm (0.12 Inch), $\sigma_D = 0.68 \sigma_{YS}$ and $(a/2c)_i \cong 0.37$

SPECIMEN NUMBER	THICKNESS, t cm (INCH)	WIDTH, w cm (INCH)	TEST CONDITIONS AT	GROSS STRESS, G MN/m ² (KSI)	FLAW DEPTH, a cm (INCH)	FLAW WIDTH, $2c$ cm (INCH)	$a/2c$	a/t	TEST ENVIRONMENT	IRWIN K_I MN/m ^{3/2} (KSI \sqrt{IN})	K_I WITH M_K MN/m ^{3/2} (KSI \sqrt{IN})	REMARKS (NUMBER OF CYCLES REFER TO TOTAL CYCLES)		
OST-10A	0.315 (0.124)	5.11 (2.01)	1	734.3 (106.5)	0.163 (0.064)	0.427 (0.168)	0.38	0.52	ARGON	42.6 (38.8)	44.5 (40.5)	CYCLIC TEST TERMINATED AT FLAW BREAKTHROUGH AT 128 CYCLES. SPECIMEN FAILED IN RT AIR.		
			2		$a = t$	0.864 (0.340)				0.37	1.00		60.4 (55.0)	—
			3		$a = t$	0.864 (0.340)				0.37	1.00		71.2 (64.8)	—
OST-18A	0.306 (0.120)	5.11 (2.01)	1	734.3 (106.5)	0.130 (0.051)	0.351 (0.138)	0.37	0.43	ARGON	38.6 (35.1)	39.8 (36.2)	CYCLIC TEST TERMINATED AT FLAW BREAKTHROUGH AT 342 CYCLES. SPECIMEN FAILED IN RT AIR.		
			2		$a = t$	0.737 (0.290)				0.41	1.00		56.3 (51.2)	—
			3		$a = t$	0.737 (0.290)				0.41	1.00		71.4 (65.0)	—
OST-11A	0.290 (0.114)	5.11 (2.01)	1	734.3 (106.5)	0.156 (0.061)	0.406 (0.160)	0.38	0.54	SALT WATER	41.5 (37.8)	43.6 (39.7)	CYCLIC TEST TERMINATED AT 39 CYCLES. SPECIMEN FAILED IN RT AIR.		
			2		$a = t$	0.762 (0.300)				0.27	0.70		70.4 (64.1)	86.9 (79.1)
			3		$a = t$	0.762 (0.300)				0.27	0.70		70.4 (64.1)	86.9 (79.1)
OST-19A	0.310 (0.122)	5.11 (2.01)	1	734.3 (106.5)	0.130 (0.051)	0.396 (0.156)	0.33	0.42	SALT WATER	40.4 (36.8)	42.2 (38.4)	CYCLIC TEST TERMINATED AT FLAW BREAKTHROUGH AT 59 CYCLES. SPECIMEN FAILED IN RT AIR.		
			2		$a = t$	1.270 (0.500)				0.23	0.93		67.3 (61.2)	—
			3		$a = t$	1.270 (0.500)				0.23	0.93		68.8 (62.6)	—

- 1 INITIAL CYCLIC CONDITIONS
 2 TERMINATION OF CYCLIC TEST
 3 FAILURE

Table 33: 6AL-4V STA Titanium (WT Direction) Cyclic Flaw Growth Data at 295°K (72° F) in Argon and Salt Water at 10 cpm; $t = 0.16$ cm (0.063 Inch), $\sigma_0 = 0.68 \sigma_{YS}$ and $(a/2c)_i \cong 0.10$

SPECIMEN NUMBER	THICKNESS, t cm (INCH)	WIDTH, W cm (INCH)	TEST CONDITIONS AT	GROSS STRESS, G MN/m ² (KSI)	FLAW DEPTH, a cm (INCH)	FLAW WIDTH, $2c$ cm (INCH)	$a/2c$	a/t	TEST ENVIRONMENT	IRWIN K_I MN/m ^{3/2} (KSI \sqrt{IN})	K_I WITH M_K MN/m ^{3/2} (KSI \sqrt{IN})	REMARKS (NUMBER OF CYCLES REFER TO TOTAL CYCLES)
ST6-7	0.160 (0.063)	5.08 (2.00)	1	734.3 (106.5)	0.081 (0.032)	0.787 (0.310)	0.10	0.51	ARGON	40.7 (37.0)	48.7 (44.3)	CYCLIC TEST TERMINATED AT FLAW BREAKTHROUGH AT 128 CYCLES. SPECIMEN FAILED IN RT AIR.
			2		$a = t$	0.787 (0.310)	0.20	1.00		51.6 (46.9)		
			3	860.5 (124.8)	$a = t$	0.787 (0.310)	0.20	1.00		AIR	61.3 (55.8)	
ST6-15	0.155 (0.061)	5.11 (2.01)	1	734.3 (106.5)	0.064 (0.025)	0.635 (0.250)	0.10	0.41	ARGON	38.0 (32.8)	40.3 (36.7)	CYCLIC TEST TERMINATED AT FLAW BREAKTHROUGH AT 342 CYCLES. SPECIMEN FAILED IN RT AIR.
			2		$a = t$	0.724 (0.285)	0.21	1.00		50.1 (45.6)		
			3	863.9 (125.3)	$a = t$	0.724 (0.285)	0.21	1.00		AIR	59.9 (54.5)	
ST6-8	0.157 (0.062)	5.11 (2.01)	1	734.3 (106.5)	0.086 (0.034)	0.787 (0.310)	0.11	0.55	SALT WATER	41.7 (37.9)	51.4 (46.8)	CYCLIC TEST TERMINATED AT 39 CYCLES. SPECIMEN FAILED IN RT AIR.
			2		0.140 (0.055)	0.940 (0.370)	0.15	0.89		51.0 (46.4)		
			3	798.4 (115.8)	0.140 (0.055)	0.940 (0.370)	0.15	0.89	AIR	55.9 (50.9)		
ST6-16	0.155 (0.061)	5.05 (1.99)	1	734.3 (106.5)	0.056 (0.022)	0.635 (0.250)	0.09	0.36	SALT WATER	34.2 (31.1)	37.6 (34.2)	CYCLIC TEST TERMINATED AT FLAW BREAKTHROUGH AT 59 CYCLES. SPECIMEN FAILED IN RT AIR.
			2		$a = t$	0.838 (0.330)	0.19	1.00		51.8 (47.1)		
			3	829.5 (120.3)	$a = t$	0.838 (0.330)	0.19	1.00	AIR	59.1 (53.8)		

- 1 INITIAL CYCLIC CONDITIONS
 2 TERMINATION OF CYCLIC TEST
 3 FAILURE

Table 34: 2219-T87 Aluminum Cyclic Flaw Growth Data at 78°K (-320°F) After Cryogenic Proof Test;
 $t = 1.27 \text{ cm (0.50 Inch)}$, $\sigma_0 = 0.67 \sigma_{ys}$ and $(a/2c)_j \cong 0.39$

SPECIMEN NUMBER	THICKNESS, t cm (INCH)	WIDTH, W cm (INCH)	TEST CONDITIONS AT	GROSS STRESS, G MN/m ² (KSI)	FLAW DEPTH, a cm (INCH)	FLAW WIDTH, 2c cm (INCH)	a/2c	a/t	TEST ENVIRONMENT	IRWIN K _I MN/m ^{3/2} (KSI √IN)	K _I WITH M _K MN/m ^{3/2} (KSI √IN)	REMARKS
OA54-3	1.270 (0.500)	12.70 (5.00)	1	407.5 (59.1)	0.584 (0.230)	1.537 (0.605)	0.38	0.46	LN ₂	45.8 (41.7)	47.4 (43.1)	SPECIMEN PROOF TESTED AND THEN CYCLED FOR 862 CYCLES. SPECIMEN MARKED AND CYCLE TEST RE-STARTED. TEST TERMINATED IMMED. PRIOR TO FAILURE AT 1584 CYCLES; SPECIMEN THEN FAILED AT RT. (FLAW SIZE BEFORE AND AFTER MARKING EQUAL)
			2		0.602 (0.237)	1.600 (0.630)				0.38	0.47	
			3	302.0 (43.8)	0.602 (0.237)	1.600 (0.630)	0.38	0.47		33.8 (30.8)	35.2 (32.0)	
			4		0.665 (0.262)	1.956 (0.770)				0.40	0.62	
			5	259.3 (37.6)	1.106 (0.435)	3.937 (1.550)	0.28	0.87		51.1 (46.5)	—	
			6		1.105 (0.435)	3.937 (1.550)				0.28	0.87	
OA54-7	1.275 (0.502)	12.70 (5.00)	1	407.5 (59.1)	0.523 (0.206)	1.321 (0.520)	0.40	0.41	LN ₂	42.5 (38.7)	43.5 (39.6)	SPECIMEN PROOF TESTED; THEN CYCLED FOR 487 CYCLES AND GRIP STUD FAILED; CYCLIC TEST RE-STARTED AND TEST TERMINATED IMMED. PRIOR TO FAILURE AT 2375 CYCLES; SPECIMEN THEN FAILED AT RT.
			2		0.549 (0.216)	1.346 (0.530)				0.41	0.43	
			3	302.0 (43.8)	0.549 (0.216)	1.346 (0.530)	0.41	0.43		31.2 (28.4)	31.9 (29.0)	
			4		0.659 (0.350)	2.184 (0.860)				0.41	0.70	
			5	265.5 (38.5)	1.143 (0.450)	3.556 (1.400)	0.32	0.90		49.7 (45.2)	—	
			6		1.143 (0.450)	3.556 (1.400)				0.32	0.90	
OA54-4	1.280 (0.504)	12.70 (5.00)	1	445.4 (64.6)	0.366 (0.144)	0.914 (0.360)	0.40	0.29	LN ₂	39.1 (35.6)	39.8 (36.2)	SPECIMEN PROOF TESTED; THEN CYCLED FOR 3772 CYCLES AND TEST TERMINATED IMMED. PRIOR TO FAILURE; SPECIMEN THEN FAILED IN RT AIR.
			2		0.389 (0.153)	0.965 (0.380)				0.40	0.30	
			3	302.0 (43.8)	0.389 (0.153)	0.965 (0.380)	0.40	0.30		26.5 (24.1)	26.9 (24.5)	
			5		0.978 (0.385)	3.378 (1.330)				0.29	0.76	
			6	265.5 (38.5)	0.978 (0.385)	3.378 (1.330)	0.29	0.76		42.0 (38.2)	52.5 (47.8)	
			6		0.323 (0.127)	0.902 (0.355)				0.36	0.25	
OA54-8	1.280 (0.504)	12.70 (5.00)	1	453.0 (65.7)	0.323 (0.127)	0.902 (0.355)	0.36	0.25	LN ₂			39.3 (35.8)
			2		0.335 (0.132)	0.902 (0.355)				0.37	0.26	39.5 (35.9)
			3	302.0 (43.8)	0.335 (0.132)	0.902 (0.355)	0.37	0.26				25.4 (23.1)
			5		0.991 (0.390)	3.048 (1.200)				0.33	0.77	46.0 (41.9)
			6	265.5 (38.5)	0.991 (0.390)	3.048 (1.200)	0.33	0.77		—	—	
			6		0.991 (0.390)	3.048 (1.200)				0.33	0.77	—

 INITIAL CONDITIONS
 PROOF LOAD
 START OF CYCLIC TEST
 CYCLIC TEST INTERRUPTED
 TERMINATION OF CYCLIC TEST
 FAILURE

Table 35: 2219-T87 Aluminum Cyclic Flaw Growth Data at 78°K (-320°F) After Cryogenic Proof Test;
 $t = 1.27 \text{ cm (0.50 Inch)}$, $\sigma_0 = 0.67 \sigma_{ys}$ and $(a/2c)_i \cong 0.28$

SPECIMEN NUMBER	THICKNESS, t cm (INCH)	WIDTH, W cm (INCH)	TEST CONDITIONS AT	GROSS STRESS, G MN/m ² (KSI)	FLAW DEPTH, a cm (INCH)	FLAW WIDTH, $2c$ cm (INCH)	$a/2c$	a/t	TEST ENVIRONMENT	IRWIN K_I MN/m ^{3/2} (KSI $\sqrt{\text{IN}}$)	K_I WITH M_K MN/m ^{3/2} (KSI $\sqrt{\text{IN}}$)	REMARKS
OA51-3	1.275 (0.502)	20.32 (8.00)	1	407.5 (59.1)	0.467 (0.184)	1.753 (0.690)	0.27	0.37	LN ₂	46.8 (42.6)	49.3 (44.9)	SPECIMEN PROOF TESTED; THEN CYCLED FOR 1533 CYCLES AND TEST TERMINATED IMMEDIATELY PRIOR TO FAILURE; SPECIMEN FAILED IN RT AIR.
			2		0.493 (0.194)	1.753 (0.690)	0.28	0.39		47.3 (43.0)	49.7 (45.2)	
			3	302.0 (43.8)	0.493 (0.194)	1.753 (0.690)	0.28	0.39		34.1 (31.0)	35.8 (32.6)	
			4		1.067 (0.420)	3.556 (1.400)	0.30	0.84	49.1 (44.7)	63.2 (57.6)		
			5	278.5 (40.1)	1.067 (0.420)	3.556 (1.400)	0.30	0.84	AIR	45.3 (41.2)	58.2 (53.0)	
OA51-7	1.280 (0.504)	20.32 (8.00)	1	407.5 (59.1)	0.380 (0.148)	1.478 (0.582)	0.25	0.29	LN ₂	42.6 (38.8)	44.6 (40.6)	SPECIMEN PROOF TESTED; THEN CYCLED FOR 2300 CYCLES AND TEST TERMINATED IMMEDIATELY PRIOR TO FAILURE; SPECIMEN FAILED IN RT AIR.
			2		0.394 (0.155)	1.478 (0.582)	0.27	0.31		43.0 (39.1)	45.1 (41.0)	
			3	302.0 (43.8)	0.394 (0.155)	1.478 (0.582)	0.27	0.31		31.0 (28.2)	32.4 (29.5)	
			4		1.029 (0.405)	3.556 (1.400)	0.29	0.80	48.8 (44.4)	62.4 (56.8)		
			5	277.2 (40.2)	1.029 (0.405)	3.556 (1.400)	0.29	0.80	AIR	45.2 (41.1)	57.7 (52.5)	
OA51-4	1.283 (0.505)	20.32 (8.00)	1	453.0 (65.7)	0.274 (0.108)	0.978 (0.385)	0.28	0.21	LN ₂	39.8 (36.2)	40.6 (36.9)	SPECIMEN PROOF TESTED; THEN CYCLED FOR 5322 CYCLES AND TEST TERMINATED IMMEDIATELY PRIOR TO FAILURE; SPECIMEN FAILED IN RT AIR.
			2		0.295 (0.116)	0.991 (0.390)	0.30	0.23		40.4 (36.8)	41.3 (37.6)	
			3	302.0 (43.8)	0.295 (0.116)	0.991 (0.390)	0.30	0.23		26.9 (23.6)	26.5 (24.1)	
			4		1.067 (0.420)	3.810 (1.500)	0.28	0.83	50.2 (45.7)	65.9 (60.0)		
			5	288.2 (38.9)	1.067 (0.420)	3.810 (1.500)	0.28	0.83	AIR	44.8 (40.8)	58.9 (53.6)	
OA51-8	1.273 (0.501)	20.32 (8.00)	1	456.4 (66.2)	0.248 (0.098)	0.813 (0.320)	0.31	0.20	LN ₂	37.0 (33.7)	37.6 (34.2)	SPECIMEN PROOF TESTED; THEN CYCLED FOR 7613 CYCLES AND TEST TERMINATED IMMEDIATELY PRIOR TO FAILURE; SPECIMEN FAILED IN RT AIR.
			2		0.262 (0.103)	0.813 (0.320)	0.32	0.21		37.3 (33.9)	37.8 (34.4)	
			3	302.0 (43.8)	0.262 (0.103)	0.813 (0.320)	0.32	0.21		23.7 (21.6)	24.1 (21.9)	
			4		1.130 (0.445)	3.962 (1.560)	0.29	0.89	51.4 (46.8)	—		
			5	266.1 (38.6)	1.130 (0.445)	3.962 (1.560)	0.29	0.89	AIR	45.5 (41.4)	—	

061

1 INITIAL CONDITIONS
 2 PROOF LOAD

3 START OF CYCLIC TEST
 4 TERMINATION OF CYCLIC TEST

5 FAILURE

Table 36: 2219-T87 Aluminum Cyclic Flaw Growth Data at 78°K (-320°F) After Cryogenic Proof Test; $t = 1.27 \text{ cm (0.50 Inch)}$, $\sigma_D = 0.91 \sigma_{YS}$ and $(a/2c)_i \cong 0.40$ and 0.10

SPECIMEN NUMBER	THICKNESS, t cm (INCH)	WIDTH, W cm (INCH)	TEST CONDITIONS AT	GROSS STRESS, G MN/m ² (KSI)	FLAW DEPTH, a cm (INCH)	FLAW WIDTH, 2c cm (INCH)	a/2c	a/t	TEST ENVIRONMENT	IRWIN K _I MN/m ^{3/2} (KSI √IN)	K _I WITH MK MN/m ^{3/2} (KSI √IN)	REMARKS
OCA54-1	1.278 (0.503)	12.70 (5.00)	1	453.0 (65.7)	0.307 (0.121)	0.767 (0.302)	0.40	0.24	LN ₂	36.5 (33.2)	36.9 (33.6)	SPECIMEN PROOF TESTED AND THEN CYCLED FOR 202 CYCLES. SPECIMEN MARKED AND CYCLE TEST RE-STARTED. TEST TERMINATED IMMEDIATELY PRIOR TO FAILURE AT 1269 CYCLES; SPECIMEN FAILED IN LN ₂
			2		0.338 (0.133)	0.851 (0.335)	0.40	0.26		38.5 (35.0)	39.0 (35.5)	
			3		0.338 (0.133)	0.851 (0.335)	0.40	0.26		34.8 (31.5)	35.2 (32.0)	
			4	412.3 (59.8)	?	?	-	-		-	-	
			5		?	?	-	-		-	-	
			6		0.813 (0.320)	2.464 (0.970)	0.33	0.64		58.0 (52.8)	65.4 (59.5)	
			7	0.813 (0.320)	2.464 (0.970)	0.33	0.64	-		-		
OCA54-3	1.273 (0.501)	12.70 (5.00)	1	453.0 (65.7)	0.228 (0.090)	0.582 (0.229)	0.39	0.18	LN ₂	31.8 (28.9)	31.9 (29.0)	SPECIMEN PROOF TESTED AND THEN CYCLED FOR 206 CYCLES. SPECIMEN MARKED AND CYCLE TEST RE-STARTED. TEST TERMINATED IMMEDIATELY PRIOR TO FAILURE AT 2191 CYCLES; SPECIMEN FAILED IN LN ₂
			2		0.261 (0.099)	0.584 (0.230)	0.43	0.20		31.9 (29.0)	32.0 (29.1)	
			3		0.261 (0.099)	0.584 (0.230)	0.43	0.20		28.8 (26.2)	28.9 (26.3)	
			4	412.3 (59.8)	?	?	-	-		-	-	
			5		?	?	-	-		-	-	
			6		0.813 (0.320)	2.286 (0.900)	0.36	0.64		56.4 (51.3)	62.1 (56.5)	
			7	421.3 (61.1)	0.813 (0.320)	2.286 (0.900)	0.36	0.64		57.7 (52.5)	63.6 (57.9)	
OCA51-3	1.273 (0.501)	20.32 (8.00)	1	453.0 (65.7)	0.224 (0.088)	2.134 (0.840)	0.11	0.18	LN ₂	44.1 (40.1)	45.3 (41.2)	SPECIMEN PROOF TESTED; THEN CYCLED FOR 66 CYCLES AND TEST TERMINATED IMMEDIATELY PRIOR TO FAILURE; SPECIMEN THEN FAILED AT RT.
			2		0.274 (0.108)	2.134 (0.840)	0.13	0.22		47.7 (43.4)	49.3 (44.9)	
			3	412.3 (59.8)	0.274 (0.108)	2.134 (0.840)	0.13	0.22		42.5 (38.7)	44.1 (40.1)	
			6		0.493 (0.194)	2.134 (0.840)	0.23	0.39		50.8 (46.2)	54.3 (49.4)	
			7		358.5 (52.0)	0.493 (0.194)	2.134 (0.840)	0.23		0.39	44.5 (40.5)	
OCA51-1A	1.288 (0.507)	20.32 (8.00)	1	453.0 (65.7)	0.130 (0.051)	1.397 (0.550)	0.09	0.10	LN ₂	34.1 (31.0)	34.5 (31.4)	SPECIMEN PROOF TESTED; THEN CYCLED FOR 668 CYCLES AND TEST TERMINATED IMMEDIATELY PRIOR TO FAILURE; SPECIMEN THEN FAILED AT RT.
			2		0.142 (0.056)	1.397 (0.550)	0.10	0.11		35.3 (32.1)	35.9 (32.7)	
			3	412.3 (59.8)	0.142 (0.056)	1.397 (0.550)	0.10	0.11		31.5 (28.7)	32.0 (29.1)	
			6		0.572 (0.225)	1.702 (0.670)	0.34	0.44		48.4 (44.0)	50.7 (46.1)	
			7		372.3 (54.0)	0.572 (0.225)	1.702 (0.670)	0.34		0.44	44.1 (40.1)	

161

1 INITIAL CONDITIONS
 2 PROOF LOAD
 3 START OF CYCLIC TEST
 4 DIMPLING OCCURRED
 5 RE-START OF CYCLIC TEST AFTER DIMPLING AND MARKING
 6 TERMINATION OF CYCLIC TEST
 7 FAILURE

Table 37: 2219-T87 Aluminum Cyclic Flaw Growth Data at 78°K (-320°F) After Cryogenic Proof Test; $t = 0.38 \text{ cm (0.15 Inch)}$, $\sigma_D = 0.67 \sigma_{YS}$ and $(a/2c)_i \cong 0.37$

SPECIMEN NUMBER	THICKNESS, t cm (INCH)	WIDTH, W cm (INCH)	TEST CONDITIONS AT	GROSS STRESS, G MN/m ² (KSI)	FLAW DEPTH, a cm (INCH)	FLAW WIDTH, 2c cm (INCH)	a/2c	a/t	TEST ENVIRONMENT	IRWIN K _I MN/m ^{3/2} (KSI √IN)	K _I WITH M K MN/m ^{3/2} (KSI √IN)	REMARKS	
OA14-3	0.394 (0.155)	8.89 (3.50)	1	407.5 (59.1)	0.300 (0.118)	0.787 (0.310)	0.38	0.76	LN ₂	32.9 (29.9)	37.1 (33.8)	SPECIMEN PROOF TESTED; THEN CYCLED FOR 1050 CYCLES TO BREAKTHROUGH. CYCLING CONTINUED FOR TOTAL OF 1450 CYCLES. SPECIMEN FAILED IN RT AIR.	
			2		0.310 (0.122)	0.813 (0.320)				33.3 (30.3)	38.2 (34.8)		
			3	302.0 (43.8)	0.310 (0.122)	0.813 (0.320)	0.38	0.79		24.2 (22.0)	27.7 (25.2)		
			5		a = t	1.181 (0.465)				0.33	1.00		28.8 (26.2)
			6	337.9 (49.0)	a = t	—	—	—	1.00	AIR	—		—
			OA14-7	0.396 (0.156)	8.89 (3.50)	1	407.5 (59.1)	0.246 (0.097)	0.660 (0.260)	0.37	0.62		LN ₂
2	0.249 (0.098)	0.665 (0.262)				30.1 (27.4)		32.6 (29.7)					
3	302.0 (43.8)	0.249 (0.098)				0.665 (0.262)	0.37	0.63	21.9 (19.9)	23.6 (21.5)			
5		a = t				1.130 (0.445)			0.35	1.00	28.2 (25.7)	—	
6	333.0 (48.3)	a = t				1.130 (0.445)	0.35	1.00	AIR	31.9 (29.0)	—		
OA14-8	0.356 (0.140)	8.89 (3.50)				1	453.0 (65.7)	0.198 (0.078)	0.533 (0.210)	0.37	0.56	LN ₂	30.3 (27.6)
			2	0.236 (0.093)	0.660 (0.260)	33.6 (30.6)		37.5 (34.1)					
			3	302.0 (43.8)	0.236 (0.093)	0.660 (0.260)	0.36	0.66	21.7 (19.7)	24.1 (21.9)			
			5		a = t	1.067 (0.420)			0.33	1.00	27.4 (24.9)		—
			6	410.3 (59.5)	a = t	1.067 (0.420)	0.33	1.00	AIR	38.5 (35.0)	—		
			OA14-4	0.389 (0.153)	8.89 (3.50)	1	431.6 (62.6)	0.229 (0.090)	0.622 (0.245)	0.37	0.59	LN ₂	31.0 (28.2)
2	0.241 (0.095)	0.635 (0.250)				31.4 (28.6)		33.7 (30.7)					
3	302.0 (43.8)	0.241 (0.095)				0.635 (0.250)	0.38	0.62	21.3 (19.4)	23.0 (20.9)			
4		?				?			—	—	—		—
5	a = t	1.041 (0.410)				0.36	1.00	27.4 (24.9)	—				
6	343.4 (49.8)	a = t				1.041 (0.410)	0.36	1.00	AIR	31.8 (28.9)	—		

1 INITIAL CONDITIONS
2 PROOF LOAD

3 START OF CYCLIC TEST
4 CYCLIC TEST INTERRUPTION

5 TERMINATION OF CYCLIC TEST
6 FAILURE

Table 38: 2219-T87 Aluminum Cyclic Flow Growth Data at 78°K (-320°F) After Cryogenic Proof Test;
 $t = 0.38$ cm (0.15 Inch), $\sigma_0 = 0.67 \sigma_{ys}$ and $(a/2c)_i \cong 0.11$

SPECIMEN NUMBER	THICKNESS, t cm (INCH)	WIDTH, W cm (INCH)	TEST CONDITIONS AT	GROSS STRESS, G MN/m ² (KSI)	FLAW DEPTH, a cm (INCH)	FLAW WIDTH, 2c cm (INCH)	a/2c	a/t	TEST ENVIRONMENT	IRWIN K _I MN/m ^{3/2} (KSI √IN)	K _I WITH M _K MN/m ^{3/2} (KSI √IN)	REMARKS
OA11-3	0.394 (0.155)	12.70 (5.00)	1	382.0 (55.4)	0.211 (0.083)	2.388 (0.940)	0.09	0.54	LN ₂	35.5 (32.3)	44.0 (40.0)	SPECIMEN PROOF TESTED; THEN CYCLED FOR 70 CYCLES TO BREAK- THROUGH; SPECIMEN FAILED IN RT AIR.
			2		0.312 (0.123)	2.388 (0.940)	0.13	0.79		41.4 (37.7)	62.6 (57.0)	
			3	302.0 (43.8)	0.312 (0.123)	2.388 (0.940)	0.13	0.79	AIR	31.9 (29.0)	48.2 (43.9)	
			4		a = t	2.388 (0.940)	0.17	1.00		34.6 (31.5)		
			5	293.7 (42.6)	a = t	2.388 (0.940)	0.17	1.00	34.2 (31.1)			
OA11-7	0.394 (0.155)	12.70 (5.00)	1	407.5 (59.1)	0.206 (0.081)	2.032 (0.800)	0.10	0.52	LN ₂	37.4 (34.0)	45.4 (41.3)	SPECIMEN PROOF TESTED; THEN CYCLED FOR 406 CYCLES TO BREAKTHROUGH; SPECIMEN FAILED IN RT AIR.
			2		0.262 (0.103)	2.032 (0.800)	0.13	0.67		41.0 (37.3)	55.4 (50.4)	
			3	302.0 (43.8)	0.262 (0.103)	2.032 (0.800)	0.13	0.67	AIR	28.2 (26.6)	39.8 (36.0)	
			4		a = t	2.210 (0.870)	0.18	1.00		34.2 (31.1)		
			5	302.0 (43.8)	a = t	2.210 (0.870)	0.18	1.00	34.7 (31.6)			
OA11-8	0.391 (0.154)	12.70 (5.00)	1	448.2 (65.0)	0.150 (0.059)	1.168 (0.460)	0.13	0.38	LN ₂	34.7 (31.6)	38.1 (34.7)	SPECIMEN PROOF TESTED; THEN CYCLED FOR 2803 CYCLES TO BREAKTHROUGH; SPECIMEN FAILED IN RT AIR.
			2		0.168 (0.066)	1.168 (0.460)	0.14	0.43		36.2 (32.9)	40.4 (36.8)	
			3	302.0 (43.8)	0.168 (0.066)	1.168 (0.460)	0.14	0.43	AIR	23.1 (21.0)	25.8 (23.5)	
			4		a = t	1.422 (0.560)	0.28	1.00		30.6 (27.8)		
			5	335.8 (48.7)	a = t	1.422 (0.560)	0.28	1.00	34.9 (31.8)			

- 1 INITIAL CONDITIONS
 2 PROOF LOAD
 3 START OF CYCLIC TEST
 4 TERMINATION OF CYCLIC TEST
 5 FAILURE

Table 39: 2219-T87 Aluminum Cyclic Flaw Growth Data at 78°K (-320°F) After Cryogenic Proof Test; $t = 0.38$ cm (0.15 Inch), $\sigma_0 = 0.76 \sigma_{ys}$ and $(a/2c) \cong 0.37$

SPECIMEN NUMBER	THICKNESS, t cm (INCH)	WIDTH, W cm (INCH)	TEST CONDITIONS AT	GROSS STRESS, G MN/m ² (KSI)	FLAW DEPTH, a cm (INCH)	FLAW WIDTH, $2c$ cm (INCH)	$a/2c$	a/t	TEST ENVIRONMENT	IRWIN K_I MN/m ^{3/2} (KSI√IN)	K_I WITH M_K MN/m ^{3/2} (KSI√IN)	REMARKS		
OCA14-1	0.368 (0.145)	8.89 (3.50)	1	453.0 (65.7)	0.140 (0.055)	0.391 (0.154)	0.36	0.38	LN ₂	25.9 (23.6)	26.7 (24.3)	SPECIMEN PROOF TESTED AND THEN CYCLED FOR 1020 CYCLES. SPECIMEN MARKED AND CYCLE TEST RE-STARTED. TEST TERMINATED AT 1985 CYCLES AT BREAKTHROUGH; SPECIMEN FAILED IN LN ₂		
			2		0.140 (0.055)	0.391 (0.154)				25.9 (23.6)	26.7 (24.3)			
			3	343.4 (49.8)	0.140 (0.055)	0.391 (0.154)	0.36	0.38		19.1 (17.4)	19.7 (17.9)			
			4		0.178 (0.070)	0.432 (0.170)				20.3 (18.5)	20.8 (18.9)			
			5	412.3 (59.8)	0.183 (0.072)	0.432 (0.170)	0.42	0.50		24.7 (22.5)	25.3 (23.0)			
			6		$a = t$	1.041 (0.410)	0.35	1.00		38.0 (34.6)	—			
			7	425.4 (61.7)	$a = t$	1.041 (0.410)	0.35	1.00		39.3 (35.8)	—			
OCA14-3	0.394 (0.155)	8.89 (3.50)	1	453.0 (65.7)	0.224 (0.088)	0.579 (0.228)	0.38	0.57	LN ₂	31.7 (28.8)	33.3 (30.3)	SPECIMEN PROOF TESTED AND THEN CYCLED FOR 513 CYCLES. SPECIMEN MARKED AND CYCLE TEST RE-STARTED. TEST TERMINATED AT 2063 CYCLES AT BREAKTHROUGH; SPECIMEN FAILED IN LN ₂		
			2		0.224 (0.088)	0.579 (0.228)				0.38	0.57		31.7 (28.8)	33.3 (30.3)
			3	343.4 (49.8)	0.224 (0.088)	0.579 (0.228)	0.38	0.57		23.4 (21.3)	24.6 (22.4)			
			4		0.249 (0.098)	0.635 (0.250)				0.39	0.63		24.5 (22.3)	26.2 (23.8)
			5		0.251 (0.099)	0.635 (0.250)				0.40	0.64		24.5 (22.3)	26.2 (23.8)
			6	$a = t$	1.207 (0.475)	0.33	1.00	33.2 (30.2)		—				
			7	410.3 (59.5)	$a = t$	1.207 (0.475)	0.33	1.00		40.3 (36.7)	—			

- 1 INITIAL CONDITIONS
- 2 PROOF LOAD
- 3 START OF CYCLIC TEST
- 4 DIMPLING OCCURRED
- 5 RE-START OF CYCLIC TEST AFTER DIMPLING AND MARKING
- 6 TERMINATION OF CYCLIC TEST
- 7 FAILURE

Table 40: 2219-T87 Aluminum Cyclic Flaw Growth Data at 78^oK (-320^oF) After Cryogenic Proof Test; t = 0.38 cm (0.15 Inch), $\sigma_0 = 0.91 \sigma_{ys}$ and (a/2c); $\cong 0.11$





SPECIMEN NUMBER	THICKNESS, t cm (INCH)	WIDTH, W cm (INCH)	TEST CONDITIONS AT	GROSS STRESS, G MN/m ² (KSI)	FLAW DEPTH, a cm (INCH)	FLAW WIDTH, 2c cm (INCH)	a/2c	a/t	TEST ENVIRONMENT	IRWIN K _I MN/m ^{3/2} (KSI √IN)	K _I WITH M _K MN/m ^{3/2} (KSI √IN)	REMARKS
OCA11-1	0.384 (0.151)	12.70 (5.00)	1	453.0 (65.7)	0.124 (0.049)	0.953 (0.375)	0.13	0.33	LN ₂	32.0 (29.1)	34.6 (31.5)	SPECIMEN PROOF TESTED AND THEN CYCLED FOR 253 CYCLES. SPECIMEN MARKED AND CYCLE TEST RE-STARTED. TEST TERMINATED AT 692 CYCLES AT BREAKTHROUGH; SPECIMEN FAILED IN LN ₂
			2		?	?				-	-	
			3	412.3 (59.8)	?	?	-	-		-	-	
			4		0.150 (0.059)	0.953 (0.375)	0.16	0.39		30.4 (27.7)	33.3 (30.3)	
			5		0.157 (0.062)	0.953 (0.375)	0.17	0.41		31.0 (28.2)	34.1 (31.0)	
			6		a = t	1.575 (0.620)	0.24	1.00		44.2 (40.2)	-	
			7	416.5 (60.4)	a = t	1.575 (0.620)	0.24	1.00		44.7 (40.7)	-	
OCA11-3	0.381 (0.150)	12.70 (5.00)	1	453.0 (65.7)	0.099 (0.039)	1.067 (0.420)	0.09	0.26	LN ₂	29.8 (27.1)	31.5 (28.7)	SPECIMEN PROOF TESTED AND THEN CYCLED FOR 286 CYCLES. SPECIMEN MARKED AND CYCLE TEST RE-STARTED. TEST TERMINATED AT 898 CYCLES AT BREAKTHROUGH; SPECIMEN THEN FAILED AT RT.
			2		?	?				-	-	
			3	412.3 (59.8)	?	?	-	-		-	-	
			4		0.122 (0.048)	1.067 (0.420)	0.11	0.32		28.8 (26.2)	31.1 (28.3)	
			5		0.135 (0.053)	1.067 (0.420)	0.13	0.35		29.9 (27.2)	32.5 (29.6)	
			6		a = t	1.346 (0.530)	0.28	1.00		42.0 (38.2)	-	
			7	380.6 (55.2)	a = t	1.346 (0.530)	0.28	1.00		AIR	39.3 (35.8)	

- 1 INITIAL CONDITIONS
 2 PROOF LOAD
 3 START OF CYCLIC TEST
 4 DIMPLING OCCURRED
 5 RE-START OF CYCLIC TEST AFTER DIMPLING AND MARKING
 6 TERMINATION OF CYCLIC TEST
 7 FAILURE

Table 41: 6AL-4V STA Titanium (Rt Direction) Cyclic Flaw Growth Data at 295°K (72°F) After An Ambient Proof Test; t = 0.54 cm (0.21 Inch), $\sigma_0 = 0.77 \sigma_{YS}$ and $(a/2c)_i \cong 0.37$

SPECIMEN NUMBER	THICKNESS, t cm (INCH)	WIDTH, W cm (INCH)	TEST CONDITIONS AT	GROSS STRESS, G MN/m ² (KSI)	FLAW DEPTH, a cm (INCH)	FLAW WIDTH, 2c cm (INCH)	a/2c	a/t	TEST ENVIRONMENT	IRWIN K _I MN/m ^{3/2} (KSI √IN)	K _I WITH M K MN/m ^{3/2} (KSI √IN)	REMARKS (NUMBER OF CYCLES REFER TO TOTAL CYCLES)
OCT24-1	0.549 (0.216)	7.62 (3.00)	1	944.6 (137.0)	0.147 (0.058)	0.401 (0.158)	0.37	0.27	AIR	54.2 (49.3)	55.3 (50.3)	SPECIMEN PROOF TESTED AND THEN CYCLED FOR 93 CYCLES. SPECIMEN MARKED AND CYCLE TEST RE-STARTED. FLAW BREAKTHROUGH OCCURRED AT 870 CYCLES BUT CYCLED FOR 885 CYCLES. SPECIMEN THEN FAILED AT RT.
			2		0.150 (0.059)	0.401 (0.158)	0.37	0.27		54.2 (49.3)	55.3 (50.3)	
			3	820.5 (119.0)	0.150 (0.059)	0.401 (0.158)	0.37	0.27		46.5 (42.3)	47.5 (43.2)	
			4		0.155 (0.061)	0.401 (0.158)	0.39	0.28		46.6 (42.4)	47.6 (43.3)	
			5		0.155 (0.061)	0.401 (0.158)	0.39	0.28		46.6 (42.4)	47.6 (43.3)	
			6	a = t	1.270 (0.500)	0.43	1.00	83.4 (75.9)		—		
			7	a = t	1.270 (0.500)	0.43	1.00	80.6 (73.3)		—		
OCT24-2	0.531 (0.209)	7.65 (3.01)	1	944.6 (137.0)	0.150 (0.059)	0.417 (0.164)	0.36	0.28	AIR	55.1 (50.1)	56.5 (51.4)	SPECIMEN PROOF TESTED AND THEN CYCLED FOR 110 CYCLES. SPECIMEN MARKED AND CYCLE TEST RE-STARTED. FLAW BREAKTHROUGH OCCURRED AT 750 CYCLES BUT CYCLED FOR 759 CYCLES. SPECIMEN THEN FAILED AT RT.
			2		0.152 (0.060)	0.417 (0.164)	0.37	0.29		55.1 (50.1)	56.5 (51.4)	
			3	820.5 (119.0)	0.152 (0.060)	0.417 (0.164)	0.37	0.29		47.4 (43.1)	48.5 (44.1)	
			4		?	?	—	—		—	—	
			5		?	?	—	—		—	—	
			6	a = t	1.270 (0.500)	0.42	1.00	83.3 (75.8)		—		
			7	a = t	1.270 (0.500)	0.42	1.00	83.3 (75.8)		—		
OCT24-3	0.538 (0.212)	7.62 (3.00)	1	944.6 (137.0)	0.203 (0.080)	0.533 (0.210)	0.38	0.38	AIR	62.6 (57.0)	64.2 (58.4)	SPECIMEN PROOF TESTED AND THEN CYCLED FOR 80 CYCLES. SPECIMEN MARKED AND CYCLE TEST RE-STARTED. FLAW BREAKTHROUGH OCCURRED AT 384 CYCLES BUT CYCLED FOR 394 CYCLES. SPECIMEN THEN FAILED AT RT.
			2		0.206 (0.081)	0.533 (0.210)	0.39	0.38		62.6 (57.0)	64.1 (58.3)	
			3	820.5 (119.0)	0.206 (0.081)	0.533 (0.210)	0.39	0.38		53.7 (48.9)	55.1 (50.1)	
			4		0.218 (0.086)	0.607 (0.239)	0.36	0.41		57.0 (51.9)	58.9 (53.6)	
			5		0.221 (0.087)	0.610 (0.240)	0.36	0.41		57.3 (52.1)	59.0 (53.7)	
			6	a = t	1.524 (0.600)	0.35	1.00	90.2 (82.1)		—		
			7	a = t	1.524 (0.600)	0.35	1.00	89.3 (81.3)		—		

96L

 INITIAL CONDITIONS
 PROOF LOAD
 START OF CYCLIC TEST
 DIMPLING OCCURRED


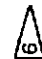

 RE-START OF CYCLIC TEST AFTER DIMPLING AND MARKING
 TERMINATION OF CYCLIC TEST
 FAILURE

Table 42: 6AL-4V STA Titanium (RT Direction) Cyclic Flaw Growth Data at 295°K (72°F) After An Ambient Proof Test; t = 0.54 cm (0.21 Inch), $\sigma_0 = 0.77 \sigma_{ys}$ and $(a/2c)_i = 0.10$

SPECIMEN NUMBER	THICKNESS, t cm (INCH)	WIDTH, W cm (INCH)	TEST CONDITIONS AT	GROSS STRESS, G MN/m ² (KSI)	FLAW DEPTH, a cm (INCH)	FLAW WIDTH, 2c cm (INCH)	a/2c	a/t	TEST ENVIRONMENT	IRWIN K _I MN/m ^{3/2} (KSI√IN)	K _I WITH M _K MN/m ^{3/2} (KSI√IN)	REMARKS (NUMBER OF CYCLES REFER TO TOTAL CYCLES)
OCT21-1	0.533 (0.210)	10.19 (4.01)	1	944.6 (137.0)	0.097 (0.038)	0.991 (0.390)	0.10	0.18	AIR	59.6 (54.2)	61.2 (55.7)	SPECIMEN PROOF TESTED AND DIMPLED AFTER 99 CYCLES; TEST TERMINATED AT 509 CYCLES. SPECIMEN THEN FAILED AT RT.
			2		0.099 (0.039)	0.991 (0.390)	0.10	0.19		60.2 (54.8)	61.9 (56.3)	
			3	820.5 (119.0)	0.099 (0.039)	0.991 (0.390)	0.10	0.19		51.1 (46.5)	52.5 (47.8)	
			4		0.109 (0.043)	0.991 (0.390)	0.11	0.21		53.1 (48.3)	54.7 (49.8)	
			5		0.112 (0.044)	0.991 (0.390)	0.11	0.21		53.6 (48.8)	55.4 (50.4)	
			6	0.335 (0.132)	1.397 (0.550)	0.24	0.63	81.1 (73.8)		97.8 (89.0)		
			7	799.8 (116.0)	0.335 (0.132)	1.397 (0.550)	0.24	0.63		78.8 (71.7)	95.2 (86.6)	
OCT21-2	0.544 (0.214)	10.19 (4.01)	1	944.6 (137.0)	0.097 (0.038)	0.991 (0.390)	0.10	0.18	AIR	59.6 (54.2)	61.2 (55.7)	SPECIMEN PROOF TESTED AND DIMPLED AFTER 99 CYCLES; TEST TERMINATED AT 422 CYCLES. SPECIMEN THEN FAILED AT RT.
			2		0.102 (0.040)	0.991 (0.390)	0.10	0.19		60.8 (55.3)	62.5 (56.9)	
			3	820.5 (119.0)	0.102 (0.040)	0.991 (0.390)	0.10	0.19		51.7 (47.0)	53.1 (48.3)	
			4		0.112 (0.044)	0.991 (0.390)	0.11	0.21		53.6 (48.8)	55.3 (50.3)	
			5		0.117 (0.046)	0.991 (0.390)	0.12	0.22		54.5 (49.6)	56.5 (51.4)	
			6	0.366 (0.144)	1.372 (0.540)	0.27	0.67	82.1 (74.7)		99.6 (90.6)		
			7	774.3 (112.3)	0.366 (0.144)	1.372 (0.540)	0.27	0.67		77.5 (70.5)	93.5 (85.1)	
OCT21-3	0.541 (0.213)	10.19 (4.01)	1	944.6 (137.0)	0.140 (0.055)	1.397 (0.550)	0.10	0.26	AIR	71.5 (65.1)	75.7 (68.9)	SPECIMEN PROOF TESTED AND DIMPLED AFTER 83 CYCLES; TEST TERMINATED IMMED. PRIOR TO FAILURE AT 131 CYCLES. SPECIMEN THEN FAILED AT RT.
			2		0.145 (0.057)	1.397 (0.550)	0.10	0.27		72.5 (66.0)	77.0 (70.1)	
			3	820.5 (119.0)	0.145 (0.057)	1.397 (0.550)	0.10	0.27		61.5 (56.0)	65.5 (59.6)	
			4		0.180 (0.071)	1.397 (0.550)	0.13	0.33		67.0 (61.0)	72.6 (66.1)	
			5		0.185 (0.073)	1.397 (0.550)	0.13	0.34		67.8 (61.7)	73.5 (66.9)	
			6	0.295 (0.116)	1.600 (0.630)	0.18	0.54	80.9 (73.6)		95.7 (87.1)		
			7	766.0 (111.1)	0.295 (0.116)	1.600 (0.630)	0.18	0.54		75.0 (68.2)	88.8 (80.8)	

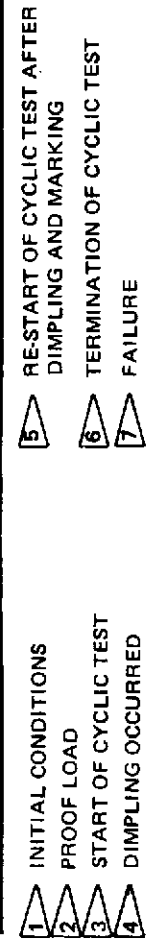






Table 42: (Continued)

SPECIMEN NUMBER	THICKNESS, t cm (INCH)	WIDTH, W cm (INCH)	TEST CONDITIONS AT	GROSS STRESS, G MN/m ² (KSI)	FLAW DEPTH, a cm (INCH)	FLAW WIDTH, 2c cm (INCH)	a/2c	a/t	TEST ENVIRONMENT	IRWIN K _I MN/m ^{3/2} (KSI √IN)	K _I WITH M _K MN/m ^{3/2} (KSI √IN)	REMARKS (NUMBER OF CYCLES REFER TO TOTAL CYCLES)
OCT 21-4	0.541 (0.213)	10.19 (4.01)	1	944.6 (137.0)	0.137 (0.054)	1.402 (0.552)	0.10	0.25	AIR	71.0 (64.6)	75.1 (68.3)	SPECIMEN PROOF TESTED AND DIMPLED AFTER 63 CYCLES; TEST TERMINATED IMMEDIATELY PRIOR TO FAILURE AT 105 CYCLES. SPECIMEN THEN FAILED AT RT.
			2		0.145 (0.057)	1.402 (0.552)	0.10	0.27		72.5 (66.0)	77.1 (70.2)	
			3	820.5 (119.0)	0.145 (0.057)	1.402 (0.552)	0.10	0.27		61.7 (56.1)	65.5 (59.6)	
			4		0.175 (0.069)	0.142 (0.552)	0.13	0.32		68.4 (60.4)	71.8 (65.3)	
			5		0.178 (0.070)	0.402 (0.552)	0.13	0.33		66.7 (60.7)	72.2 (65.7)	
			6		0.274 (0.108)	1.461 (0.575)	0.19	0.51		77.7 (70.7)	89.6 (81.5)	
			7		0.274 (0.108)	1.461 (0.575)	0.19	0.51		75.0 (68.2)	86.4 (78.6)	

Table 43: 6Al-4V STA Titanium (RT Direction) Cyclic Flow Growth Data at 295°K (72°F) After an Ambient Proof Test; $t = 0.16$ cm (0.063 inch), $\sigma_D = 0.77 \sigma_{YS}$ and $(a/2c)_i \cong 0.33$

SPECIMEN NUMBER	THICKNESS, t cm (INCH)	WIDTH, W cm (INCH)	TEST CONDITIONS AT	GROSS STRESS, G MN/m ² (KSI)	FLAW DEPTH, a cm (INCH)	FLAW WIDTH, 2c cm (INCH)	a/2c	a/t	TEST ENVIRONMENT	IRWIN K_I MN/m ^{3/2} (KSI √IN)	K_I WITH M/K MN/m ^{3/2} (KSI √IN)	REMARKS (NUMBER OF CYCLES REFER TO TOTAL CYCLES)
OCT 64-1	0.152 (0.060)	3.81 (1.50)	1	944.6 (137.0)	0.028 (0.011)	0.089 (0.035)	0.31	0.18	AIR	25.1 (22.8)	25.4 (23.1)	SPECIMEN PROOF TESTED AND THEN CYCLED FOR 125 CYCLES WHEN SPECIMEN DIMPLED. SPECIMEN MARKED AND CYCLE TEST RE-STARTED. TEST TERMINATED AT FLAW BREAKTHROUGH AT 1866 CYCLES SPECIMEN THEN FAILED AT RT.
			2		0.028 (0.011)	0.089 (0.035)				25.1 (22.8)	25.4 (23.1)	
			3		0.028 (0.011)	0.089 (0.035)				21.5 (19.6)	21.8 (19.8)	
			4	820.5 (119.0)	?	?	—	—		—	—	
			5		?	?	—	—		—	—	
			6		a = t	0.437 (0.172)	0.35	1.00		48.2 (43.9)	—	
			7	1002.5 (145.4)	a = t	0.437 (0.172)	0.35	1.00		60.1 (54.7)	—	
OCT 64-2	0.152 (0.060)	3.81 (1.50)	1	944.6 (137.0)	0.028 (0.011)	0.094 (0.037)	0.30	0.18	AIR	25.6 (23.3)	25.9 (23.6)	SPECIMEN PROOF TESTED AND THEN CYCLED FOR 37 CYCLES WHEN SPECIMEN DIMPLED. SPECIMEN MARKED AND CYCLE TEST RE-STARTED. TEST TERMINATED AT FLAW BREAKTHROUGH AT 3150 CYCLES. SPECIMEN THEN FAILED AT RT.
			2		0.028 (0.011)	0.094 (0.037)				25.6 (23.3)	25.9 (23.6)	
			3		0.028 (0.011)	0.094 (0.037)				21.9 (19.9)	22.2 (20.2)	
			4	820.5 (119.0)	?	?	—	—		—	—	
			5		?	?	—	—		—	—	
			6		a = t	0.457 (0.180)	0.33	1.00		49.1 (44.7)	—	
			7	1004.6 (145.7)	a = t	0.457 (0.180)	0.33	1.00		63.9 (58.1)	—	
OCT 64-3	0.152 (0.060)	3.81 (1.50)	1	944.6 (137.0)	0.076 (0.030)	0.196 (0.077)	0.39	0.50	AIR	37.9 (34.5)	39.2 (35.7)	SPECIMEN PROOF TESTED AND THEN CYCLED FOR 38 CYCLES WHEN SPECIMEN DIMPLED. SPECIMEN MARKED AND CYCLE TEST RE-STARTED. TEST TERMINATED AT FLAW BREAKTHROUGH AT 540 CYCLES. SPECIMEN THEN FAILED AT RT.
			2		0.079 (0.031)	0.198 (0.078)				38.2 (34.8)	39.6 (36.0)	
			3		0.079 (0.031)	0.198 (0.078)				32.9 (29.9)	34.0 (30.9)	
			4	820.5 (119.0)	?	?	—	—		—	—	
			5		?	?	—	—		—	—	
			6		a = t	0.457 (0.180)	0.33	1.00		49.1 (44.7)	—	
			7	921.2 (133.6)	a = t	0.457 (0.180)	0.33	1.00		55.7 (50.7)	—	

66 L

 INITIAL CONDITIONS
 PROOF LOAD
 START OF CYCLIC TEST
 DIMPLING OCCURRED




 RESTART OF CYCLIC TEST AFTER DIMPLING AND MARKING
 TERMINATION OF CYCLIC TEST
 FAILURE

Table 44: 6Al-4V STA Titanium (RT Direction) Cyclic Flaw Growth Data at 295°K (72° F) After an Ambient Proof Test; $t = 0.16 \text{ cm (0.063 inch)}$, $\sigma_D = 0.77\sigma_{VS}$ and $(a/2c)_i \cong 0.09$

SPECIMEN NUMBER	THICKNESS, t cm (INCH)	WIDTH, W cm (INCH)	TEST CONDITIONS AT	GROSS STRESS, G MN/m ² (KSI)	FLAW DEPTH, a cm (INCH)	FLAW WIDTH, 2c cm (INCH)	a/2c	a/t	TEST ENVIRONMENT	IRWIN K _I MN/m ^{3/2} (KSI √IN)	K _I WITH M _K MN/m ^{3/2} (KSI √IN)	REMARKS
OCT 61 -1	0.157 (0.062)	5.08 (2.00)	1	944.6 (137.0)	0.025 (0.010)	0.302 (0.119)	0.08	0.16	AIR	31.0 (28.2)	31.8 (28.9)	SPECIMEN PROOF TESTED AND THEN CYCLED FOR 106 CYCLES WHEN SPECIMEN DIMPLED. SPECIMEN MARKED AND CYCLE TEST RE-STARTED. FLAW BREAKTHROUGH OCCURRED AT 1110 CYCLES. SPECIMEN THEN FAILED AT RT.
			2		0.028 (0.011)	0.302 (0.119)	0.09	0.18		32.2 (29.3)	33.1 (30.1)	
			3	820.5 (119.0)	0.028 (0.011)	0.302 (0.119)	0.09	0.18		27.4 (24.9)	28.1 (25.6)	
			4		?	?	—	—		—	—	
			5		?	?	—	—		—	—	
			6	a = t	0.559 (0.220)	0.28	1.00	53.0 (48.2)		—		
			7	a = t	0.559 (0.220)	0.28	1.00	—		—		
OCT 61 -2	0.157 (0.062)	5.11 (2.01)	1	944.6 (137.0)	0.250 (0.010)	0.284 (0.112)	0.09	0.16	AIR	30.9 (28.1)	31.5 (28.7)	SPECIMEN PROOF TESTED AND THEN CYCLED FOR 90 CYCLES WHEN SPECIMEN DIMPLED. SPECIMEN MARKED AND CYCLE TEST RE-STARTED; SPECIMEN FAILED
			2		0.028 (0.011)	0.284 (0.112)	0.10	0.18		32.1 (29.2)	32.9 (29.9)	
			3	0.028 (0.011)	0.284 (0.112)	0.10	0.18	27.3 (24.8)		27.9 (25.4)		
			4	?	?	—	—	—		—		
			5	?	?	—	—	—		—		
			6	a = t	0.584 (0.230)	0.27	1.00	53.7 (48.9)		—		
			7	a = t	0.584 (0.230)	0.27	1.00	—		—		
OCT 61 -3	0.160 (0.063)	5.08 (2.00)	1	944.6 (137.0)	0.058 (0.023)	0.549 (0.216)	0.11	0.37	AIR	45.9 (41.8)	50.4 (45.9)	SPECIMEN PROOF TESTED AND THEN CYCLED FOR 96 CYCLES WHEN SPECIMEN DIMPLED. SPECIMEN MARKED AND CYCLE TEST RE-STARTED. FLAW BREAKTHROUGH OCCURRED AT 1176 CYCLES BUT CYCLED FOR 1224 CYCLES. SPECIMEN THEN FAILED AT RT.
			2		0.061 (0.024)	0.549 (0.216)	0.11	0.38		46.6 (42.4)	50.8 (46.7)	
			3	0.061 (0.024)	0.549 (0.216)	0.11	0.38	39.7 (36.1)		43.6 (39.7)		
			4	0.071 (0.028)	0.549 (0.216)	0.13	0.44	42.1 (39.3)		47.8 (43.5)		
			7	0.076 (0.030)	0.549 (0.216)	0.14	0.48	43.2 (39.3)		49.8 (45.3)		

1 INITIAL CONDITIONS
 2 PROOF LOADS
 3 START OF CYCLIC TEST

4 DIMPLING OCCURRED
 5 RESTART OF CYCLIC TEST AFTER DIMPLING AND MARKING

6 TERMINATION OF CYCLIC TEST
 7 FAILURE

Table 45: 6Al-4V STA Titanium (WT Direction) Cyclic Flaw Growth Data at 295°K (72° F) in Argon at 10 cpm After an Ambient Proof Test; $t = 0.31$ cm (0.12 inch); $\sigma_0 = 0.68 \sigma_{YS}$ and $(a/2c)_i \cong 0.38$

SPECIMEN NUMBER	THICKNESS, t cm (INCH)	WIDTH, W cm (INCH)	TEST CONDITIONS AT	GROSS STRESS, G MN/m ² (KSI)	FLAW DEPTH, a cm (INCH)	FLAW WIDTH, $2c$ cm (INCH)	$a/2c$	a/t	TEST ENVIRONMENT	IRWIN K_I MN/m ^{3/2} (KSI \sqrt{IN})	K_I WITH M_K MN/m ^{3/2} (KSI \sqrt{IN})	REMARKS (NUMBER OF CYCLES REFER TO TOTAL CYCLES)
OST-8A	0.310 (0.122)	5.08 (2.00)	1	979.1 (142.0)	0.163 (0.064)	0.422 (0.166)	0.39	0.53	AIR	57.7 (52.5)	60.2 (54.8)	SPECIMEN PROOF TESTED. FLAW BREAKTHROUGH OCCURRED AT 735 CYCLES INTO CYCLIC TEST BUT CYCLED FOR 747 CYCLES. SPECIMEN FAILED IN RT AIR.
			2		0.165 (0.065)	0.483 (0.190)	0.34	0.53		61.1 (55.6)	65.5 (59.6)	
			3	734.3 (106.5)	0.165 (0.065)	0.483 (0.190)	0.34	0.53	ARGON	44.8 (40.8)	48.0 (43.7)	
			4		$a = t$	0.775 (0.305)	0.40	1.00		57.6 (52.4)	—	
			5	762.6 (110.6)	$a = t$	0.775 (0.305)	0.40	1.00	AIR	60.0 (54.6)	—	
OST-9A	0.302 (0.119)	5.11 (2.01)	1	979.1 (142.0)	0.163 (0.064)	0.422 (0.166)	0.39	0.54	AIR	57.7 (52.5)	60.3 (54.9)	SPECIMEN PROOF TESTED. FLAW BREAKTHROUGH OCCURRED AT 800 CYCLES INTO CYCLIC TEST BUT CYCLED FOR 875 CYCLES. SPECIMEN FAILED IN RT AIR.
			2		0.168 (0.066)	0.432 (0.170)	0.39	0.56		58.5 (53.2)	61.2 (55.7)	
			3	734.3 (106.5)	0.168 (0.066)	0.432 (0.170)	0.39	0.56	ARGON	43.0 (39.1)	45.1 (41.0)	
			4		$a = t$	0.757 (0.298)	0.40	1.00		56.9 (51.8)	—	
			5	815.7 (118.3)	$a = t$	0.757 (0.298)	0.40	1.00	AIR	63.6 (57.9)	—	
OST-16A	0.320 (0.126)	5.11 (2.01)	1	979.1 (142.0)	0.132 (0.052)	0.361 (0.142)	0.37	0.41	AIR	53.2 (48.4)	54.8 (49.9)	SPECIMEN PROOF TESTED AND THEN CYCLED FOR 1240 CYCLES WHEN FLAW BREAKTHROUGH OCCURRED. SPECIMEN FAILED IN RT AIR.
			2		0.135 (0.053)	0.366 (0.144)	0.37	0.42		53.6 (48.8)	55.3 (50.3)	
			3	734.3 (106.5)	0.135 (0.053)	0.366 (0.144)	0.37	0.42	ARGON	39.3 (35.8)	40.6 (36.9)	
			4		$a = t$	0.889 (0.350)	0.36	1.00		61.2 (55.7)	—	
			5	818.4 (118.7)	$a = t$	0.889 (0.350)	0.36	1.00	AIR	68.7 (62.5)	—	
OST-17A	0.302 (0.119)	5.08 (2.00)	1	979.1 (142.0)	0.130 (0.051)	0.373 (0.147)	0.35	0.43	AIR	53.9 (49.0)	56.0 (51.0)	SPECIMEN PROOF TESTED AND THEN CYCLED FOR 1088 CYCLES WHEN FLAW BREAKTHROUGH OCCURRED. SPECIMEN FAILED IN RT AIR.
			2		0.135 (0.053)	0.381 (0.150)	0.35	0.45		54.5 (49.6)	56.8 (51.7)	
			3	734.3 (106.5)	0.135 (0.053)	0.381 (0.150)	0.35	0.45	ARGON	40.0 (36.4)	41.7 (37.9)	
			4		$a = t$	0.864 (0.340)	0.35	1.00		60.1 (54.7)	—	
			5	799.8 (116.0)	$a = t$	0.864 (0.340)	0.35	1.00	AIR	65.8 (59.9)	—	

1 INITIAL CONDITIONS
2 PROOF LOAD

3 START OF CYCLIC TEST
4 TERMINATION OF CYCLIC TEST

5 FAILURE

Table 46: 6Al-4V STA Titanium (WT Direction) Cyclic Flaw Growth Data at 295°K (72°F) in Argon at 10 cpm After an Ambient Proof Test; $t = 0.16 \text{ cm (0.063 inch)}$, $\sigma_D = 0.68 \sigma_{YS}$ and $(a/2c)_i = 0.10$

SPECIMEN NUMBER	THICKNESS, t cm (INCH)	WIDTH, W cm (INCH)	TEST CONDITIONS AT	GROSS STRESS, G MN/m ² (KSI)	FLAW DEPTH, a cm (INCH)	FLAW WIDTH, $2c$ cm (INCH)	$a/2c$	a/t	TEST ENVIRONMENT	IRWIN K_I MN/m ^{3/2} (KSI $\sqrt{\text{IN}}$)	K_I WITH M_K MN/m ^{3/2} (KSI $\sqrt{\text{IN}}$)	REMARKS
ST6-5	0.157 (0.062)	5.11 (2.01)	1	979.1 (142.0)	0.079 (0.031)	0.795 (0.313)	0.10	0.50	AIR	55.7 (50.7)	66.3 (60.3)	SPECIMEN PROOF TESTED. FLAW BREAKTHROUGH OCCURRED AT 302 CYCLES INTO CYCLIC TEST. SPECIMEN THEN FAILED IN RT AIR.
			2		0.094 (0.037)	0.795 (0.313)	0.12	0.60		59.6 (54.2)	76.4 (69.5)	
			3	734.3 (106.5)	0.094 (0.037)	0.795 (0.313)	0.12	0.60	ARGON	43.1 (39.2)	55.2 (50.2)	
			4		$a = t$	0.826 (0.325)	0.19	1.00		51.8 (47.1)	—	
			5	861.9 (125.0)	$a = t$	0.826 (0.325)	0.19	1.00	AIR	61.8 (56.2)	—	
ST6-6	0.160 (0.063)	5.11 (2.01)	1	979.1 (142.0)	0.076 (0.030)	0.780 (0.307)	0.10	0.48	AIR	54.8 (49.9)	64.3 (58.5)	SPECIMEN PROOF TESTED. FLAW BREAKTHROUGH OCCURRED AT 405 CYCLES INTO CYCLIC TEST. SPECIMEN THEN FAILED IN RT AIR.
			2		0.089 (0.035)	0.780 (0.307)	0.11	0.56		58.1 (52.9)	72.2 (65.7)	
			3	734.3 (106.5)	0.089 (0.035)	0.780 (0.307)	0.11	0.56	ARGON	42.0 (38.2)	52.2 (47.5)	
			4		$a = t$	0.813 (0.320)	0.20	1.00		51.9 (47.2)	—	
			5	863.3 (125.2)	$a = t$	0.813 (0.320)	0.20	1.00	AIR	62.0 (56.4)	—	
ST6-13	0.157 (0.062)	5.11 (2.01)	1	979.1 (142.0)	0.061 (0.024)	0.622 (0.245)	0.10	0.39	AIR	49.0 (44.6)	54.3 (49.4)	SPECIMEN PROOF TESTED. FLAW BREAKTHROUGH OCCURRED AT 651 CYCLES INTO CYCLIC TEST. SPECIMEN THEN FAILED IN RT AIR.
			2		0.066 (0.026)	0.622 (0.245)	0.11	0.42		50.6 (46.0)	56.8 (51.7)	
			3	734.3 (106.5)	0.066 (0.026)	0.622 (0.245)	0.11	0.42	ARGON	36.5 (33.2)	41.0 (37.3)	
			4		$a = t$	0.686 (0.270)	0.23	1.00		49.7 (45.2)	—	
			5	906.0 (131.4)	$a = t$	0.686 (0.270)	0.23	1.00	AIR	62.5 (56.9)	—	
ST6-14	0.157 (0.062)	5.11 (2.01)	1	979.1 (142.0)	0.061 (0.024)	0.640 (0.252)	0.10	0.39	AIR	49.2 (44.8)	54.5 (49.6)	SPECIMEN PROOF TESTED. FLAW BREAKTHROUGH OCCURRED AT 565 CYCLES INTO CYCLIC TEST. SPECIMEN THEN FAILED IN RT AIR.
			2		0.064 (0.025)	0.640 (0.252)	0.10	0.40		50.0 (45.5)	55.6 (50.6)	
			3	734.3 (106.5)	0.064 (0.025)	0.640 (0.252)	0.10	0.40	ARGON	36.0 (32.8)	40.1 (36.5)	
			4		$a = t$	0.762 (0.300)	0.21	1.00		51.0 (46.4)	—	
			5	856.4 (124.2)	$a = t$	0.762 (0.300)	0.21	1.00	AIR	60.2 (54.8)	—	

1 INITIAL CONDITIONS
2 PROOF LOAD

3 START OF CYCLIC TEST
4 TERMINATION OF CYCLIC TEST

5 FAILURE

Table 47: 6Al-4V STA Titanium (WT Direction) Cyclic Flaw Growth Data at 295°K (72° F) in Salt Water at 10 cpm
 After an Ambient Proof Test; $t = 0.31$ cm (0.12 inch), $\sigma_D = 0.68 \sigma_{ys}$ and $(a/2c)_i \cong 0.38$

SPECIMEN NUMBER	THICKNESS, t cm (INCH)	WIDTH, W cm (INCH)	TEST CONDITIONS AT	GROSS STRESS, G MN/m ² (KSI)	FLAW DEPTH, a cm (INCH)	FLAW WIDTH, $2c$ cm (INCH)	$a/2c$	a/t	TEST ENVIRONMENT	IRWIN K_I MN/m ^{3/2} (KSI \sqrt{IN})	K_I WITH M_K MN/m ^{3/2} (KSI \sqrt{IN})	REMARKS (NUMBER OF CYCLES REFER TO TOTAL CYCLES)	
OST -6A	0.307 (0.121)	5.08 (2.00)	1	961.9 (139.5)	0.157 (0.062)	0.422 (0.166)	0.37	0.51	AIR	56.5 (51.4)	59.1 (53.8)	SPECIMEN PROOF TESTED. TEST TERMINATED AFTER 58 CYCLES INTO CYCLIC TEST. SPECIMEN THEN FAILED IN RT AIR.	
			2		0.168 (0.066)	0.533 (0.210)	0.31	0.55		62.4 (56.8)	68.2 (62.1)		
			3		734.3 (106.5)	0.168 (0.066)	0.533 (0.210)	0.31	0.55	SALT WATER	46.6 (42.4)		51.0 (46.4)
			4			0.241 (0.095)	1.016 (0.400)	0.24	0.79		61.0 (55.5)		81.7 (74.3)
			5		761.2 (110.4)	0.241 (0.095)	1.016 (0.400)	0.24	0.79	AIR	63.3 (57.6)		84.8 (77.2)
OST -7A	0.318 (0.125)	5.11 (2.01)	1	979.1 (142.0)	0.155 (0.061)	0.442 (0.174)	0.35	0.49	AIR	58.7 (53.4)	61.8 (56.2)	SPECIMEN PROOF TESTED. TEST TERMINATED AFTER 72 CYCLES INTO CYCLIC TEST. SPECIMEN THEN FAILED IN RT AIR.	
			2		0.157 (0.062)	0.457 (0.180)	0.34	0.50		59.6 (54.2)	63.0 (57.3)		
			3	734.3 (106.5)	0.157 (0.062)	0.457 (0.180)	0.34	0.50	SALT WATER	43.6 (39.7)	46.2 (42.0)		
			4		0.254 (0.100)	1.041 (0.410)	0.24	0.80		62.1 (56.5)	83.4 (75.9)		
			5	781.9 (113.4)	0.254 (0.100)	1.041 (0.410)	0.24	0.80	AIR	66.4 (60.4)	89.2 (81.2)		
OST -14A	0.307 (0.121)	5.11 (2.01)	1	979.1 (142.0)	0.142 (0.056)	0.376 (0.148)	0.38	0.46	AIR	54.4 (49.5)	56.4 (51.3)	SPECIMEN PROOF TESTED. TEST TERMINATED AFTER 82 CYCLES INTO CYCLIC TEST. SPECIMEN THEN FAILED IN RT AIR.	
			2		0.145 (0.057)	0.381 (0.150)	0.38	0.47		54.8 (49.9)	56.8 (51.7)		
			3	734.3 (106.5)	0.145 (0.057)	0.381 (0.150)	0.38	0.47	SALT WATER	40.2 (36.6)	41.7 (37.9)		
			4		0.259 (0.102)	0.914 (0.360)	0.28	0.84		60.0 (54.6)	79.0 (71.9)		
			5	811.5 (117.7)	0.259 (0.102)	0.914 (0.360)	0.28	0.84	AIR	66.8 (60.8)	87.9 (80.0)		
OST -15A	0.315 (0.124)	5.08 (2.00)	1	979.1 (142.0)	0.132 (0.052)	0.340 (0.134)	0.39	0.42	AIR	51.9 (47.2)	53.2 (48.4)	SPECIMEN PROOF TESTED. TEST TERMINATED AFTER 91 CYCLES INTO CYCLIC TEST. SPECIMEN THEN FAILED IN RT AIR.	
			2		0.135 (0.053)	0.343 (0.135)	0.39	0.43		52.1 (47.4)	53.4 (48.6)		
			3	734.3 (106.5)	0.135 (0.053)	0.343 (0.135)	0.39	0.43	SALT WATER	38.2 (34.8)	39.2 (35.7)		
			4		0.246 (0.097)	0.940 (0.370)	0.26	0.78		59.9 (54.5)	78.0 (71.0)		
			5	736.4 (106.8)	0.246 (0.097)	0.940 (0.370)	0.26	0.78	AIR	60.1 (54.7)	78.2 (71.2)		

1 INITIAL CONDITIONS
 2 PROOF LOAD

3 START OF CYCLIC TEST
 4 TERMINATION OF CYCLIC TEST

5 FAILURE

Table 48: 6Al-4V STA Titanium (WT Direction) Cyclic Flaw Growth Data at 295°K (72° F) in Salt Water at 10 cpm After an Ambient Proof Test; $t = 0.16$ cm (0.063 inch), $\sigma_0 = 0.68 \sigma_{YS}$ and $(a/2c)_i \cong 0.10$

SPECIMEN NUMBER	THICKNESS, t cm (INCH)	WIDTH, W cm (INCH)	TEST CONDITIONS AT	GROSS STRESS, G MN/m ² (KSI)	FLAW DEPTH, a cm (INCH)	FLAW WIDTH, $2c$ cm (INCH)	$a/2c$	a/t	TEST ENVIRONMENT	IRWIN K_I MN/m ^{3/2} (KSI √IN)	K_I WITH M_K MN/m ^{3/2} (KSI √IN)	REMARKS
ST6 -3	0.157 (0.062)	5.11 (2.01)	1	975.0 (141.4)	0.084 (0.033)	0.787 (0.310)	0.11	0.53	AIR	56.7 (51.6)	69.2 (63.0)	SPECIMEN PROOF TESTED. FLAW BREAKTHROUGH OCCURRED AT 45 CYCLES INTO CYCLIC TEST. SPECIMEN THEN FAILED IN RT AIR.
			2		0.089 (0.035)	0.787 (0.310)	0.11	0.57		57.9 (52.7)	72.5 (66.0)	
			3	734.3 (106.5)	0.089 (0.035)	0.787 (0.310)	0.11	0.57	SALT WATER	42.1 (38.3)	52.6 (47.9)	
			4		$a = t$	0.965 (0.380)	0.16	1.00		53.3 (48.5)	—	
			5	860.5 (124.8)	$a = t$	0.965 (0.380)	0.16	1.00	AIR	53.5 (57.8)	—	
ST6 -4	0.160 (0.063)	5.11 (2.01)	1	882.6 (128.0)	0.081 (0.032)	0.787 (0.310)	0.10	0.51	AIR	49.9 (45.4)	59.8 (54.4)	SPECIMEN PROOF TESTED. FLAW BREAKTHROUGH OCCURRED AT 14 CYCLES INTO CYCLIC TEST. SPECIMEN THEN FAILED IN RT AIR.
			2		0.104 (0.041)	0.787 (0.310)	0.13	0.65		55.0 (50.0)	73.2 (66.6)	
			3	734.3 (106.5)	0.104 (0.041)	0.787 (0.310)	0.13	0.65	SALT WATER	44.7 (40.7)	59.7 (54.3)	
			4		$a = t$	1.168 (0.460)	0.14	1.00		55.3 (50.3)	—	
			5	748.8 (108.6)	$a = t$	1.168 (0.460)	0.14	1.00	AIR	55.4 (51.3)	—	
ST6 -11	0.155 (0.061)	5.00 (1.97)	1	979.1 (142.0)	0.061 (0.024)	0.622 (0.245)	0.10	0.39	AIR	49.0 (44.6)	54.4 (49.5)	SPECIMEN PROOF TESTED. FLAW BREAKTHROUGH OCCURRED AT 100 CYCLES INTO CYCLIC TEST. SPECIMEN THEN FAILED IN RT AIR.
			2		0.066 (0.026)	0.622 (0.245)	0.11	0.43		50.6 (46.0)	57.1 (52.0)	
			3	734.3 (106.5)	0.066 (0.026)	0.622 (0.245)	0.11	0.43	SALT WATER	36.5 (33.2)	41.2 (37.5)	
			4		$a = t$	0.864 (0.340)	0.18	1.00		52.0 (47.3)	—	
			5	841.2 (122.0)	$a = t$	0.864 (0.340)	0.18	1.00	AIR	60.3 (54.9)	—	
ST6 -12	0.155 (0.061)	5.08 (2.00)	1	979.1 (142.0)	0.064 (0.025)	0.635 (0.250)	0.10	0.41	AIR	49.9 (45.4)	55.8 (50.8)	SPECIMEN PROOF TESTED. FLAW BREAKTHROUGH OCCURRED AT 73 CYCLES INTO CYCLIC TEST. SPECIMEN THEN FAILED IN RT AIR.
			2		0.069 (0.027)	0.635 (0.250)	0.11	0.44		51.4 (46.8)	58.7 (53.4)	
			3	734.3 (106.5)	0.069 (0.027)	0.635 (0.250)	0.11	0.44	SALT WATER	37.1 (33.8)	42.4 (38.6)	
			4		$a = t$	0.889 (0.350)	0.17	1.00		52.3 (47.6)	—	
			5	818.4 (118.7)	$a = t$	0.889 (0.350)	0.17	1.00	AIR	58.9 (53.6)	—	

1 INITIAL CONDITIONS
2 PROOF LOAD

3 START OF CYCLIC TEST
4 TERMINATION OF CYCLIC TEST

5 FAILURE

Table 49: 6Al-4V STA Titanium (WT Direction) Cyclic Flaw Growth Data at 295° K (72° F) in Salt Water at 0.2 cpm After an Ambient Proof Test; $t = 0.31$ (0.12 inch), $\sigma_0 = 0.68 \sigma_{ys}$ and $(a/2c)_i \cong 0.38$

SPECIMEN NUMBER	THICKNESS, t cm (INCH)	WIDTH, W cm (INCH)	TEST CONDITIONS AT	GROSS STRESS, G MN/m ² (KSI)	FLAW DEPTH, a cm (INCH)	FLAW WIDTH, $2c$ cm (INCH)	$a/2c$	a/t	TEST ENVIRONMENT	IRWIN K_I MN/m ^{3/2} (KSI√IN)	K_I WITH MK MN/m ^{3/2} (KSI√IN)	REMARKS
OST-4A	0.307 (0.121)	5.08 (2.00)	1	979.1 (142.0)	0.160 (0.063)	0.419 (0.165)	0.38	0.52	AIR	57.5 (52.3)	60.0 (54.6)	SPECIMEN PROOF TESTED, THEN SPECIMEN FAILED AFTER 2.5 MINUTES OF FIRST CYCLE INTO CYCLIC TEST.
			2		0.163 (0.064)	0.429 (0.169)	0.38	0.53		38.1 (52.9)	61.0 (55.5)	
			3	734.3 (106.5)	0.163 (0.064)	0.429 (0.169)	0.38	0.53	SALT WATER	42.6 (38.8)	44.6 (40.6)	
OST-5A	0.310 (0.122)	5.08 (2.00)	1	979.1 (142.0)	0.152 (0.060)	0.414 (0.163)	0.37	0.49	AIR	57.0 (51.9)	59.6 (54.2)	SPECIMEN PROOF TESTED, THEN SPECIMEN FAILED AFTER 3.4 MINUTES OF 19TH CYCLE INTO CYCLIC TEST.
			2		0.157 (0.062)	0.424 (0.167)	0.37	0.51		57.7 (52.5)	60.4 (55.0)	
			3	734.3 (106.5)	0.157 (0.062)	0.424 (0.167)	0.37	0.51	SALT WATER	42.4 (38.6)	44.4 (40.4)	
			5		0.165 (0.065)	0.437 (0.172)	0.38	0.53		43.0 (39.1)	44.9 (40.9)	
OST-12A	0.310 (0.122)	5.11 (2.01)	1	979.1 (142.0)	0.130 (0.051)	0.345 (0.136)	0.38	0.42	AIR	52.1 (47.4)	53.6 (48.8)	SPECIMEN PROOF TESTED AND THEN CYCLED FOR 260 CYCLES. TEST TERMINATED AND SPECIMEN MARKED AND FAILED IN RT AIR.
			2		0.132 (0.052)	0.351 (0.138)	0.38	0.43		52.5 (47.8)	54.1 (49.2)	
			3	734.3 (106.5)	0.132 (0.052)	0.351 (0.138)	0.38	0.43	SALT WATER	38.6 (35.1)	39.8 (36.2)	
			4		0.152 (0.060)	0.411 (0.162)	0.37	0.49		41.8 (38.0)	43.5 (39.6)	
			5	—	0.152 (0.062)	0.483 (0.190)	0.33	0.51	AIR	—	—	
OST-13A	0.310 (0.122)	5.11 (2.01)	1	979.1 (142.0)	0.127 (0.050)	0.333 (0.131)	0.38	0.41	AIR	51.2 (46.6)	52.5 (47.8)	SPECIMEN PROOF TESTED, THEN SPECIMEN FAILED AFTER 1.3 MINUTES OF 475TH CYCLE INTO CYCLIC TEST.
			2		0.130 (0.051)	0.335 (0.132)	0.39	0.42		51.4 (46.8)	52.8 (48.0)	
			3	734.3 (106.5)	0.130 (0.051)	0.335 (0.132)	0.39	0.42	SALT WATER	37.8 (34.4)	38.8 (35.3)	
			5		0.183 (0.072)	0.508 (0.200)	0.36	0.59		46.3 (42.1)	49.9 (45.4)	

- 1 INITIAL CONDITIONS
 2 PROOF LOAD
 3 START OF CYCLIC TEST
 4 TERMINATION OF CYCLIC TEST
 5 FAILURE

Table 50: 6Al-4V STA Titanium (WT Direction) Cyclic Flaw Growth Data at 295°K (72° F) in Salt Water at 0.2 cpm After an Ambient Proof Test, $t = 0.16$ cm (0.063 inch), $\sigma_D \cong 0.68 \sigma_{YS}$ and $(a/2c)_i \cong 0.10$

SPECIMEN NUMBER	THICKNESS, t cm (INCH)	WIDTH, W cm (INCH)	TEST CONDITIONS AT	GROSS STRESS, G MN/m ² (KSI)	FLAW DEPTH, a cm (INCH)	FLAW WIDTH, 2c cm (INCH)	a/2c	a/t	TEST ENVIRONMENT	IRWIN K_I MN/m ^{3/2} (KSI √IN)	K_I WITH M_K MN/m ^{3/2} (KSI √IN)	REMARKS
ST6 -1	0.157 (0.062)	5.08 (2.00)	1	961.9 (139.5)	0.079 (0.031)	0.770 (0.303)	0.10	0.50	AIR	54.3 (49.4)	64.6 (58.8)	SPECIMEN PROOF TESTED, THEN SPECIMEN FAILED AFTER 1.5 MINUTES OF 15TH CYCLE INTO CYCLIC TEST.
			2		0.097 (0.038)	0.770 (0.303)	0.13	0.61		58.8 (53.5)	76.1 (69.2)	
			3	734.3 (106.5)	0.097 (0.038)	0.770 (0.303)	0.13	0.61	SALT WATER	43.4 (39.5)	56.2 (51.1)	
			4		0.107 (0.042)	0.770 (0.303)	0.14	0.68		45.1 (41.0)	61.1 (55.6)	
ST6 -2	0.150 (0.059)	5.11 (2.01)	1	896.4 (130.0)	0.091 (0.036)	0.762 (0.300)	0.12	0.61	AIR	53.0 (48.2)	68.7 (62.5)	SPECIMEN PROOF TESTED, THEN SPECIMEN FAILED AFTER 1.2 MINUTES OF 23RD CYCLE INTO CYCLIC TEST.
			2		0.107 (0.042)	0.762 (0.300)	0.14	0.71		56.2 (51.1)	78.2 (71.2)	
			3	673.6 (97.7)	0.107 (0.042)	0.762 (0.300)	0.14	0.71	SALT WATER	40.9 (37.2)	57.0 (51.9)	
			4		0.127 (0.050)	0.838 (0.330)	0.15	0.85		44.1 (40.1)	68.0 (61.9)	
ST6 -9	0.157 (0.062)	5.08 (2.00)	1	973.6 (141.2)	0.058 (0.023)	0.635 (0.250)	0.09	0.37	AIR	48.0 (43.7)	53.0 (48.2)	SPECIMEN PROOF TESTED, THEN SPECIMEN FAILED AFTER 0.7 MINUTE OF 157TH CYCLE INTO CYCLIC TEST.
			2		0.064 (0.025)	0.635 (0.250)	0.10	0.40		49.6 (45.1)	55.2 (50.2)	
			3	734.3 (106.5)	0.064 (0.025)	0.635 (0.250)	0.10	0.40	SALT WATER	36.0 (32.8)	40.1 (36.5)	
			4		0.117 (0.046)	0.681 (0.268)	0.17	0.74		45.5 (41.4)	63.3 (57.6)	
ST6 -10	0.157 (0.062)	5.08 (2.00)	1	979.1 (142.0)	0.058 (0.023)	0.622 (0.245)	0.09	0.37	AIR	48.2 (43.9)	53.2 (48.4)	SPECIMEN PROOF TESTED, THEN SPECIMEN FAILED AFTER 0.8 MINUTE OF 54TH CYCLE INTO CYCLIC TEST.
			2		0.074 (0.029)	0.622 (0.245)	0.12	0.47		52.8 (48.0)	61.0 (55.5)	
			3	734.3 (106.5)	0.074 (0.029)	0.622 (0.245)	0.12	0.47	SALT WATER	38.1 (34.7)	44.1 (40.1)	
			4		0.091 (0.036)	0.622 (0.245)	0.15	0.58		41.3 (37.6)	51.4 (46.8)	



- 1 INITIAL CONDITIONS
- 2 PROOF LOAD
- 3 START OF CYCLIC TEST
- 4 FAILURE


**Table 51: Proof Overload Effects on da/dN for 2219-T87 Aluminum at 78°K (-320°F)
(WT Direction)**

CYCLIC STRESS LEVEL σ_o/σ_{ys}	MATERIAL THICKNESS, cm (INCH)			
	1.27 (0.50)		0.38 (0.15)	
	INITIAL FLAW SHAPE		INITIAL FLAW SHAPE	
	$\cong 0.40$	$\cong 0.10$	$\cong 0.40$	$\cong 0.10$
0.67	MODERATE RETARDATION INITIALLY	NO TEST RESULTS	SIGNIFICANT RETARDATION INITIALLY	MODERATE TO SIGNIFICANT RETARDATION INITIALLY
0.91	SLIGHT, IF ANY, RETARDATION INITIALLY	SLIGHT, IF ANY, RETARDATION INITIALLY	NO DISCERNIBLE EFFECT	SIGNIFICANT RETARDATION INITIALLY

$\sigma_{PROOF} = 0.85 \text{ --- } 1.0 \sigma_{ys}$ AT 78°K (-320°F)

Table 52: Proof Overload Effects on da/dN in Inert Environment for 6Al-4V STA Titanium at 295°K (72°F)

CYCLIC STRESS LEVEL σ_o/σ_{ys}	MATERIAL THICKNESS, cm (INCH)					
	0.54 (0.21)		0.31 (0.12)		0.16 (0.063)	
	$(a/2c)_i$		$(a/2c)_i$		$(a/2c)_i$	
	$\cong 0.40$	$\cong 0.10$	$\cong 0.40$	$\cong 0.10$	$\cong 0.40$	$\cong 0.10$
0.68 	NO TEST RESULTS		SIGNIFICANT RETARDATION INITIALLY	NO TEST RESULTS		SIGNIFICANT RETARDATION INITIALLY
0.77 	SLIGHT, IF ANY, RETARDATION INITIALLY	NO DISCERNIBLE EFFECT	NO TEST RESULTS		SIGNIFICANT RETARDATION INITIALLY	SLIGHT RETARDATION INITIALLY

 $\sigma_p = 0.91 \sigma_{ys}$ AT 295°K (72°F) & FLAW ORIENTATION OF WT


 $\sigma_p = 0.89 \sigma_{ys}$ AT 295°K (72°F) & FLAW ORIENTATION OF RT

Table 53: 6Al-4V STA Titanium (WT Direction) Sustained Load Flow Growth Data at 295°K (72°F) in Salt Water, $t = 0.54$ cm (0.21 inch), $\sigma_0 = 0.68 \sigma_{YS}$ and $(a/2c)_i \cong 0.37$

SPECIMEN NUMBER	THICKNESS, t cm (INCH)	WIDTH, W cm (INCH)	TEST CONDITIONS AT	GROSS STRESS, G MN/m ² (KSI)	FLAW DEPTH, a cm (INCH)	FLAW WIDTH, 2c cm (INCH)	a/2c	a/t	TEST ENVIRONMENT	IRWIN K _I MN/m ^{3/2} (KSI √IN)	K _I WITH M _K MN/m ^{3/2} (KSI √IN)	REMARKS
XT-5	0.531 (0.209)	4.90 (1.93)	3	568.8 (82.5)	0.279 (0.110)	0.749 (0.295)	0.37	0.53	SALT WATER	43.2 (39.3)	45.4 (41.3)	SPECIMEN FAILED IN 0.25 MIN.
XT-4	0.544 (0.214)	4.90 (1.93)	3	734.3 (106.5)	0.175 (0.069)	0.488 (0.192)	0.36	0.32	SALT WATER	45.3 (41.2)	48.6 (42.4)	SPECIMEN FAILED IN 0.72 MIN.
OST2 -1	0.533 (0.210)	5.08 (2.00)	1	979.1 (142.0)	0.170 (0.067)	0.467 (0.184)	0.36	0.32	AIR	60.6 (55.1)	62.2 (56.6)	SPECIMEN PROOF TESTED AND THEN SUSTAIN LOADED FOR 8.0 HOURS WITH NO FLAW GROWTH. SPECIMEN THEN MARKED AND FAILED IN RT AIR.
			2		0.173 (0.068)	0.490 (0.193)				61.8 (56.2)	63.6 (57.9)	
			3	734.3 (106.5)	0.173 (0.068)	0.490 (0.193)	0.35	0.32	SALT WATER	45.4 (41.3)	46.7 (42.5)	
			4	0.173 (0.068)	0.490 (0.193)	45.4 (41.3)				46.7 (42.5)		
			5	1041.1 (151.0)	0.185 (0.073)	0.528 (0.208)	0.36	0.35	AIR	67.9 (61.8)	70.0 (63.7)	
OST2 -2	0.531 (0.209)	5.08 (2.00)	1	979.1 (142.0)	0.188 (0.074)	0.528 (0.208)	0.36	0.35	AIR	64.2 (58.4)	66.2 (60.2)	SPECIMEN PROOF TESTED AND THEN A SLIGHT MARK APPLIED. SPECIMEN FAILED IN 1.33 MINUTES OF BEING SUSTAIN LOADED.
			2		0.191 (0.075)	0.594 (0.234)				67.4 (61.3)	70.0 (63.7)	
			3	734.3 (106.5)	0.193 (0.076)	0.597 (0.235)	0.32	0.36	SALT WATER	49.6 (45.1)	51.4 (46.8)	
OST2 -3	0.536 (0.211)	5.08 (2.00)	1	979.1 (142.0)	0.185 (0.073)	0.485 (0.191)	0.38	0.35	AIR	61.9 (56.3)	63.4 (57.7)	SPECIMEN PROOF TESTED AND THEN SUSTAIN LOADED FOR 7.0 HOURS WITH NO FLAW GROWTH. SPECIMEN THEN MARKED AND FAILED IN RT AIR.
			2		0.191 (0.075)	0.559 (0.220)				65.7 (59.8)	68.0 (61.9)	
			3	734.3 (106.5)	0.191 (0.075)	0.559 (0.220)	0.34	0.36	SALT WATER	48.1 (43.8)	49.9 (45.4)	
			4	0.198 (0.078)	0.635 (0.250)	50.8 (46.2)				52.9 (48.1)		
			5	946.0 (137.2)	0.249 (0.098)	0.762 (0.300)	0.33	0.46	AIR	73.6 (67.0)	77.8 (70.8)	
OST2 -4	0.533 (0.210)	5.08 (2.00)	1	979.1 (142.0)	0.178 (0.070)	0.478 (0.188)	0.37	0.33	AIR	61.3 (55.8)	62.9 (57.2)	SPECIMEN PROOF TESTED AND THEN A SLIGHT MARK APPLIED. SPECIMEN FAILED IN 1.7 MINUTES OF BEING SUSTAIN LOADED.
			2		0.188 (0.074)	0.500 (0.197)				62.8 (57.1)	64.4 (58.6)	
			3	734.3 (106.5)	0.193 (0.076)	0.503 (0.198)	0.38	0.36	SALT WATER	46.3 (42.1)	47.4 (43.1)	

1 INITIAL CONDITIONS
 2 PROOF LOAD
 3 START OF SUSTAINED LOAD TEST

4 TERMINATION OF SUSTAINED LOAD TEST
 5 FAILURE

Table 54: 6Al-4V STA Titanium (WT Direction) Sustained Load Flaw Growth Data at 295°K (72° F) in Salt Water, $t = 0.31$ cm (0.12 inch), $\sigma_0 = 0.68 \sigma_{YS}$ and $(a/2c)_i \cong 0.37$

SPECIMEN NUMBER	THICKNESS, t cm (INCH)	WIDTH, W cm (INCH)	TEST CONDITIONS AT	GROSS STRESS, G MN/m ² (KSI)	FLAW DEPTH, a cm (INCH)	FLAW WIDTH, $2c$ cm (INCH)	$a/2c$	a/t	TEST ENVIRONMENT	IRWIN K_I MN/m ^{3/2} (KSI \sqrt{IN})	K_I WITH M/K MN/m ^{3/2} (KSI \sqrt{IN})	REMARKS
OST -2A	0.306 (0.120)	5.08 (2.00)	3	734.3 (106.5)	0.127 (0.050)	0.340 (0.134)	0.37	0.42	SALT WATER	38.0 (34.6)	39.1 (35.6)	SPECIMEN FAILED IN 1.10 MIN.
OST2 -7	0.312 (0.123)	5.08 (2.00)	3	734.3 (106.5)	0.157 (0.062)	0.417 (0.164)	0.38	0.50	SALT WATER	42.1 (38.3)	43.9 (39.9)	SPECIMEN FAILED IN 1.02 MIN.
OST -1A	0.318 (0.125)	5.08 (2.00)	1	979.1 (142.0)	0.175 (0.069)	0.465 (0.183)	0.38	0.55	AIR	60.6 (55.1)	63.9 (58.1)	SPECIMEN PROOF TESTED AND THEN SUSTAIN LOADED FOR 8.0 HOURS WITH NO FLAW GROWTH. SPECIMEN THEN MARKED AND FAILED IN RT AIR.
			2		0.178 (0.070)	0.470 (0.185)				60.9 (55.4)	64.3 (58.5)	
			3	734.3 (106.5)	0.178 (0.070)	0.470 (0.185)	0.38	0.56	SALT WATER	44.7 (40.7)	47.3 (43.0)	
			4	1037.0 (150.4)	0.178 (0.070)	0.470 (0.185)	0.38	0.56	SALT WATER	44.7 (40.7)	47.3 (43.0)	
			5		0.193 (0.076)	0.544 (0.214)				69.5 (63.2)	75.6 (68.8)	
OST -3A	0.315 (0.124)	5.08 (2.00)	1	979.1 (142.0)	0.127 (0.050)	0.351 (0.138)	0.36	0.40	AIR	52.4 (47.7)	54.0 (49.1)	SPECIMEN PROOF TESTED AND THEN SUSTAIN LOADED FOR 8.0 HOURS WITH NO FLAW GROWTH. SPECIMEN THEN MARKED AND FAILED IN RT AIR.
			2		0.130 (0.051)	0.353 (0.139)				52.6 (47.9)	54.3 (49.4)	
			3	734.3 (106.5)	0.130 (0.051)	0.353 (0.139)	0.37	0.41	SALT WATER	38.7 (35.2)	39.8 (36.2)	
			4	0.130 (0.051)	0.353 (0.139)	0.37	0.41	38.7 (35.2)		39.8 (36.2)		
			5	1054.2 (152.9)	0.145 (0.057)	0.381 (0.150)	0.38	0.46	AIR	59.5 (54.1)	61.5 (56.0)	

- 1 INITIAL CONDITIONS
 2 PROOF LOAD
 3 START OF SUSTAINED LOAD TEST
 4 TERMINATION OF SUSTAINED LOAD TEST
 5 FAILURE

Table 55: 6Al-4V STA Titanium (WT Direction) Sustained Load Flaw Growth Data at 295°K (72°F) in Salt Water;
 $t = 0.16 \text{ cm (0.063 inch)}$, $\sigma_0 = 0.62 \text{ - } 0.76 \sigma_{YS}$ and $(a/2c)_i \cong 0.09$

SPECIMEN NUMBER	THICKNESS, t cm (INCH)	WIDTH, W cm (INCH)	TEST CONDITIONS AT	GROSS STRESS, G MN/m ² (KSI)	FLAW DEPTH, a cm (INCH)	FLAW WIDTH, 2c cm (INCH)	a/2c	a/t	TEST ENVIRONMENT	IRWIN K _I MN/m ^{3/2} (KSI√IN)	K _I WITH M _K MN/m ^{3/2} (KSI√IN)	REMARKS	
OST6 -2	0.155 (0.061)	5.08 (2.00)	3	734.3 (106.5)	0.058 (0.023)	0.709 (0.279)	0.08	0.38	SALT WATER	35.2 (32.0)	38.9 (35.4)	SPECIMEN SUSTAIN LOADED FOR 7.0 HOURS WITH NO FLAW GROWTH. SPECIMEN THEN MARKED AND FAILED IN RT AIR.	
			4		0.058 (0.023)	0.709 (0.279)	0.08	0.38		35.2 (32.0)	38.9 (35.4)		
			5		950.8 (137.9)	0.097 (0.038)	0.709 (0.279)	0.14	0.62	AIR	57.4 (52.2)		74.4 (67.7)
OST6 -3	0.160 (0.063)	5.08 (2.00)	3	734.3 (106.5)	0.069 (0.027)	0.762 (0.300)	0.09	0.43	SALT WATER	37.8 (34.4)	43.0 (39.1)		SPECIMEN SUSTAIN LOADED FOR 7.0 HOURS WITH NO SCC FLAW GROWTH. SPECIMEN MARKED AND SUSTAIN LOADED FOR 7.0 HOURS WITH NO SCC FLAW GROWTH. SPECIMEN MARKED AND SUSTAIN LOADED. SPECIMEN FAILED IN 0.33 MIN.
			4		0.071 (0.028)	0.762 (0.300)	0.09	0.44		38.4 (34.9)	44.1 (40.1)		
			3		0.079 (0.031)	0.762 (0.300)	0.10	0.49		40.0 (36.4)	47.3 (43.0)		
			4		0.084 (0.033)	0.762 (0.300)	0.11	0.52		41.0 (37.3)	49.6 (45.1)		
			3		0.094 (0.037)	0.762 (0.300)	0.12	0.59		42.9 (39.0)	54.4 (49.5)		
ST6 -17	0.160 (0.063)	5.08 (2.00)	3	832.2 (120.7)	0.069 (0.027)	0.787 (0.310)	0.09	0.43	SALT WATER	43.6 (39.7)	49.6 (45.1)	SPECIMEN FAILED IN 0.43 MIN.	
ST6 -19	0.155 (0.061)	5.08 (2.00)	3	832.2 (120.7)	0.066 (0.026)	0.635 (0.250)	0.10	0.43	SALT WATER	42.0 (38.2)	47.5 (43.2)	SPECIMEN FAILED IN 0.30 MIN.	
ST6 -20	0.157 (0.062)	5.08 (2.00)	1	979.1 (142.0)	0.069 (0.027)	0.635 (0.250)	0.11	0.44	AIR	51.4 (46.8)	58.5 (53.2)	SPECIMEN PROOF TESTED AND THEN SUSTAIN LOADED. SPECIMEN FAILED IN 0.50 MIN.	
			2		0.069 (0.027)	0.635 (0.250)	0.11	0.44		51.4 (46.8)	58.5 (53.2)		
			3		832.2 (120.7)	0.069 (0.027)	0.635 (0.250)	0.11	0.44	SALT WATER	42.6 (38.8)		48.5 (44.1)

- 1 INITIAL CONDITIONS
 2 PROOF LOAD
 3 START OF SUSTAINED LOAD TEST
 4 TERMINATION OF SUSTAINED LOAD TEST
 5 FAILURE

